Instituto de Tecnología Sábato

International Center for Advanced Studies

INSTITUTO DE CIENCIAS FÍSICAS
UNIVERSIDAD NACIONAL DE SAN MARTÍN

Precision in Drell Yan lepton pair production at hadron colliders

PhD candidate: Manuel Der

Supervisor: **Prof. Dr. Daniel de Florian**

July 27, 2023
Buenos Aires

To Moma, Joa, Ale and Guada.

To Pau and my beloved nephews.

To the memory of Duly Rey and Marta Vega Martínez.

Abstract

Over the last decade and given the impressive agreement between the Standard Model (SM) and the LHC experiments, particle physics has progressively become a precision science. In this scenario, where both SM and Beyond the Standard Model (BSM) physics must be tested through small deviations between theory and experiment, Drell Yan lepton pair production happens to gather the important properties of a precision observable. As the experimental determination for Drell Yan reaches the percent level, the study of this mechanism works both as an important testground for the Standard Model and as a way to evaluate alternative BSM theories, as well. Therefore, theory must be ready for this appointment by producing equally accurate instruments to correctly interpret the available high-precision data.

One of the ways to access the Drell Yan mechanism is the inclusive cross-section. In this sense, in the first part of this work we complete the set of NNLO initial state corrections to the neutral current contributions to Drell Yan lepton pair production. We add both the mixed QCD$\otimes$QED and the NNLO QED terms to the perturbative expansion of the production of a Z boson in hadronic collisions. Specifically, we obtain these corrections by exploiting the resemblance between the abelian part of QCD and the EW $f\bar{f}\gamma$ vertex to develop a suitable *abelianisation* procedure to extract the mixed order $\mathcal{O}(\alpha_s\alpha)$ and even the pure electromagnetic $\mathcal{O}(\alpha^2)$ results.

Furthermore, in order to offer an integral description of the mechanism, we dig deeper and focus on the fully exclusive calculation of the mixed QCD$\otimes$QED correction terms. In order to achieve this goal, we extend the q_T-subtraction method, originally developed to address pure QCD corrections, to apply it to the calculation of the mixed NNLO contributions. We present the explicit expressions for the subtraction term and the hard factor, therefore providing all the ingredients needed for the application of the formalism up to $\mathcal{O}(\alpha_s\alpha)$. We compute the mixed QCD$\otimes$QED corrections and study the phenomenological impact at the level of kinematical distributions.

Our exclusive computation was implemented within a parton level Monte Carlo code, which allows the user to apply arbitrary kinematical cuts on the final-state leptons and to compute the specified distributions in the form of bin histograms. The kinematical dependence of the full differential calculation, together with the magnitude of the inclusive result, were shown to be relevant and highly non trivial at the LHC energies.

Keywords: Drell Yan, Mixed corrections , Abelianisation, q_T-Subtraction.

Resumen

Durante la última década y debido al impresionante acuerdo entre el Modelo Estándar (SM) y los experimentos del LHC, la física de partículas ha comenzado a convertirse en una ciencia de precisión. En este contexto, en el que tanto el SM como las teorías de física más allá del Modelo Estándar (BSM) deben ser contrastados a través de pequeñas desviaciones entre las predicciones teóricas y el experimento, el mecanismo de Drell-Yan ha resultado ser un excelente observable de precisión. Mientras que la determinación experimental se encuentra en el nivel porcentual, el estudio de este mecanismo sirve como un importante campo de pruebas para el Modelo Estándar, tanto como una forma de evaluar teorías alternativas de nueva física. Consecuentemente, la teoría debe estar preparada para este desafío y producir instrumentos adecuados para interpretar correctamente los datos de alta precisión que hay disponibles.

Una de las formas de acceder al mecanismo Drell-Yan es a través de la sección eficaz inclusiva. En este sentido, en la primera parte de esta Tesis completamos el conjunto de correcciones de estado inicial de NNLO para las contribuciones de corriente neutra de la producción de pares de leptones en colisiones hadrónicas. En particular, añadimos tanto los términos mixtos QCD$\otimes$QED como los términos de NNLO de QED a la expansión perturbativa de la producción de un bosón Z. Estas correcciones son obtenidas a partir de la similitud entre la parte abeliana de QCD y el vértice EW $f\bar{f}\gamma$, que nos permite desarrollar un procedimiento de *abelianización* adecuado para calcular los resultados mixtos de orden $\mathcal{O}(\alpha_s\alpha)$ e incluso los puramente electromagnéticos de orden $\mathcal{O}(\alpha^2)$.

Además, con el fin de ofrecer una descripción integral del mecanismo, focalizamos la segunda parte de esta Tesis en el cálculo totalmente exclusivo de los términos mixtos QCD$\otimes$QED. Para lograr este objetivo extendemos el método de sustracción de q_T, originalmente desarrollado para abordar correcciones puras de QCD, y lo aplicamos al cálculo de las contribuciones mixtas de NNLO. En este trabajo presentamos las expresiones explícitas para el término de sustracción y el factor H, proporcionando así todos los ingredientes necesarios para la aplicación del formalismo hasta orden $\mathcal{O}(\alpha_s\alpha)$. Finalmente, presentamos un estudio del impacto fenomenológico de las correcciones mixtas al nivel de las distribuciones cinemáticas.

Nuestro cálculo se encuentra implementado en códigos de tipo Monte Carlo, que permiten al usuario aplicar cortes cinemáticos arbitrarios a los leptones en el estado final y calcular las distribuciones especificadas en forma de histogramas. La dependencia cinemática de los cálculos exclusivos, junto con la magnitud del resultado inclusivo, han demostrado ser relevantes y altamente no triviales para las energías del LHC.

Palabras clave: Drell Yan, Correcciones mixtas, Abelianización, Sustracción de q_T.

Contents

List of Figures

List of Tables

CHAPTER 1

Introduction

It is clear that, over the last decades, the Standard Model of particle physics (SM) has been strongly established as the theory for the fundamental interactions. These series of quantum theories developed to describe the dynamics of elementary particles were successfully unified, which represents one of the greatest achievements for the physics of the twentieth century. Furthermore, experiments have strongly supported the SM theory, which also offered accurate predictions for reachable observables, at each energy level tested [1].

The Standard Model, technically speaking, is a gauge theory that describes the dynamics of the 12 spin $1/2$ fermions (and their antiparticles) under the three fundamental forces, which are represented by the specific exchange of a spin 1 boson particle. Each fermion is charged under the SM symmetry group $\mathrm{U}(1) \times \mathrm{SU}(2) \times \mathrm{SU}(3)$ and the mediators are photons (γ) for the $\mathrm{U}(1)$ symmetry group of electromagnetism, $W^{\pm}$ and Z bosons for the $\mathrm{SU}(2)$ symmetry group of the weak force, and 8 gluons for the strong interactions.

Nevertheless, explicit mass terms can't be added to the Lagrangian without breaking the symmetries of the SM. Therefore, a mechanism known as Electroweak Symmetry Breaking (EWSB) was developed to break the $\mathrm{U}(1) \times \mathrm{SU}(2)$ symmetry of the SM into the electromagnetic and weak interactions, thus providing also masses to the $W^{\pm}$ and Z bosons through an interaction with a new scalar field under $\mathrm{U}(1) \times \mathrm{SU}(2)$. This new field would also generate masses for the fermions through Yukawa interactions, making the SM fully compatible with the experimental observations. Finally, the excitation of this scalar field predicted a new 0-spin particle, now known as the Higgs boson. In this sense, the search for the Higgs boson

and the study of its properties have become a major focus of all particle accelerators.

Since the SM was first postulated, a path of experimental confirmation has been pursued and the observation of all the predicted particles was the main purpose of many experiments. This journey culminated in the discovery of the Higgs boson, which was first observed in 2012 by ATLAS and CMS experiments at CERN [3–5]. Furthermore, over the last years, and especially since the measurement of the Higgs, discoveries have made the way for a high luminosity era, and thus particle physics has progressively become a precision science [6–9].

While new physics may be measured through the direct observation of notorious peaks on kinematical distributions, searching for small deviations from some SM observables might also be a suitable way, especially if Beyond the Standard Model (BSM) physics is above the energy scale of the experiment. On the other hand, despite its overall success, the SM is known to be incomplete, mainly due to the existence of some unresolved issues, such as the existence of Dark Matter or the Naturalness problem, among others. In this sense, many BSM theories were postulated in order to address some of these issues, but so far, there has been a remarkable agreement between the SM and the experiments at the Large Hadron Collider (LHC) at CERN. This is why new physics is considered to arise at higher energies, above the TeV scale and thus, the discovery of BSM physics is likely to hide in precision experiments.

In this context, the impressive high precision experiments at the LHC, which are reaching the percent scale, demanded a theoretical upgrade to match the accuracy achieved.

Broadly speaking, the standard procedure to obtain theoretical predictions in Quantum Field Theories (QFT) is to perform a perturbative expansion in powers of the coupling constant. In the case of the LHC, given that the experiments are initiated by hadron collisions, this perturbative procedure, which is carried out at the partonic level, has to be combined with the non-perturbative contribution of the parton distribution functions in order to get complete reliable predictions for full hadronic processes.

In this sense, the way to systematically enhance the precision of a calculation is not lineal, and requires getting the relevant contributions within the perturbative expansion in powers of the coupling constants. In the case of the LHC and, in order to reach the percent level, partonic cross sections have to be calculated at least at Next to Next to Leading Order (NNLO) for most of the observables. This means being able to obtain the series in the strong coupling up to $\mathcal{O}(\alpha_s^2)$. Additionally, ElectroWeak (EW) corrections may also become necessary, given that $\alpha_s^2 \sim \alpha$. In fact, for many observables the EW corrections happen to exceed the few

percent level (e.g. [10, 11]).

From all the experiments at the LHC, the inclusive lepton pair production (Drell Yan process [12]) gathers some important properties that make it work as an important testground of perturbative Quantum Chromodynamics (QCD). On the one hand, it offers a sensitive way to study parton distribution functions (PDFs) [13–15]. From weak bosons production, charge asymmetry measurements and invariant mass dependencies have also helped to extract precise information on both the quarks valence structure functions and the separation of quarks flavours, as well. On the other hand, knowing the behavior of charged-current (CC) and neutral-current (NC) processes has allowed to perform high-precision measurements of fundamental Electroweak parameters, like Z and W widths and masses and the EW mixing angle. With W and Z bosons in final or intermediate states of hadronic processes, some clean production channels can be characterized with great levels of precision by studying leptonic decay modes. This has also served to accurately calibrate detector components, which was important for further measurements [16].

In addition, the Drell-Yan process is not only relevant to test SM predictions, but also to evaluate alternative BSM theories, where W and Z bosons usually appear as final or intermediate states in the decay of particles predicted in new physics models, like new gauge interactions, supersymmetry or heavy resonances [17]. For these reasons, the study of Drell Yan processes and, in general, theoretical and experimental explorations of multiple EW gauge boson productions, becomes a priority in the development of current high-energy physics. Advancements in our understanding of Drell Yan mechanism will have deep implications for our knowledge of fundamental interactions and the search for new physics.

In terms of accuracy, the Drell Yan mechanism also constitutes a clear example of the statements of a precision observable. The experimental precision is at the percent level at the LHC for the total cross section, and the differential distributions are also measured at an impressively high accuracy. On the theoretical side, the perturbative QCD corrections have been computed at next-to-leading order (NLO) in Ref. [18], at NNLO for the inclusive cross section in Refs. [19–21] and considering differential distributions in Refs. [22–28]. In addition, $\mathrm{N^3LL}$ results in association with the $\mathrm{N^3LO}$ have been also presented in Refs. [29–31]. Recently, the $\mathrm{N^3LO}$ QCD corrections have been obtained for the inclusive cross section of the production of a lepton pair via virtual photon exchange [32], and for the production of on-shell massive vector bosons as well [33–35]. Furthermore, $\mathrm{N^3LO}$ QCD corrections for the

Drell Yan mechanism have been presented at the differential level, for certain kinematical distributions [36–38].

However, computing several terms in the α_s expansion is not enough to reach the ultimate accuracy goal, since EW corrections, i.e. $\mathcal{O}(\alpha^n)$, are also expected to be important contributions.

In this sense, and considering that the improvement in statistics over the last years has made higher-order corrections experimentally noticeable, having access to QCD (and QED) corrections to these processes has become of great importance to put the previous predictions on a firmer ground. For instance, it is important to achieve a better comprehension of the so-called Sudakov regime, where large logarithmic EW factors play an important role, and of the order $\mathcal{O}(\alpha_s\alpha)$, that represent the first QCD corrections to these large EW factors, or even $\mathcal{O}(\alpha^2)$ corrections.

Furthermore, recent work has been performed to include QED effects in the evolution of parton distributions, by providing explicit expressions for splitting kernels up to $\mathcal{O}(\alpha_s\alpha)$ [39] and $\mathcal{O}(\alpha^2)$ [40] and by the determination of precise photon distributions in the proton within the LUXqed approach [41, 42] . The availability of these QED corrected parton distributions is essential to match the theoretical calculations at the partonic level.

From the point of view of partonic cross-sections, the $\mathcal{O}(\alpha_s\alpha)$ and $\mathcal{O}(\alpha)$ corrections represent the first EW and mixed order contributions to Drell-Yan pair production in the general expansion

$$d\sigma = \sum_{i,j} \alpha_s^i \alpha^j d\sigma^{(i,j)}, \tag{1.0.1}$$

where pure EW $d\sigma^{(0,j)}$ and QCD $d\sigma^{(i,0)}$ corrections, as well as *mixed order* contributions, which combine effects of the two interactions, arise.

In the case of the EW contributions, exclusive computations for NLO-EW corrections to CC-DY are available in Refs. [43–45] and for NC-DY, in Refs. [46, 47]. Finally, progress towards the computation of NNLO-EW has been accomplished in recent years too [48–51]. On the other hand, for the case of the QCD-EW corrections, mixed contributions have been presented for NC-DY and CC-DY in Refs. [52–58].

Additionally, due to the previous lack of full calculations of the NNLO mixed-order terms $\mathcal{O}(\alpha_s\alpha)$, different approaches have also been followed to approximately combine the QCD and QED/EW corrections [59–63], by either assuming the full factorization or the additive

combination of the strong and electroweak contributions. Particularly, partial exclusive results have been presented for the resonance region, by using the pole approximation [64–66]. Technically speaking, these corrections represent the first term in the fixed order expansion that takes into account, at the same time, *mixed* effects from the strong and electroweak interactions. The computation of the mixed QCD⊗QED $\mathcal{O}(\alpha_s\alpha)$ corrections to the inclusive on-shell production of a Z boson in hadronic collisions, and the later characterization of all the differential distributions in various kinematical regimes, together with the extension of the theoretical methods in order to take into account both strong and EW interactions, are the main goals of this Thesis.

This work is organized as follows: in Chapter 2 we review the formulation of the Standard Model and the formalism of perturbative QCD, the assumptions in the partonic model, which allow us to achieve general formulations and handle the calculation of hadronic cross sections, the main observable to access through the LHC experiments. Furthermore, we review the main available methods to obtain the higher order corrections within the perturbation theory. In Chapter 3 we will address the complete set of Next to Next to Leading Order contributions (i.e. all the terms that correspond to $i + j \leq 2$ in Eq. (1.0.1)) to the inclusive production of a Z boson in hadronic collisions. In order to obtain these contributions, we will develop a suitable *abelianisation* procedure to handle the non-abelian QCD results and construct the mixed order and the pure EW terms, which are presented in the appendices. After this, in Chapter 4 we will discuss the NNLO mixed QCD⊗QED initial state corrections to the Drell Yan mechanism, and study their relevance in a number of observables at a fully exclusive level. Furthermore, aiming to achieve these results, we extend the FKS and q_T-subtraction formalisms, originally developed to address pure QCD corrections, in order to apply them to the calculation of QCD⊗QED mixed contributions. Our results are of value for transverse-momentum resummation at the corresponding logarithmic accuracy. Finally, our conclusions are presented in Chapter 5.

CHAPTER 2

Precision Physics

During the second half of the 20th century, and after the successful generalization of electrodynamics as a quantum-relativistic theory, a new and someway similar theory was developed in order to explain the strong interactions. In this chapter we will review some of the concepts of these two theories, especially focusing on the facts that make it possible to perform perturbative expansions in powers of the coupling constants. We will emphasize on the factorization properties of the amplitudes in the soft and collinear limits, and refer to hadronic collisions through short and long range factorizations within the naive parton model. We will discuss the evolution of the parton distribution functions and comment on the running of the coupling constants. Finally, we will make use of all these ingredients to review the method developed by Frixione, Kunszt and Signer in Ref. [67] (the so called FKS-subtraction, useful to calculate Next to Leading Order QCD corrections), so that we can apply it to the calculation of the mixed QCD$\otimes$QED contributions to Drell Yan.

2.1 SM Lagrangian and Perturbation Theory

In order to explain the dynamics of the elementary particles, the Standard Model Lagrangian includes several terms that describe the behavior of the quantum fields and their interactions. In this sense, there is a term devoted to the electroweak (EW) theory, and a strong (QCD) term that characterizes the color interactions between quarks and gluons. Both EW and QCD are gauge theories, based on local symmetries, which play a crucial role in determining the

main interactions and properties of the SM particles and therefore, also the observables.

2.1.1 Electroweak Theory

On the one hand, the electroweak theory unifies the electromagnetic and weak interactions, and the Lagrangian of this sector reads:

$$\mathcal{L}_{\text{EW}} = -\frac{1}{4}B_{\mu\nu}B^{\mu\nu} - \frac{1}{4}W^i_{\mu\nu}W^{i\mu\nu} + \mathcal{L}_F \tag{2.1.1}$$

Here, the first two terms involve the field strength tensors, $B_{\mu\nu}$ and $W^i_{\mu\nu}$ ($i = 1, 2, 3$), which represent the electromagnetic and weak gauge fields, respectively. These gauge fields interact with the fundamental particles and actually carry the forces associated with the electromagnetic and weak interactions. The third term represents the EW Lagrangian for the fermions ψ_f, which after the Electroweak Symmetry Breaking (EWSB), is (see Chapter 10 in Ref. [1] for more details) can be expressed as

$$\begin{aligned}\mathcal{L}_F = &\sum_f \overline{\psi}_f \left(i\not{\partial} - \frac{m_f H}{v}\right)\psi_f \\ &- \frac{g}{2\sqrt{2}}\sum_f \overline{\psi}_f\gamma^\mu\left(1-\gamma^5\right)\left(T^+W^+_\mu + T^-W^-_\mu\right)\psi_f \\ &- e\sum_f Q_i\overline{\psi}_f\gamma^\mu\psi_f A_\mu - \frac{g}{2\cos\theta_W}\sum_f \overline{\psi}_f\gamma^\mu(g^i_V - g^i_A\gamma^5)\psi_f Z_\mu.\end{aligned} \tag{2.1.2}$$

Here, $\theta_W = \tan^{-1}(g'/g)$ is the mixing angle, with g and g' the coupling constants associated with the SU(2) and U(1) gauge symmetries, respectively. On the other hand, $e = g\,\sin\,\theta_W$ is the absolute value of the electron charge, such that the fine-structure constant is defined as $\alpha \equiv e^2/4\pi$. Furthermore,

$$\begin{aligned}A_\mu &= B_\mu\,\cos\,\theta_W + W^3_\mu\,\sin\,\theta_W \\ W^\pm_\mu &= \frac{W^1_\mu \mp iW^2_\mu}{\sqrt{2}} \\ Z_\mu &= -B_\mu\,\sin\,\theta_W + W^3_\mu\,\cos\,\theta_W\end{aligned} \tag{2.1.3}$$

are the photon field (γ) and the charged ($W^\pm$) and neutral (Z) weak boson fields, respectively. The Yukawa coupling of H to ψ_f in the first term in $\mathcal{L}_F$ is $gm_f/2M_W$. The second term in $\mathcal{L}_F$ represents the charged-current weak interaction, where T^+ and T^- are the customary raising and lowering operators. The third term in $\mathcal{L}_F$ describes electromagnetic interactions

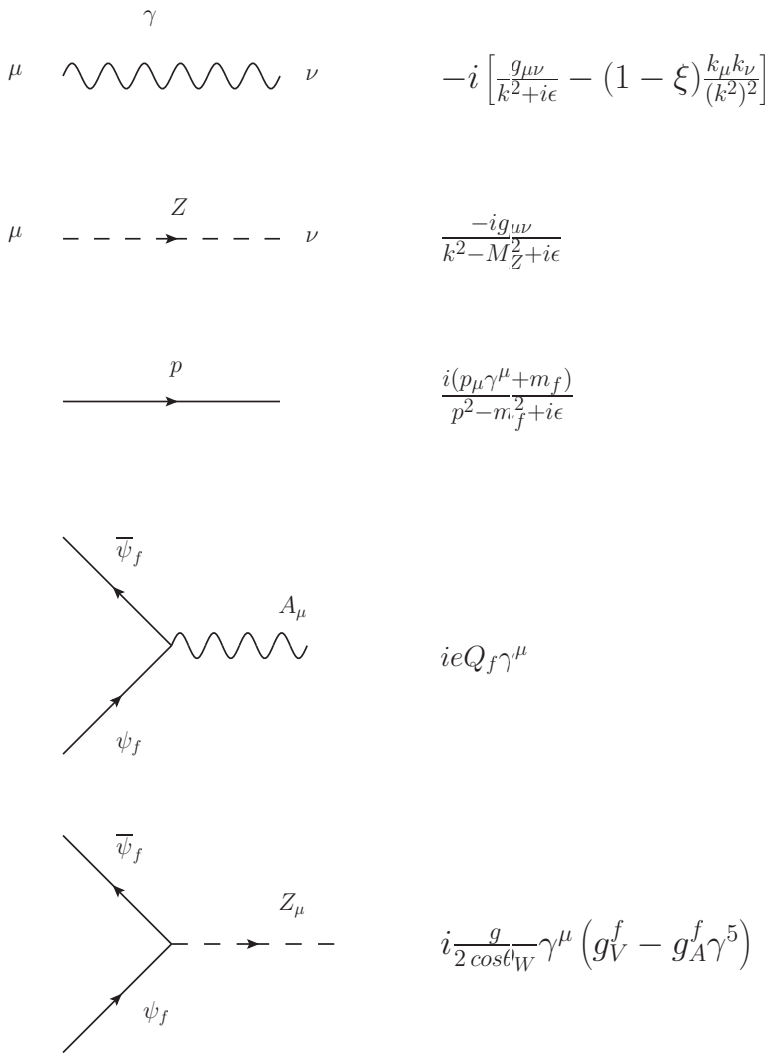

Figure 2.1: Some of the Feynman Rules for the EW sector of the Standard Model, specifically concerning γ and Z bosons and their interaction vertices $\overline{f}f\gamma$ and $\overline{f}fZ$ with fermions. These rules are obtained from the EW piece of the Lagrangian in Eq. (2.1.2).

(QED) [68, 69] and the last is the weak neutral-current interaction [70–72]. Within this last term, the vector and axial-vector couplings are

$$\begin{aligned} g_V^f &= t_{3L}(f) - 2Q_i \sin^2\theta_W \\ g_A^f &= t_{3L}(f) \end{aligned} \tag{2.1.4}$$

where $t_{3L}(f)$ is the weak isospin of fermion f ($+1/2$ for u_i and ν_i, and $-1/2$ for d_i and e_i) and Q_f is the charge of ψ_f in units of e.

Within the electroweak sector 2.1.1, we can identify the quantum electrodynamics (QED) part, which specifically describes the electromagnetic interactions. This is by itself an abelian

gauge theory that can be obtained after imposing a local U(1) symmetry to the Lagrangian, where the photon emerges as a massless spin 1 gauge field that assures the conservation of the electric current. According to QED, all spin-$1/2$ charged particles interact through the electromagnetic field, with a strength proportional to the fine-structure constant α[1].

By isolating the electromagnetic field and its interaction with charged particles, we obtain the QED Lagrangian:

$$\mathcal{L}_{\text{QED}} = -\frac{1}{4}F_{\mu\nu}F^{\mu\nu} + \sum_f \overline{\psi}_f \left(i\gamma^\mu D_\mu - m_f\right)\psi_f \tag{2.1.5}$$

where γ_μ are the Dirac matrices and $F_{\mu\nu}$ represents the electromagnetic field strength tensor, given by

$$F_{\mu\nu} = \partial_\mu A_\nu - \partial_\nu A_\mu \tag{2.1.6}$$

and A_μ is the electromagnetic four-potential of Eq. (2.1.3). On the other hand, D_μ is the covariant derivative, which includes the electromagnetic interaction. It is given by

$$D_\mu = \partial_\mu - ieA\mu \tag{2.1.7}$$

with $-e$ the electron charge. Finally, the sum over f in Eq. (2.1.5) includes all the charged fermions, denoted by ψ_f, with masses m_f. In figure 2.1 we can see the Feynman rules for some of the electroweak interactions addressed in this work, according to the Lagrangian of Eq. (2.1.2).

2.1.2 Quantum Chromodynamics

On the other hand, Quantum Chromodynamics (QCD) is the other fundamental pillar of the SM. In fact, this is a non abelian field theory dedicated to describe the strong interactions between quarks and gluons. Unlike QED, isolated colored particles have never been seen, but only inside hadrons, which are complex states mainly formed by a collection of quarks and gluons, among other fields. This is why the strong interaction has to be explored in hadron collisions, like those that take place in the LHC.

The Lagrangian of the QCD sector reads

[1] At the scale of the W boson mass, $\alpha(\text{M}_W^2) \simeq 1/128 \simeq 0.008$.

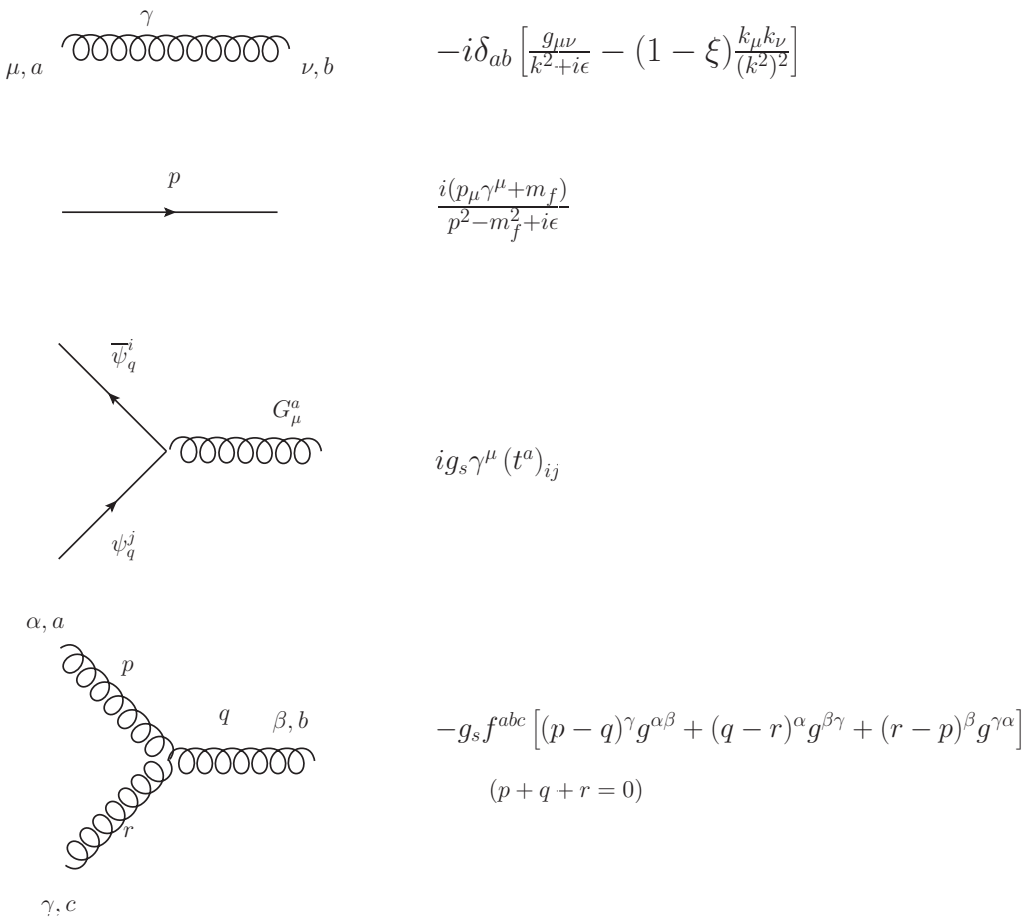

Figure 2.2: Some of the Feynman Rules for QCD, important to the development of this thesis. The ggg and $\overline{q}qg$ vertices were obtained from the strong piece of the SM Lagrangian in Eq. (2.1.8).

$$\mathcal{L}_{QCD} = -\frac{1}{4}G^a_{\mu\nu}G^{a\mu\nu} + \sum_q \overline{\psi}_q\left(i\gamma^\mu D_\mu - m_q\right)\psi_q. \tag{2.1.8}$$

Here, the first term represents the field strength tensor for the gluon field, denoted by

$$G^a_{\mu\nu} = \partial_\mu G^a_\nu - \partial_\nu G^a_\mu + g_S f^{abc}G^b_\mu G^c_\nu, \tag{2.1.9}$$

where a is the color index, and f^{abc} the structure constants of SU(3). The gluon fields G^a_μ are the gauge bosons associated with the strong force[2]. On the other hand, the second term in Eq. (2.1.8) involves the quarks with mass m_q, denoted by ψ_q, which are the fundamental spin $1/2$ particles that experience the strong force. Additionally, this term encodes the interactions

[2]Note that this definition implies, contrary to that of the electromagnetic strength tensor in Eq. (2.1.6), that the term $G^a_{\mu\nu}G^{a\mu\nu}$ involves interactions between the gauge bosons through 3 and 4-gluon vertices, with strengths $\sim g_S$ and $\sim g_S^2$, respectively.

between quarks and gluons through the covariant derivative for the QCD sector, which is given by

$$D_\mu = \partial_\mu - ig_S t^a G^a_\mu. \tag{2.1.10}$$

Here, λ_a are the Gell-Mann matrices, the generators of the SU(3) color group, with the relation $t^a = \frac{\lambda^a}{2}$, and g_S is the strong coupling constant, such that $\alpha_s = g_S^2/4\pi$. In figure 2.2 we can see the Feynman rules for some of the QCD interactions to be addressed in this thesis. These are obtained by means of the QCD lagrangian in Eq. (2.1.8).

Here, by comparing the second terms of Eqs. (2.1.5) and (2.1.8), together with the definition of the covariant derivatives (2.1.7) and (2.1.10), we see how similar the structures are for the fermion-fermion-boson vertices in each case. It is clear that, apart from the couplings and the color factors, the abelian parts of the interactions have the same shape, for both QCD and QED theories[3].

2.2 Radiative Corrections

On the theoretical side, the way to obtain reliable predictions of the SM observables, such as cross sections or decay rates with acceptable levels of precision and accuracy, is to perform perturbative expansions in terms of the coupling constants. In hadron collisions (see section 2.3), the largest contributions usually come from the interaction of two colored partons, which are proportional to $\alpha_s = g_s^2/(4\pi)$ and constitute the first and simplest term, i.e. the Leading Order (LO) in the perturbative series.

In general, the way to systematically enhance the precision of a calculation is to get higher order terms in the perturbative expansion. For example, given the generic process of two incoming partons, each with momenta k_1 and k_2, as the one shown in figure 2.3, this expansion can be written as

$$\sigma(k_1, k_2; \{p_n\}; \alpha_s, \alpha) = \alpha_s^k \alpha^\ell \sum_{i,j=0} \alpha_s^i \alpha^j \sigma^{(i,j)}(k_1, k_2, ; \{p_i\}), \tag{2.2.1}$$

where the powers k and ℓ characterize the order of the first non-vanishing term of the

[3]Here, and all along this thesis, by *abelian* we mean all the terms and contributions that don't involve the structure constants f^{abc}. In fact, they constitute exactly the commutator of the group generators (λ_a for SU(3) in this case), and thus they encode all the non-abelian effects that may arise within the interaction.

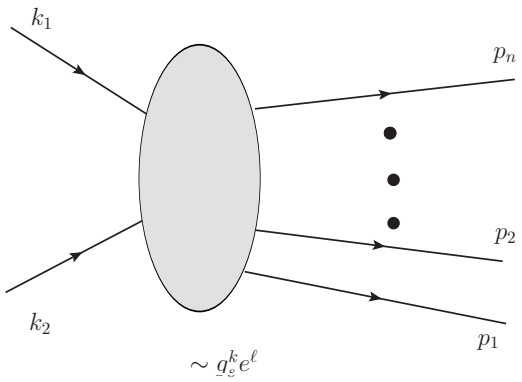

Figure 2.3: Feynman diagram corresponding to the generic scattering of two incoming partons with momenta k_1 and k_2 at Leading Order.

series and $\{p_i\}$ the momenta of the final state particles. In addition, the terms of the form $\sigma^{(i,0)}$ symbolize pure QCD corrections, usually denoted as NLO (Next to Leading Order), NNLO (Next to Next to Leading Order) and so on. On the other hand, the terms $\sigma^{(0,j)}$ are the EW corrections and finally, $\sigma^{(i,j)}|_{i,j\neq 0}$ are the so called mixed order corrections, which include combined effects of both the electroweak and the strong interactions. If α and α_s are small, then the first estimated value for the cross section is given by

$$\alpha_s^k \alpha^\ell \sigma^{(0,0)}(k_1, k_2; \{p_i\}) = \int_n d\sigma^B \tag{2.2.2}$$

where the Born cross section $d\sigma^B$ is given by the integration of the absolute squared value of the matrix element $\mathcal{M}_n^{(0,0)}(\{p_i\})$ over the phase space $d\phi_n$, times a measurement function $\mathcal{S}$ and a flux factor:

$$d\sigma^B = \frac{d\phi_n}{2(k_1+k_2)^2} \mid \mathcal{M}_n^{(0,0)}(\{p_i\}) \mid^2 \mathcal{S}(\{p_i\}), \tag{2.2.3}$$

$$d\phi_n = (2\pi)^4 \delta^4 \left(k_1 + k_2 - \sum_{i=1}^{n} p_i \right) \prod_{i=1}^{n} \frac{d^4 p_i}{(2\pi)^3} \delta_+(p_i^2). \tag{2.2.4}$$

In this equation, $\mathcal{M}^{(0,0)}$ is computed following the Feynman Rules, while the measurement function $\mathcal{S}$ accurately specifies the observable to be calculated. Interesting values for $\mathcal{S}$ are $\mathcal{S} = 1$ along all the integration region, that corresponds to the inclusive cross-section, and $\mathcal{S} = \delta(\phi_n - \phi_{n,0})$ which indicates the fully differential cross section in the phase-space point $\phi_{n,0}$.

Moreover, in order to achieve a higher precision, some of the following orders (in the sense of Eq. (2.2.1)) might be required. While Leading Order calculations are thus taken into account, Next to Leading Order contributions involve the computation of two different terms (see figure 2.4). On the one hand, there are corrections due to the real emission of an extra particle, which imply one more parton in the final state. On the other hand, virtual corrections, which have the same final state as the born cross section, must also be considered. For the sake of simplicity and without loosing generality, from now on throughout this chapter we will focus exclusively on pure QCD corrections to illustrate the calculation of NLO contributions. This means that the second index, according to Eq. (2.2.1), will take a constant 0 value and will be understood, in the following equations. These pure QCD contributions constitute by themselves gauge-invariant corrections to the relevant observables and their structure is in general analogous to that of the other interactions at this order. Furthermore, given the dominant value of g_S they are, for most of the processes in the LHC, the main contributions to take into account[4]. Specifically, regarding the NLO QCD corrections from the real and virtual sides, we have

$$\begin{aligned}\sigma^{NLO} &= \int_{n+1} d\sigma^R + \int_n d\sigma^V \\ &= \int_{n+1} \frac{d\phi_{n+1}}{2(k_1+k_2)^2} \mid \mathcal{M}^{(0)}_{n+1} \mid^2 \mathcal{S}_{n+1} \\ &+ \int_n \frac{d\phi_n}{2(k_1+k_2)^2} \left[\mathcal{M}^{(1)\dagger}_n \mathcal{M}^{(0)}_n + \mathcal{M}^{(0)\dagger}_n \mathcal{M}^{(1)}_n\right] \mathcal{S}_n. \end{aligned} \tag{2.2.5}$$

In order to tackle this calculation, some important limits must be considered. First of all, the virtual $\mathcal{M}^{(1)}_n$ amplitude might contain ultraviolet (UV) divergences originated from the unconstrained loop momenta p_ℓ in the limit $p_\ell \to \infty$ (see the virtual contribution in figure 2.4). On the other hand, infrared (IR) divergences are also present in the limit $p_\ell \to 0$ if the particle in the loop is massless (see the diagram in figure 2.4b). As the final results should be finite, these infinities have to be handled in order to obtain a reliable prediction for the NLO cross section.

In the case of UV divergences, one can absorb them by renormalizing the fields or the parameters in the theory, like the couplings or the masses, at the price of adding a depen-

[4]Later in this thesis, when it is needed, we will recover the EW notation by recalling the second index, in the sense of Eq. (2.2.1)

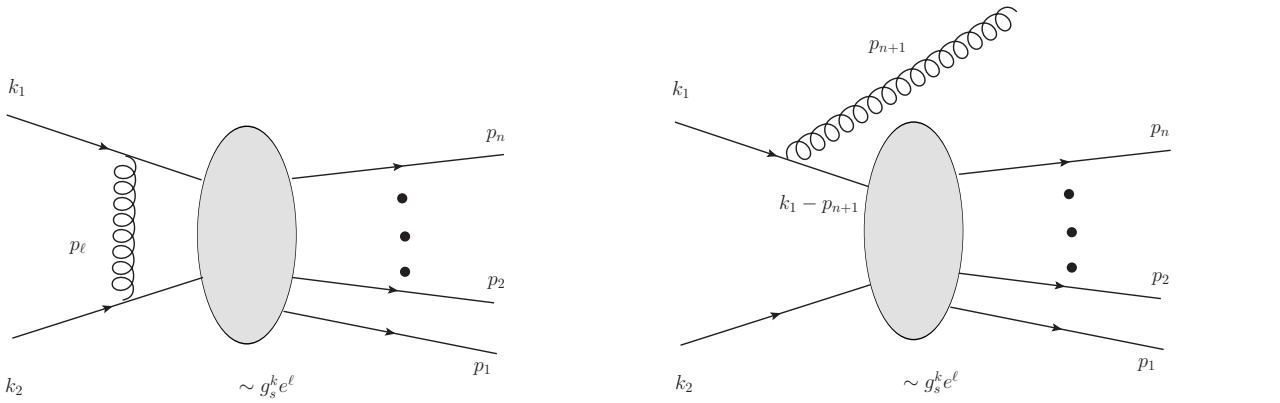

(a) Next to Leading Order correction due to a virtual gluon with momentum p_ℓ.

(b) Next to Leading Order correction due to the emission of a real gluon with momentum p_{n+1}.

Figure 2.4: Feynman diagrams corresponding to the generic scattering of two incoming partons with momenta k_1 and k_2 at Next to Leading Order.

dence on a so called renormalization scale μ_R (see section 2.2.3 for a deeper discussion on renormalization). On the other hand, IR singularities can be handled differently. It has been shown [73–75] that although some IR divergences may arise during the calculation of loop diagrams in partial transition probabilities, they always cancel when considering the total probability. In the case of Eq. (2.2.5), they cancel with those arising from the integration over the phase space of the real term $\int_{n+1} d\sigma^R$. In this integration, the singular behavior happens to be associated with the momentum of the extra massless particle whenever it becomes soft or collinear (for instance, $p_{n+1} \to 0$ in figure 2.4).

To illustrate, if we had an extra gluon emitted from one of the initial legs with momentum p_{n+1}, as we can see in figure 2.4b, the propagator of the virtual particle reads

$$\frac{1}{(k_1 - p_{n+1})^2 - m^2} = \frac{-1}{2k_1.p_{n+1}} = \frac{1}{2 \mid \mathbf{k}_1 \mid\mid \mathbf{p}_{n+1} \mid (\cos\theta - \sqrt{1 + m^2/ \mid \mathbf{k}_1 \mid^2})} \tag{2.2.6}$$

where m is the mass of the incoming particle with momentum k_1, such that $k_1^2 = m^2$, and θ is the angle between the 3-momenta $\mathbf{k}_1$ and $\mathbf{p}_{n+1}$. As can be seen, there are 2 regions where this propagator becomes singular. From one side, $\mid \mathbf{p}_{n+1} \mid \to 0$ leads to a divergence, associated with the soft limit $p^0_{n+1} \to 0$, where the emitted gluon has vanishing energy. From the other, the limit $\theta \to 0$ can also lead to a singular region, whenever the initial leg is massless, i.e. $m = 0$. This is the collinear limit, in which the gluon is emitted in the same direction than the initial state parton.

To be able to compute a reliable observable, we need to handle these divergent contributions to obtain an infrared-safe quantity. This means that the Next-to-Leading-Order corrections to the observable must truly approach the expression for the previous order in the unresolved regions. In order to achieve this, we have to understand each singular behavior and either absorb or cancel all the singular terms with other parts of the calculation.

2.2.1 Soft Limit

In the case of the soft limit, we consider a gluon of momentum p_{n+1} and color a, such as the one emitted from the initial leg in figure 2.4b, in the limit $p_{n+1} \to 0$. In this region, we can nearly factorize the amplitude into a divergent piece that depends on the energy and angle of the emitted gluon, and a second piece which is precisely the amplitude omitting that gluon. The reason why the factorization is not exact is originated in the color correlations. The emission of a soft gluon does not affect the momenta and spins of the radiating hard partons, but it always carries away color charge, no matter how soft the gluon is.

In order to address the behavior of the amplitude in this limit, let us first consider the case in which the emitting particle is an external final state quark[5] of momentum p_i and color $c_i = 1, ..N_C$ (see figure 2.5a). We simultaneously regularize ultraviolet and infrared singularities by using dimensional regularization. This involves the analytic continuation of loop momenta to $d = 4 - 2\epsilon$ space-time dimensions and the introduction of a scale μ, such that $g_s \to g_s \mu^\epsilon$. In this case we can write the amplitude for the process $\mathcal{M}_{n+1}$, involving the soft gluon and other n external partons of momenta $\{p_1, ..., p_n\}$ and colors $\{c1, ..., c_n\}$ as [6]

$$\mathcal{M}_{n+1}^{(c1,...,c_n;a)}(p_1, ..., p_n; p_{n+1}) = g_s \mu^\epsilon \bar{u}(p_i) \, (t^a)_{c_i \beta} \, \epsilon_\mu(p_{n+1}) \gamma^\mu \frac{\not{p}_i + \not{p}_{n+1}}{(p_i + p_{n+1})^2} \tilde{\mathcal{M}}_n^\beta, \tag{2.2.7}$$

where $\bar{u}$ is the Dirac spinor of quark i, $t^a = \lambda^a/2$ is the $a^{\text{th.}}$ Gell-Mann matrix, $\epsilon(p_{n+1})$ is the polarization vector of the emitted gluon, γ^μ are the Dirac matrices in four-vector notation and $\not{p} = p_\mu \gamma^\mu$. Finally, $\tilde{\mathcal{M}}_n^\beta$ is the n-particle matrix element with an off-shell quark i, such that $\mathcal{M}_n^\beta = \bar{u}(p_i)\tilde{\mathcal{M}}_n^\beta$.

We can easily see that in the limit $p_{n+1} \to 0$, where the momentum of the gluon becomes soft, the amplitude $\mathcal{M}$ of Eq. (2.2.7) takes the form

[5] It is important to note that if the emitting particle was an internal off-shell parton, then the amplitude would not be singular in the soft limit.

[6] This formalism also works with an extra arbitrary number of external particles with no color (photons, leptons, Higgs or vector bosons, among others).

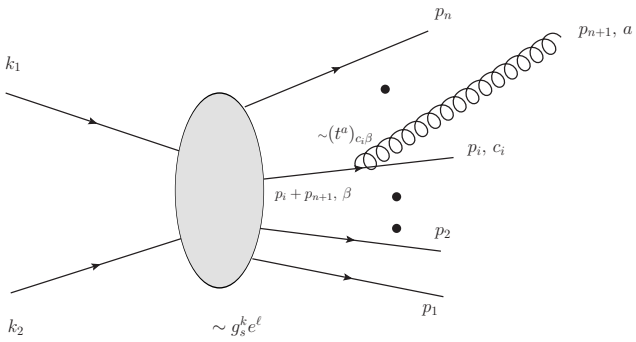

(a) Soft gluon emission from an external final state quark with momentum p_i and color c_i.

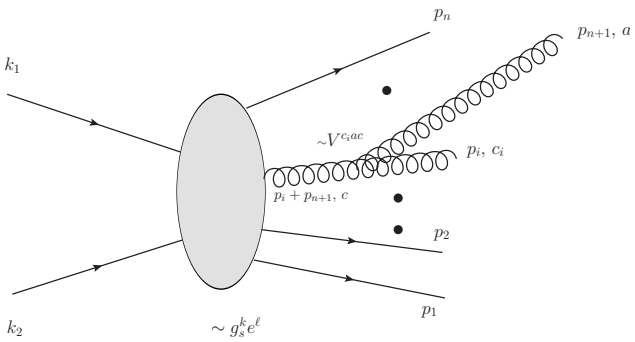

(b) Soft gluon emission from an external final state gluon with momentum p_i and color c_i.

Figure 2.5: Diagrams used to illustrate the emission of a soft gluon in a generic scattering process.

$$\begin{aligned}\mathcal{M}_{n+1}^{(c1,\ldots,c_n;a)}(p_1,\ldots,p_n;p_{n+1}) &\simeq g_s\mu^\epsilon \bar{u}(p_i)\,(t^a)_{c_i\beta}\,\epsilon_\mu(p_{n+1})\gamma^\mu \frac{\not{p}_i}{2\,p_i\cdot p_{n+1}}\tilde{\mathcal{M}}_n^\beta \\ &= g_s\mu^\epsilon\,\epsilon(p_{n+1})\left[\frac{p_i^\mu}{p_i\cdot p_{n+1}}\right](t^a)_{c_i\beta}\mathcal{M}_n^\beta.\end{aligned} \tag{2.2.8}$$

In the last line, we have used the anticommutation identities for the gamma matrices $\{\gamma^\mu,\gamma^\nu\}=2\eta^{\mu\nu}$ and the Dirac equation for massless quarks: $\bar{u}(p_i)\not{p}_i=0$. Likewise, with a little extra work we can see that this factorization, which we achieved in Eq. (2.2.8) for the emission of a soft gluon from a an external final state quark leg, is also valid for an initial antiquark leg, and even more, with the corresponding replacement $(t^a)_{c_i\beta}\to(\bar{t}^a)_{c_i\beta}=-(t^a)_{\beta c_i}$, for emissions from final state anti-quarks and initial quark legs, respectively.

On the other hand, let us consider the different case of the soft gluon radiation generated from a gluon line i of color $c_i=1,\ldots N_C^2-1$ (see figure 2.5b). In this case, the amplitude becomes

$$\mathcal{M}_{n+1}^{(c1,\ldots,c_n;a)}(p_1,\ldots,p_n;p_{n+1}) = \mu^\epsilon\epsilon^\mu(p_{n+1})\epsilon^\lambda(p_i)\,V_{\mu\nu\lambda}^{c_i ac}(-p_i,-p_{n+1},p_i+p_{n+1})\,D_\beta^\nu(p_i+p_{n+1})\,\tilde{\mathcal{M}}_n^{c,\beta}, \tag{2.2.9}$$

where $D_\beta^\nu(p_i+p_{n+1})$ is the gluon propagator, which can be expressed in a physical gauge, i.e. removing the unphysical polarizations and the ghosts, and taking the arbitrary n^μ vector to be orthogonal to the gluon polarization vector $\epsilon^\mu(p_i)$, such that $n.\epsilon(p_i)=0$. On the other hand, $V_{\mu\nu\lambda}^{abc}(p,q,r)$ is the triple gluon vertex (see figure 2.2), depending of the QCD structure constants f^{abc} for p, q and r ($p+q+r=0$)

$$
\begin{aligned}
V^{\alpha\beta\gamma}_{abc}(p,q,r) &= -g_s f^{abc}\left[(p-q)^\gamma g^{\alpha\beta} + (q-r)^\alpha g^{\beta\gamma} + (r-p)^\beta g^{\gamma\alpha}\right] \\
V^{abc}_{\mu\nu\lambda}(-p_i,-p_{n+1},p_i+p_{n+1}) &= -g_s f^{abc}\left[(p_{n+1}-p_i)_\nu\, g_{\mu\lambda} + (-p_i-2p_{n+1})_\lambda\, g_{\mu\nu}\right. \\
&\quad \left. +(2p_i+p_{n+1})_\mu\, g_{\nu\lambda}\right].
\end{aligned}
\tag{2.2.10}
$$

Finally, $\tilde{\mathcal{M}}^\beta_n$ is the n-particle matrix element with an off-shell gluon i, such that $\mathcal{M}^c_n = \epsilon_\sigma(p_i)\tilde{\mathcal{M}}^{c,\sigma}_n$.

It is easy to see that, in the limit $p_{n+1} \to 0$, the amplitude of Eq. (2.2.9) behaves as

$$
\begin{aligned}
\mathcal{M}^{(c1,\ldots,c_n;a)}_{n+1}(p_1,\ldots,p_n;p_{n+1}) &\simeq -g_s\mu^\epsilon \epsilon^\mu(p_{n+1})\epsilon^\lambda(p_i)\, f^{c_i ac}\left[(-p_i)_\nu\, g_{\mu\lambda} + (-p_i)_\lambda\, g_{\mu\nu} + (2p_i)_\mu\, g_{\nu\lambda}\right] \times \\
&\quad \times \frac{-i}{(p_i+p_{n+1})^2+i\epsilon}\left[g^\nu_\beta - \frac{n^\nu\, p_{i\beta} + p_i^\nu\, n_\beta}{n\cdot(p_i+p_{n+1})}\right]\tilde{\mathcal{M}}^{c,\beta}_n \\
&= g_s\mu^\epsilon \epsilon_\mu(p_{n+1})\left[\frac{{p_i}^\mu}{p_i\cdot p_{n+1}}\right](if^{c_i ac})\,\mathcal{M}^c_n.
\end{aligned}
\tag{2.2.11}
$$

As we can note by comparing Eqs. (2.2.8) and (2.2.11), the soft limit behaves just the same, with the exception of the color factors $(t^a)_{c_i\beta}$ and $(if^{c_i ac})$, which are related to the color index and the nature of the emitter. This general behavior, that has been addressed in Refs. [76–79] allows us to express the soft limit in a general shape, by defining the color charge operator $\mathbf{T}_i$ to describe the color correlations produced by a soft gluon of color a. In this sense:

$$
\mathbf{T}_i \equiv \langle a|T^a_i, \tag{2.2.12}
$$

where given $\{|c_1,\ldots,c_m\rangle\}$ a generic color basis of the interacting QCD partons, $\mathbf{T}_i$ acts as

$$
\langle a,c_1,\ldots,c_i,\ldots,c_m|\mathbf{T}_i|b_1,\ldots,b_i,\ldots,b_m\rangle = \delta_{c_1b_1}\ldots T^a_{c_ib_i}\ldots\delta_{c_mb_m}, \tag{2.2.13}
$$

where it is important to note that $T^a_{c_ib_i}$ has to take different values, depending on the particle that radiates the soft gluon. In this sense, $T^a_{cb} \equiv if^{abc}$ if the particle i is a gluon, $T^a_{cb} \equiv (t^a)_{bc}$ if the emitting particle is a final-state quark or an initial-state antiquark and $T^a_{cb} \equiv (-t^a)_{cb}$ if the emitting particle is an initial-state quark or a final-state antiquark.

With this definition, the algebra for the color-charge operator is:

$$T_i^a \, T_j^a \equiv \boldsymbol{T}_i \cdot \boldsymbol{T}_j = \boldsymbol{T}_j \cdot \boldsymbol{T}_i \quad \text{if} \;\; i \neq j; \qquad \boldsymbol{T}_i^2 = C_i, \tag{2.2.14}$$

where C_i is the Casimir operator, i.e. $C_i = C_A = N_c$ if i is a gluon and $C_i = C_F = (N_c^2 - 1)/2N_c$ if i is a quark or antiquark.

Note that, by definition, each vector $|\mathcal{M}(p_1, \ldots, p_m)\rangle$ is a color-singlet state. Therefore color conservation is simply

$$\sum_{i=1}^{m} \boldsymbol{T}_i \, |\mathcal{M}(p_1, \ldots, p_m)\rangle = 0 \, . \tag{2.2.15}$$

On the other hand, the dependence of the matrix element $\mathcal{M}$ on the color indices $c_1, ..., c_m$ is written as

$$\mathcal{M}_{c_1,...,c_m}(p_1, ..., p_m) \equiv \langle c_1, ..., c_m | \mathcal{M}(p_1, ..., p_m)\rangle, \tag{2.2.16}$$

where the ket $|\mathcal{M}(p_1, ..., p_m)\rangle$ is a vector in the m-parton color space.

Within this formalism, a generic soft limit for a gluon emission can be generally written following the factorization formula

$$\langle a | \mathcal{M}(q, p_1, ..., p_m)\rangle \simeq g_s \mu^{\epsilon} \epsilon^{\mu}(q) J_{\mu}^{a}(q) | \mathcal{M}(p_1, ..., p_m)\rangle \tag{2.2.17}$$

where q is the momentum of the soft gluon and $\mathcal{M}(p_1, ..., p_m)\rangle$ is the amplitude without the soft gluon. Finally, the factor $\mathbf{J}^{\mu}(q)$ is the tree level soft gluon current, that depends on the momentum q and on the momenta and color charges of the hard partons in the matrix element as well.

$$\mathbf{J}^{\mu}(q) = \sum_{i=1}^{m} \mathbf{T}_i \frac{p_i^{\mu}}{p_i . q}. \tag{2.2.18}$$

In the right hand side of Eq. (2.2.17), the "$\simeq$" means that all the contributions less singular than $1/q$ have been neglected in the limit $q \to 0$.

As a matter of fact, it is clear that the soft limit has some general important properties that may help to achieve a better understanding of the scattering amplitudes, and reach higher precision levels in the calculations. Here, given the similarity between the QED vertex and

the abelian piece of the strong interactions (see comments in section 2.1.2), and taking into account the aim of this work, which is to characterize the mixed corrections, it is important to comment that we could easily extend this expression (2.2.17) to also address the soft photon radiation, by making some simple replacements:

$$\begin{aligned} g_s &\to e\, q_i \\ T^a_{c_i b_i} &\to \delta_{c_i b_i}. \end{aligned} \tag{2.2.19}$$

Here, in the case of pure QED interactions, the soft radiation does not carry any color, and thus the a index makes no sense anymore. As a consequence, in this case the amplitude does exactly factorize in the soft limit.

Finally, in order to express the relations at the level of the squared amplitude $|\mathcal{M}|^2$, which is that of the differential cross section $d\sigma$, we can write

$$|\mathcal{M}(p_1, ...p_n; q)|^2 \simeq -2g_s^2\mu^{2\epsilon} \sum_{i,j=1} \mathbf{S}_{ij}(q)|\mathcal{M}_{(ij)}(p_1, ..., p_n)|^2 \tag{2.2.20}$$

where $\mathbf{S}_{ij}$ is the eikonal function and $\mathcal{M}_{(ij)}$ is the *color-correlated* amplitude:

$$\begin{aligned} \mathbf{S}_{ij}(q) &= \frac{p_i.p_j}{2(p_i.q)(p_j.q)}, \\ |\mathcal{M}_{(ij)}(p_1, ..., p_n)|^2 &= \langle \mathcal{M}(p_1, ..., p_n)|\mathbf{T}_i\mathbf{T}_j|\mathcal{M}(p_1, ..., p_n)\rangle. \end{aligned} \tag{2.2.21}$$

2.2.2 Collinear Limit

On the other hand, as we commented in section 2.2, the case in which two (or more) particles become collinear also leads to a divergent behavior in the amplitude. This phenomenon has been studied in detail in Ref. [80], and higher order contributions to this behavior have been addressed in Refs. [81–87].

In order to show the collinear limit in a suitable way to perform NLO calculations, we will consider the $(n+1)$-particle tree level amplitude

$$\mathcal{M}_{n+1}^{c_1,...,c_m;c_a,...;s_1,...,s_m;s_a,...}(p_1, ..., p_m; p_a, ...) \tag{2.2.22}$$

and the associated vector in the color + helicity space

$$|1, ..., m; a, ...\rangle_{n+1} \tag{2.2.23}$$

in the sense of reference [79], where indices $1, .., m$ indicate final state QCD partons, and $a, ..$ indicate partons in the initial state. Additionally, we parametrize the momenta p_i and p_j of the partons i and j as

$$\begin{aligned} p_i^\mu &= zp^\mu + k_\perp - \frac{k_\perp^2}{z}\frac{n^\mu}{2pn} \\ p_j^\mu &= (1-z)p^\mu - k_\perp^\mu - \frac{k_\perp^2}{1-z}\frac{n^\mu}{2pn} \end{aligned} \tag{2.2.24}$$

where p^μ is a light-like vector that represents the collinear direction and n^μ is another light-like direction to determine how we approach the collinear limit. Thus, $k_\perp$ is a vector perpendicular to p^μ and n^μ, such that

$$2p_i.p_j = -\frac{k_\perp^2}{z(1-z)}\,, \tag{2.2.25}$$

and the collinear limit corresponds to $k_\perp \to 0$.

Furthermore, it can be seen that in the limit where $p_i||p_j$, the matrix element squared behaves as follows [79]:

$$\begin{aligned} |\mathcal{M}(p_1, ..., p_{n+1})|^2 &= {}_{n+1,a}\langle 1, ..., m; a, ...|1, ..., m; a, ...\rangle_{n+1,a} \to \\ \to \frac{1}{p_i.p_j} g_s^2 \mu^{2\epsilon}\, {}_{n,a}\langle 1, ..., m; a, ...|\hat{P}_{(ij),i}(z, k_\perp; \epsilon)|1, ..., m; a, ...\rangle_{n,a} \end{aligned} \tag{2.2.26}$$

where g_s is the strong coupling in d-dimensions, and the n-parton matrix element can be obtained by replacing the partons i and j in Eq. (2.2.22) with a single parton ij, that represents the partons i and j in the collinear limit, in such a way that its momentum is $p^\mu = p_i^\mu + p_j^\mu$. Besides, the flavour of ij is given by the rule: $anything + gluon \to anything$ and $quark + antiquark \to gluon$.

In this case, contrary to the soft limit, the collinear radiation does involve spin correlations. The kernel $\hat{P}_{(ij),i}$ is the d-dimensional Altarelli-Parisi splitting function, which represents the splitting $ij \to i + j$. It depends on the momentum fraction z involved in the collinear splitting, but also on the helicity of the parton ij in the n-parton matrix element and on the transverse

momentum $k_\perp$, which add an azimuthal dependence on the angle on the emitted particle[7]. Note that, because of these spin correlations, the matrix element squared cannot be simply factorized in Eq. (2.2.26), and thus, this equation has to be regarded as a limiting formula, rather than a factorization one. The case of the implementation in the calculation of QCD cross sections always requires a careful treatment of momentum conservation away from the collinear limit.

As has been stated in the comments below the formulation in Eq. (2.2.23), so far we have considered the case in which two final-state partons in $\mathcal{M}_{m+1,a...}$ become collinear. In general, one has to deal also with the case in which a final-state parton i becomes collinear to an initial-state parton a. For the sake of completeness we also address the limiting behavior corresponding to this last collinear case, which is straightforward with the definition

$$\begin{aligned} p_i^\mu &= (1-x)p_a^\mu + k_\perp - \frac{k_\perp^2}{1-x}\frac{n^\mu}{2p_a n} \\ 2p_i.p_a &= -\frac{k_\perp^2}{1-x} \quad k_\perp \to 0, \end{aligned} \tag{2.2.27}$$

where the corresponding splitting process $a \to ai + i$ involves the transition from the initial state parton a to the initial state parton ai with the associated emission of the final state parton i. Here, the corresponding behavior in the collinear limit is

$$\begin{aligned} &|\mathcal{M}(p_1,...,p_{n+1})|^2 = {}_{n+1,a}\langle 1,...,m;a,...|1,...,m;a,...\rangle_{n+1,a} \to \\ &\to \frac{1}{x}\frac{1}{p_i.p_a} g_s^2 \mu^{2\epsilon}\, {}_{n,ai}\langle 1,...,m;ai,...|\hat{P}_{a(ai)}(z,k_\perp;\epsilon)|1,...,m;ai,...\rangle_{n,ai} \end{aligned} \tag{2.2.28}$$

Note the main difference with respect to Eq. (2.2.26). The initial-state parton ai carries the momentum $x\,p_a^\mu$, which also introduces the additional factor $1/x$ in Eq. (2.2.28).

The explicit expressions of $\hat{P}_{ab}(z,k_\perp;\epsilon)$ for the splitting processes

$$a(p) \longrightarrow b(zp + k_\perp + \mathcal{O}(k_\perp^2)) + c((1-z)p - k_\perp + \mathcal{O}(k_\perp^2)), \tag{2.2.29}$$

are

$$\langle s|\hat{P}_{qq}(z,k_\perp;\epsilon)|s'\rangle = \delta_{ss'}\, C_F \left[\frac{1+z^2}{1-z} - \epsilon(1-z)\right] , \tag{2.2.30}$$

[7] Although this azimuthal dependence is not usually relevant for NLO calculations, since its average over the azimuthal angle of the collinearly emitted parton is zero, it is of some importance to include the explicit form, since it could improve the numerical treatment of some local subtraction terms.

$$\langle s|\hat{P}_{qg}(z,k_\perp;\epsilon)|s'\rangle = \delta_{ss'}\, C_F \left[\frac{1+(1-z)^2}{z} - \epsilon z\right] \quad , \tag{2.2.31}$$

$$\langle \mu|\hat{P}_{qq}(z,k_\perp;\epsilon)|\nu\rangle = T_R \left[-g^{\mu\nu} + 4z(1-z)\frac{k_\perp^\mu k_\perp^\nu}{k_\perp^2}\right] \quad , \tag{2.2.32}$$

$$\langle \mu|\hat{P}_{gg}(z,k_\perp;\epsilon)|\nu\rangle = 2C_A \left[-g^{\mu\nu}\left(\frac{z}{1-z}+\frac{1-z}{z}\right) - 2(1-\epsilon)z(1-z)\frac{k_\perp^\mu k_\perp^\nu}{k_\perp^2}\right] \quad , \tag{2.2.33}$$

where the spin indices of the parent parton a have been denoted by s, s' if a is a fermion and μ, ν if a is a gluon.

Finally we recall the most commonly used expressions for the kernels P_{ab} at LO in QCD for each of the splitting processes as presented in Ref. [80] after the corresponding average over the polarizations of the parton a[8]:

$$\begin{aligned}
P_{qq}^{(1,0)}(x) &= C_F\left[\frac{1+x^2}{(1-x)_+} + \frac{3}{2}\delta(1-x)\right] = C_F\, p_{qq}(x) + \frac{3\,C_F}{2}\delta(1-x)\,, \\
P_{qg}^{(1,0)}(x) &= T_R\left[x^2+(1-x)^2\right] = T_R\, p_{qg}(x)\,, \\
P_{gq}^{(1,0)}(x) &= C_F\left[\frac{1+(1-x)^2}{x}\right] = C_F\, p_{gq}(x)\,, \\
P_{gg}^{(1,0)}(x) &= 2C_A\left[\frac{x}{(1-x)_+} + \frac{1-x}{x} + x(1-x)\right] + 2\beta_0\delta(1-x)\,,
\end{aligned} \tag{2.2.34}$$

with $\beta_0 = (11N_C - 4n_F T_R)/12$ and the usual plus distribution defined as

$$\int_0^1 dx\, \frac{f(x)}{(1-x)_+} = \int_0^1 dx\, \frac{f(x)-f(1)}{1-x}\,, \tag{2.2.35}$$

for any regular test function f. Additionally, $N_C = 3$ and $T_R = 1/2$ for the SU(3) color symmetry group.

Note that some of the splitting functions in Eq. (2.2.34) are divergent for $z \to 0, 1$. These divergences are the soft singularities addressed in section 2.2.1. Thus, when using the limits (2.2.20) or (2.2.26) to approximate the singular behavior of $|\mathcal{M}(p_1,...,p_{n+1})|^2$ we must be careful to avoid double counting the soft and collinear divergences in the overlapping region (see

[8]Note that in the AP formulation there is a slightly different labeling for the partons in the kernels. While $\hat{P}_{(ij),i}(z)$ in Ref. [79], which we followed to obtain our results, stands for the probability density of finding, inside a parton ij, another parton i with fraction z of the parent momentum, the labeling in the following equations 2.2.34 and 2.2.36 corresponds to $\hat{P}_{i,(ij)}$ (i.e. the indices are crossed). This new labeling will be, unless made explicit, the understood for all the following deductions in this work. Furthermore, in order not to confuse the QCD or the QED corrections for the kernels, we now include the full QCD⊗QED notation in the sense of 2.2.1 to indicate both strong and electromagnetic contributions to the splitting functions.

section 2.4 for a deeper discussion on this topic).

Finally, the same similarity reasons between QED and QCD that we previously discussed for the soft limits also hold here and, regarding the emission of collinear radiation coming from QED interactions, we could address these effects by taking care of the color factors, for the LO and even for higher order contributions to the splitting kernels, just in the way discussed in reference [39], where high order QED and mixed corrections were presented to the Altarelli-Parisi splitting functions. Here, we recall the expressions for the Leading Order QED contributions to the kernels [88]:

$$\begin{aligned} P_{qq}^{(0,1)}(x) &= e_q^2 \left[p_{qq}(x) + \frac{3}{2}\delta(1-x) \right] , \\ P_{q\gamma}^{(0,1)}(x) &= N_C \, e_q^2 \, p_{qg}(x) \, , \\ P_{\gamma q}^{(0,1)}(x) &= e_q^2 \, p_{gq}(x) \, , \\ P_{\gamma\gamma}^{(0,1)}(x) &= -\frac{2}{3} \sum_f e_f^2 \, \delta(1-x) \, , \end{aligned} \tag{2.2.36}$$

where an explicit dependence on the quark electromagnetic (EM) charge arises. Likewise, the sum over fermion charges in the $P_{\gamma\gamma}^{(0,1)}$ kernel corresponds to the definition

$$\sum_f e_f^2 = N_C \sum_q^{n_F} e_q^2 + \sum_l^{n_L} e_l^2 \, , \tag{2.2.37}$$

with n_F and n_L the number of quark and lepton flavours, respectively. As it is clear, with the exception of $P_{\gamma\gamma}$ (that at LO in QED only receives the δ-contribution, while its parent P_{gg} also involves non-abelian terms) all the other splitting kernels at this order could be constructed by carefully handling the color factors, with no further changes within their functional dependence.

2.2.3 Evolution of the couplings

In order to achieve a detailed understanding of the underlying physics, we will address the behavior of the QCD coupling constant, and its relation with two key phenomena that characterize strong interactions: confinement and asymptotic freedom.

As was first discussed in section 2.1, all the fundamental interactions are proportional to a coupling constant that states how strong the fields may couple to each other. From the

Standard Model Lagrangian, the procedure to obtain theoretical predictions, such as a cross section, is to perform perturbative expansions in powers of this coupling constant. In this way, all the quantities are generally expressed in terms of the coupling at a given known scale, which is preferably close to the typical scale of the process studied. Thus, the coupling at this scale actually indicates the effective strength of the interaction in the process. As it can be expected, this value may be different for different energy scales. In fact, this dependence is known as the running of the couplings constants. Moreover, despite theory can not predict the value of the coupling, its dependence on the energy scale inherent to the process can indeed be calculated.

In the case of QCD, all the particles that can be found isolated in nature are color singlets. In this sense, the color confinement refers then to the fact that quarks and gluons are always confined in bound states known as hadrons. Specifically, this phenomenon is due to the behavior of the strong coupling, which becomes larger (and so the force stronger) as particles are more separated, so that it isn't likely that low energy partons can escape an hadron. It is important to note that this is a non perturbative effect, which cannot be fully understood through perturbative series in powers of g_s , and other considerations have to be taken.

As a matter of fact, in order to gain insights into the distribution of QCD partons within hadrons and the subsequent hadronization process, the Parton Distribution Functions (PDFs) and fragmentation functions have to be *determined*. These distributions are fundamental quantities that provide essential information about the momentum and spatial distribution of partons inside hadrons, and they are essential for predicting the outcome of high-energy scattering processes. However, the determination of PDFs and fragmentation functions heavily relies on experimental data (for a more comprehensive discussion on PDFs, see section 2.3.1).

Contrary to this, one can calculate the running of the strong coupling constant within the perturbative region. This running arises due to quantum effects, which cause the g_s coupling to depend on the energy scale at which it is probed. In this region, the running involves the resolution of the following renormalization group equation for α_s:

$$\beta^{\text{QCD}} = \frac{d\log(\alpha_s)}{d\log(\mu^2)} = -\sum b_n \alpha_s^{n+1}(\mu^2), \tag{2.2.38}$$

where β^{QCD} is the logarithmic derivative of the coupling constant, the $b_n \equiv \beta_n/\pi^{n+1}$ are the coefficients multiplying each power of α_s and μ is an arbitrary energy scale. Both the

value of the coupling, as well as the exact form of each of the coefficients (specifically the ones that define higher orders in the expansion), depend on the renormalization scheme in which the coupling is defined. This means that they depend on the convention used to subtract infinities in the context of renormalization and generally, the most common choice is the $\overline{\text{MS}}$ scheme [89–91]. Once a convention is stated, the value of α_s is always determined in terms of a known value at a given scale as, for example, the mass of one of the electroweak bosons, which serves as a reference value for the coupling. For instance, α_s has been determined to be $\alpha_s(M_Z^2) = 0.1179 \pm 0.0009$ at the scale of the Z boson mass M_Z. In figure 2.6 one can find a summary of the most recent determinations for each of the studies performed. As we can see, this constitutes a reasonable and stable value for the strong coupling.

On the theoretical side, the first results for the running $\alpha_s(\mu^2)$ were obtained in Refs. [92,93] where Gross, Wilczek and Politzer achieved the first calculation of the β-function for a Yang-Mills theory. At the lowest order, the resolution of Eq. (2.2.38) reads

$$\alpha_s(\mu^2) = \frac{\alpha_s(\mu_0^2)}{1 + \alpha_s(\mu_0^2)\,\frac{\beta_0}{\pi}\,\log\left(\mu^2/\mu_0^2\right)}, \tag{2.2.39}$$

where β_0 stands for the first coefficient of Eq. (2.2.38)

$$\beta_0 \equiv \frac{11C_A - 4n_F T_R}{12} \tag{2.2.40}$$

with $C_A = N_C = 3$ the Casimir invariant of SU(3) and n_F the number of active light quark flavours in the theory. As can be easily observed, the value of β_0 is positive for QCD, which implies that $\alpha_s(\mu^2)$ vanishes when $\mu^2 \to \infty$ (i.e. at high energies). These results show that the strong force becomes weaker for processes involving large momentum transfers (i.e. at very high energies or very short distances)[9]. This theoretical result shapes the so called *asymptotic freedom*, and justifies the perturbative expansions in powers of α_s for energy scales in the $100\text{GeV} - \text{TeV}$ range, where the hadrons could just be seen as a collection of almost-free partons that are weakly interacting. What is more, this behavior is supported by the experimental evidences, where the available measurements of α_s at different energy scales Q agree with the limiting behavior of Eq. (2.2.39), as can be seen in figure 2.7.

On the other hand, although this result does not hold for very low energy scales, one can easily see that Eq. (2.2.39) diverges for small values of μ. This defines a scale

[9] Given that this perturbative result relies on the smallness of α_s, any further argumentation coming from this result only holds within the perturbative region where $\alpha_s < 1$.

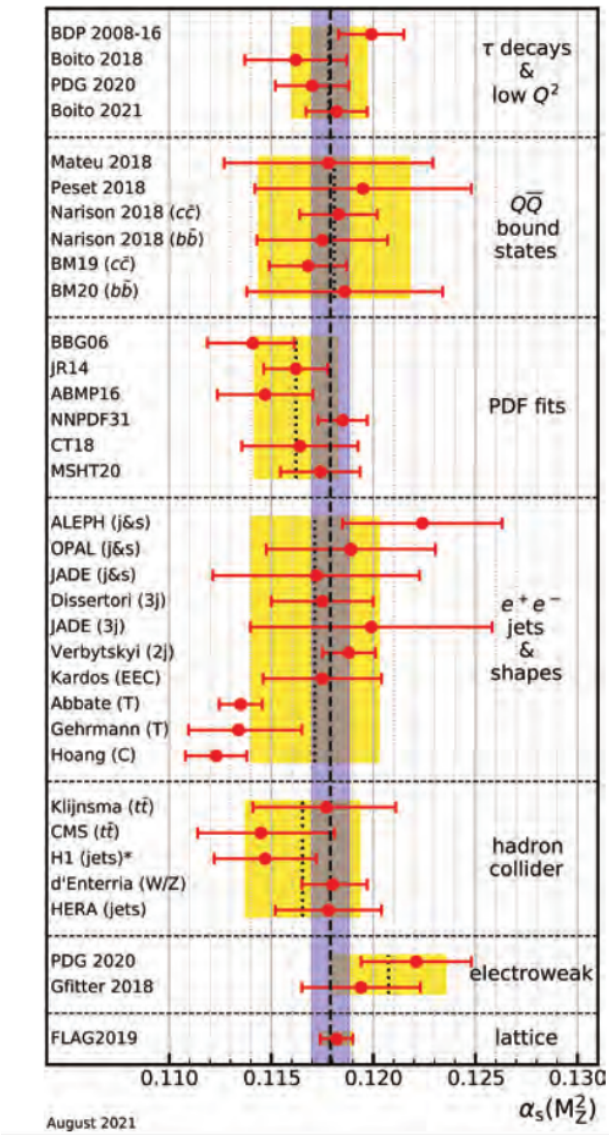

Figure 2.6: Summary presented in Ref. [1] for the determinations of $\alpha_s(M_Z^2)$ according to the experiments within the main sub-fields. The yellow (light shaded) bands and dotted lines indicate the pre-average values of each sub-field. The dashed line and blue (dark shaded) band represent the final world average value of $\alpha_s(M_Z^2)$. The "$*$" symbol within the "hadron colliders" sub-field indicates a determination including a simultaneous fit of the PDFs.

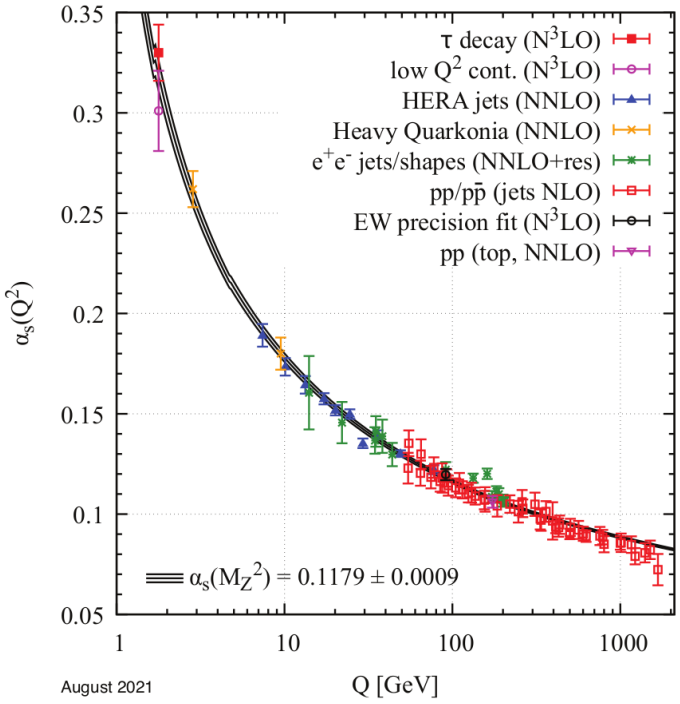

Figure 2.7: Summary presented in Ref. [1] for the measurements of $\alpha_s(Q^2)$ as a function of the energy scale Q. The respective degree of QCD perturbation theory used in the extraction of $\alpha_s(Q^2)$ is indicated in brackets.

$$\Lambda_{\text{QCD}} \equiv \mu_0 \exp\left[-\frac{\pi}{\beta_0 \alpha_s(\mu_0^2)}\right] \tag{2.2.41}$$

that represents a typical hadronic limit where the strong interactions become *stronger*, which agrees with the confinement of color but also indicates that the theory does not admit perturbative expansions any more in this region, and thus all the effects taking place below this Λ_{QCD} scale must be addressed through non-perturbative analysis.

Furthermore, if deeper perturbative effects were required, more terms can also be considered in the perturbative expansion of the β function, apart from the pure QCD contributions in Eq. (2.2.38). These might be important in order to offer a complete description of any observable (such as the cross section) to a certain mixed order, in the sense of Eq. (2.2.1). Here, the presence of electromagnetic interactions inside loops may lead to mixed terms in the running

$$\begin{aligned}\beta^{QCD} &= \frac{d\log(\alpha_s)}{d\log(\mu^2)} = -\sum_{i=0}^{\infty} b_{i0}\,\alpha_s^{i+1} - \sum_{i=0,j=1}^{\infty} b_{ij}\,\alpha_s^{i+1}\alpha^j \\ \beta^{QED} &= \frac{d\log(\alpha)}{d\log(\mu^2)} = -\sum_{j=0}^{\infty} b'_{0j}\,\alpha^{j+1} - \sum_{i=1,j=0}^{\infty} b'_{ij}\,\alpha_s^{i}\alpha^{j+1}\,,\end{aligned} \tag{2.2.42}$$

where now the first index refers to QCD orders, and the second one to QED ones, in a sense that $b_{i0} \equiv \beta_i^{QCD}/\pi^{i+1}$, $b'_{0j} \equiv \beta_j^{QED}/\pi^{j+1}$. Additionally, $b_{ij} = \beta_{ij}/\pi^{(i+j+1)}$ and $b'_{ij} = \beta'_{ij}/\pi^{(i+j+1)}$, with $\beta_{ij}|_{i,j\neq 0}$, $\beta'_{ij}|_{i,j\neq 0}$ are the mixed β-coefficients.

The first result for the mixed β function was calculated in Ref. [94] in order to reach a leading mixed order contribution for the resummation formula.

2.3 Hadronic Collisions

As has been mentioned, hadronic collisions are the crucial tool for studying and testing the behavior of the strong force, which is described by quantum chromodynamics. In this sense, they involve a complex interplay of strong, electromagnetic, and weak interactions and both perturbative and non-perturbative effects, which have to be understood and considered to access an hadronic cross section.

In general, the cross section for a generic hard scattering process

$$H_1(K_1) + H_2(K_2) \to F(Q) + X \tag{2.3.1}$$

where the collision of the two hadrons H_1 and H_2 with momenta K_1 and K_2 produces the final-state system F, accompanied by an arbitrary final state X, can be obtained by calculating

$$\sigma_F(K_1,K_2) = \sum_{a_1,a_2}\int_0^1 dx_1 \int_0^1 dx_2\, f_{a_1}^{(H_1)}(x_1)\, f_{a_2}^{(H_2)}(x_2)\, \hat{\sigma}_{F\,a_1a_2}(x_1K_1, x_2K_2) + \mathcal{O}\left(\frac{\Lambda_{QCD}}{Q}\right)^p . \tag{2.3.2}$$

Here, we have made a factorization assumption, based on the so called *naive parton model*, where the pair $a_1,\ a_2$ denote each partonic channel contributing to the production of the final state F, and x_1 and x_2 are the respective momentum fractions that each parton carries out of each hadron. The assumption indicates that the cross section can be essentially obtained by convoluting the low and high energy contributions. On the one hand, $f_{a_1}^{(H_1)}(x_1)$ and $f_{a_2}^{(H_2)}(x_2)$

are the parton distributions functions (PDF), which represent a probability density of finding each parton a_1 and a_2 within the hadrons H_1 and H_2 with momentum fractions x_1 and x_2, respectively. These PDFs are process-independent, in the sense that they only depend on the specific hadrons and partons being considered, and they characterize all the factorizable long-distance mechanisms that cannot be accessed through theory. On the other hand, $\hat{\sigma}_{F\,a_1 a_2}$ is the partonic cross section for the production of the final state F, which can be calculated in perturbation theory because it involves all the short distance (i.e. high energy) parton scattering effects.

Finally, all the terms that escape the factorization assumption (i.e. the terms that are process-dependent and also non-perturbative, and therefore non-factorizable) are considered in $(\Lambda_{QCD}/Q)^p$, which states the relation between the non-perturbative effects scale Λ_{QCD} and the hard scale Q of the process, where p is a non-negative integer that characterizes the power suppression of higher-order QCD corrections in the perturbative expansion, such that its value depends on the specific process and observable being considered.

2.3.1 Parton distribution functions

Nevertheless, it is really important to notice that this factorization assumption, which serves as a reasonable ground to express hadronic cross sections by separating between perturbative calculations and experimental determinations, involves certain degree of arbitrariness.

In principle, the collinear emission of a parton b with momentum fraction z from an initial leg a could be considered both as a real emission correction to the hard process, or as a correction to the PDF itself. In fact, we might directly find a parton b with momentum fraction $\zeta = zx$, instead of first finding in the hadron a parton a with momentum fraction x, followed by a further splitting $a(xP) \to b(zxP)$ (see figure 2.8). This arbitrariness shapes a factorization-scheme dependence, where all the PDFs could be in principle redefined by convoluting them with some process independent perturbative function. MS [89,90] DIS [18] and $\overline{\text{MS}}$ [91] are some of the most commonly used factorization schemes. As we know, the physical quantities cannot depend on such an arbitrary election, which makes the partonic cross section also depend on the factorization scheme, in such a way that the total final contribution is independent.

This situation introduces a dependence on the so called factorization scale μ_F, where the partonic cross section can be cast in the form

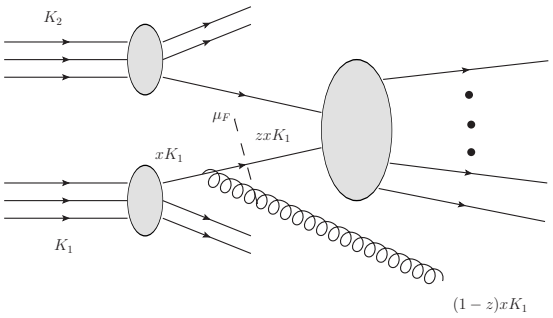

(a) Initial state collinear emission as a correction to the PDF.

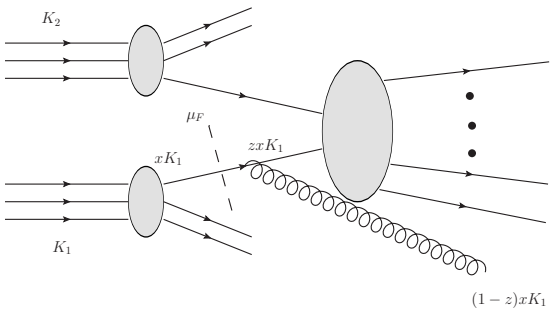

(b) Initial state collinear emission as a real emission correction to the hard process.

Figure 2.8: Arbitrariness within the factorization assumption. A NLO correction given by an initial state collinear emission could be seen as a correction to $\hat{\sigma}_{F\,a_1a_2}$, as well as a correction to the PDF $f_a^{(H_1)}(x)$.

$$\hat{\sigma}_{F\,a_1a_2}(p_1,p_2) = \sum_{b_1,b_2}\int_0^1 dz_1 \int_0^1 dz_2\, \hat{\sigma}_{F\,b_1b_2}(z_1p_1, z_2p_2;\mu_F)\Gamma_{b_1a_1}(z_1;\mu_F)\Gamma_{b_2a_2}(z_2;\mu_F). \tag{2.3.3}$$

In this sense, while at the Leading Order there is no loss of momentum due to extra radiation from the incoming partons, at higher orders the situation is different. Whereas the quantity $\hat{\sigma}_{F\,b_1b_2}$ is finite, the transition functions $\Gamma_{b_1a_1}(z_1;\mu_F)$ and $\Gamma_{b_2a_2}(z_2;\mu_F)$ encode the singular behavior of collinear emissions of partons carrying a momentum fraction of $(1-z_1)$ and $(1-z_2)$, respectively. Furthermore, as we anticipated, we could redefine the PDFs so that these transition contributions are absorbed within the functions $f_{a_1}^{(H_1)}(x_1)$ and $f_{a_2}^{(H_2)}(x_2)$ in Eq. (2.3.2):

$$\bar{f}_b^{(H)}(x;\mu_F) = \sum_a \int_x^1 \frac{dz}{z} f_a^{(H)}\left(\frac{x}{z}\right)\Gamma_{ba}(z;\mu_F) \equiv \sum_a \left(f_a^{(H)}\otimes\Gamma_{ba}\right)(x). \tag{2.3.4}$$

In this sense, as in the case of the coupling constants, the parton distributions also depend on the energy scale of the interaction and they must usually be "evolved" from a known initial scale to the scale of the interaction. After the redefinitions in Eq. (2.3.4), the hadronic cross section takes the form

$$\sigma_F(K_1,K_2) = \sum_{a_1,a_2}\int_0^1 dx_1 \int_0^1 dx_2\, \bar{f}_{a_1}^{(H_1)}(x_1;\mu_F)\,\bar{f}_{a_2}^{(H_2)}(x_2;\mu_F)\,\hat{\sigma}_{F\,a_1a_2}(x_1K_1, x_2K_2;\mu_F), \tag{2.3.5}$$

where the partonic distributions $\bar{f}_a^{(H)}(x;\mu_F)$ are now corrected by the transition functions $\Gamma_{ba}(z;\mu_F)$, which are computable order by order in perturbation theory, and each order is controlled by the splitting kernels defined in section 2.2.2. Specifically, in the case of the NLO QCD corrections, the expression for $\Gamma_{ab}(z)$ in the $\overline{\text{MS}}$ scheme, obtained through dimensional regularization, is

$$\Gamma_{ab}(z) = \delta_{ab}\delta(1-z) - \frac{1}{\epsilon}\frac{\alpha_s}{2\pi}P_{ab}^{(1)}(z) + \mathcal{O}(\alpha_s^2). \tag{2.3.6}$$

In this way we can address the calculation of radiative corrections with collinear singularities, which is essential to compute higher-order terms in the perturbative expansion of the cross section. In fact, it is common to express the hadronic cross section in 2.3.5 in terms of *subtracted* partonic cross sections $\bar{\sigma}_{F\,ab}$, in which the singularities due to collinear emissions from the incoming partons are cancelled by suitable counterterms originated in Eq. (2.3.6). Explicitly,

$$\begin{aligned}
\bar{\sigma}_{ab\to F}^{(0)}(p_1,p_2) &= \hat{\sigma}_{ab\to F}^{(0)}(p_1,p_2;\mu_F) \\
\bar{\sigma}_{ab\to F}^{(1)}(p_1,p_2) &= \hat{\sigma}_{ab\to F}^{(1)}(p_1,p_2) + \sigma^{(ct+)} + \sigma^{(ct-)}
\end{aligned} \tag{2.3.7}$$

with

$$\begin{aligned}
\sigma^{(ct+)} &= \frac{1}{\epsilon}\sum_{a_1}\int_0^1 dz\,\hat{\sigma}_{a_1 b\to F}^{(0)}(zp_1,p_2)P_{a_1 a}^{(1)}(z) \\
\sigma^{(ct-)} &= \frac{1}{\epsilon}\sum_{b_1}\int_0^1 dz\,\hat{\sigma}_{a b_1\to F}^{(0)}(p_1,zp_2)P_{b_1 b}^{(1)}(z).
\end{aligned} \tag{2.3.8}$$

Here, as we can see, these are in fact NLO contributions (i.e. $\mathcal{O}(\alpha_s)$ corrections) with Born kinematics, that subtract the singular behavior of the hard scattering $ab \to F$ with extra particle emissions that result collinear to the incoming partons, and can be addressed by convoluting the Altarelli-Parisi splitting kernels with the Leading Order partonic cross section $\sigma_{F\,ab}^{(0)}$. In practice, these contributions are to be cancelled with infrared singular terms coming from the real and virtual parts of the NLO in Eq. (2.3.7) (see section 2.4 for a deeper discussion on this subtraction). Furthermore, the expressions above do not depend on the explicit decomposition of the phase space element in each case. As a consequence, their validity extends to the full differential form of the cross section $d\sigma$, without further modifications.

On the other hand, although the μ_F cancellation would be exact when doing the complete (i.e. to all orders) calculation of a cross section, the truncation at a given order n formally adds a μ_F dependence of order $n+1$. This fact and the actual μ_F (and μ_R) dependences at a given order may help estimate the size of higher order terms in the expansion, which is often used as an uncertainty estimator within theoretical calculations.

2.4 NLO Calculations and the FKS Method

As has been previously stated, the calculation of higher order corrections in perturbation theory brings the need to handle the infrared divergences that arise within the computation of each separate term in these contributions (see section 2.2 for a deeper discussion on the ways in which IR divergences appear). For this reason, Frixione, Kunszt and Signer developed a method [67] (the so called FKS-subtraction) to calculate Next To Leading Order contributions to hadronic cross sections. Although it was first developed to address the three-jet production in hadronic collisions, it actually provides a systematic approach to include higher-order corrections in a broad spectrum of physical observables. The aim of the method is to achieve the analytic cancellation of the divergent parts in the sum, which defines any infrared-safe physical observable, just as, for instance, a cross section. In fact, such an analytic treatment of the divergences is essential for the amplitudes to be numerically evaluated within a computer code, which is generally the case.

In this section we will discuss and schematize the FKS-subtraction method [67,95] in order to address the NLO corrections to a generic hadronic process[10]. We will see in detail how to handle both initial state and final state collinear singularities, as well as soft singularities, which complete the set of infrared divergences appearing at NLO. Later in this work, the FKS subtraction will be used to deal with the mixed NLO contributions to the production of Z+jet in hadronic collisions (i.e. all the double-real and real-virtual terms that contribute to the production of a Z boson at $\mathcal{O}(\alpha_s\alpha)$. See Chapter 4 for details on this calculation). Let us begin with the expression for a differential hadronic cross section for the process $H_1\, H_2 \to F$, where F is a state composed by N particles that, in this case, could have color charge. This cross section, according to the factorization assumption (see Eq. (2.3.2)), can be written as:

[10] In fact, the following assumptions could also be made for processes that are not purely hadronic, like $d\hat{\sigma}_{\gamma a_2}$ (photon-hadron cross sections) and $d\hat{\sigma}_{e a_2}$ (DIS cross sections), or not hadronic at all, such as the e^+e^- cross section $d\hat{\sigma}_{e^+e^-}$, among others. See the formulation in Ref. [95] in terms of $L^{(AB)}_{a_1 a_2}$ to fully address these cases.

$$d\sigma^{(H_1H_2)}(K_1,K_2) = \sum_{a_1a_2} \int dx_1 dx_2 f_{a_1}^{(H_1)}(x_1) f_{a_2}^{(H_2)}(x_2) d\hat{\sigma}_{a_1a_2}(x_1K_1, x_2K_2)\,, \tag{2.4.1}$$

where H_1 and H_2 are the incoming hadrons, with momenta K_1 and K_2 respectively, $f_{a_i}^{(H_i)}$ is the distribution function for the parton a_i in the hadron H_i, and $d\hat{\sigma}_{a_1a_2}$ is the short-distance partonic cross section for each channel a_1a_2 of a 2-parton scattering. We consider that any ultraviolet divergence has already been properly renormalized, and thus we will especially make focus on the IR divergences appearing at NLO. On the one hand, given that the incident particles come from hadrons, the singular behavior introduced by collinear emissions from the partons a_1 and a_2 can be regulated by means of the collinear counterterms presented in section 2.3.1 (see particularly Eq. (2.3.8)). On the other hand, as has been previously commented, the Kinoshita-Lee-Nauenberg theorem [73–75] guarantees that for sufficiently inclusive observables, the remaining IR divergences appearing in real and virtual terms in the unresolved regions cancel against each other when considering the whole contribution. The goal will be to show and perform the cancellation analytically, by expressing the real corrections in a suitable form along the integration region, in such a way that each differential term will have one soft-collinear divergence at the worst.

We start by considering both the LO and the NLO QCD contributions to $d\hat{\sigma}_{a_1a_2}(x_1K_1, x_2K_2)$ in Eq. (2.4.1)

$$d\hat{\sigma}_{a_1a_2} = d\hat{\sigma}^{(0)}_{a_1a_2} + d\hat{\sigma}^{(1)}_{a_1a_2}\,. \tag{2.4.2}$$

On the one hand, $d\hat{\sigma}^{(0)}_{a_1a_2}$ is free of divergences and can be computed exactly by recalling the equation (2.2.3) in section 2.2

$$d\hat{\sigma}^{(0)}_{a_1a_2} = \mathcal{A}^{(N,0)}(\{a_l\}_1^{N+2}) \mathcal{S}_N d\phi_N, \tag{2.4.3}$$

Here, $\mathcal{A}^{(N,0)}$ is the leading order squared averaged partonic amplitude for the process $H_1\,H_2 \to F$ with N particles in the final state (see, for example, figure 2.3), which includes the flux, structure and all the statistical factors. On the other hand, at the Next to Leading Order, $d\hat{\sigma}^{(1)}_{a_1a_2}$ is composed by the sum of three terms

$$d\hat{\sigma}^{(1)}_{a_1a_2} = d\sigma^{(v)}_{a_1a_2} + d\sigma^{(r)}_{a_1a_2} + d\sigma^{(c)}_{a_1a_2}\,, \tag{2.4.4}$$

where

$$d\sigma^{(r)}_{a_1 a_2} = \mathcal{A}^{(N+1)}(\{a_l\}_1^{N+3})\mathcal{S}_{N+1}d\phi_{N+1} \tag{2.4.5}$$

is the contribution from the tree diagrams of $(N+1)$-parton corrections, and

$$d\sigma^{(v)}_{a_1 a_2} = \mathcal{A}^{(N,1)}(\{a_l\}_1^{N+2})\mathcal{S}_{N}d\phi_{N} \tag{2.4.6}$$

is the contribution of the QCD-loop corrections to $a_1\, a_2 \to F$, with born kinematics (see, for instance, figures 2.4b and 2.4a, respectively). In addition, $d\sigma^{(c)}_{a_1 a_2}$ is the contribution of the initial state collinear counterterms (see Eq. (2.3.8)).

We know that, although the virtual and real quantities defined in Eqs. (2.4.6) and (2.4.5) and the collinear counterterms are infrared divergent, their sum in Eq. (2.4.4) is finite, and thus the divergences will cancel according to the KLN theorem, if $\mathcal{S}$ is *infrared-safe*.

In this sense, we need the measurement function $\mathcal{S}_{N+1}(\phi_{N+1})$ for the $(N+1)$-particle phase space to be equal to the measurement function $\mathcal{S}_N(\phi_N)$ of the LO kinematics in the unresolved regions. This condition defines a safe mapping in the regions where i becomes soft and $i \parallel j$, that allows the cancellation to happen:

$$\begin{aligned} \mathcal{S}_{N+1}(...,k_{i-1},k_i,k_{i+1},...) &\xrightarrow{k_i\to 0} \mathcal{S}_N(...,k_{i-1},k_{i+1},...) \\ \mathcal{S}_{N+1}(...,k_i,k_j,...) &\xrightarrow{k_i\parallel k_j} \mathcal{S}_N(...,k_i+k_j,...). \end{aligned} \tag{2.4.7}$$

Starting from this point (2.4.7), we have to explore each divergent region in the NLO corrections and show the explicit cancellation of all the poles appearing in the expressions. Thus we will be able to get the NLO contributions as a sum of terms, each of them suitable for numerical integration.

In order to achieve the cancellation, we will first address the virtual contributions. Although the calculation of the loop corrections $d\sigma^{(v)}_{a_1 a_2}$ is often complicated, the structure of the divergent terms is straightforward [96–98] and can be expressed by recalling the result in Eq. (3.1) in Ref. [67]:

$$\mathcal{A}^{(N,1)}(\{a_l\}_{1,N+2};\{k_l\}_{1,N+2}) = \frac{\alpha_s}{2\pi}\frac{(4\pi)^\epsilon}{\Gamma(1-\epsilon)}\left(\frac{\mu^2}{Q^2}\right)^\epsilon \quad \mathcal{V}(\{a_l\}_{1,N+2};\{k_l\}_{1,N+2})\,, \tag{2.4.8}$$

where

$$\mathcal{V}(\{a_l\}_{1,N+2};\{k_l\}_{1,N+2}) = -\left(\frac{1}{\epsilon^2}\sum_{n=1}^{N+2} C(a_n) + \frac{1}{\epsilon}\sum_{n=1}^{N+2}\gamma(a_n)\right)\mathcal{A}^{(N,0)}(\{a_l\}_{1,N+2};\{k_l\}_{1,N+2}) + \frac{1}{2\epsilon}\sum_{\substack{n,m=1\\ n\neq m}}^{N+2}\log\frac{2k_n\cdot k_m}{Q^2}\frac{1}{8\pi^2}\mathcal{A}^{(N,0)}_{mn}(\{a_l\}_{1,N+2};\{k_l\}_{1,N+2}) + \mathcal{A}^{(N,1)}_{NS}(\{a_l\}_{1,N+2};\{k_l\}_{1,N+2})\,. \tag{2.4.9}$$

with

$$C(g) = C_A = N_c\,, \qquad \gamma(g) = \frac{11C_A - 4T_R n_F}{6}\,, \tag{2.4.10}$$

$$C(q) = C_F = \frac{N_c^2-1}{2N_c}\,, \qquad \gamma(q) = \frac{3}{2}C_F\,. \tag{2.4.11}$$

Here, μ is the renormalization scale and Q is the Ellis-Sexton scale, an arbitrary mass scale introduced in Ref. [98] to facilitate the writing of the result[11]. On the other hand, $\mathcal{A}^{(N,0)}_{mn}$ are the color-linked Born squared amplitudes as defined in Ref. [67], with the additional normalization of $16\pi^2$ with respect to our definition in Eq. (2.2.21). On top of that, they satisfy

$$\sum_{\substack{n=1\\ n\neq m}}^{N+2}\mathcal{A}^{(N,0)}_{mn}(\{a_l\}_{1,N+2};\{k_l\}_{1,N+2}) = 16\,C(a_m)\,\pi^2\mathcal{A}^{(N,0)}(\{a_l\}_{1,N+2};\{k_l\}_{1,N+2})\,. \tag{2.4.12}$$

Finally, $\mathcal{A}^{(N,1)}_{NS}$ represents all the non-divergent terms of the virtual contributions.

The key points from now on in order to perform the subtraction are that the N partonic phase space can be completely factorized out of the $(N+1)$-body partonic kinematics in the unresolved limits. Additionally, we exactly know the behavior of the amplitude $\mathcal{A}^{(N+1)}(\{a_l\}_1^{N+3})$ in these limits and, furthermore, the measurement function $\mathcal{S}_{N+1}$ can be constructed in such a way that it reduces to $\mathcal{S}_N$ in each of the infrared limits, thus guaranteeing that the cancellation can be carried out and that the Next to Leading Order contribution $d\hat{\sigma}^{(1)}_{a_1a_2}$ is finite. According to Eq. (2.4.7), we specifically need

[11] It is important to note that, in the end, the final result does not depend on the election of Q. In fact, the variation of Q could be useful for cross-checking the result of the calculation.

$$\lim_{k_i^0 \to 0} \mathcal{S}_{N+1} = \mathcal{S}_N \,, \qquad \lim_{\vec{k}_i \| \vec{k}_j} \mathcal{S}_{N+1} = \mathcal{S}_N \,, \tag{2.4.13}$$

$$\lim_{\vec{k}_i \| \vec{k}_1} \mathcal{S}_{N+1} = \mathcal{S}_N \,, \qquad \lim_{\vec{k}_i \| \vec{k}_2} \mathcal{S}_{N+1} = \mathcal{S}_N \,, \tag{2.4.14}$$

with 1 and 2 the initial state partons, $i, j \neq 1, 2$ and $i \neq j$. These can be seen as a definition for the conditions that must be fulfilled by the measurements functions to induce an infrared-safe cross section. What is more, these conditions also imply that, at least at the NLO, the only non-vanishing multiple infrared limits for $\mathcal{S}_{N+1}$ are the soft-collinear ones, which allows us to deal only with one soft-collinear divergence at the worst[12].

2.4.1 Separation of singularities

The main objective ahead is to fully organize $d\hat{\sigma}^{(1)}_{a_1 a_2}$ into $(N+1)$-parton and N-parton contributions, such that the whole NLO correction can be expressed as

$$d\hat{\sigma}^{(1)}_{a_1 a_2} = d\hat{\sigma}^{(1,N+1)}_{a_1 a_2} + d\hat{\sigma}^{(1,N)}_{a_1 a_2}, \tag{2.4.15}$$

where

$$\begin{aligned} d\hat{\sigma}^{(1,N+1)}_{a_1 a_2} &= \sum_i \left(d\sigma^{(in,f)}_{a_1 a_2, i} + \sum_j^{[i]} d\sigma^{(out,f)}_{a_1 a_2, ij} \right) \\ d\hat{\sigma}^{(1,N)}_{a_1 a_2} &= d\sigma^{(v)}_{a_1 a_2} + d\sigma^{(s)}_{a_1 a_2} + d\hat{\sigma}^{(in,+)}_{a_1 a_2} + d\hat{\sigma}^{(in,-)}_{a_1 a_2} + d\sigma^{(c)}_{a_1 a_2} + d\sigma^{(out,+)}_{a_1 a_2}. \end{aligned} \tag{2.4.16}$$

Here, each term is either finite or its singularities evidently cancel with those of the others, so that $d\hat{\sigma}^{(1,N+1)}_{a_1 a_2}$ and $d\hat{\sigma}^{(1,N)}_{a_1 a_2}$ will be suitable for the numerical evaluation.

In the following, we will show how to achieve each term in the separation of Eq. (2.4.15) by regulating the divergences due to the integration over the infrared singular regions in the real part of the differential cross section $d\sigma^{(r)}_{a_1 a_2}$. First, we will profit from the decomposition

$$\mathcal{S}_{N+1} = \sum_{i=3}^{N+3} \mathcal{S}_i^{(sing)} = \sum_{i=3}^{N+3} \left(\mathcal{S}_i^{(0)} + \sum_{\substack{j=3 \\ j \neq i}}^{N+3} \mathcal{S}_{ij}^{(1)} \theta(k_{jT}^2 - k_{iT}^2) \right). \tag{2.4.17}$$

[12] See the reasoning in section 2 in Ref. [95] and the specific measurement function used to address the three jet cross section to Next to Leading Order in Ref. [67].

where the functions $\mathcal{S}_i^{(0)}$ and $\mathcal{S}_{ij}^{(1)}$ in Eq. (2.4.17) are defined by their behavior in the neighborhood of the infrared singular regions. In particular

$$\mathcal{S}_i^{(0)} \neq 0 \quad \text{only if} \quad k_i^0 \to 0, \;\; \vec{k}_i \parallel \vec{k}_1 \,, \;\; \vec{k}_i \parallel \vec{k}_2 \,, \tag{2.4.18}$$

$$\mathcal{S}_{ij}^{(1)} \neq 0 \quad \text{only if} \quad k_i^0 \to 0, \;\; k_j^0 \to 0, \;\; \vec{k}_i \parallel \vec{k}_j \,. \tag{2.4.19}$$

As can be easily seen, this decomposition accomplishes the expected property of having one soft-collinear singularity at most in each term. Note that $\mathcal{S}_i^{(0)}$ and $\mathcal{S}_{ij}^{(1)}$ are exactly 0 in other infrared singular regions than the specified in Eqs. (2.4.18) and (2.4.19), and that they could be redefined by any other measurement term that also vanishes in these limits [13].

Next, we can replace the decomposition (2.4.17) in the differential form of the real contribution (2.4.5) and thus split $d\sigma^{(r)}_{a_1 a_2}$ in a sum of terms that exclusively encode the singularities associated to parton i[14]

$$d\sigma^{(r)}_{a_1 a_2} = \sum_{i=3}^{N+3} d\sigma^{(sing)}_{a_1 a_2, \, i}. \tag{2.4.20}$$

Here, each $d\sigma^{(sing)}_{a_1 a_2, \, i}$ is proportional to $\mathcal{S}_i^{(sing)}$ in Eq. (2.4.17).

In order to show the final result in Eq. (2.4.15), we have to choose suitable partonic kinematic variables to perform the subtraction for each term $d\sigma^{(sing)}_{a_1 a_2, \, i}$. In the case of Frixione, Kunszt and Signer, they decided to use the energy and angle variables instead of transverse momenta and rapidities. This election shows a number of advantages with respect to the previous subtraction methods. In fact, the soft integrals become much simpler in this way, and the FKS formalism is still valid for inclusive production of any number of jets.

With this election, we write the momenta of the initial state partons 1 and 2 in the partonic center-of-mass frame, as

$$\begin{aligned} k_1 &= \frac{\sqrt{S}}{2}(1, \vec{0}, 1) \\ k_2 &= \frac{\sqrt{S}}{2}(1, \vec{0}, -1) \end{aligned} \tag{2.4.21}$$

[13] This was the case with the additional term $\mathcal{S}_i^{(fin)}$ in the three jet calculation of [67], while in the calculation of the Drell Yan mixed contributions at a fully differential level, we chose to absorb $\mathcal{S}_i^{(fin)}$ within $\mathcal{S}_i^{(sing)}$ when defining the NLO measurement function, as suggested in Ref. [95] (see Chapter 4 of the present work).

[14] Note that the θ function in Eq. (2.4.17) assures that each term $\mathcal{S}_{ij}^{(1)}\theta(k_{jT}^2 - k_{iT}^2)$ does not get contributions when j is soft. Furthermore, the region in which $i \parallel j$ contributes to both $\mathcal{S}_i^{(sing)}$ and $\mathcal{S}_j^{(sing)}$, but the $\theta(k_{jT}^2 - k_{iT}^2)$ in Eq. (2.4.17) prevents any double counting.

where $\sqrt{S}$ is the partonic center-of-mass energy and $\vec{0}$ is the null vector in $(2-2\epsilon)$-dimensional space. Furthermore, the momentum for a generic final state parton i, can be written as

$$k_i = \frac{\sqrt{S}}{2}\xi_i \left(1, \sqrt{1-y_i^2}\vec{e}_{iT}, y_i\right). \tag{2.4.22}$$

Here, $\vec{e}_{iT}$ is a unit vector in the $(2-2\epsilon)$-dimensional transverse momentum space, $-1 \leq y_i \leq 1$ and $0 \leq \xi_i \leq 1$ are the angle and energy variables for the parton i.

As we can see, this parametrization implies that when $\xi_i \to 0$, the parton i gets soft, while on the other hand, the limit $y_i \to \pm 1$ indicates the collinear limits $i \parallel 1$ and $i \parallel 2$, respectively.

Moreover, the general $(N+1)$-body phase space $d\phi_{N+1}$ can be expressed as a product of the invariant measure over the variables of parton i and $d\phi$ as

$$\begin{aligned} d\phi_{N+1} &= d\phi d\phi_i \\ d\phi_i &= \frac{d^{3-2\epsilon}k_i}{(2\pi)^{3-2\epsilon}\,2k_i^0} = \frac{1}{2(2\pi)^{3-2\epsilon}}\left(\frac{\sqrt{S}}{2}\right)^{2-2\epsilon} \xi_i^{1-2\epsilon}\left(1-y_i^2\right)^{-\epsilon} d\xi_i dy_i d\Omega_i^{(2-2\epsilon)}, \end{aligned} \tag{2.4.23}$$

where $d\Omega_i^{(2-2\epsilon)}$ is the angular measure in $2-2\epsilon$ dimensions. Additionally, $d\phi$ is the remaining part of the $(N+1)$ phase space element, in the sense of Eq. (2.2.3). Now we can regulate the soft singularities of $d\sigma^{(sing)}_{a_1a_2,\,i}$ by multiplying the invariant amplitude squared by ξ_i^2.

$$\begin{aligned} d\sigma^{(sing)}_{a_1a_2,\,i} &= \xi_i^2 \;\; \mathcal{A}^{(N+1)}(\{a_l\}_1^{N+3})\, \mathcal{S}_i^{(sing)} d\phi d\phi_i \\ &= \xi_i^2 \;\; \mathcal{A}^{(N+1)}(\{a_l\}_1^{N+3})\, \mathcal{S}_i^{(sing)} d\phi \\ &\times \frac{1}{2(2\pi)^{3-2\epsilon}}\left(\frac{\sqrt{S}}{2}\right)^{2-2\epsilon} \xi_i^{-1-2\epsilon}\left(1-y_i^2\right)^{-\epsilon} d\xi_i dy_i d\Omega_i^{(2-2\epsilon)}. \end{aligned} \tag{2.4.24}$$

Thus, we could therefore isolate the ϵ-divergences by using the identity

$$\xi_i^{-1-2\epsilon} = -\frac{\xi_{cut}^{-2\epsilon}}{2\epsilon}\delta(\xi_i) + \left(\frac{1}{\xi_i}\right)_c - 2\epsilon\left(\frac{\log\xi_i}{\xi_i}\right)_c + \mathcal{O}(\epsilon^2), \tag{2.4.25}$$

where ξ_{cut} is an arbitrary parameter satisfying the condition $0 < \xi_{cut} \leq 1$, and the distributions

in the right hand side are defined as follows

$$< \left(\frac{1}{\xi_i}\right)_c , f > = \int_0^1 d\xi_i \frac{f(\xi_i) - f(0)\theta(\xi_{cut} - \xi_i)}{\xi_i} , \tag{2.4.26}$$

$$< \left(\frac{\log \xi_i}{\xi_i}\right)_c , f > = \int_0^1 d\xi_i \left[f(\xi_i) - f(0)\theta(\xi_{cut} - \xi_i) \right] \frac{\log \xi_i}{\xi_i} . \tag{2.4.27}$$

As it is clear, this parametrization allows us to separate the $\sim \delta(\xi_i)$ soft term from the others. We write

$$\begin{aligned}
d\sigma^{(sing)}_{a_1 a_2, i} &= d\sigma^{(s)}_{a_1 a_2, i} + d\sigma^{(ns)}_{a_1 a_2, i} \\
d\sigma^{(s)}_{a_1 a_2, i} &= -\frac{\xi_{cut}^{-2\epsilon}}{2\epsilon} \delta(\xi_i) d\xi_i \left(\xi_i^2 \ \mathcal{A}^{(N+1)}(\{a_l\}_1^{N+3}) \right) \ \mathcal{S}_i^{(sing)} d\phi \\
&\quad \times \frac{1}{2(2\pi)^{3-2\epsilon}} \left(\frac{\sqrt{S}}{2} \right)^{2-2\epsilon} \left(1 - y_i^2\right)^{-\epsilon} dy_i d\Omega_i^{(2-2\epsilon)} . \\
d\sigma^{(ns)}_{a_1 a_2, i} &= \left[\left(\frac{1}{\xi_i}\right)_c - 2\epsilon \left(\frac{\log \xi_i}{\xi_i}\right)_c \right] \left(\xi_i^2 \ \mathcal{A}^{(N+1)}(\{a_l\}_1^{N+3}) \right) \ \mathcal{S}_i^{(sing)} d\phi \\
&\quad \times \frac{1}{2(2\pi)^{3-2\epsilon}} \left(\frac{\sqrt{S}}{2} \right)^{2-2\epsilon} \left(1 - y_i^2\right)^{-\epsilon} d\xi_i dy_i d\Omega_i^{(2-2\epsilon)} .
\end{aligned} \tag{2.4.28}$$

While the quantity $d\sigma^{(s)}_{a_1 a_2, i}$ contains singularities due to the parton i becoming soft, the term $d\sigma^{(ns)}_{a_1 a_2, i}$ is free of them, but it does contain collinear singularities.

On top of that, by taking into account the decomposition of $\mathcal{S}_i^{(sing)}$ in Eq. (2.4.17) we can also fully disentangle the collinear singularities of $d\sigma^{(ns)}_{a_1 a_2, i}$:

$$d\sigma^{(ns)}_{a_1 a_2, i} = d\sigma^{(in)}_{a_1 a_2, i} + \sum_j^{[i]} d\sigma^{(out)}_{a_1 a_2, ij}, \tag{2.4.29}$$

where[15]

[15]The superindex $[i]$ in the sum in Eq. (2.4.29) means that j can take the values 3, ..., $N+3$ with the exclusion of i.

$$d\sigma^{(in)}_{a_1a_2,i} = \left[\left(\frac{1}{\xi_i}\right)_c - 2\epsilon\left(\frac{\log\xi_i}{\xi_i}\right)_c\right]\left(\xi_i^2\ \mathcal{A}^{(N+1)}(\{a_l\}_{1,N+3})\right)\mathcal{S}_i^{(0)}d\phi$$
$$\times\ \frac{1}{2(2\pi)^{3-2\epsilon}}\left(\frac{\sqrt{S}}{2}\right)^{2-2\epsilon}\left(1-y_i^2\right)^{-\epsilon}d\xi_i dy_i d\Omega_i^{(2-2\epsilon)}\,, \tag{2.4.30}$$

$$d\sigma^{(out)}_{a_1a_2,ij} = \left[\left(\frac{1}{\xi_i}\right)_c - 2\epsilon\left(\frac{\log\xi_i}{\xi_i}\right)_c\right]\left(\xi_i^2\ \mathcal{A}^{(N+1)}(\{a_l\}_{1,N+3})\right)\mathcal{S}_{ij}^{(1)}\theta(k_{jT}^2-k_{iT}^2)d\phi$$
$$\times\ \frac{1}{2(2\pi)^{3-2\epsilon}}\left(\frac{\sqrt{S}}{2}\right)^{2-2\epsilon}\left(1-y_i^2\right)^{-\epsilon}d\xi_i dy_i d\Omega_i^{(2-2\epsilon)}\,. \tag{2.4.31}$$

By construction, Eq. (2.4.30) contains only initial state collinear singularities, while Eq. (2.4.31) contains only final state ones.

So far, we managed to express the real part $d\sigma^{(r)}_{a_1a_2}$ of the cross section as a sum of terms with singular behaviors well defined, and properly isolated.

$$d\sigma^{(r)}_{a_1a_2} = \sum_i\left(d\sigma^{(s)}_{a_1a_2,i} + d\sigma^{(in)}_{a_1a_2,i} + \sum_j^{[i]} d\sigma^{(out)}_{a_1a_2,ij}\right). \tag{2.4.32}$$

Now that we have isolated the soft limit, we will deal with the collinear singularities. As for the term $\sigma^{(in)}_{a_1a_2,i}$, the divergences due to parton i becoming collinear to one of the incoming partons can simultaneously be regulated by multiplying the invariant amplitude squared by the factor $(1-y_i^2) = (1+y_i)(1-y_i)$. Eq. (2.4.30) becomes

$$d\sigma^{(in)}_{a_1a_2,i} = \left[\left(\frac{1}{\xi_i}\right)_c - 2\epsilon\left(\frac{\log\xi_i}{\xi_i}\right)_c\right]\left((1-y_i^2)\xi_i^2\ \mathcal{A}^{(N+1)}(\{a_l\}_{1,N+3})\right)\mathcal{S}_i^{(0)}d\phi$$
$$\times\ \frac{1}{2(2\pi)^{3-2\epsilon}}\left(\frac{\sqrt{S}}{2}\right)^{2-2\epsilon}\left(1-y_i^2\right)^{-1-\epsilon}d\xi_i dy_i d\Omega_i^{(2-2\epsilon)}\,. \tag{2.4.33}$$

We use the identity

$$\left(1-y_i^2\right)^{-1-\epsilon} = -\frac{(2\delta_I)^{-\epsilon}}{2\epsilon}\Big[\delta(1-y_i)+\delta(1+y_i)\Big] + \mathcal{P}(y_i) + \mathcal{O}(\epsilon), \tag{2.4.34}$$

where

$$\mathcal{P}(y_i) = \frac{1}{2}\left[\left(\frac{1}{1-y_i}\right)_{\delta_I} + \left(\frac{1}{1+y_i}\right)_{\delta_I}\right]. \tag{2.4.35}$$

Here δ_I is an arbitrary parameter satisfying the condition $0 < \delta_I \leq 2$, and we defined

$$< \left(\frac{1}{1-y_i}\right)_{\delta_I}, f > = \int_{-1}^{1} dy_i \, \frac{f(y_i) - f(1)\theta(y_i - 1 + \delta_I)}{1 - y_i}\,, \tag{2.4.36}$$

$$< \left(\frac{1}{1+y_i}\right)_{\delta_I}, f > = \int_{-1}^{1} dy_i \, \frac{f(y_i) - f(-1)\theta(-y_i - 1 + \delta_I)}{1 + y_i}\,. \tag{2.4.37}$$

Therefore, by using Eq. (2.4.34), Eq. (2.4.33) can be splitted into three terms, the first two proportional to $\delta(1+y_i)$ and $\delta(1-y_i)$ respectively, which contain the collinear singularities (and in which the invariant amplitude can be substituted with its collinear limit), and the third one which is finite in the limits $y_i \to \pm 1$. Explicitly

$$d\sigma^{(in)}_{a_1 a_2, i} = d\sigma^{(in,+)}_{a_1 a_2, i} + d\sigma^{(in,-)}_{a_1 a_2, i} + d\sigma^{(in,f)}_{a_1 a_2, i}\,, \tag{2.4.38}$$

where

$$\begin{aligned} d\sigma^{(in,f)}_{a_1 a_2, i} = {} & \mathcal{P}(y_i) \left[\left(\frac{1}{\xi_i}\right)_c - 2\epsilon \left(\frac{\log \xi_i}{\xi_i}\right)_c \right] \frac{1}{2(2\pi)^{3-2\epsilon}} \left(\frac{\sqrt{S}}{2}\right)^{2-2\epsilon} \\ & \times \left((1-y_i^2)\xi_i^2 \;\; \mathcal{A}^{(N+1)}(\{a_l\}_{1,N+3}) \right) \mathcal{S}_i^{(0)} d\phi d\xi_i dy_i d\Omega_i^{(2-2\epsilon)}\,, \end{aligned} \tag{2.4.39}$$

and

$$\begin{aligned} d\sigma^{(in,\pm)}_{a_1 a_2, i} = {} & -\frac{(2\delta_I)^{-\epsilon}}{2\epsilon} \delta(1 \mp y_i) \left[\left(\frac{1}{\xi_i}\right)_c - 2\epsilon \left(\frac{\log \xi_i}{\xi_i}\right)_c \right] \frac{1}{2(2\pi)^{3-2\epsilon}} \left(\frac{\sqrt{S}}{2}\right)^{2-2\epsilon} \\ & \times \left((1-y_i^2)\xi_i^2 \;\; \mathcal{A}^{(N+1)}(\{a_l\}_{1,N+3}) \right) \mathcal{S}_i^{(0)} d\phi d\xi_i dy_i d\Omega_i^{(2-2\epsilon)}\,. \end{aligned} \tag{2.4.40}$$

The subtraction prescriptions of $\mathcal{P}(y_i)$, which regulate initial state divergences, and the decomposition in Eq. (2.4.17), which guarantees that $\mathcal{S}_i^{(0)}$ does not get contributions from final state collinear divergences, assure that Eq. (2.4.39) is finite, and therefore we can set $\epsilon = 0$:

$$\begin{aligned} d\sigma^{(in,f)}_{a_1 a_2, i} = {} & \frac{1}{2} \left(\frac{1}{\xi_i}\right)_c \left[\left(\frac{1}{1-y_i}\right)_{\delta_I} + \left(\frac{1}{1+y_i}\right)_{\delta_I} \right] \frac{1}{2(2\pi)^3} \left(\frac{\sqrt{S}}{2}\right)^2 \\ & \times \left((1-y_i^2)\xi_i^2 \;\; \mathcal{A}^{(N+1)}(\{a_l\}_{1,N+3}) \right) \mathcal{S}_i^{(0)} d\phi d\xi_i dy_i d\varphi_i\,. \end{aligned} \tag{2.4.41}$$

Since all the divergences have been properly regulated, this quantity in Eq. (2.4.41) can be numerically integrated. On the other hand, all the remaining initial state collinear singularities

are still encoded within $d\sigma^{(in,\pm)}_{a_1 a_2,i}$.

Now, we concentrate in $d\sigma^{(out)}_{a_1 a_2,ij}$ in Eq. (2.4.32), which contains final state collinear divergences corresponding to the limit $i \parallel j$. We can follow a path similar to the initial state case and regulate the final state divergences.

First, we can parametrize the momentum of parton j as

$$k_j = \frac{\sqrt{S}}{2}\xi_j \left(1, \hat{k}_j\right), \quad \hat{k}_j = \hat{p}_j R, \quad \hat{p}_j = \left(\sqrt{1-y_j^2}\vec{e}_{jT}, y_j\right). \tag{2.4.42}$$

where R is the $3-2\epsilon$ dimensional rotation matrix that rotates $(\vec{0}, 1)$ into the parton i 3-momentum $(\sqrt{1-y_i^2}\vec{e}_{iT}, y_i)$ of the definition (2.4.22). This parametrization leads to the product

$$k_i \cdot k_j = \left(\frac{\sqrt{S}}{2}\right)^2 \xi_i \xi_j \left(1 - y_j\right). \tag{2.4.43}$$

Therefore, in the limit $y_j \to 1$ the partons i and j become collinear to each other.

Due to the known universal behavior of the collinear limits, we can regulate final state divergences by multiplying the invariant amplitude squared by the factor $(1-y_j)$. Moreover, with this definition (2.4.42) we can factorize the j-part out of the $d\phi$ piece of the phase space in a similar way as in Eq. (2.4.23) and write:

$$d\phi = d\tilde{\phi} d\phi_j \tag{2.4.44}$$

$$= d\tilde{\phi}\, \frac{1}{2(2\pi)^{3-2\epsilon}} \left(\frac{\sqrt{S}}{2}\right)^{2-2\epsilon} \xi_j^{1-2\epsilon} \left(1-y_j^2\right)^{-\epsilon} d\xi_j dy_j d\Omega_j^{(2-2\epsilon)}, \tag{2.4.45}$$

where, from Eq. (2.4.23),

$$d\tilde{\phi} = (2\pi)^{4-2\epsilon}\delta^{4-2\epsilon}\left(k_1 + k_2 - \sum_{l=3}^{N+3} k_l\right) \prod_l^{[ij]} \frac{d^{3-2\epsilon}k_l}{(2\pi)^{3-2\epsilon}\, 2k_l^0}. \tag{2.4.46}$$

In this way, we can write the piece with the final state collinear singularities of Eq. (2.4.31) as

$$
\begin{aligned}
d\sigma^{(out)}_{a_1a_2,ij} = & \left[\left(\frac{1}{\xi_i}\right)_c - 2\epsilon\left(\frac{\log\xi_i}{\xi_i}\right)_c\right]\left((1-y_j)\xi_i^2\ \ \mathcal{A}^{(N+1)}(\{a_l\}_{1,N+3})\right) \\
& \times \mathcal{S}^{(1)}_{ij}\theta(k^2_{jT}-k^2_{iT})d\tilde{\phi}\left(\frac{1}{2(2\pi)^{3-2\epsilon}}\left(\frac{\sqrt{S}}{2}\right)^{2-2\epsilon}\right)^2\left(1-y_i^2\right)^{-\epsilon}d\xi_i dy_i d\Omega_i^{(2-2\epsilon)} \\
& \times \xi_j^{1-2\epsilon}\left(1-y_j\right)^{-1-\epsilon}\left(1+y_j\right)^{-\epsilon}d\xi_j dy_j d\Omega_j^{(2-2\epsilon)}\,.
\end{aligned}
\tag{2.4.47}
$$

We can therefore split $d\sigma^{(out)}_{a_1a_2,ij}$ into two terms, by using the identity

$$
\left(1-y_j\right)^{-1-\epsilon} = -\frac{(\delta_o)^{-\epsilon}}{\epsilon}\delta(1-y_j) + \left(\frac{1}{1-y_j}\right)_{\delta_o} + \mathcal{O}(\epsilon),
\tag{2.4.48}
$$

where $0<\delta_o\leq 2$ and the $()_{\delta_o}$ distribution was defined in Eq. (2.4.36). Thus:

$$
d\sigma^{(out)}_{a_1a_2,ij} = d\sigma^{(out,+)}_{a_1a_2,ij} + d\sigma^{(out,f)}_{a_1a_2,ij}\,,
\tag{2.4.49}
$$

where $d\sigma^{(out,+)}_{a_1a_2,ij}$ is proportional to $\delta(1-y_j)$ and $d\sigma^{(out,f)}_{a_1a_2,ij}$ is free of singularities, and therefore suitable for numerical integration, after setting $\epsilon=0$. Explicitly:

$$
\begin{aligned}
d\sigma^{(out,f)}_{a_1a_2,ij} = & \left(\frac{1}{\xi_i}\right)_c\left(\frac{1}{1-y_j}\right)_{\delta_o}\left((1-y_j)\xi_i^2\xi_j\ \ \mathcal{A}^{(N+1)}(\{a_l\}_{1,N+3})\right)\mathcal{S}^{(1)}_{ij}\theta(k^2_{jT}-k^2_{iT}) \\
& \times\left(\frac{1}{2(2\pi)^3}\left(\frac{\sqrt{S}}{2}\right)^2\right)^2 d\tilde{\phi}d\xi_i d\xi_j dy_i dy_j d\varphi_i d\varphi_j
\end{aligned}
\tag{2.4.50}
$$

and

$$
\begin{aligned}
d\sigma^{(out,+)}_{a_1a_2,ij} = & -\frac{(2\delta_o)^{-\epsilon}}{\epsilon}\delta(1-y_j)dy_j\left[\left(\frac{1}{\xi_i}\right)_c - 2\epsilon\left(\frac{\log\xi_i}{\xi_i}\right)_c\right] \\
& \times\left((1-y_j)\xi_i^2\ \ \mathcal{A}^{(N+1)}(\{a_l\}_{1,N+3})\right)\mathcal{S}^{(1)}_{ij}\theta(k^2_{jT}-k^2_{iT}) \\
& \times\left(\frac{1}{2(2\pi)^{3-2\epsilon}}\left(\frac{\sqrt{S}}{2}\right)^{2-2\epsilon}\right)^2 d\tilde{\phi}\,\xi_j^{1-2\epsilon}\left(1-y_i^2\right)^{-\epsilon}d\xi_i d\xi_j dy_i d\Omega_i^{(2-2\epsilon)}d\Omega_j^{(2-2\epsilon)}\,.
\end{aligned}
\tag{2.4.51}
$$

Here, the last expression $d\sigma^{(out,+)}_{a_1a_2,ij}$ encodes the final state collinear behavior and can be exactly evaluated in the collinear limit.

2.4.2 Cancellation of singularities

As we can see, after all these considerations we finally got to express the NLO corrections $d\hat{\sigma}^{(1)}_{a_1a_2}$ in Eq. (2.4.4) as a sum of $(N+1)$ and N-final state parton contributions, just in the way anticipated in Eq. (2.4.15).

On the one hand,

$$d\hat{\sigma}^{(1,N+1)}_{a_1a_2} = \sum_i \left(d\sigma^{(in,f)}_{a_1a_2,i} + \sum_j^{[i]} d\sigma^{(out,f)}_{a_1a_2,ij} \right), \tag{2.4.52}$$

where these $(N+1)$-parton quantities are given in Eqs. (2.4.41) and (2.4.50), respectively. They are finite, and suitable for numerical integration in 4 dimensions.

On the other hand, from Eq. 2.4.15 we see that there is still the term $d\hat{\sigma}^{(1,N)}_{a_1a_2}$. It is formed by both the virtual part $d\sigma^{(v)}_{a_1a_2}$ and the collinear counterterms of Eqs. (2.4.6) and (2.3.8), respectively, and by the remaining divergent pieces of $d\sigma^{(r)}_{a_1a_2}$: $d\sigma^{(s)}_{a_1a_2,\,i}$, $d\sigma^{(in,\pm)}_{a_1a_2,i}$ and $d\sigma^{(out,+)}_{a_1a_2,ij}$, summed over the partons (these quantities are specified in Eqs. (2.4.28), (2.4.40) and (2.4.51), respectively).

$$\begin{aligned} d\sigma^{(s)}_{a_1a_2} &= \sum_i d\sigma^{(s)}_{a_1a_2,i} \\ d\hat{\sigma}^{(in,\pm)}_{a_1a_2} &= \sum_i d\hat{\sigma}^{(in,\pm)}_{a_1a_2,i} \\ d\sigma^{(out,+)}_{a_1a_2} &= \sum_i \sum_j^{[i]} d\sigma^{(out,+)}_{a_1a_2,ij}\,, \end{aligned} \tag{2.4.53}$$

so that

$$d\hat{\sigma}^{(1,N)}_{a_1a_2} = d\sigma^{(v)}_{a_1a_2} + d\sigma^{(s)}_{a_1a_2} + d\hat{\sigma}^{(in,+)}_{a_1a_2} + d\hat{\sigma}^{(in,-)}_{a_1a_2} + d\sigma^{(c)}_{a_1a_2} + d\sigma^{(out,+)}_{a_1a_2}. \tag{2.4.54}$$

Here, we will profit from the known universal behavior of the amplitudes in the soft and collinear limits (see sections 2.2.1 and 2.2.2) to achieve Born-like expressions for the quantities in Eq. (2.4.53). Thus, their poles will cancel against each other and with the ones originated from the virtual amplitudes $d\sigma^{(v)}_{a_1a_2}$, as well as from the counterterms in Eq. (2.3.8), which arise from the evolution of the PDFs. The cancellation will leave finite remainders dependent on the factorization scale μ_F, which will be suitable for numerical computation.

In order to show that the separation above leads to an explicit cancellation of singularities,

we will first address $d\sigma^{(s)}_{a_1 a_2, i}$. Here we can recall the expression (2.2.20) for the soft limit and write (after relabeling the partons in Eq. (2.2.20) so that i takes the soft particle and m and n the emitters)

$$\lim_{\xi_i \to 0} \mathcal{A}^{(N+1)}(\{a_l\}_{1,N+3}; \{k_l\}_{1,N+3}) = \delta_{g a_i} \frac{\alpha_s \mu^{2\epsilon}}{2\pi} \sum_{\substack{n,m \\ n<m}}^{[i]} \frac{k_n \cdot k_m}{k_n \cdot k_i \; k_m \cdot k_i} \mathcal{A}^{(N,0)}_{mn} \left(\{a_l\}^{[i]}_{1,N+3}; \{k_l\}^{[i]}_{1,N+3} \right), \tag{2.4.55}$$

where n and m in the sum run also over the values 1 and 2 (incoming partons), $k_n \cdot k_m / (k_n \cdot k_i \; k_m \cdot k_i)$ is the eikonal function and $\mathcal{A}^{(N,0)}_{mn}$ are the color-linked Born squared amplitudes as defined in Ref. [67] with the additional factor of $16\pi^2$, which explains the different normalizations between Eqs. (2.4.55) and (2.2.20). Note that the conservation of the fermionic number implies that, regarding the NLO QCD contributions, only the soft gluon contribution is different from 0 in the limit (2.4.55).

Furthermore, by replacing the expression (2.4.55) in $d\sigma^{(s)}_{a_1 a_2, i}$, and taking into account the limits (2.4.13) and the phase space reduction

$$\lim_{\xi_i \to 0} d\phi_N = d\phi_N \left(k_1, k_2 \to \{k_l\}^{[i]}_{3,N+3} \right), \tag{2.4.56}$$

the soft component in Eq. (2.4.28) becomes therefore

$$\begin{aligned} d\sigma^{(s)}_{a_1 a_2, i} = & -\frac{\alpha_s}{2\pi} \frac{\xi_{cut}^{-2\epsilon}}{2\epsilon} \frac{2^{2\epsilon}}{2(2\pi)^{3-2\epsilon}} \left(\frac{S}{\mu^2} \right)^{-\epsilon} \\ & \times \sum_{\substack{n,m \\ n<m}}^{[i]} \mathcal{A}^{(N,0)}_{mn} \left(\{a_l\}^{[i]}_{1,N+3}; \{k_l\}^{[i]}_{1,N+3} \right) \mathcal{S}_3([i]) \, d\phi_N \left(k_1, k_2 \to \{k_l\}^{[i]}_{3,N+3} \right) \\ & \times \delta(\xi_i) \left(\frac{\sqrt{S}}{2} \right)^2 \frac{k_n \cdot k_m}{k_n \cdot k_i \; k_m \cdot k_i} \xi_i^2 \left(1 - y_i^2 \right)^{-\epsilon} d\xi_i dy_i d\Omega_i^{(2-2\epsilon)} . \end{aligned} \tag{2.4.57}$$

as can be seen, the dependence of $d\sigma^{(s)}_{a_1 a_2, i}$ on y_i and Ω_i is fully contained in the last line. Therefore, the integral over $d\xi_i$, dy_i and $d\Omega_i^{(2-2\epsilon)}$ can be performed explicitly. This analytical integration leads to the product of a form factor and the color linked cross section element $d\sigma^{(0)}_{mn}$, with one less particle in the final state:

$$d\sigma^{(s)}_{a_1a_2} = \sum_i d\sigma^{(s)}_{a_1a_2,i} = \frac{\alpha_s}{2\pi}\frac{1}{2}\sum_{\substack{n,m=1\\ n\neq m}}^{N+2}\left(\mathcal{I}^{(div)}_{mn} + \mathcal{I}^{(reg)}_{mn}\right)\; d\sigma^{(0)}_{mn}(\{a_l\}_{1,N+2}) \tag{2.4.58}$$

where

$$d\sigma^{(0)}_{mn}\left(\{a_l\}_{1,N+2};\{k_l\}_{1,N+2}\right) = \mathcal{A}^{(N,0)}_{mn}\left(\{a_l\}_{1,N+2};\{k_l\}_{1,N+2}\right)\,\mathcal{S}_N\,d\phi_N\left(k_1,k_2\to\{k_l\}_{3,N+2}\right) \tag{2.4.59}$$

and

$$\mathcal{I}^{(div)}_{mn} = \frac{1}{8\pi^2}\frac{(4\pi)^\epsilon}{\Gamma(1-\epsilon)}\left(\frac{\mu^2}{Q^2}\right)^\epsilon\left[\frac{1}{\epsilon^2} - \frac{1}{\epsilon}\left(\log\frac{2k_n\cdot k_m}{Q^2} - \log\frac{4E_nE_m}{\xi^2_{cut}S}\right)\right], \tag{2.4.60}$$

$$\begin{aligned}\mathcal{I}^{(reg)}_{mn} = \frac{1}{8\pi^2}\Bigg[&\frac{1}{2}\log^2\frac{\xi^2_{cut}S}{Q^2} + \log\frac{\xi^2_{cut}S}{Q^2}\log\frac{k_n\cdot k_m}{2E_nE_m} - \mathrm{Li}_2\left(\frac{k_n\cdot k_m}{2E_nE_m}\right)\\ &+\frac{1}{2}\log^2\frac{2k_n\cdot k_m}{E_nE_m} - \log\left(4-\frac{2k_n\cdot k_m}{E_nE_m}\right)\log\frac{k_n\cdot k_m}{2E_nE_m} - 2\log^2 2\Bigg].\end{aligned} \tag{2.4.61}$$

Here E_n is the energy of the parton n in the partonic center-of-mass frame

$$E_n = \frac{(k_1+k_2)\cdot k_n}{\sqrt{S}}\,. \tag{2.4.62}$$

and Q is the Ellis-Sexton scale.

On the other hand, we have also the terms with the initial state collinear singularities, $d\hat{\sigma}^{(in,+)}_{a_1a_2}$ and $d\hat{\sigma}^{(in,-)}_{a_1a_2}$ in Eq. (2.4.54). These are proportional to $\delta(1\mp y_i)$, which allows as to take the collinear limits $i\parallel 1$ and $i\parallel 2$, respectively.

Given that $d\hat{\sigma}^{(in,-)}_{a_1a_2}$ is completely analogous, we will focus on the case of $d\hat{\sigma}^{(in,+)}_{a_1a_2}$. First of all, we write the collinear limit for the squared amplitude, following the limiting behavior of Eq. (2.2.28). Here, we could easily get rid of the azimuthal part (i.e. the $k_\perp$-dependence in Eq. (2.2.28)), because the integral over $d\Omega_i^{(2-2\epsilon)}$ is 0 at the NLO. As for the z-dependence, we have:

$$\begin{aligned}&\lim_{y_i\to 1}\mathcal{A}^{(N+1)}(\{a_l\}_{1,N+3};\{k_l\}_{1,N+3}) =\\ &\qquad\frac{4\pi\alpha_s\mu^{2\epsilon}}{k_i\cdot k_1}P^<_{S(a_1,\bar{a}_i)a_1}(z,\epsilon)\mathcal{A}^{(N,0)}\left(S(a_1,\bar{a}_i),a_2,\{a_l\}^{[i]}_{3,N+3};zk_1,k_2,\{k_l\}^{[i]}_{3,N+3}\right),\end{aligned} \tag{2.4.63}$$

where $P^<_{ab}(z,\epsilon)$ is the Altarelli-Parisi kernel for $z<1$ in $4-2\epsilon$ dimensions and $S(c,d)$ is

the flavour of the parton which can split into two partons of flavour c and d.

Here, by definition, if the splitting into the flavours c and d is not possible, $P^{<}_{S(c,d)a}$ is zero. Additionally, the z parameter is defined in the collinear limit according to Eq. (2.2.27), as $k_i = (1-z)k_1$. If we consider the parametrization of k_i in Eq. (2.4.22), we have

$$\xi_i \equiv 1 - z \quad \text{if} \quad y_i = 1\,. \tag{2.4.64}$$

Furthermore, if we write explicitly the product of k_i and k_1, and consider the factors ξ_i^2 and $(1-y_i^2)$ of Eq. (2.4.40), we have

$$\lim_{y_i\to 1}\left(1-y_i^2\right)\xi_i^2\mathcal{A}^{(N+1)}(\{a_l\}_{1,N+3};\{k_l\}_{1,N+3}) = \tag{2.4.65}$$

$$8\pi\alpha_s\mu^{2\epsilon}\left(\frac{2}{\sqrt{S}}\right)^2\xi_i P^{<}_{S(a_1,\bar{a}_i)a_1}(1-\xi_i,\epsilon)$$
$$\times\,\mathcal{A}^{(N,0)}\left(S(a_1,\bar{a}_i),a_2,\{a_l\}^{[i]}_{3,N+3};(1-\xi_i)k_1,k_2,\{k_l\}^{[i]}_{3,N+3}\right). \tag{2.4.66}$$

Now we recall the whole expression for $d\sigma^{(in,+)}_{a_1a_2,i}$ in Eq. (2.4.40). We have formally obtained the limit for the average squared amplitude, and with all the remaining factors, together with the phase space reduction

$$\lim_{\vec{k}_i\parallel\vec{k}_1} d\phi = d\phi_N\left((1-\xi_i)k_1,k_2\to\{k_l\}^{[i]}_{3,N+3}\right), \tag{2.4.67}$$

and the infrared safe behavior of $\mathcal{S}_{N+1}$ in the collinear limit (2.4.13), we get

$$\begin{aligned} d\sigma^{(in,+)}_{a_1a_2,i} = &-\frac{\alpha_s}{2\pi}\sum_d\left(\frac{1}{\bar{\epsilon}}-\log\frac{S\delta_I}{2\mu^2}\right)\left[\left(\frac{1}{\xi_i}\right)_c - 2\epsilon\left(\frac{\log\xi_i}{\xi_i}\right)_c\right]\xi_i P^{<}_{da_1}(1-\xi_i,\epsilon)\\ &\times\;\mathcal{A}^{(N,0)}\left(d,a_2,\{a_l\}^{[i]}_{3,N+3};(1-\xi_i)k_1,k_2,\{k_l\}^{[i]}_{3,N+3}\right)\\ &\times\,\mathcal{S}_3([i])d\phi_N\left((1-\xi_i)k_1,k_2\to\{k_l\}^{[i]}_{3,N+3}\right)d\xi_i\,. \end{aligned} \tag{2.4.68}$$

where the azimutal angle has been integrated out

$$\int d\Omega_i^{(2-2\epsilon)} = \frac{2\pi^{1-\epsilon}}{\Gamma(1-\epsilon)}\,. \tag{2.4.69}$$

and

$$\frac{1}{\bar{\epsilon}} = \frac{1}{\epsilon} - \gamma_E + \log 4\pi. \tag{2.4.70}$$

We can now show that the divergent part of Eq. (2.4.68) is cancelled by the collinear counterterm of Eq. (2.3.8). In order to achieve this goal we can rewrite Eq. (2.3.8) in terms of the variable ξ_i in the collinear limit

$$\begin{aligned} d\sigma^{(cnt+)}_{a_1 a_2} = \frac{\alpha_s}{2\pi} \sum_d \left\{ \frac{1}{\bar{\epsilon}} \left[\left(\frac{1}{\xi_i} \right)_c \xi_i P^{<}_{da_1}(1-\xi_i, 0) + \delta_{da_1} \delta(\xi_i) \Big(\gamma(d) + 2C(d) \log \xi_{cut} \Big) \right] \right\} \\ \times \quad \mathcal{A}^{(N,0)} \left(d, a_2, \{a_l\}^{[i]}_{3,N+3}; (1-\xi_i)k_1, k_2, \{k_l\}^{[i]}_{3,N+3} \right) \\ \times \, \mathcal{S}_3([i]) d\phi_N \left((1-\xi_i)k_1, k_2 \to \{k_l\}^{[i]}_{3,N+3} \right) d\xi_i \,, \end{aligned} \tag{2.4.71}$$

where the AP kernels have been put in the form

$$P_{ab}(z,0) = \frac{(1-z)P^{<}_{ab}(z,0)}{(1-z)_+} + \gamma(a)\delta_{ab}\delta(1-z)\,, \tag{2.4.72}$$

$$2C(a)\delta_{ab}\delta(1-z) = \delta(1-z)(1-z)P^{<}_{ab}(z,0)\,, \tag{2.4.73}$$

with $C(a)$ and $\gamma(a)$ the Casimir operators for the flavour a and the contributions from virtual graphs to the Altarelli-Parisi kernels P_{aa}, as defined in Eqs. (2.4.10) and (2.4.11).

Also, the following identity has been used

$$\delta(1-y_i) \left(\frac{1}{1-z} \right)_+ = \delta(1-y_i) \left[\left(\frac{1}{\xi_i} \right)_c + \delta(\xi_i) \log \xi_{cut} \right]. \tag{2.4.74}$$

Now we compute the quantity

$$d\hat{\sigma}^{(in,+)}_{a_1 a_2, i} = d\sigma^{(in,+)}_{a_1 a_2, i} + d\sigma^{(cnt+)}_{a_1 a_2} \tag{2.4.75}$$

using

$$P^{<}_{ab}(z,\epsilon) = P^{<}_{ab}(z,0) + \epsilon P'^{<}_{ab}(z,0)\,, \tag{2.4.76}$$

we have

$$
\begin{aligned}
d\hat{\sigma}^{(in,+)}_{a_1a_2,i} = & \frac{\alpha_s}{2\pi}\frac{1}{\bar{\epsilon}}\Big(\gamma(a_1) + 2C(a_1)\log\xi_{cut}\Big) \\
& \times \mathcal{A}^{(N,0)}\left(\{a_l\}^{[i]}_{1,N+3};\{k_l\}^{[i]}_{1,N+3}\right)\mathcal{S}_3([i])d\phi_N\left(k_1,k_2\to\{k_l\}^{[i]}_{3,N+3}\right) \\
& + \frac{\alpha_s}{2\pi}\sum_d\Bigg\{\xi_i P^{<}_{da_1}(1-\xi_i,0)\Bigg[\left(\frac{1}{\xi_i}\right)_c\log\frac{S\delta_I}{2\mu^2} + 2\left(\frac{\log\xi_i}{\xi_i}\right)_c\Bigg] \\
& \qquad - \xi_i P'^{<}_{da_1}(1-\xi_i,0)\left(\frac{1}{\xi_i}\right)_c\Bigg\} \\
& \times \mathcal{A}^{(N,0)}\left(d,a_2,\{a_l\}^{[i]}_{3,N+3};(1-\xi_i)k_1,k_2,\{k_l\}^{[i]}_{3,N+3}\right) \\
& \times\mathcal{S}_3([i])d\phi_N\left((1-\xi_i)k_1,k_2\to\{k_l\}^{[i]}_{3,N+3}\right)d\xi_i\,.
\end{aligned}
\tag{2.4.77}
$$

As it is clear, we check that the subtracted $d\hat{\sigma}^{(in,+)}_{a_1a_2,i}$ quantity does not contain any pole associated with pure collinear singularities (corresponding to the non-soft region $z<1$). The pole part of this equation, which originates from the δ term in the flavour-diagonal Altarelli-Parisi kernels, cancels a corresponding term in the soft-virtual contribution. As for the remaining part, it is finite, and can be numerically evaluated.

Finally, by summing over i we can get the $d\hat{\sigma}^{(in,+)}_{a_1a_2}$ contribution to Eq. (2.4.54) as

$$
\begin{aligned}
d\hat{\sigma}^{(in,+)}_{a_1a_2} = & \sum_i d\hat{\sigma}^{(in,+)}_{a_1a_2,i} \\
= & \frac{\alpha_s}{2\pi}\left(\frac{(4\pi)^\epsilon}{\Gamma(1-\epsilon)}\left(\frac{\mu^2}{Q^2}\right)^\epsilon\frac{1}{\epsilon} - \log\frac{\mu^2}{Q^2}\right) \\
& \times\Big(\gamma(a_1) + 2C(a_1)\log\xi_{cut}\Big)\;\; d\sigma^{(0)}(\{a_l\}_{1,N+2};\{k_l\}_{1,N+2}) \\
& + \frac{\alpha_s}{2\pi}\sum_d\Bigg\{\xi P^{<}_{da_1}(1-\xi,0)\Bigg[\left(\frac{1}{\xi}\right)_c\log\frac{S\delta_I}{2\mu^2} + 2\left(\frac{\log\xi}{\xi}\right)_c\Bigg] \\
& \qquad - \xi P'^{<}_{da_1}(1-\xi,0)\left(\frac{1}{\xi}\right)_c\Bigg\} \\
& \times\; d\sigma^{(0)}(d,a_2,\{a_l\}_{3,N+3};(1-\xi)k_1,k_2,\{k_l\}_{3,N+2})\,d\xi\,,
\end{aligned}
\tag{2.4.78}
$$

where $d\sigma^{(0)}$ is the born cross section of equation (2.4.3). As for the $d\hat{\sigma}^{(in,-)}_{a_1a_2}$ term, the treatment is completely analogous, and the result is

$$
\begin{aligned}
d\hat{\sigma}^{(in,-)}_{a_1 a_2} = & \frac{\alpha_s}{2\pi}\left(\frac{(4\pi)^\epsilon}{\Gamma(1-\epsilon)}\left(\frac{\mu^2}{Q^2}\right)^\epsilon \frac{1}{\epsilon} - \log\frac{\mu^2}{Q^2}\right) \\
& \times\Big(\gamma(a_2) + 2C(a_2)\log\xi_{cut}\Big)\; d\sigma^{(0)}(\{a_l\}_{1,N+2};\{k_l\}_{1,N+2}) \\
& + \frac{\alpha_s}{2\pi}\sum_d \Bigg\{\xi P^{<}_{da_2}(1-\xi,0)\left[\left(\frac{1}{\xi}\right)_c \log\frac{S\delta_I}{2\mu^2} + 2\left(\frac{\log\xi}{\xi}\right)_c\right] \\
& \qquad - \xi P'^{<}_{da_2}(1-\xi,0)\left(\frac{1}{\xi}\right)_c\Bigg\} \\
& \times\; d\sigma^{(0)}(a_1, d, \{a_l\}_{3,N+3}; k_1, (1-\xi)k_2, \{k_l\}_{3,N+2})\, d\xi\,.
\end{aligned}
\tag{2.4.79}
$$

Finally, the last remaining term to deal with is $d\sigma^{(out,+)}_{a_1 a_2, ij}$ in Eq. (2.4.53). Here we could, as anticipated, take a similar path as in the initial state collinear terms. In this case, we can conveniently define the extra momentum p in the unresolved region

$$
p \equiv k_i + k_j \tag{2.4.80}
$$

such that

$$
\xi_i = (1-z)\xi_p, \quad \xi_j = z\xi_p, \quad \Rightarrow \quad d\xi_i d\xi_j = \xi_p d\xi_p dz\,. \tag{2.4.81}
$$

Thus, we have

$$
\delta(1-y_j)\,(k_i+k_j) \equiv \delta(1-y_j)p = \delta(1-y_j)\frac{\sqrt{S}}{2}\xi_p\left(1, \sqrt{1-y_i^2}\vec{e}_{iT}, y_i\right), \tag{2.4.82}
$$

Which defines ξ_p in a way consistent to Eq. (2.4.22). In fact, in the collinear limit this parameter is proportional to the energy of the parton that eventually splits into the two collinear partons i and j.

By taking into account the definition of the extra momentum p, the factors ξ_i^2 and $(1-y_j)$ in Eq. (2.4.51) and cancelling the $k_\perp$-dependence in the splitting, given the azimuthal symmetry at NLO, we have

$$\lim_{y_j\to 1}\left[\left((1-y_j)\xi_i^2\ \mathcal{A}^{(N+1)}(\{a_l\}_{1,N+3})\right)\mathcal{S}_{ij}^{(1)}\theta(k_{jT}^2-k_{iT}^2)\right]=$$
$$\lim_{y_j\to 1}\left((1-y_j)\xi_i^2\ \frac{4\pi\alpha_s\mu^{2\epsilon}}{k_i\cdot k_j}P^{<}_{a_ja_p}(z,\epsilon)\mathcal{A}^{(N,0)}\left(\{a_l\}^{[ij]}_{1,N+3;p};\{k_l\}^{[ij]}_{1,N+3;p}\right)\right)\mathcal{S}_{ij}^{(1)}\theta(k_{jT}^2-k_{iT}^2)=$$
$$4\pi\alpha_s\mu^{2\epsilon}\left(\frac{\sqrt{S}}{2}\right)^{-2}\frac{1-z}{z}\,\theta\left(z-\frac{1}{2}\right)\mathcal{S}_N([ij])\times\ \left[P^{<}_{a_ja_p}(z,\epsilon)\mathcal{A}^{(N,0)}\left(\{a_l\}^{[ij]}_{1,N+3;p};\{k_l\}^{[ij]}_{1,N+3;p}\right)\right], \tag{2.4.83}$$

with

$$a_p=S(a_i,a_j). \tag{2.4.84}$$

Additionally, with the definition in Eq. (2.4.81), the phase space measure in the third line of Eq. (2.4.51), corresponding to $d\phi_{N+1}$ with the i,j element factorized out, becomes

$$d\mu=\left(\frac{1}{2(2\pi)^{3-2\epsilon}}\left(\frac{\sqrt{S}}{2}\right)^{2-2\epsilon}\right)^2 d\tilde{\phi}\,z^{1-2\epsilon}dz\,\xi_p^{2-2\epsilon}d\xi_p\left(1-y_i^2\right)^{-\epsilon}dy_i d\Omega_i^{(2-2\epsilon)}d\Omega_j^{(2-2\epsilon)}\,. \tag{2.4.85}$$

Finally, we integrate over $d\Omega_j^{(2-2\epsilon)}$, which adds a factor $2\pi^{1-\epsilon}/\Gamma(1-\epsilon)$, and we get

$$\begin{aligned}d\sigma^{(out,+)}_{a_1a_2,ij}=&-\frac{(2\delta_o)^{-\epsilon}}{\epsilon}\frac{2\pi^{1-\epsilon}}{\Gamma(1-\epsilon)}4\pi\alpha_s\mu^{2\epsilon}\left(\frac{\sqrt{S}}{2}\right)^{-2}\left[\mathcal{D}^{(0)}(z)-2\epsilon\,\mathcal{D}^{(1)}(z)\right]\theta\left(z-\frac{1}{2}\right)\\&\times\,dz\,(1-z)\,z^{-2\epsilon}\ P^{<}_{a_ja_p}(z,\epsilon)\mathcal{A}^{(N,0)}\left(\{a_l\}^{[ij]}_{1,N+3;p};\{k_l\}^{[ij]}_{1,N+3;p}\right)\mathcal{S}_3([ij])\\&\times\left(\frac{1}{2(2\pi)^{3-2\epsilon}}\left(\frac{\sqrt{S}}{2}\right)^{2-2\epsilon}\right)^2 d\tilde{\phi}\,\xi_p^{1-2\epsilon}d\xi_p\left(1-y_i^2\right)^{-\epsilon}dy_i d\Omega_i^{(2-2\epsilon)}\,.\end{aligned} \tag{2.4.86}$$

where we can see that the last line agrees with the definition of the N-particle phase space, according to the definition (2.4.81). Therefore, we have

$$\begin{aligned}d\sigma^{(out,+)}_{a_1a_2,ij}=&-\frac{\alpha_s}{2\pi}\left(\frac{1}{\bar{\epsilon}}-\log\frac{S\delta_o}{2\mu^2}\right)\ \left[\mathcal{I}^{(0)}_{a_ja_p}-2\epsilon\,\mathcal{I}^{(1)}_{a_ja_p}\right]\\&\times\,\mathcal{A}^{(N,0)}\left(\{a_l\}^{[ij]}_{1,N+3;p};\{k_l\}^{[ij]}_{1,N+3;p}\right)\mathcal{S}_3([ij])d\phi_N\left(k_1,k_2\to\{k_l\}^{[ij]}_{3,N+3;p}\right),\end{aligned} \tag{2.4.87}$$

with

$$\mathcal{I}_{ab}^{(0)} = \int_0^1 dz\, z^{-2\epsilon}\,(1-z)\,P_{ab}^{<}(z,\epsilon)\,\theta\left(z-\frac{1}{2}\right)\mathcal{D}^{(0)}(z)\,, \tag{2.4.88}$$

$$\mathcal{I}_{ab}^{(1)} = \int_0^1 dz\, z^{-2\epsilon}\,(1-z)\,P_{ab}^{<}(z,\epsilon)\,\theta\left(z-\frac{1}{2}\right)\mathcal{D}^{(1)}(z)\,, \tag{2.4.89}$$

and $\mathcal{D}^{(0)}$ and $\mathcal{D}^{(1)}$ the expressions for the subtraction terms in Eq. (2.4.31) by means of z

$$\mathcal{D}^{(0)}(z) = \left(\frac{1}{1-z}\right)_+ + \log\left(\frac{\xi_p}{\xi_{cut}}\right)\delta(1-z), \tag{2.4.90}$$

$$\mathcal{D}^{(1)}(z) = \left(\frac{\log(1-z)}{1-z}\right)_+ + \log\xi_p\left(\frac{1}{1-z}\right)_+ + \frac{1}{2}\left(\log^2\xi_p - \log^2\xi_{cut}\right)\delta(1-z). \tag{2.4.91}$$

Finally, we managed to arrange $d\sigma^{(out,+)}_{a_1a_2,ij}$ as a product of a Born-like cross section with LO kinematics, and a term dependent upon the Altarelli-Parisi kernels, which completely describes the collinear splitting. We can sum over i,j the quantities $d\sigma^{(out,+)}_{a_1a_2,ij}$ and recover the quantity in Eq. (2.4.54)

$$d\sigma^{(out,+)}_{a_1a_2} = \sum_i \sum_j^{[i]} d\sigma^{(out,+)}_{a_1a_2,ij}\,, \tag{2.4.92}$$

In the end, we can address the integration of Eqs. (2.4.88) and (2.4.89) and get the expression

$$\begin{aligned} d\sigma^{(out,+)}_{a_1a_2} = {} & \frac{\alpha_s}{2\pi}\frac{(4\pi)^\epsilon}{\Gamma(1-\epsilon)}\left(\frac{\mu^2}{Q^2}\right)^\epsilon \; d\sigma^{(0)}(\{a_l\}_{1,N+2}) \\ & \times\frac{1}{\epsilon}\sum_{j=3}^{N+2}\left[\gamma(a_j) - 2C(a_j)\log\frac{2E_j}{\xi_{cut}\sqrt{S}}\right] \\ & + \frac{\alpha_s}{2\pi}\; d\sigma^{(0)}(\{a_l\}_{1,N+2}) \\ & \times\sum_{j=3}^{N+2}\left[\gamma'(a_j) - \log\frac{S\delta_o}{2Q^2}\left(\gamma(a_j) - 2C(a_j)\log\frac{2E_j}{\xi_{cut}\sqrt{S}}\right)\right. \\ & \left. +2C(a_j)\left(\log^2\frac{2E_j}{\sqrt{S}} - \log^2\xi_{cut}\right) - 2\gamma(a_j)\log\frac{2E_j}{\sqrt{S}}\right]. \end{aligned} \tag{2.4.93}$$

with

$$\gamma'(g) = \frac{67}{9}C_A - \frac{2\pi^2}{3}C_A - \frac{23}{9}T_R N_f \,, \tag{2.4.94}$$

$$\gamma'(q) = \frac{13}{2}C_F - \frac{2\pi^2}{3}C_F \,. \tag{2.4.95}$$

As it is clear, the divergent term cancels its analogous in the virtual contribution, and also the $\sim C(a_j)$ piece of $d\sigma^{(s)}_{a_1 a_2}$. This final cancellation accomplishes the desired goal of cancelling all the infrared divergent pieces within Eq. (2.4.54) and making the whole NLO contributions suitable for numerical computations.

Moreover, along this work the FKS method has shown useful to obtain the mixed $\mathcal{O}(\alpha_s\alpha)$ contributions to the partonic cross section of a $Z + a$ system in hadronic collisions, where by a we mean the broad definition of parton, which includes quarks, antiquarks, gluons and also photons. Specifically, this calculation involves several terms that constitute important steps towards the computation of the NNLO mixed QCD⊗QED corrections to the production of an off shell Z boson in hadronic collisions.

On the one hand, FKS has been used to address the NLO QCD terms for the production of $Z\gamma$, and $Z\overset{(-)}{q}$ in $\overset{(-)}{q}\gamma$ channels. These are $\mathcal{O}(\alpha)$ contributions to the Z-production process with the additional $\mathcal{O}(\alpha_s)$ corrections of an extra gluon, and can be fully addressed with this formalism.

On the other hand, the FKS subtraction has also helped us getting the QED corrections to Zg, as well as $Z\overset{(-)}{q}$ in $\overset{(-)}{q}g$ channels. It is worth noticing that in this case, where the subtraction was applied to obtain NLO electromagnetic contributions, we had to deal with QED divergences, instead of the singularities inherent to QCD corrections, which were studied all along this section. In this sense, although the way to proceed is nearly the same, the structure of the divergent terms has to be slightly modified to take care of the electromagnetic interactions. Specifically, concerning the soft and collinear limits, one has to take into account the changes in Eq. (2.2.19) and the QED splitting functions in Eq. (2.2.36) to address the soft and collinear electromagnetic radiation. In fact, the introduction of these new expressions in the formalism leads to some modifications in the coefficients C, γ, γ' and the kernels themselves.

In the following we present the modified coefficients for the expressions in the Eq. (2.4.54), which allow us to apply the formalism for the calculation of the NLO QED contributions.

First of all, in the case of quark-initiated electromagnetic radiation, the coefficients $C(a)$ and $\gamma(a)$ participating in the virtual term $\mathcal{V}$ in Eq. (2.4.8), and in the real-divergent pieces $d\sigma^{(s)}_{a_1a_2}$, $d\sigma^{(in,\pm)}_{a_1a_2}$ and $d\sigma^{(out,+)}_{a_1a_2}$ in Eqs. (2.4.58), (2.4.78), (2.4.79) and (2.4.93), respectively, acquire the form

$$\begin{aligned} C^{\text{QED}}(q) &= e_q^2\,, \\ \gamma^{\text{QED}}(q) &= \frac{3}{2}e_q^2\,. \end{aligned} \tag{2.4.96}$$

In addition, the coefficient $\gamma'(q)$ needed to compute the quantity $d\sigma^{(out,+)}_{a_1a_2}$ in Eq. (2.4.93) becomes:

$$\gamma'^{\text{QED}}(q) = \frac{13}{2}e_q^2 - \frac{2\pi^2}{3}e_q^2\,. \tag{2.4.97}$$

Finally, all the expressions involving the Altarelli-Parisi splitting kernels in the quantities in Eq. (2.4.54) (see Eqs. (2.4.78), (2.4.79), (2.3.8) and (2.4.93)) have to be adapted by changing $P^{(1,0)}_{ab} \to P^{(0,1)}_{ab}$ according to Eqs. (2.2.34) and (2.2.36), respectively.

These modified coefficients allow the complete application of the FKS formalism to obtain the NLO QED corrections to the production of Zg, and $Z\overset{(-)}{q}$ in $\overset{(-)}{q}g$ channels. What is more, all these contributions, together with the NLO QCD terms for the production of $Z\gamma$ and $Z\overset{(-)}{q}$ in $\overset{(-)}{q}\gamma$ channels, constitute the complete single-virtual plus one parton emission and double-real emission correction terms within the calculation of NNLO QCD⊗QED contributions to the Drell Yan full differential cross section (see Chapter 4 for more details on this topic).

CHAPTER 3

Inclusive Drell Yan Production

As has been previously pointed out, the study of the Drell Yan mechanism is crucial towards a deeper understanding of particle physics. This experiment provides a precise way to access the electroweak sector, serves as a crucial background for new physics searches, brings important insights into parton distribution functions, and offers opportunities for testing the limits of our current theoretical framework.

In order to offer a complete description of this process along various kinematic conditions, in this Chapter we will address the calculation of the full set of NNLO QED⊕QCD corrections (i.e. all the terms that satisfy $i + j \leq 2$ in the sense of Eq. (1.0.1)) to the inclusive Drell Yan cross section. In order to achieve this goal we will first review the NLO and the NNLO QCD corrections, presented in Ref. [19], and also the ones for the corresponding NLO QED part [46, 47]. Finally, mixed corrections coming from diagrams with simultaneous QCD and QED vertices, as well as pure NNLO QED contributions, are to be studied. We will characterize the importance of each different contribution in the perturbative expansion by comparing the K factors for different energies, and we will discuss the interesting behavior in the vicinity of the LHC center of mass energy $\sqrt{S} \sim 14$ TeV. Moreover, in the case of the mixed corrections, we will study in detail the contribution from each of the channels involved in the Drell Yan process to the mixed K factor. Finally, we will see how the the inclusion of the NNLO corrections diminishes the dependence on the factorization and renormalization scales, thus indicating the convergence of the perturbative series.

In this work, we will especially make focus on the neutral current contributions, which

are mediated by a Z boson. The figure 3.1 shows the leading order diagram for the Z boson production in hadronic collisions, originated in a $q\overline{q}$ annihilation.

From the theoretical side, the contributions for a general (i.e. including the decay of the gauge boson) perturbative calculation of Drell-Yan can be roughly characterized into the following subsets: on the one hand, *purely factorizable* terms that arise due to initial state (*production*, from the initial state partons) and final state (*decay*, from the final state leptons) emissions and, on the other hand, *non-factorizable* terms originated by soft photon exchanges between the production and the decay. As for the non-factorizable $\mathcal{O}(\alpha\alpha_s)$ terms, they have been shown [64–66] to have a negligible impact on the cross section, allowing to treat effectively Drell-Yan in the (resonant) limit of the decoupling between the production and decay processes, at least for the achieved experimental accuracy. Additionally, the mixed contributions are by themselves a gauge-invariant set of the complete Drell-Yan cross section calculation at $\mathcal{O}(\alpha\alpha_s)$, even for charged current contributions to the mechanism.

The presentation of the complete set of NNLO corrections to Drell Yan and, furthermore, the computation through a suitable *abelianisation procedure* of the so called mixed QCD$\otimes$QED $\mathcal{O}(\alpha\alpha_s)$ contributions to the inclusive on-shell production of a Z boson will be the main goals of this Chapter. Finally, counting with analytical expressions for the total cross section will be useful to establish a subtraction method to compute differential distributions for different observables at $\mathcal{O}(\alpha\alpha_s)$ by extending the q_T- subtraction method [99] originally developed for pure QCD corrections, so that it can also address mixed contributions. See Chapter 4 for a deeper discussion of this mechanism.

In principle a full computation of QCD$\otimes$QED $\mathcal{O}(\alpha\alpha_s)$ terms involves, as in any NNLO calculation, the evaluation of double-virtual, single-virtual plus one parton emission and double parton emission contributions, where parton in this Chapter will always refer to quarks, antiquarks, gluons, and photons. Most of the needed double real contributions were presented in Ref. [100], including the case of W boson production which is not discussed in this work [1], while the master integrals for the two-loop calculation were obtained in Ref. [101].

The structure of this Chapter is as follows: first we will introduce useful notation and recall the NLO QCD and NLO QED corrections ($\sigma_Z^{(1,0)}$ and $\sigma_Z^{(0,1)}$ in the sense of Eq. (1.0.1)) to the production of a Z boson, as presented in Ref. [19] and [46, 47], respectively. Next we will address the NNLO QCD contributions in relation with the calculation in Ref. [19] (see

[1] Only the contribution from the interference of QCD and QED $qq \to qq$ diagrams is missing in Ref. [100].

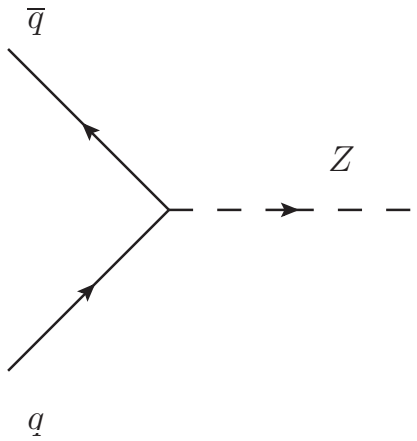

Figure 3.1: The Leading Order contribution to the production of the Z boson in hadronic collisions given a by $q\bar{q}$ annihilation.

section 3.1.2). After this, regarding the mixed corrections, instead of following the path of a dedicated calculation for each term, we will profit from the NNLO $\mathcal{O}(\alpha_s^2)$ contributions, by pointing out the abelian component, and obtain the corresponding QCD⊗QED $\mathcal{O}(\alpha\alpha_s)$ corrections (see section 3.2.1). Furthermore, we will discuss the phenomenological impact for the inclusive cross section at different hadronic energies. Finally, we will show how the same approach is useful to calculate the QED^2 $\mathcal{O}(\alpha^2)$ corrections, completing, therefore, the set of NNLO contributions in QCD⊕QED (i.e. all terms that correspond to $i + j = 2$ in Eq. (1.0.1)).

3.1 First orders and NNLO QCD Corrections

3.1.1 Background and Notation

In general, the cross section for the production of a Z boson in hadronic collisions can be written as

$$\frac{d\sigma^Z}{dQ^2} = \tau\sigma_Z(Q^2, M_Z^2)W_Z(\tau, Q^2), \tag{3.1.1}$$

where σ_Z is the point-like LO cross section, $\sqrt{S}$ is the hadronic centre-of-mass energy, Q the invariant mass of the produced Z, $\tau = \frac{Q^2}{S}$ and $W_Z(\tau, Q^2)$ is the hadronic structure function.

The point-like cross section that appears in Eq. (3.1.1) is defined as[2]

$$\sigma_Z(Q^2, M_Z^2) = \frac{\pi\alpha}{4M_Z \sin^2\theta_W \cos^2\theta_W} \frac{1}{N_C} \frac{\Gamma_{Z\to X}}{(Q^2 - M_Z^2)^2 + M_Z^2\Gamma_Z^2}, \tag{3.1.2}$$

where $N_C = 3$ is the number of quark colors, θ_W is the weak mixing angle (with $\sin^2\theta_W = 0.23$), $M_Z = 91.187$ GeV and Γ_Z are the mass and width of the Z, and $\Gamma_{Z\to X}$ is the partial width due to the decay of the Z to X (e.g. for leptonic decay, $X = \ell\bar{\ell}$). The narrow-width approximation used along this calculation consists on making the following replacement

$$\frac{1}{(Q^2 - M_Z^2)^2 + M_Z^2\Gamma_Z^2} \to \frac{\pi}{M_Z\Gamma_Z}\delta(Q^2 - M_Z^2). \tag{3.1.3}$$

ensuring the decoupling of the production and decay mechanisms. The hadronic structure function appearing in Eq. (3.1.1) can be written as a sum of contributions of different orders

$$W_Z(\tau, Q^2) = \int_0^1 \mathrm{d}x_1 \int_0^1 \mathrm{d}x_2 \int_0^1 \mathrm{d}x\, \delta(\tau - x x_1 x_2) \sum_{i,j} \left(\frac{\alpha_s}{\pi}\right)^i \left(\frac{\alpha}{\pi}\right)^j w_Z^{(i,j)}(x, x_1, x_2, Q^2), \tag{3.1.4}$$

where the dependencies on the factorization μ_F and renormalization μ_R scales are understood. Within this notation, the coefficients $w_Z^{(i,j)}$ are the ones that encode the perturbative corrections at different orders, along with the partonic distributions and the specific couplings and factors for each of the channels involved in the Z production.

For the LO, the channel is $q\bar{q}$ (see figure 3.1), and the contribution is essentially that of $\sigma_Z(Q^2, M_Z^2)$ in Eq. (3.1.2), plus the weak couplings to the Z boson and the partonic distributions, so that $w_Z^{(0,0)}$ can be expressed as

$$w_Z^{(0,0)} = \sum_{i\in Q,\bar{Q}} c_i q_i(x_1)\bar{q}_i(x_2)\delta(1 - x). \tag{3.1.5}$$

Here, $q_i(x_1)$ and $\bar{q}_i(x_2)$ are the distribution functions for the quark and antiquark i, respectively, and $c_i = v_i^2 + a_i^2$, with v_i and a_i defined as the vector and axial couplings of

[2] In order to separate the QED contributions computed here from the *weak* induced effects, we will consider the coupling between the Z boson and the quarks as an *effective coupling* and do not take into account self-energy insertions in the Z (and eventually γ) propagator.

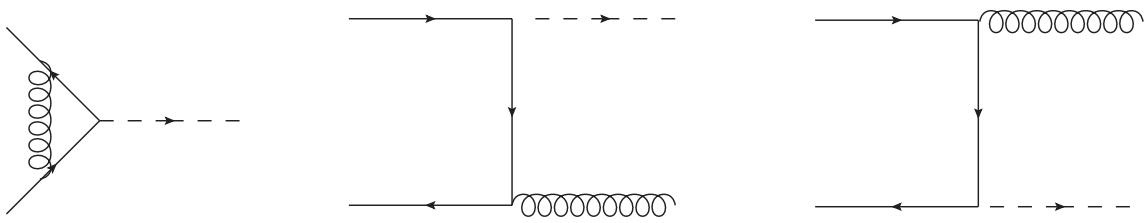

(a) Diagrams contributing to the order α_s correction to Drell Yan.

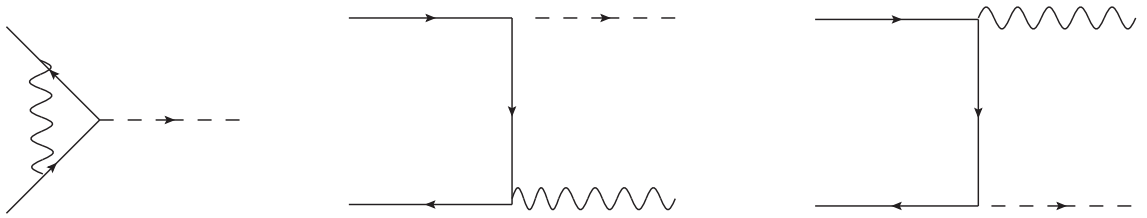

(b) Diagrams contributing to the order α correction to Drell Yan.

Figure 3.2: The $q\bar{q}$ channel for the Next to Leading Order contribution to the production of the Z boson in hadronic collisions. Diagrams contributing to qg and $q\gamma$ channels can be obtained from the real contributions presented in this figure via crossing.

particle i:

$$v_u = 1 - \frac{8}{3}\sin^2\theta_W, \qquad a_u = -1, \tag{3.1.6}$$

$$v_d = -1 + \frac{4}{3}\sin^2\theta_W, \qquad a_d = 1, \tag{3.1.7}$$

$$v_e = -1 + 4\sin^2\theta_W, \qquad a_e = 1. \tag{3.1.8}$$

On the other hand, regarding the NLO corrections, there are contributions from two different parton subprocesses in each case. Let us consider the NLO QCD corrections (see figure 3.2a). Here, we have to take into account the contribution coming from a real gluon emission from one of the quark legs ($q\bar{q} \to Zg$ squared) and also the interference between the one loop corrections to $q\bar{q}$, originated from a virtual gluon between legs 1 and 2, with the leading order diagram of figure 3.1. Additionally, we must also consider the qg channel, that shows up for the first time in this order[3]. The diagrams for this new channel can be obtained from the real emission diagrams in figure 3.2a via crossing. In this sense, the coefficient $w_Z^{(1,0)}$ can be expressed as

[3]Here and from now on, by q we mean any quark or antiquark considered for the production.

$$w_Z^{(1,0)} = \sum_{i\in Q,\bar{Q}} \Big\{ c_i q_i(x_1)\bar{q}_i(x_2) C_F \Delta_{q\bar{q}}^{(1)}(x) + \\ \left(q_i(x_1)g(x_2) + g(x_1)q_i(x_2)\right) c_i \Delta_{qg}^{(1)}(x) \Big\} \tag{3.1.9}$$

where $g(x)$ is the gluon distribution function, $C_A = N_C$ and $C_F = (N_C^2 - 1)/2N_C$ are the Casimir operators of SU(3) and, $\Delta_{q\bar{q}}^{(1)}(x)$ and $\Delta_{qg}^{(1)}(x)$ the QCD correction functions for $q\bar{q}$ and qg channels at first order, respectively. These corrections can be calculated by using n-dimensional regularization, as was first done in Refs. [18,102,103]. Recalling these results, the non-pole expressions, that constitute the DY NLO QCD correction terms, are

$$\Delta_{q\bar{q}}^{(1)} = 8\mathcal{D}_0(x)L_{\mu_F} + 16\mathcal{D}_1(x) + \delta(x-1)(6L_{\mu_F} + 8\zeta_2 - 16) \\ - 4L_{\mu_F}(x+1) - \frac{4\left(x^2+1\right)\log(x)}{1-x} - 8(x+1)\log(1-x) \tag{3.1.10}$$

$$\Delta_{qg}^{(1)} = \frac{1}{2}\left(2\left(2x^2 - 2x + 1\right)\left(L_{\mu_F} + 2\log(1-x) - \log(x)\right) - 7x^2 + 6x + 1\right), \tag{3.1.11}$$

where we define the following distributions

$$\mathcal{D}_i(x) = \left[\frac{\log^i(1-x)}{1-x}\right]_+ \tag{3.1.12}$$

that appear in the soft terms regularizing the divergence of soft emission ($x \approx 1$) and whose action is as usual, according to

$$\int_0^1 \mathcal{D}_i(x) f(x) \mathrm{d}x = \int_0^1 \frac{\log^i(1-x)}{1-x}\left[f(x) - f(1)\right] \mathrm{d}x\,. \tag{3.1.13}$$

We also consider an auxiliary variable to write the dependence on the factorization scale,

$$L_{\mu_F} = -\log\left(\frac{\mu_F^2}{Q^2}\right), \tag{3.1.14}$$

where μ_F is the factorization scale and Q the invariant mass of the produced Z[4].

On the other hand, if we wanted to calculate the NLO QED corrections to Drell Yan, we could take the same approach as in the NLO QCD case. These contributions (which were

[4]Here we amend the definition of L_{μ_F} given in Eq.(B.3) of ref [2] by adding the corresponding missing -1 factor to the $\log(\mu_F^2/Q^2)$

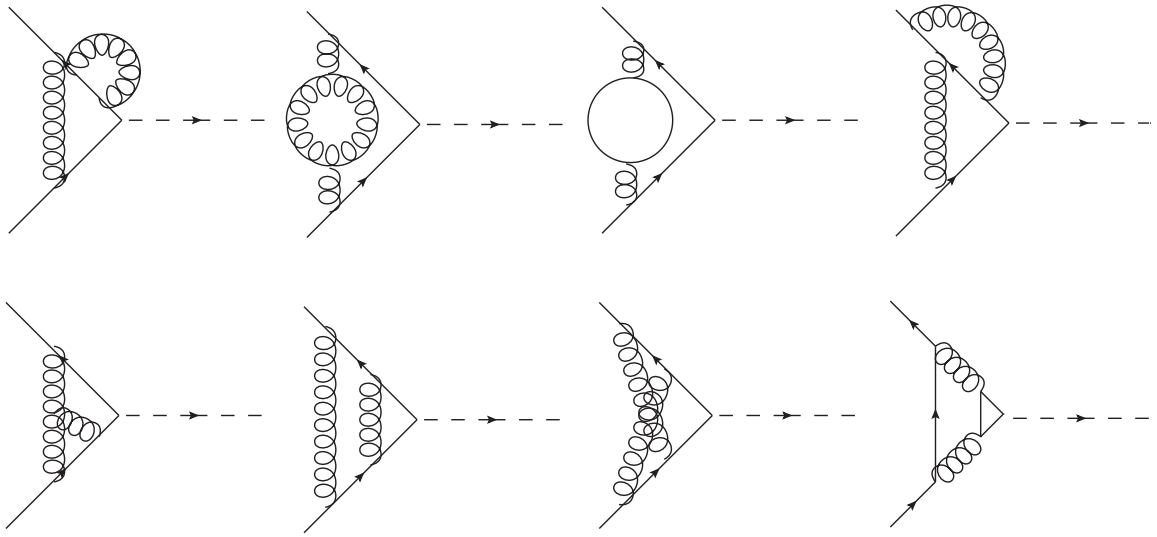

Figure 3.3: Two-loop diagrams contributing to the NNLO QCD corrections to Drell Yan.

first carried out in Refs. [46,47]) arise from partonic diagrams for Z production containing QED (i.e. e-order) vertices, where we would have to consider the terms coming from a real photon emission from one of the quark legs ($q\bar{q} \to Z\gamma$ squared, as showed in Fig. 3.2b) and also the interference between the one loop corrections to $q\bar{q}$, originated from a virtual photon between legs 1 and 2 (see the virtual diagram in figure 3.2b), with the leading order diagram of figure 3.1.

In this case, the results for the NLO QED corrections may be easily obtained in dimensional regularization, which we can express within this notation as

$$\begin{aligned} w_Z^{(0,1)} = \sum_{i \in Q,\bar{Q}} \big\{ & c_i q_i(x_1)\bar{q}_i(x_2) e_i^2 \Delta_{q\bar{q}}^{(1)}(x) \\ & \left(q_i(x_1)\gamma(x_2) + \gamma(x_1)q_i(x_2)\right) c_i 2C_A e_i^2 \Delta_{qg}^{(1)}(x) \big\}. \end{aligned} \tag{3.1.15}$$

Here, $\gamma(x)$ stands for the photon distribution within the proton (that has been recently determined by the LUXqed approach [41,42]) and the electric charges of the quarks e_i for the QED coupling. As can be notably seen, $\Delta_{q\bar{q}}^{(1)}(x)$ and $\Delta_{qg}^{(1)}(x)$ are the same correction functions than in the previous QCD case, which means that, for the next to leading order, the QCD and QED contributions are almost equal for each channel. In fact, the main differences, apart from the gluon and photon PDFs and flux factors, are the color structures arising from each QCD vertex, which are to be changed by the electric charge times a δ of color, in the QED case.

This behavior is not surprising, given that the QED $q\bar{q}\gamma$ and the QCD $q\bar{q}g$ vertices have the same structure, except for the color factors and the couplings. Furthermore, in this case

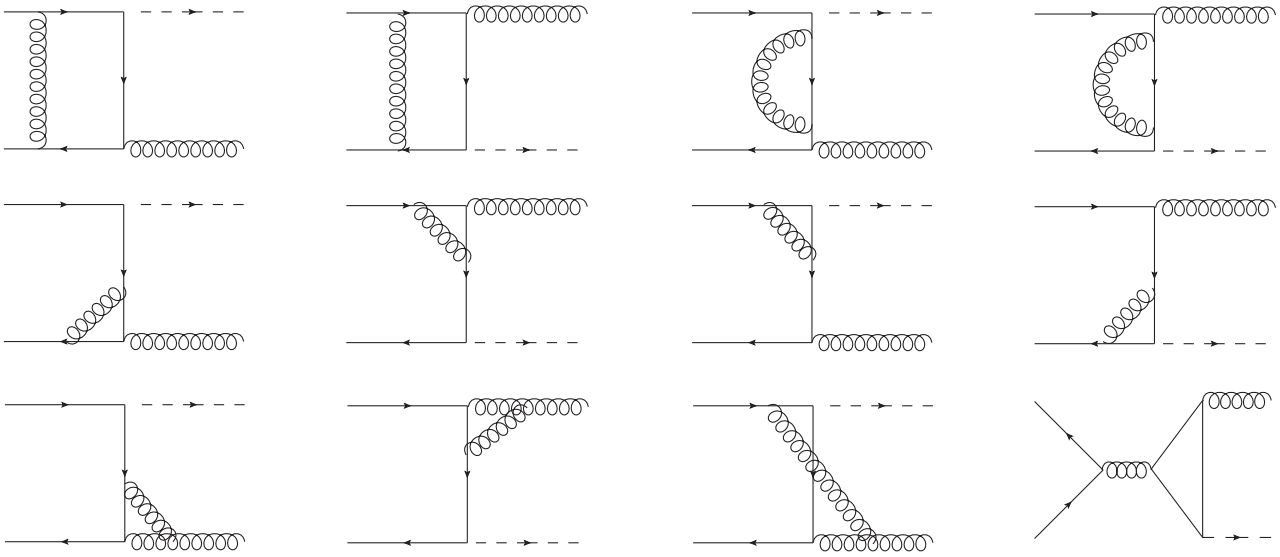

Figure 3.4: One-loop plus one parton emission diagrams contributing to the NNLO QCD corrections to Drell Yan.

of NLO corrections to Drell Yan, none of the non-abelian QCD vertices is present in the diagrams, which makes the calculations almost entirely analogous. This similarity will be very useful to complete the next order.

3.1.2 NNLO QCD Results

In order to improve the theoretical precision for the process and match the accuracy achieved at the LHC, we should go one step further and address the NNLO corrections.

While the full set of next to next to leading order contributions to the Drell Yan cross section (in the sense of Eq. (1.0.1)) is formed by pure QCD, pure QED and also mixed order terms, we will first discuss the pure NNLO QCD terms, which were completed for the first time in Ref. [19]. These are expected to be the biggest at this order, given that $\alpha_s^2 > \alpha_s\alpha > \alpha^2$.

In principle, the computation of $\mathcal{O}(\alpha_s^2)$ terms involves, as any NNLO calculation, the evaluation of double-virtual, single-virtual plus one parton emission and double parton emission contributions. Additionally, in this case one has to consider a greater number of parton subprocesses: $q\bar{q}$ and qg, as in the NLO case, but also qq and gg, which complete the set of parton-parton reactions at this order.

For the sake of completeness and in order to present the full set of topologies inherent to the NNLO corrections, which will also be crucial to obtain the mixed QCD$\otimes$QED and pure NNLO QED terms, we recall the relevant diagrams for the NNLO QCD contributions, as

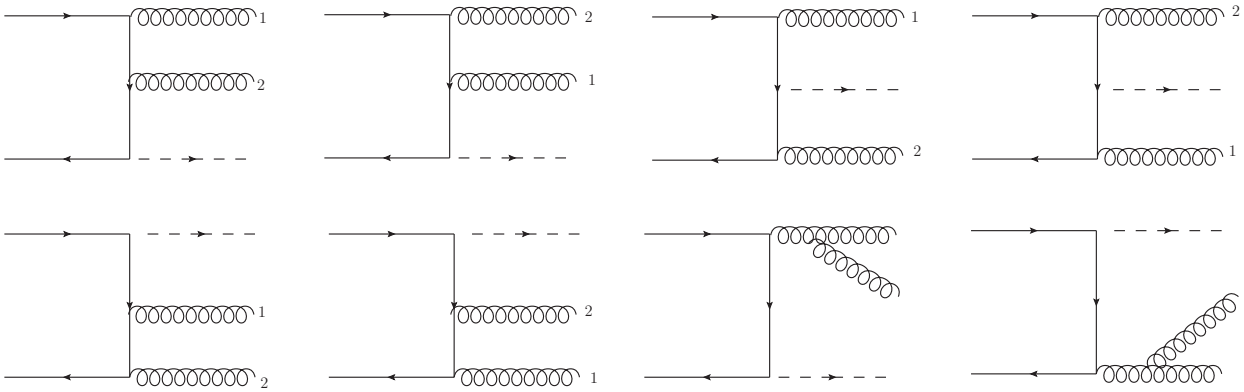

Figure 3.5: Double-real diagrams contributing to the NNLO QCD corrections to Drell Yan.

presented in Ref. [19] in figures (3.3-3.7). Whereas the topologies in the figures for stand for quark-initiated processes, the diagrams for all the quark channels, as well as the remaining qg and gg contributions can be obtained from these diagrams via crossing.

The calculation of the terms in figures (3.3-3.7) was carried out in pieces as follows: the qq process was calculated in Ref. [104] (see figure 3.7), the soft and virtual gluon contributions from the $q\bar{q}$ process with two gluons or a quark pair in the final state were determined in Refs. [105, 106] (see figures (3.3-3.6)), and the computation of the gg subprocess was performed in Ref. [107] (see fig. 3.5). Finally, the hard gluon contribution to the $q\bar{q}$ subprocess (figures (3.4-3.6)), the $\mathcal{O}(\alpha_s)$ correction to the qg subprocess (figures 3.4 and 3.5) and all the possible interference terms between the various $q\bar{q} \to q\bar{q}Z$ subprocesses (figures (3.6-3.7)) were obtained in Ref. [19], thus completing the $\mathcal{O}(\alpha_s^2)$ corrections.

Here, in order to present the full set of NNLO corrections to the Drell-Yan Z production, we recall the order α_s^2 results from [19] and rewrite them in the notation of Eq. (3.1.4), as performed in Ref. [2]:

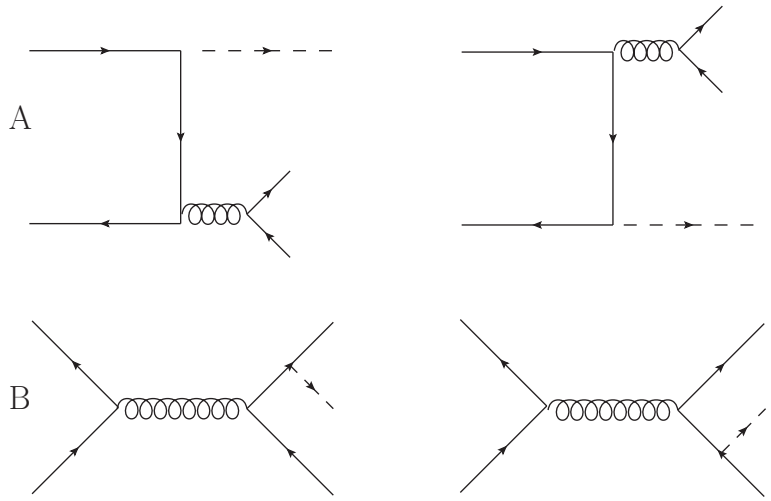

Figure 3.6: $q\bar{q}$ annihilation diagrams contributing to the NNLO QCD corrections to Drell Yan.

$$
\begin{aligned}
w_Z^{(2,0)} = & \sum_{i\in Q,\bar{Q}} q_i(x_1)\bar{q}_i(x_2) \\
& \times \Bigg\{ c_i C_F \left(C_A \Delta_{q\bar{q}}^{(2)C_A}(x) + C_F \Delta_{q\bar{q}}^{(2)C_F}(x) + n_F \Delta_{q\bar{q}}^{(2)n_F}(x) + \beta_0^{QCD} \Delta_{q\bar{q}}^{(1)}(x) \log\left(\frac{\mu_R^2}{\mu_F^2}\right)\right) \\
& + \sum_{k\in Q} \left[c_k \Delta_{q\bar{q}}^{(2)f}(x) + a_i a_k \Delta_{q\bar{q}}^{(2)ax}(x) \right] C_F \Bigg\} \\
& + \sum_{i\in Q,\bar{Q}} c_i q_i(x_1) q_i(x_2) \Delta_{qq}^{(2)\text{id}}(x) C_F \left(C_F - \frac{1}{2} C_A \right) \\
& + \sum_{i,j\in Q,\bar{Q}} q_i(x_1) q_j(x_2) C_F \left[(c_i + c_j) \Delta_{qq}^{(2)\text{ non-id}}(x) + v_i v_j \Delta_{q_i q_j}^{(2)\text{non-id, V}}(x) + a_i a_j \Delta_{qq}^{(2)\text{non-id, A}}(x) \right] \\
& + \sum_{i\in Q,\bar{Q}} (q_i(x_1) g(x_2) + g(x_1) q_i(x_2)) c_i \\
& \qquad \times \left[C_A \Delta_{qg}^{(2)C_A}(x) + C_F \Delta_{qg}^{(2)C_F}(x) + \beta_0^{QCD} \Delta_{qg}^{(1)}(x) \log\left(\frac{\mu_R^2}{\mu_F^2}\right) \right] \\
& + g(x_1) g(x_2) \left(\sum_{k\in Q} c_k \right) \left(\Delta_{gg}^{(2)C_A}(x) + \Delta_{gg}^{(2)C_F}(x) \right)
\end{aligned}
\tag{3.1.16}
$$

where several correction terms Δ were introduced. Here we denote with a C_A superscript the corrections coming from the non-abelian part of the contributions (only relevant for the NNLO QCD contributions), with n_F the ones that involve a sum over fermion families and with C_F the rest of the abelian contributions. All the Δ correction terms needed for Eq. (3.1.16) are detailed in the Appendix A.

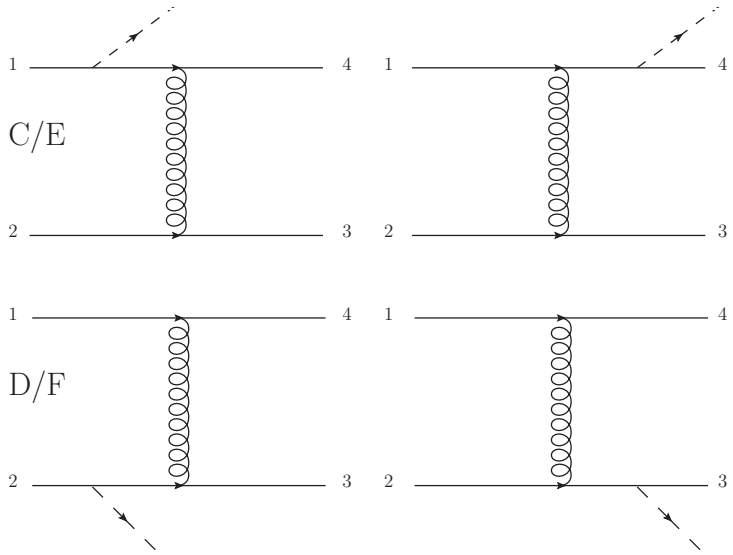

Figure 3.7: Gluon exchange graphs contributing to the NNLO QCD corrections to Drell Yan. The topologies here address the subprocesses $q\bar{q} \to Zq\bar{q}$ and $qq \to Zqq$ with both identical and non-identical quarks in the initial or the final state.

3.2 NNLO Mixed QCD⊗QED and QED^2 corrections

Once the pure QCD contributions have been presented, one can address the calculation of Drell Yan corrections that involve QED vertices at the partonic level. The most important, after the consideration of the NLO QED terms in Eq. (3.1.15), are the NNLO mixed contributions to the production of a Z boson. These, together with the NNLO QED terms, involve the calculation of a large number of Feynman diagrams, but the relevant topologies are fully included within those of the NNLO QCD, which were shown in the previous section in the figures (3.3-3.7). As has been stated when presenting to the NLO corrections in Eqs. (3.1.9) and (3.1.15), and checked all along this work in every QCD quantity calculated, the resemblance between the QED vertex and the abelian $q\bar{q}g$ QCD interaction usually makes it possible to convert QCD quantities into QED ones. Besides, a first *abelianisation procedure* was developed in order to obtain the QED corrections to the Altarelli-Parisi splitting kernels, in Refs. [39, 40].

In this sense, there might be a mapping between the QCD result for Drell Yan and both the mixed QCD⊗QED and pure electromagnetic corrections, if one could get rid of the non-abelian terms in the calculation and handle color and flux factors within the abelian QCD part. As we pointed out in Ref. [2], there are interestingly two ways to obtain these mixed QCD⊗QED and QED^2 contributions. On the one hand, one could approach the same way as

in the NNLO QCD case and compute all the diagrams for each partonic channel involved in the production. But on the other, we could observe that the relevant diagrams and topologies that take part in the calculation are completely included within the set needed for the NNLO QCD case, except for the fact the QCD corrections involve $q\bar{q}g$ and ggg vertices, while the other involve only $q\bar{q}\gamma$ ones. On top of that, we could take advantage of the similar structures of the QCD $q\bar{q}g$-vertex and the QED $q\bar{q}\gamma$-vertex by observing that these abelian QCD contributions could be converted to QED ones by taking care of the color and flux factors. Additionally, the diagrams containing gluons self-interactions, which arise exclusively from the non-abelian part of QCD, do not have any correlation with the mixed order nor with the NNLO QED terms, and thus do not contribute in these cases.

In the next section we will analyze the contributing diagrams for each interaction and take the corresponding abelian limit from the existing NNLO QCD calculation. Thus we will obtain the mixed QCD⊗QED terms.

3.2.1 Abelianisation

To calculate the mixed contributions we need to compute the correction terms for the $q\bar{q}$, qq, qg, $q\gamma$ and $g\gamma$ channels. In order to schematize the procedure used to accomplish the mixed order and without loosing generality, we describe the algorithm of *gluon-photon interchange* taking as an example the most relevant $q\bar{q}$ channel. Furthermore, all the remaining contributions for the other channels could be obtained via crossing.

First of all, we analyze all the topologies inherent to each partonic subprocess in QCD and determine the corresponding color factors, coming from the color structure in the vertices. Then we replace a gluon by a photon in each diagram and profit from the similarity in QED and QCD fermion coupling factors to pin down the abelian parts of both calculations. Moreover, given that the photon has no color, non-abelian terms (i.e. all the terms arising from NNLO QCD diagrams that contain three or four gluon vertices) do not contribute to QED corrections and therefore can be thrown out. Thus, we recalculate the color factors for the mixed topologies attained identifying changes and substitutions to be made in previous QCD results in order to obtain mixed order QCD⊗QED correction terms.

For the explicit case of the $q\bar{q}$ channel, in order to show how the method works and given that the color factors in the partonic cross section only depend on the QCD structure, we concentrate on diagrams with double real emission which appear only to tree level (the same

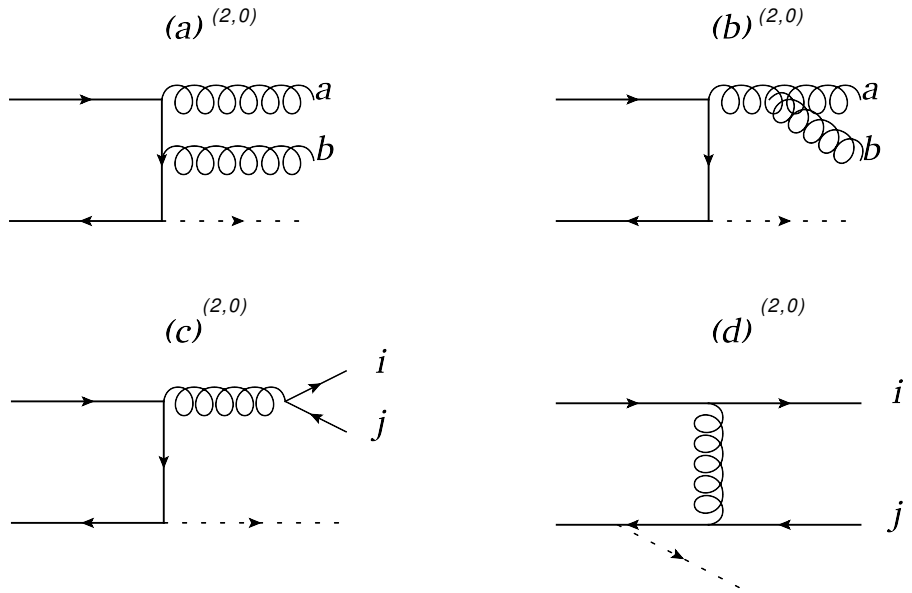

Figure 3.8: Some of the diagrams contributing to NNLO QCD corrections to Drell-Yan.

considerations can be applied to the two-loop and one-loop plus real emission contributions). As can be observed in figure 3.8, and check in figures (3.3-3.7), there are four kinds of diagrams to consider, which we will label with the supra-index (k, l) according to the total number of QCD (k) and QED (l) vertices for each topology. It is also important to note that the order of external momenta does affect the color structure of the diagram. In this sense, we will refer as (a) to the diagram showed in figure 3.8, while (a') represents the corresponding diagram obtained after crossing the final state parton lines. There we can recognize different color factors, according to the configurations of color matrix traces in the calculation of each contribution to the partonic cross section.

For example, terms corresponding to the calculation of $\left|(a)^{(2,0)}\right|^2$ in NNLO QCD result proportional to $\frac{1}{2N_C^2} Tr\left[T^b T^a T^a T^b\right] = \frac{1}{2N_C} C_F^2$, where the N_C^2 in the denominator arises due to the average over the color factor of the incoming quarks and the symmetry factor $1/2$ is due to the appearance of two identical gluons in the final state. For the case of $\left[(a)^{(2,0)} \times (a'^*)^{(2,0)}\right]$ both abelian and non-abelian contributions appear resulting in a factor $\frac{1}{2N_C^2} Tr\left[T^b T^a T^b T^a\right] = \frac{1}{2N_C} C_F\left(C_F - C_A/2\right)$ and, when considering terms from $\left[(b)^{(2,0)} \times (a^*)^{(2,0)}\right]$, they result proportional to $\frac{1}{2N_C^2}\ f^{abc} Tr\left[T^c T^a T^b\right] = \frac{1}{2N_C^2}\ Tr\left[[T^a, T^b] T^a T^b\right] = -\frac{1}{2N_C}(C_F C_A/2)$, a purely non-abelian contribution.

Once color factors are characterized for each term, we choose a gluon in the diagram, replace it by a photon and recalculate the color structure, thus obtaining modified diagrams with the corresponding new factors for QCD⊗QED corrections. These are shown in figure 3.9.

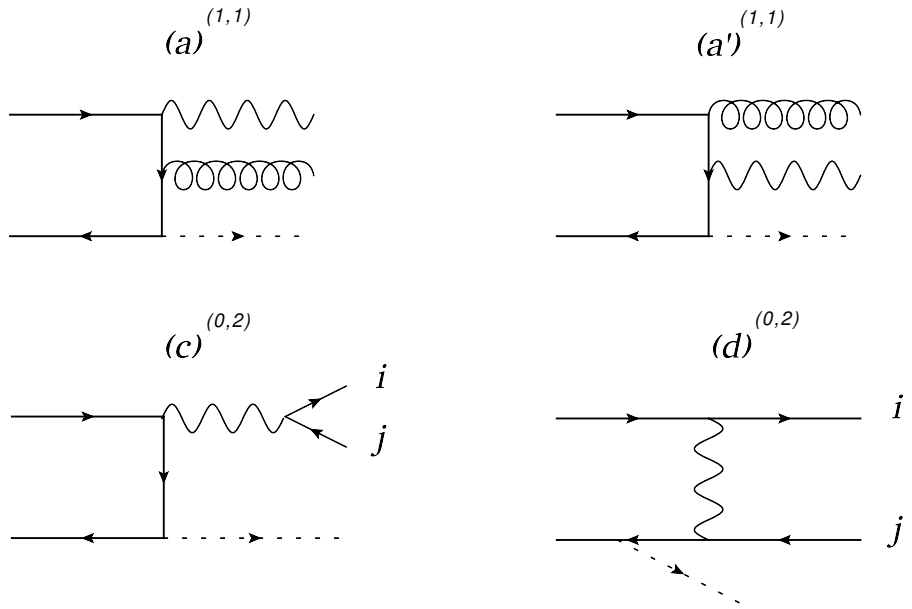

Figure 3.9: Diagrams that result after applying the abelianisation procedure to the real NNLO QCD corrections in figure 3.8.

Naturally, all the diagrams of type (b) (i.e. topologies containing at least one 3-gluon-vertex), which always contribute to second order for the NNLO QCD calculation in this process, vanish when considering the abelian limit.

Taking this into account, we find that the modified factors for $\left|(a)^{(1,1)}\right|^2$ and $\left[(a)^{(1,1)} \times (a'^*)^{(1,1)}\right]$ are both given by $\frac{e_q^2}{N_C^2} Tr[T^a T^a] = \frac{e_q^2}{N_C} C_F$, where we have included the charge of the quark for the QED coupling, while the non-abelian one obviously vanishes. Here we may notice that all the color factors proportional to C_A, which corresponds to non-abelian part of the calculation, could be thrown out when considering the abelian limit, while the ones proportional to C_F^2 are to be replaced by $2e_q^2 C_F$, thus obtaining QCD⊗QED factors in each case. It is worth noticing by performing the same analysis for the topology shown in figure 3.8c, i.e. the production of a $q\bar{q}$ pair, that also the color factor T_R vanishes when the similar contribution is analyzed in the QCD⊗QED case, since the result for $\left[(c)^{(2,0)} \times (c^*)^{(0,2)}\right]$ becomes proportional to $Tr[T^a]$. Therefore, since terms proportional to both C_A and T_R are vanishing, the same occurs for terms proportional to β_0^{QCD} in the original pure QCD calculation, consistent with the fact that no renormalization is needed at this order either for the QED or QCD couplings[5]. Same wise, only a few contributions survive in the products of the type $\left[(c)^{(2,0)} \times (d^*)^{(0,2)}\right]$ and $\left[(d)^{(2,0)} \times (d'^*)^{(0,2)}\right]$, i.e. the interference of amplitudes with one photon and with one

[5] As stated above, we consider the Born coupling between the quarks and the Z in the sense of an effective coupling.

Color factors in $q\bar{q}$			
diagram	α_s^2	$\alpha \times \alpha_s$	α^2
$\lvert(a)\rvert^2$	C_F^2	$2e_q^2 C_F$	e_q^4
$(d) \times (d^*)$	$C_F T_R$	0	$C_A\, e_i^2 e_j^2$
$(c) \times (c^*)$	$n_F\, C_F T_R$	0	$e_q^2 \left[N_C \sum_{k\epsilon Q} e_k^2 + \sum_{k\epsilon L} e_k^2 \right]$
$(a) \times (a'^*)$	$C_F^2 - \frac{C_F\, C_A}{2}$	$2e_q^2 C_F$	e_q^4
$(d) \times (d'^*)$	$C_F^2 - \frac{C_F\, C_A}{2}$	$2e_q^2 C_F$	e_q^4
$(b) \times (a^*)$	$-\frac{C_F\, C_A}{2}$	0	0
$(c) \times (d^*)$	$C_F^2 - \frac{C_F\, C_A}{2}$	$2e_q^2 C_F$	e_q^4

Table 3.1: Color factors corresponding to $q\bar{q}$ channel for each contribution to NNLO QCD⊕QED corrections to Drell-Yan, up to an overall $\frac{1}{2N_C}$ factor. Focusing on α^2 factors, the third column includes sums over sets of quark (Q) and lepton (L) final state charges, while e_i and e_j refer to different quark flavour charges in the scattering.

gluon exchange.

This strategy can be extended for all the topologies in $q\bar{q}$. In Table 3.1 we show the different color factors (after factorizing an overall factor of $1/2N_C$) for diagrams contributing to $\sigma^{(2,0)}$, and the resulting ones after the abelianisation procedure corresponding to $\sigma^{(1,1)}$. The replacements in the color structures needed to go from the NNLO QCD coefficients to the QCD⊗QED ones can be directly read from the entries in Table 3.1.

As an important feature, this method shows to be versatile in order to obtain NNLO QED corrections to Drell-Yan as well (i.e. the calculation of $\sigma^{(0,2)}$), if a deeper abelian limit is considered in this case. Here, by turning two gluons into photons from the topologies of NNLO QCD calculation one can recover correction terms up to second order in α, thus completing the set of QCD⊕QED NNLO corrections to Drell-Yan, in the sense of Eq. (4.3.1). The corresponding color factors (including electric charges of both quarks and leptons that might appear in the final state) are also shown in Table 3.1 for the $q\bar{q}$ channel.

The same occurs for other channels, after treating carefully the initial flux factor, which depends on the color properties of initial state particles. For instance, both $q\gamma$ and qg contributions to $\sigma^{(1,1)}$ can be obtained from the qg calculation for NNLO QCD corrections, by choosing the initial or final state gluon, respectively, to perform the abelianisation and following the procedure detailed above. Particularly, in the case of γg channel, we have performed as a

check the explicit calculation of the fixed order corrections, finding perfect agreement with the result obtained by applying the abelianisation procedure.

By following this path, we managed to calculate all the expressions for the Mixed QCD⊗QED and QED^2 correction coefficients $w^{(1,1)}$ and $w^{(0,2)}$, which read:

$$
\begin{aligned}
w_Z^{(1,1)} = & \sum_{i\in Q,\bar{Q}} q_i(x_1)\bar{q}_i(x_2)c_i 2e_i^2 C_F \Delta_{q\bar{q}}^{(2)C_F}(x) \\
& + \sum_{i\in Q,\bar{Q}} q_i(x_1)q_i(x_2)c_i 2e_i^2 C_F \Delta_{qq}^{(2)\mathrm{id}}(x) \\
& + \sum_{i\in Q,\bar{Q}} \left[2C_A C_F (q_i(x_1)\gamma(x_2) + \gamma(x_1)q_i(x_2)) + (q_i(x_1)g(x_2) + g(x_1)q_i(x_2))\right] \\
& \qquad \times c_i e_i^2 \Delta_{qg}^{(2)C_F}(x) \\
& + \left(g(x_1)\gamma(x_2) + \gamma(x_1)g(x_2)\right) 2C_A \left(\sum_{k\in Q} c_k e_k^2\right) \Delta_{gg}^{(2)}(x) \qquad (3.2.1)
\end{aligned}
$$

$$
\begin{aligned}
w_Z^{(0,2)} = & \sum_{i\in Q,\bar{Q}} q_i(x_1)\bar{q}_i(x_2) \\
& \times \left\{ c_i e_i^2 \left(e_i^2 \Delta_{q\bar{q}}^{(2)C_F}(x) + 2\left[N_C \sum_{k\in Q} e_k^2 + \sum_{k\in L} e_k^2\right] \Delta_{q\bar{q}}^{(2)n_F}(x) + \beta_0^{QED} \Delta_{q\bar{q}}^{(1)}(x) \log\left(\frac{\mu_R^2}{\mu_F^2}\right)\right)\right. \\
& + \sum_{k\in Q} \left[c_k \Delta_{q\bar{q}}^{(2)f}(x) + a_i a_k \Delta_{q\bar{q}}^{(2)ax}(x)\right] 2C_A e_i^2 e_k^2 \\
& \left. + \sum_{k\in L} \left[c_k \Delta_{q\bar{q}}^{(2)f}(x) + a_i a_k \Delta_{q\bar{q}}^{(2)ax}(x)\right] 2e_i^2 e_k^2 \right\} \\
& + \sum_{i\in Q,\bar{Q}} c_i q_i(x_1) q_i(x_2) \Delta_{qq}^{(2)\mathrm{id}}(x) e_i^4 \\
& + \sum_{i,j\in Q,\bar{Q}} q_i(x_1) q_j(x_2) 2C_A e_i^2 e_j^2 \\
& \qquad \times \left[(c_i + c_j)\Delta_{qq}^{(2)\text{non-id}}(x) + v_i v_j \Delta_{q_i q_j}^{(2)\text{non-id, V}}(x) + a_i a_j \Delta_{qq}^{(2)\text{non-id, A}}(x)\right] \\
& + \sum_{i\in Q,\bar{Q}} (q_i(x_1)\gamma(x_2) + \gamma(x_1)q_i(x_2)) c_i 2C_A e_i^2 \left[e_i^2 \Delta_{qg}^{(2)C_F}(x) + \beta_0^{QED} \Delta_{qg}^{(1)\gamma}(x) \log\left(\frac{\mu_R^2}{\mu_F^2}\right)\right] \\
& + \gamma(x_1)\gamma(x_2) 4C_A \left[N_C \sum_{k\in Q} c_k e_k^4 + \sum_{k\in L} c_k e_k^4\right] \Delta_{gg}^{(2)C_F}(x). \qquad (3.2.2)
\end{aligned}
$$

These are expressed, like the results for the NNLO QCD in Eq. (3.1.16), in terms of the coefficients Δ presented in the Appendix A.

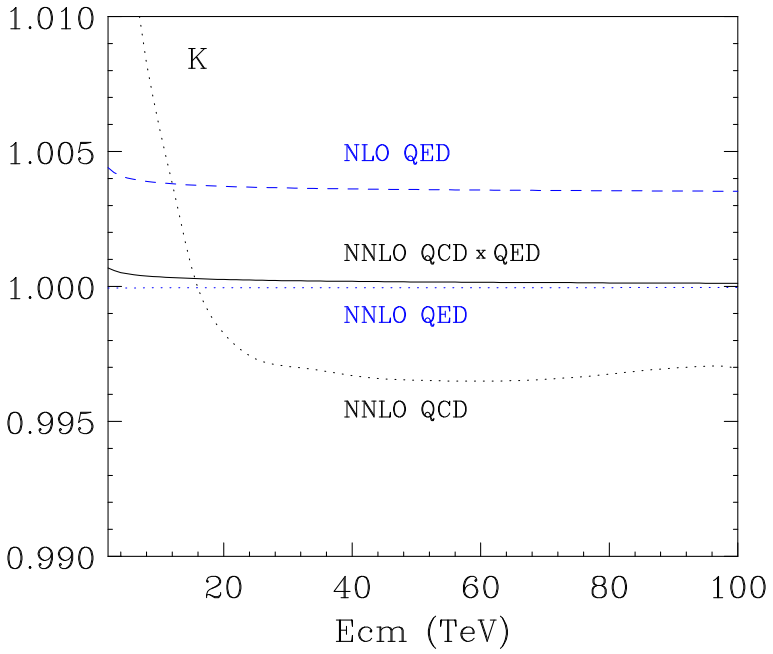

Figure 3.10: K-factors for the different distributions as defined in Eq.(3.3.1). The (blue) dashed line corresponds to K^{NLO}_{QED}, the (blue) dotted line to K^{NNLO}_{QED}, the solid line to the mixed $K^{NNLO}_{QCD\otimes QED}$ and the (black) dotted line to the pure NNLO QCD corrections K^{NNLO}_{QCD}.

3.3 NNLO Results and Phenomenology

In this section we study the phenomenology of the total inclusive cross section, i.e. in all the decay channels of the Z, within the narrow-width approximation. To this end, a specific code was written which makes use of the LHAPDF [108] package to interpolate sets of parton distribution functions.

For the phenomenological study, unless explicitly stated, we set the renormalization and factorization scales to $\mu_R = \mu_F = M_Z$. For both interactions, we set the running coupling at the corresponding renormalization scale (i.e. $\alpha(M_Z) \sim \frac{1}{128}$ [6]) and always use the parton distributions to NNLO (QCD) accuracy [13–15, 109] with the corresponding QED corrections from LUXqed [41, 42]. In figure 3.10 we plot the K-factors for different orders as a way to quantify the size of the QED and QCD corrections to Drell-Yan at different centre-of-mass energies.

Here the K-factor is defined as the ratio of the cross-section computed at a given order

[6] For the sake of simplicity we make the same choice for the value of the coupling between quarks and the Z boson in the Born cross section in Eq. (3.1.2).

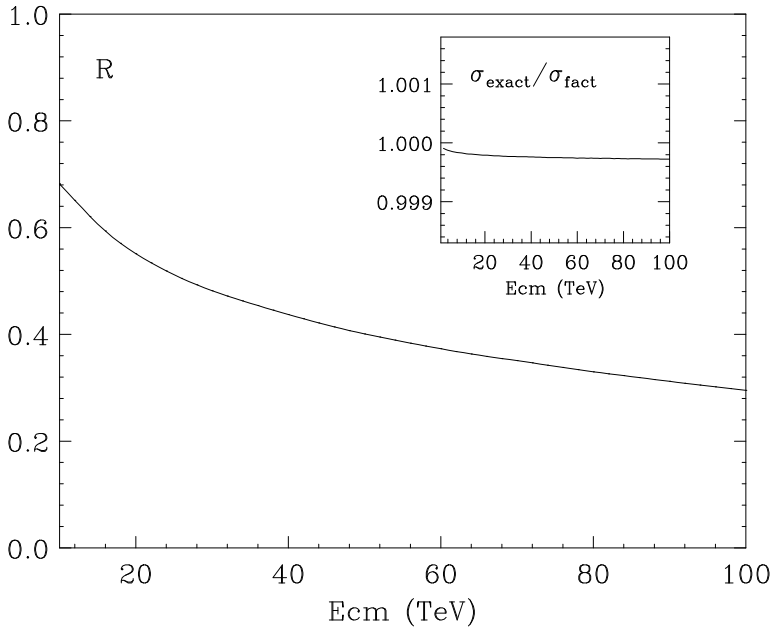

Figure 3.11: Ratio R between the exact and the factorization approximation for the mixed QCD⊗QED contributions. The inset plot shows the ratio of the cross section computed exactly and with the factorization approximation for the mixed term.

over the previous one, i.e.

$$\begin{aligned} K_{QED}^{NLO} &= \frac{\sigma^{(0,0)} + \alpha\,\sigma^{(0,1)}}{\sigma^{(0,0)}} \\ K_{QCD}^{NNLO} &= \frac{\sigma^{(0,0)} + \alpha_s\,\sigma^{(1,0)} + \alpha_s^2\,\sigma^{(2,0)}}{\sigma^{(0,0)} + \alpha_s\,\sigma^{(1,0)}} \\ K_{QED}^{NNLO} &= \frac{\sigma^{(0,0)} + \alpha\,\sigma^{(0,1)} + \alpha^2\,\sigma^{(0,2)}}{\sigma^{(0,0)} + \alpha\,\sigma^{(0,1)}} \\ K_{QCD\otimes QED}^{NNLO} &= \frac{\sigma^{(0,0)} + \alpha\,\sigma^{(0,1)} + \alpha_s\,\sigma^{(1,0)} + \alpha\alpha_s\,\sigma^{(1,1)}}{\sigma^{(0,0)} + \alpha\,\sigma^{(0,1)} + \alpha_s\,\sigma^{(1,0)}}. \end{aligned} \tag{3.3.1}$$

As can be observed, the NNLO QCD corrections are of the same (~ 5 per mille level) order, but typically with the opposite sign, as the NLO QED corrections, as expected from the simple counting $\alpha_s^2 \sim \alpha$. The mixed QCD⊗QED turn out to be positive and below the per mille level over the whole range of energies spanned in the plot. Interestingly, due to the particular dependence of the NNLO QCD corrections with the energy, with a sign change around $\sqrt{S} \sim 18$ TeV, for the LHC at $\sqrt{S} \sim 14$ TeV the mixed QCD⊗QED corrections are only a factor of ~ 3.5 smaller than the pure NNLO QCD contributions. Furthermore, for lower centre-of-mass energies $\sqrt{S} \sim 2$ TeV the mixed terms almost reach the per mille level and are just a factor of 5 smaller than the NLO QED ones, showing that the elementary counting of

couplings can fail under certain kinematical conditions. The pure NNLO QED terms, also plotted in figure 3.10, are negative but the corrections always remain at the $\mathcal{O}(10^{-5})$ level.

Even though for this particular observable the mixed QCD⊗QED contributions are small, it is interesting to study how well they can be approximated by the *factorization* assumption on QED plus QCD corrections, where it is assumed that $\kappa_{\text{fact}} = \left[K_{QED}^{NLO} \times K_{QCD}^{NLO}\right]_{\mathcal{O}(\alpha\alpha_s)} = \alpha\alpha_s \frac{\sigma^{(0,1)}\sigma^{(1,0)}}{\sigma^{(0,0)}\sigma^{(0,0)}}$, compared to the exact case $\kappa_{\text{mixed}} = \alpha\alpha_s \frac{\sigma^{(1,1)}}{\sigma^{(0,0)}}$. For that purpose, in figure 3.11 we plot the following quantity

$$R = \frac{\kappa_{\text{mixed}}}{\kappa_{\text{fact}}} = \frac{\sigma^{(0,0)}\sigma^{(1,1)}}{\sigma^{(0,1)}\sigma^{(1,0)}}, \tag{3.3.2}$$

which is the ratio between the exact and the approximated factorized contribution. As it can be observed, the factorization approach fails to reproduce the correct behavior of the mixed contribution typically by a factor of two or more. Of course, given the size of the corrections, the effect of the factorized treatment of these contributions is small at the level of the cross section, as shown in the inset plot of figure 3.11, where we show the ratio between the cross section computed exactly and within the factorization approach, but the situation might not hold for other observables or even for more exclusive distributions in Drell-Yan.

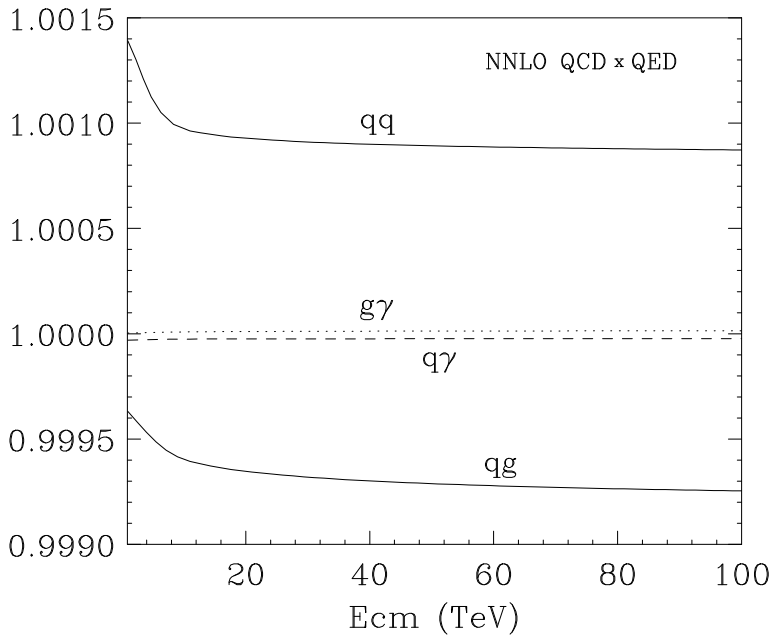

Figure 3.12: Contribution to the mixed QCD⊗QED K-factor from the different channels. Here the label q accounts for both quarks and antiquarks and qq represents the sum of $q\bar{q}$ and qq.

In figure 3.12 we show the contribution to the mixed QCD⊗QED K-factor from the

different channels. It is noticeable that the photon initiated contributions are rather small, mostly due to the size of the photon pdf in the proton, as can be observed by comparing $q\gamma$ and qg contributions, which share the same partonic coefficient apart from the color factor. It is also clear that the different signs of qq (fully dominated by the born level $q\bar{q}$ channel and exceeding the per mille level) and qg contributions conspire to reduce the effect of the mixed QCD⊗QED corrections to the Drell-Yan cross section. Again, in more exclusive distributions this partial cancellation might be spoiled by some kinematical cuts, resulting in an increase of the mixed order corrections.

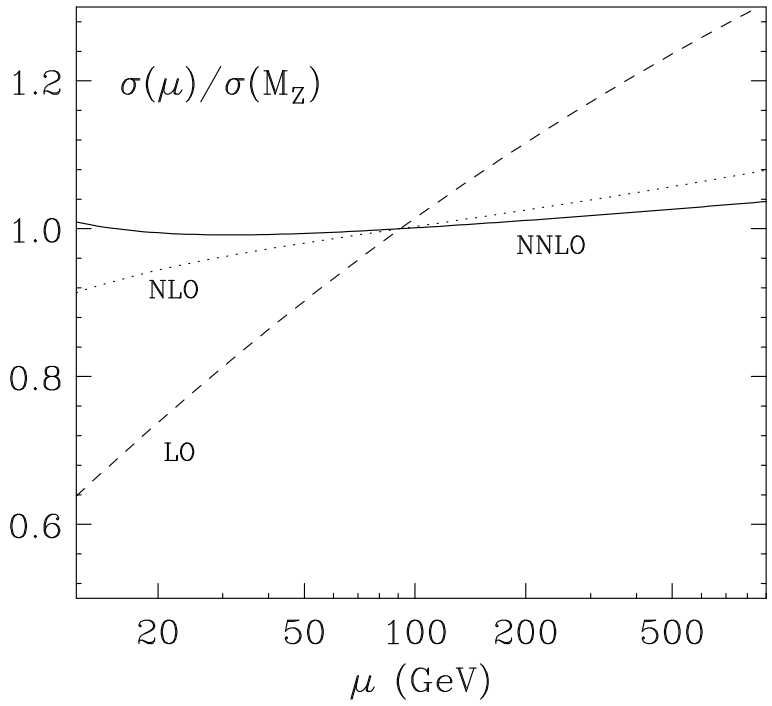

Figure 3.13: Cross sections corresponding to LO (dashes, $i+j$=0 in Eq. (4.3.1)), NLO(dots, $i+j$=0,1) and NNLO (solid, $i+j$=0,1,2) at different factorization and renormalization scales with $\mu_R = \mu_F = \mu$. All results are normalized by the corresponding cross section at $\mu = M_Z$.

Finally, we discuss the effect of the higher order contributions in the stabilization of the perturbative expansion in terms of the scale dependence for $\sqrt{S} = 13$ TeV (very similar behaviors are observed for other values of $\sqrt{S}$). In figure 3.13 we show the LO ($\sigma^{(0,0)}$), NLO ($\sigma^{(0,0)} + \alpha\,\sigma^{(0,1)} + \alpha_s\,\sigma^{(1,0)}$) and NNLO ($\sigma^{(0,0)} + \alpha\,\sigma^{(0,1)} + \alpha_s\,\sigma^{(1,0)} + \alpha\alpha_s\,\sigma^{(1,1)} + \alpha^2\,\sigma^{(0,2)} + \alpha_s^2\,\sigma^{(2,0)}$) cross sections for different values of the factorization and renormalization scales $\mu_R = \mu_F = \mu$, normalized by the corresponding value at the central scale $\mu = M_Z$. From the slope of the different curves, it is clearly visible the reduction in the scale dependence when including higher order corrections, mostly due to the dominant QCD effects but also thanks to the

inclusion of the QED and mixed contributions.

CHAPTER 4

Fully differential Drell Yan cross section at NNLO QCD⊗QED

As has been previously pointed out, high theoretical precision is needed in order to interpret the high-precision data of the LHC experiments. This scenario, together with the fact that the NNLO QCD perturbative corrections to the inclusive Drell Yan production have been found of the same order than the mixed QCD⊗QED ones at the LHC energies, motivates a new theoretical effort to go beyond NNLO QCD contributions within the kinematic distributions. In this Chapter we will focus on the mixed order QCD⊗QED corrections to Drell Yan pair production at the full differential level.

A crucial ingredient in the calculation of fully differential distributions are the so-called subtraction methods. For the case of pure QCD corrections to the hadroproduction of colorless final states, the q_T-subtraction method [99, 110, 111] has been extensively used in order to obtain NNLO-accurate predictions. In this Chapter we will extend the q_T-subtraction formalism in order to apply it to the calculation of $\mathcal{O}(\alpha_s\alpha)$ mixed corrections at a fully exclusive level. These results are of high value for transverse-momentum resummation at the corresponding logarithmic accuracy. In particular, we will describe the mixed QCD⊗QED corrections to the production of an off-shell Z boson decaying into a neutrino-antineutrino system $\nu\overline{\nu}$. We consider the simplest case of uncharged particles in the decay of the off-shell Z boson as a way to directly address the relevance of the initial state corrections to a number of exclusive observables.

In order to achieve this goal, we will first explicitly address the NNLO contributions for

each partonic channel, and handle the NLO infrared divergences due to soft and collinear emissions within the double-real and real-virtual topologies (see figures (3.4-3.7) in section 3.1.2) through the FKS-subtraction method (details for this method are shown in section 2.4), in this case slightly modified to deal with mixed order NNLO corrections with non-vanishing transverse momentum. Then we will go one step further and include the remaining $q_T = 0$ piece of the calculation by extending the q_T-subtraction method, originally developed for pure QCD processes, in order to get stability of the mixed order results within the region of small transverse momentum. In this sense, both the extension of the q_T-subtraction up to mixed order, and the calculation of the NNLO QCD⊗QED corrections to Drell Yan, are the main goals of this Chapter.

The next sections are organized as follows: first of all we describe the regions of small-q_T in the cross section by sketching the formalism of transverse momentum resummation [111–114]. In section 4.2 we introduce the q_T-subtraction, as it was originally formulated in Refs. [99,111] for the calculation of pure NNLO QCD contributions. In section 4.3 we extend the method to address the mixed QCD⊗QED corrections to Drell Yan. Finally, in section 4.4 we study the phenomenological impact of our results, by comparing the differential distributions.

4.1 Transverse-Momentum Resummation

4.1.1 Basics and notation

In order to introduce the q_T-subtraction formalism, we must first describe the general behavior of a differential cross section in the regions of small transverse momentum. To this end we will discuss the formalism as presented in Ref. [111] to calculate the q_T distribution of a generic colorless system up to NNLO in the strong coupling constant.

Let us consider the production of a system F with total invariant mass M and transverse momentum q_T, and no color in the final state. According to the QCD factorization theorem (see Eq. (2.3.2) in section 2.3), the corresponding transverse-momentum differential cross section $d\hat{\sigma}_F/dq_T^2$ for the production of F in hadronic collisions can be written as

$$\frac{d\sigma_F}{dq_T^2}(q_T, M, s) = \sum_{a,b} \int_0^1 dx_1 \int_0^1 dx_2 \, f_{a/h_1}(x_1, \mu_F^2) \, f_{b/h_2}(x_2, \mu_F^2) \, \frac{d\hat{\sigma}_{F\,ab}}{dq_T^2}(q_T, M, \hat{s}; \alpha_s(\mu_R^2), \mu_R^2, \mu_F^2) \, , \tag{4.1.1}$$

where $f_{a/h}(x,\mu_F^2)$ ($a = q_f, \bar{q}_f, g, \gamma$) are the parton densities of the colliding hadrons at the factorization scale μ_F, $d\hat{\sigma}_{F\,ab}/dq_T^2$ is the partonic cross sections, $\hat{s} = x_1 x_2 s$ is the partonic centre-of-mass energy, μ_R is the renormalization scale and $\alpha_s(q^2)$ is the running QCD coupling.

As it is well known [113,115–120], in the small-q_T region ($q_T \ll M$), the convergence of the fixed-order expansion is spoiled, since higher-order perturbative contributions to the partonic cross section $d\hat{\sigma}_{F\,ab}/dq_T^2$ are enhanced by powers of large logarithmic terms, $\ln^m(M^2/q_T^2)$. These are originated from soft and collinear final state radiation to the incoming partons that arise when considering perturbative corrections. As a consequence, to obtain reliable predictions at higher orders, these logarithmic terms have to be resummed to all orders in α_s.

To that end we can introduce the following decomposition of the partonic cross section in Eq. (4.1.1):

$$\frac{d\hat{\sigma}_{F\,ab}}{dq_T^2} = \frac{d\hat{\sigma}^{(\mathrm{res.})}_{F\,ab}}{dq_T^2} + \frac{d\hat{\sigma}^{(\mathrm{fin.})}_{F\,ab}}{dq_T^2}\,, \tag{4.1.2}$$

where the distinction between the two terms here is purely theoretical.

The first term in Eq. (4.1.2), $d\hat{\sigma}^{(\mathrm{res.})}_{F\,ab}$, contains all the logarithmically-enhanced contributions $(\alpha_s^n/q_T^2)\,\ln^m(M^2/q_T^2)$ at small q_T, and has to be evaluated by resumming them to all orders in α_s. The second term, $d\hat{\sigma}^{(\mathrm{fin.})}_{F\,ab}$, is free of such contributions, and can be computed by fixed-order truncation of the perturbative series. It is clear that we can locate any perturbative contribution proportional to $\delta(q_T)$ within $d\hat{\sigma}^{(\mathrm{res.})}_{F\,ab}$, as long as it also encodes the logarithmically-enhanced behavior. Additionally, whereas this "resummed" component could systematically be organized in classes of LL, NLL, ... terms, both the finite and resummed contributions have to be consistently matched at intermediate values of q_T, so as to obtain a theoretical prediction with uniform formal accuracy over the entire range of q_T, from $q_T \ll M$ up to $q_T \sim M$.

On the other hand, the resummation procedure has to be carried out in the impact-parameter space, to correctly take into account the kinematics constraint of transverse-momentum conservation. The resummed component of the transverse-momentum cross section in Eq. (4.1.2) is then obtained by performing the inverse Fourier (Bessel) transformation with respect to the impact parameter b. We write

$$\begin{aligned}\frac{d\hat{\sigma}^{(\mathrm{res.})}_{F\,ab}}{dq_T^2}(q_T, M, \hat{s}; \alpha_s(\mu_R^2), \mu_R^2, \mu_F^2) &= \frac{M^2}{\hat{s}} \int \frac{d^2\mathbf{b}}{4\pi}\, e^{i\mathbf{b}\cdot q_T}\, \mathcal{W}^F_{ab}(b, M, \hat{s}; \alpha_s(\mu_R^2), \mu_R^2, \mu_F^2) \\ &= \frac{M^2}{\hat{s}} \int_0^\infty db\, \frac{b}{2}\, J_0(bq_T)\, \mathcal{W}^F_{ab}(b, M, \hat{s}; \alpha_s(\mu_R^2), \mu_R^2, \mu_F^2)\,,\end{aligned} \tag{4.1.3}$$

where $J_0(x)$ is the 0th-order Bessel function.

The perturbative and process-dependent factor $\mathcal{W}^F_{ab}$ embodies the all-order dependence on the large logarithms $\ln M^2b^2$ at large b, which correspond to the q_T-space terms $\ln M^2/q_T^2$ that are logarithmically enhanced at small q_T (the limit $q_T \ll M$ corresponds to $Mb \gg 1$, since b is the variable conjugate to q_T).

Here, in order to present the corresponding structure of the logarithmic contributions, we will show some key features of the resummed partonic cross section. To this end, the N-moments of the process dependent factor $\mathcal{W}^F_{ab}$ for the all-order resummation can be organized in the form[1]

$$\mathcal{W}^F_N(b, M; \alpha_s(\mu_R^2), \mu_R^2, \mu_F^2) = \mathcal{H}^F_N\left(M, \alpha_s(\mu_R^2); M^2/\mu_R^2, M^2/\mu_F^2, M^2/Q^2\right) \times \exp\{\mathcal{G}_N(\alpha_s(\mu_R^2), L; M^2/\mu_R^2, M^2/Q^2)\} \ . \tag{4.1.4}$$

The function $\mathcal{H}^F_N$ does not depend on the impact parameter b and, therefore, it contains all the perturbative terms that behave as constants in the limit $b \to \infty$. The function $\mathcal{G}$ includes the complete dependence on b and, in particular, it contains all the terms that order-by-order in α_s are divergent when $b \to \infty$. In fact, all the large logarithmic terms $\alpha_s^n L^m$ with $1 \leq m \leq 2n$ are included in the form factor $\exp\{\mathcal{G}\}$. More importantly, all the logarithmic contributions to $\mathcal{G}$ with $n+2 \leq m \leq 2n$ are vanishing. This property [114–118] arises from the perturbative dynamics of generic gauge theories and from kinematics factorization in the impact parameter space. Additionally, this factorization between constant and logarithmic terms involves some degree of arbitrariness [121], since the argument of the large logarithms can always be rescaled as $\ln M^2b^2 = \ln Q^2b^2 + \ln M^2/Q^2$, provided that Q is independent of b and that $\ln M^2/Q^2 = \mathcal{O}(1)$ when $bM \gg 1$. To parametrize this arbitrariness we introduce a dependence on the so-called resummation scale Q, such that $Q \sim M$ (see the right-hand side of Eq. (4.1.4)). Also, we define the large logarithmic expansion parameter, L, as

$$L \equiv \ln \frac{Q^2b^2}{b_0^2} \ , \tag{4.1.5}$$

where the coefficient $b_0 = 2e^{-\gamma_E}$ ($\gamma_E = 0.5772\ldots$ is the Euler number) has a kinematical origin.

[1] the N-moments h_N of any function $h(z)$ of the variable z are defined as $h_N = \int_0^1 dz\, z^{N-1}\, h(z)$.

Now that we got all the ingredients to write $\mathcal{G}$ in a useful way, we perform a perturbative expansion in powers of a logarithmic parameter $\alpha_s L$. In this sense, $\mathcal{G}$ can be expressed as:

$$\begin{aligned}\mathcal{G}_N(\alpha_s, L; M^2/\mu_R^2, M^2/Q^2) &= L\, g^{(1)}(\alpha_s L) + g_N^{(2)}(\alpha_s L; M^2/\mu_R^2, M^2/Q^2) \\ &+ \frac{\alpha_s}{\pi}\, g_N^{(3)}(\alpha_s L; M^2/\mu_R^2, M^2/Q^2) \\ &+ \sum_{n=4}^{+\infty} \left(\frac{\alpha_s}{\pi}\right)^{n-2}\, g_N^{(n)}(\alpha_s L; M^2/\mu_R^2, M^2/Q^2) \ ,\end{aligned} \tag{4.1.6}$$

where $\alpha_s = \alpha_s(\mu_R^2)$ and the functions $g^{(n)}(\alpha_s L)$ are defined such that $g^{(n)} = 0$ when $\alpha_s L = 0$. Thus the term $Lg^{(1)}$ collects the LL contributions $\alpha_s^n L^{n+1}$; the function $g^{(2)}$ resums the NLL contributions $\alpha_s^n L^n$; $g^{(3)}$ controls the NNLL terms $\alpha_s^n L^{n-1}$, and so forth. Note that within the resummation approach, the parameter $\alpha_s L$ is formally considered as being of order unity. In this way, the ratio of two successive terms in the expansion (4.1.6) is formally of $\mathcal{O}(\alpha_s)$ (with no L enhancement). As a consequence, the resummed logarithmic expansion in Eq. (4.1.6) works as any customary fixed-order expansion in powers of α_s.

On the other hand, the function $\mathcal{H}_N^F$ in Eq. (4.1.4) does not contain large logarithmic terms to be resummed. It can be expanded in powers of $\alpha_s = \alpha_s(\mu_R^2)$ as

$$\begin{aligned}\mathcal{H}_N^F(M, \alpha_s; M^2/\mu_R^2, M^2/\mu_F^2, M^2/Q^2) &= \sigma_F^{(0)}(\alpha_s, M)\Big[1 + \frac{\alpha_s}{\pi}\, \mathcal{H}_N^{F\,(1)}(M^2/\mu_R^2, M^2/\mu_F^2, M^2/Q^2) \\ &+ \left(\frac{\alpha_s}{\pi}\right)^2 \mathcal{H}_N^{F\,(2)}(M^2/\mu_R^2, M^2/\mu_F^2, M^2/Q^2) \\ &+ \sum_{n=3}^{+\infty} \left(\frac{\alpha_s}{\pi}\right)^n \mathcal{H}_N^{F\,(n)}(M^2/\mu_R^2, M^2/\mu_F^2, M^2/Q^2)\Big] \ ,\end{aligned} \tag{4.1.7}$$

where $\sigma_F^{(0)} = \alpha_s^p\, \sigma_F^{(\mathrm{LO})}$ is the lowest-order partonic cross section for the hard-scattering process $h_1 + h_2 \to F(M, q_T)$.

In what comes to the factorization scale, the μ_F-dependence of $d\hat{\sigma}_{F\,ab}^{(\mathrm{res.})}/dq_T^2$ is due to the arbitrariness of the factorization assumption (see section 2.3.1), and therefore this dependence must be balanced with that of the PDFs. Given that the parton densities do not depend on the transverse momentum q_T, there is no reason to think μ_F can introduce any logarithmic dependence on b in the factor $\exp\{\mathcal{G}\}$. As a consequence, the perturbative expansion (4.1.7) of the function $\mathcal{H}_N^F$ depends on μ_F, while the exponent $\mathcal{G}$ of the form factor does not depend on μ_F and neither does on the factorization scheme used to define the parton densities.

Furthermore, the form factor is also process independent. It is produced by universal soft and collinear radiation from the QCD partons entering the hard-scattering process, which have nothing to do with the final state F of the collision. The dependence on the process, on the other hand, is fully taken into account by the hard-scattering function $\mathcal{H}_N^F$, that embodies contributions produced by virtual corrections at transverse-momentum scales $q_T \sim M$.

In general, in order to reduce the impact of unjustified resummed logarithms in the large-q_T region, it is common to express the form factor using a procedure inspired by that introduced in Ref. [122] to deal with kinematical constraints when performing soft-gluon resummation in e^+e^- event shapes. We consider the exponent $\mathcal{G}(\alpha_s, L)$ of the form factor in Eqs. (4.1.4) and (4.1.6) and replace

$$\mathcal{G}(\alpha_s, L) \;\longrightarrow\; \mathcal{G}(\alpha_s, \widetilde{L}) \;\; . \tag{4.1.8}$$

where $\widetilde{L}$ is defined as

$$\widetilde{L} \equiv \ln\left(\frac{Q^2 b^2}{b_0^2} + 1\right) \;\; . \tag{4.1.9}$$

In this way, within the resummation region $Qb \gg 1$ we have $\widetilde{L} = L + \mathcal{O}(1/(Qb)^2)$, and thus the replacement in Eq. (4.1.8) is fully legitimate to arbitrary logarithmic accuracy. On the other hand, although L and $\widetilde{L}$ are equivalent to organize the resummation formalism in the region $Qb \gg 1$, they lead to a different behavior of the form factor at small values of b: when $Qb \ll 1$, we have $\widetilde{L} \to 0$ and $\exp\{\mathcal{G}(\alpha_s, \widetilde{L})\} \to 1$. Therefore, the replacement (4.1.8) reduces the effect produced by the resummed contributions in the small-b region, where the use of the large-b resummation approach is no longer justified.

By following this path, one may be able to handle and compute both the hard function $\mathcal{H}_N^F$ and the form factor $\exp\{\mathcal{G}\}$ in Eq. (4.1.4), which makes it possible to get $d\hat{\sigma}_{F\,ab}^{(\mathrm{res.})}/dq_T^2$ in Eq. (4.1.1) at a given logarithmic accuracy.

Finally, with the aim to exploit the logarithmic behavior at small-q_T and establish a subtraction method to regulate the $q_T = 0$ divergences within the fixed order result, he have to exactly know the specific dependence of $\mathcal{H}_N^F$ and $\exp\{\mathcal{G}\}$ on the process, the PDFs and on the universal structure of soft and collinear radiation from the QCD partons entering the hard-scattering, respectively.

4.1.2 Perturbative coefficients

Now we must show how these ingredients in the resummed cross section can be expressed in terms of perturbative coefficients. This approach was fully formalized by Collins, Soper and Sterman in [113]. In order to achieve the expressions for $\mathcal{W}_N^F$ in Eq. (4.1.4), we can start from the consideration of the structure of the hadronic transverse-momentum differential cross section at small values of q_T. In fact, it can be written as

$$\frac{d\sigma_F}{dq_T^2}(q_T, M, s) = \frac{M^2}{s} \int_0^\infty db\, \frac{b}{2}\, J_0(bq_T)\, W^F(b, M, s) + \dots\ , \tag{4.1.10}$$

where the dots stand for terms that are not logarithmically enhanced at small q_T (large b). Considering that the quantity in Eq. (4.1.10) is the hadronic cross section, the b-space function $W^F(b, M, s)$ depends on the parton densities of the colliding hadrons. Also, it encodes all the real and virtual contributions due to soft and collinear radiation at small momenta, and the virtual corrections. As a consequence, the b-space function $W^F(b, M, s)$ will depend on the soft $A_c(\alpha_s)$ function, the flavour conserving collinear coefficients $B_c(\alpha_s)$ and the collinear functions $C_{ab}(\alpha_s, z)$, together with the parton distributions at the q_T-scale and the process-dependent factor H_c^F.

$$\begin{aligned} W_N^F(b,\ M\ ) = &\sum_c \sigma^{(0)}_{c\bar{c},\,F}(\alpha_s(M^2), M)\ H_c^F(\alpha_s(M^2))\ S_c(M, b) \\ &\times \sum_{a,b} C_{ca,\,N}(\alpha_s(b_0^2/b^2))\ C_{\bar{c}b,\,N}(\alpha_s(b_0^2/b^2))\ f_{a/h_1,\,N}(b_0^2/b^2)\ f_{b/h_2,\,N}(b_0^2/b^2). \end{aligned} \tag{4.1.11}$$

Here $f_{a/h,\,N}(\mu^2)$ are the N-moments of the parton density $f_{a/h}(z, \mu^2)$, and $\sigma^{(0)}_{c\bar{c},\,F}$ is the lowest-order cross section for the partonic subprocess $c+\bar{c} \to F$. The function $S_c(M, b)$ is the Sudakov form factor of the quark ($c = q, \bar{q}$) or of the gluon ($c = g$), and it has the following expression:

$$S_c(M, b) = \exp\left\{ -\int_{b_0^2/b^2}^{M^2} \frac{dq^2}{q^2} \left[A_c(\alpha_s(q^2))\ \ln\frac{M^2}{q^2} + B_c(\alpha_s(q^2)) \right] \right\}\ . \tag{4.1.12}$$

The functions A, B, C and H^F in Eqs. (4.1.11) and (4.1.12) are perturbative series in α_s:

$$A_c(\alpha_s) = \sum_{n=1}^{\infty} \left(\frac{\alpha_s}{\pi}\right)^n A_c^{(n)} \ , \tag{4.1.13}$$

$$B_c(\alpha_s) = \sum_{n=1}^{\infty} \left(\frac{\alpha_s}{\pi}\right)^n B_c^{(n)} \ , \tag{4.1.14}$$

$$C_{ab}(\alpha_s, z) = \delta_{ab}\,\delta(1-z) + \sum_{n=1}^{\infty} \left(\frac{\alpha_s}{\pi}\right)^n C_{ab}^{(n)}(z) \ , \tag{4.1.15}$$

$$H_c^F(\alpha_s) = 1 + \sum_{n=1}^{\infty} \left(\frac{\alpha_s}{\pi}\right)^n H_c^{F\,(n)} \ . \tag{4.1.16}$$

The functions A_c, B_c and C_{ab} are process independent, while H_c^F depends on the specific hard-scattering process.

On the other hand, comparing the partonic (Eq. (4.1.3)) and the hadronic (Eq. (4.1.11)) cross sections, we see that

$$W_N^F(b, M) = \sum_{a,b} \mathcal{W}_{ab,\,N}^F(b, M; \alpha_s(\mu_R^2), \mu_R^2, \mu_F^2)\ f_{a/h_1,\,N}(\mu_F^2)\ f_{b/h_2,\,N}(\mu_F^2) \ . \tag{4.1.17}$$

Finally, to express the resummed partonic cross section $\mathcal{W}_{ab}^F$ in terms of the perturbative coefficients in Eqs. (4.1.13)–(4.1.16), we need to replace the parton densities $f_{a/h,\,N}(b_0^2/b^2)$ in Eq. (4.1.11) for the same parton densities evaluated at the factorization scale μ_F. The substitution can be done by using

$$f_{a/h,\,N}(\mu^2) = \sum_b\ U_{ab,\,N}(\mu^2, \mu_0^2)\ f_{b/h,\,N}(\mu_0^2) \ , \tag{4.1.18}$$

where the QCD evolution operator $U_{ab,\,N}(\mu^2, \mu_0^2)$ fulfils the evolution equations

$$\frac{d\,U_{ab,\,N}(\mu^2, \mu_0^2)}{d\ln\mu^2} = \sum_c \gamma_{ac,\,N}(\alpha_s(\mu^2))\ U_{cb,\,N}(\mu^2, \mu_0^2) \ , \tag{4.1.19}$$

and $\gamma_{ab,\,N}(\alpha_s)$ are the parton anomalous dimensions or, more precisely, the N-moments of the customary Altarelli–Parisi splitting functions $P_{ab}(\alpha_s, z)$ [91]:

$$\gamma_{ab,\,N}(\alpha_s) = \int_0^1 dz\ z^{N-1}\ P_{ab}(\alpha_s, z) = \sum_{n=1}^{\infty} \left(\frac{\alpha_s}{\pi}\right)^n \gamma_{ab,\,N}^{(n)} \ . \tag{4.1.20}$$

Then, we can finally write the resummed $\mathcal{W}^F_{ab,\,N}$ factor as

$$\begin{aligned}\mathcal{W}^F_{ab,\,N}(b,M;\alpha_s(\mu_R^2),\mu_R^2,\mu_F^2)=&\sum_c \sigma^{(0)}_{c\bar{c},\,F}(\alpha_s(M^2),M)\; H_c^F(\alpha_s(M^2))\; S_c(M,b)\\ &\times\sum_{a_1,\,b_1} C_{ca_1,\,N}(\alpha_s(b_0^2/b^2))\; C_{\bar{c}b_1,\,N}(\alpha_s(b_0^2/b^2))\\ &\times U_{a_1a,\,N}(b_0^2/b^2,\mu_F^2)\; U_{b_1b,\,N}(b_0^2/b^2,\mu_F^2)\;\;,\end{aligned} \tag{4.1.21}$$

which relates the resummed partonic cross section in Eq. (4.1.4) to the perturbative coefficients in Eqs. (4.1.13)–(4.1.16) and the anomalous dimensions coefficients in Eq. (4.1.20).

Furthermore, we can express $C_N(\alpha_s(b_0^2/b^2))$ in Eq. (4.1.21) in terms of $C_N(\alpha_s(M^2))$ by evolving the strong coupling, which adds to the coefficient the renormalization-group correction:

$$C_N(\alpha_s(b_0^2/b^2)) = C_N(\alpha_s(M^2))\;\exp\left\{-\int_{b_0^2/b^2}^{M^2}\frac{dq^2}{q^2}\;\beta(\alpha_s(q^2))\;\frac{d\ln C_N(\alpha_s(q^2))}{d\ln\alpha_s(q^2)}\right\}\;\;. \tag{4.1.22}$$

Finally, we insert in Eq. (4.1.21) the solution of the evolution equation (4.1.19):

$$U_N(b_0^2/b^2,\mu_F^2) = \exp\left\{-\int_{b_0^2/b^2}^{\mu_F^2}\frac{dq^2}{q^2}\;\gamma_N(\alpha_s(q^2))\right\}\;\;. \tag{4.1.23}$$

After all these considerations, we are now in a position to express $\mathcal{W}^F_{ab,\,N}$ in the useful exponential form of Eq. (4.1.4). Once there, the calculation of the $g^{(n)}$ functions is straightforward (see Ref. [123]). With this notation, the all-order form factor $\exp\{\mathcal{G}\}$ could be expressed as

$$\mathcal{G}_N(\alpha_s(\mu_R^2),L;M^2/\mu_R^2,M^2/Q^2) = -\int_{b_0^2/b^2}^{Q^2}\frac{dq^2}{q^2}\left[A(\alpha_s(q^2))\;\ln\frac{M^2}{q^2}+\widetilde{B}_N(\alpha_s(q^2))\right]\;\;, \tag{4.1.24}$$

where the $A(\alpha_s)$ is exactly the perturbative function in Eq. (4.1.13), and $\widetilde{B}_N(\alpha_s)$ can be also expanded as

$$\widetilde{B}_N(\alpha_s) = \left(\frac{\alpha_s}{\pi}\right)\widetilde{B}_N^{(1)} + \left(\frac{\alpha_s}{\pi}\right)^2\widetilde{B}_N^{(2)} + \sum_{n=3}^{\infty}\left(\frac{\alpha_s}{\pi}\right)^n\widetilde{B}_N^{(n)}\;\;. \tag{4.1.25}$$

and expressed as follows in terms of the perturbative functions in Eqs. (2.2.38), (4.1.14), (4.1.15) and (4.1.20):

$$\widetilde{B}_N(\alpha_s) = B(\alpha_s) + 2\beta(\alpha_s)\,\frac{d\ln C_N(\alpha_s)}{d\ln\alpha_s} + 2\gamma_N(\alpha_s) \tag{4.1.26}$$

On the other hand, The expression of the hard-process function $\mathcal{H}_N^F$ in Eq. (4.1.4) is

$$\begin{aligned}\mathcal{H}_N^F(M,\alpha_s(\mu_R^2);M^2/\mu_R^2,M^2/\mu_F^2,M^2/Q^2) &= \sigma_F^{(0)}(\alpha_s(M^2),M)\;H^F(\alpha_s(M^2))\;C_N^2(\alpha_s(M^2))\\ &\times\exp\left\{\int_{M^2}^{Q^2}\frac{dq^2}{q^2}\left[A(\alpha_s(q^2))\;\ln\frac{M^2}{q^2}+\widetilde{B}_N(\alpha_s(q^2))\right]+\int_{\mu_F^2}^{M^2}\frac{dq^2}{q^2}\,2\,\gamma_N(\alpha_s(q^2))\right\}\;.\end{aligned} \tag{4.1.27}$$

Unlike the form factor $\exp\{\mathcal{G}\}$, the non-logarithmic function $\mathcal{H}_N^F$ in Eq. (4.1.27) explicitly depends on the factorization scale μ_F, on the factorization scheme (through $C_{ab,\,N}(\alpha_s)$ and $\gamma_{ab,\,N}(\alpha_s)$) and on the final-state system F (through $\sigma_F^{(0)}$ and H^F). Nonetheless, $\mathcal{H}_N^F$ does not depend on the resummation scheme, since the factor $H^F(\alpha_s)C_N^2(\alpha_s)$ is invariant under the resummation scheme transformations.

Now, for the sake of completeness and in order to have all the components to perform the q_T-subtraction at NNLO QCD and even more, to expand the formalism up to mixed NNLO QCD⊗QED, we report the expressions for all the coefficients needed to perform the resummation up to order $\mathcal{O}(\alpha_s^2)$.

The first order coefficient for the universal (i.e. independent of the process and of the factorization and resummation schemes) perturbative function $A_c(\alpha_s)$ in Eq. (4.1.13) is [111, 114, 124]

$$A_c^{(1)} = C_c\;, \tag{4.1.28}$$

where $C_c = C_F$ if $c = q, \bar{q}$ and $C_c = C_A$ if $c = g$.

The first-order coefficient $\widetilde{B}_{c,\,N}^{(1)}$ in the expansion (4.1.25) of the universal perturbative function $\widetilde{B}_N(\alpha_s)$ in Eq. (4.1.26) is

$$\widetilde{B}_{c,\,N}^{(1)} = B_c^{(1)} + 2\gamma_{cc,\,N}^{(1)}\;, \tag{4.1.29}$$

with [114, 124]

$$B_q^{(1)} = B_{\bar{q}}^{(1)} = -\frac{3}{2}\, C_F \quad , \qquad B_g^{(1)} = -\frac{1}{6}\,(11 C_A - 2N_f) \quad . \tag{4.1.30}$$

As for the first-order $C_{ab}^{(1)}$ coefficients, $C_{qg}^{(1)}$ and $C_{gq}^{(1)}$ in Eq. (4.1.15) do not depend on the process and on the resummation scheme, and were first computed in Refs. [125] and [126], respectively. Their expressions in the $\overline{\rm MS}$ factorization scheme are

$$C_{qg}^{(1)}(z) = C_{\bar{q}g}^{(1)}(z) = \frac{1}{2}\, z(1-z) \quad , \qquad C_{gq}^{(1)}(z) = C_{g\bar{q}}^{(1)}(z) = \frac{1}{2}\, C_F\, z \quad . \tag{4.1.31}$$

On the other hand, the flavour-diagonal first-order coefficients $C_{qq}^{(1)}$ and $C_{gg}^{(1)}$ and the coefficients $H_q^{F\,(1)}$ and $H_g^{F\,(1)}$ do depend on the resummation scheme. Here we recall the expressions for the coefficients $C_{qq'}^{(1)}$ and $C_{gg}^{(1)}$ in the so called *hard scheme*[2], as presented in Ref. [110]:

$$C_{qq'}^{(1)}(z) = \delta_{qq'} \frac{1}{2} C_F (1-z) \,, \tag{4.1.32}$$

$$C_{gg}^{(1)}(z) = 0 \,, \tag{4.1.33}$$

where q' stands for both quarks and antiquarks of all the possible flavours, and the $\delta_{qq'}$ ensures the complete flavour conservation at this order.

As for the process-dependent coefficient H_c^F, we specifically recall the expression for the NLO hard-virtual function $H_q^{DY\,(1)}$ for the Drell Yan mechanism, in the hard scheme, as presented in Refs. [110, 127]:

$$H_q^{DY\,(1)} = C_F \left(\frac{\pi^2}{2} - 4 \right) \quad . \tag{4.1.34}$$

Moreover, the coefficients corresponding to the second order in the expansions (4.1.13-4.1.15) for the case of quark initiated processes and even the process-dependent H_c^F function in Eq. (4.1.16) for the specific case of the Drell Yan mechanism are explicitly presented in

[2] The hard scheme is the scheme in which, order by order in perturbation theory, the coefficients $C_{ab}^{(n)}(z)$ with $n \geq 1$ do not contain any $\delta(1-z)$ term. This definition implies that all the process-dependent virtual corrections to the Born level subprocess are embodied in the resummation coefficient H_c^F. The hard-scheme expressions for the perturbative coefficients can be achieved from any other resummation scheme by simply setting the coefficient of the $\delta(1-z)$ term to zero in the expression for $C_{ab}^{(n)}(z)$ (see Eq. 4.1.15).

the Appendix B, thus completing the set of perturbative coefficients needed to perform the transverse momentum resummation up to second order in the strong coupling constant.

4.2 q_T-Subtraction

Once we have revised the logarithmic behavior of the cross section in the small-q_T region, we can exploit this known dependence to formulate a method, which was developed to cancel the infrared divergences in a practical way by exploiting the universal behavior of the associated transverse-momentum distributions in the limit $q_T \to 0$. In the next sections we will introduce the general formalism for the q_T-subtraction and discuss its usefulness to address NNLO QCD corrections. Later, we will extend the method up to the mixed order to address the QCD⊗QED contributions.

4.2.1 Background and formulation

This method was firstly devoted to obtain the NNLO QCD corrections for the production of colorless high-mass systems in hadron collisions. In fact, this implies that the LO partonic subprocess can be $q\bar{q}$ annihilation, as in the case of the Drell Yan process (or also gg fusion, as in the case of Higgs boson production). As has been previously stated, each perturbative contribution is logarithmically divergent in the region of small-q_T, and therefore the calculation has to be organized in order to achieve stability within the whole q_T spectrum.

We consider the inclusive hard-scattering reaction

$$h_1(p_1) + h_2(p_2) \to F(M, q_T) + X \,, \tag{4.2.1}$$

where the collision of the two hadrons h_1 and h_2 with momenta p_1 and p_2 produces the triggered generic final state F, without color and electric charge, such as *one* or *more* neutral vector bosons ($\gamma^*, Z, ZZ, \gamma\gamma, \ldots$), Higgs particles, and so forth. The observed final state F is accompanied by the final-state radiation X, which might be composed by either quarks, antiquarks, gluons or photons. The system F is formed by n final-state particles with momenta $q_1, q_2, \ldots, q_n$, and has total invariant mass $M^2 = (q_1 + q_2 + \cdots + q_n)^2$ and transverse momentum q_T.

The first thing to take into account is that, at the LO, the transverse momentum q_T of the

final state F is exactly 0. This means that all the terms with $q_T \neq 0$ are at least of NLO, which then correspond to the Leading Order contributions to the production of a triggered final state F + jets. Thus we can rewrite the cross section as

$$d\sigma^F_{(N)NLO}|_{q_T\neq 0} = d\sigma^{F+jets}_{(N)LO} \tag{4.2.2}$$

By keeping this in mind, we could address the whole set of NNLO contributions with $q_T \neq 0$ just as an usual NLO calculation, and then handle the IR divergences corresponding to this $q_T \neq 0$ region with one of the known NLO methods, just like, for example, FKS or the Catani-Seymour dipole subtraction (see section 2.4 for details on the FKS method).

Once this is done, The only remaining singularities of NNLO type are associated to the limit $q_T \to 0$. In this case, we can profit from the fact that the singular behavior of $d\sigma^{F+jets}_{(N)LO}$ in the $q_T \to 0$ limit is well known, and corresponds to the truncation of the resummed cross section at the same order. Thus, we can combine the results with the fixed order calculation and get fixed order results that are independent of the enhanced logarithmic contributions of the small-q_T region (see section 4.1 for a deeper discussion on the resummation formalism).

To schematize the subtraction, we will shortly sketch the general method introduced by de Florian, Grazzini, Catani and Bozzi [99, 111] to subtract the divergent behavior of $q_T = 0$ for QCD calculations. Within their notation, we can define a subtraction counterterm in the $q_T \to 0$ limit as

$$d\sigma^{CT} = d\sigma^F_{LO} \otimes \Sigma^F(q_T/Q)\, d^2\mathbf{q}_T. \tag{4.2.3}$$

where the function $\Sigma^F(q_T/Q)$ embodies the singular behavior of $d\sigma^{F+\text{jets}}$ when $q_T \to 0$, which is related to the enhanced logarithmic contributions at small-q_T, of the form

$$\Sigma^F(q_T/Q) \xrightarrow[q_T\to 0]{} \sum_{n=1}^{\infty} \left(\frac{\alpha_s}{\pi}\right)^n \sum_{k=1}^{2n} \Sigma^{F(n;k)}\, \frac{Q^2}{q_T^2} \ln^{k-1}\frac{Q^2}{q_T^2} \quad . \tag{4.2.4}$$

It is essential to note that within this notation, the coefficients $\Sigma^{F(n;k)}$ are q_T-independent. Furthermore, they are also universal, in the sense that they only involve a dependence on the partons of the LO subprocess (for instance $q\bar{q}$ annihilation in the case of Drell Yan), and do not depend on the final state F of the collision.

Therefore, in the equation (4.2.2) it is possible to regularize the divergence of $d\sigma^F_{(N)NLO}$ in

the limit $q_T \to 0$ by subtracting the expansion (4.2.4) at the same order in the coupling constant. Finally, an additional $\mathcal{H}$ term has to be considered, in order to add the corresponding finite contribution to the cross section in the limit $q_T \to 0$. This quantity is also q_T-independent, but it does depend on the specific hard-scattering subprocess of the LO diagram.

With these extra ingredients we can extend the Eq. (4.2.2) to finally include the contribution at $q_T = 0$ as

$$d\sigma^F_{(N)NLO} = \mathcal{H}^F_{(N)NLO} \otimes d\sigma^F_{LO} + \left[d\sigma^{F+\text{jets}}_{(N)LO} - d\sigma^{CT}_{(N)LO} \right] \quad . \tag{4.2.5}$$

where $\mathcal{H}$ is the hard function in Eq. (4.1.7) and admits the following expansion

$$\mathcal{H}^F = 1 + \left(\frac{\alpha_s}{\pi}\right) \mathcal{H}^{F(1)} + \left(\frac{\alpha_s}{\pi}\right)^2 \mathcal{H}^{F(2)} + \dots \quad . \tag{4.2.6}$$

Now we may note that, given that the counterterm in Eq. (4.2.3) regularizes the singularity of $d\sigma^{F+jets}$ in the limit $q_T \to 0$, the expression in the square brackets in Eq. (4.2.5) is then IR finite and integrable over q_T. As a consequence, this method shows useful to compute arbitrary infrared-safe observables for this class of processes. Furthermore, according to this method, the NLO calculation of $d\sigma^F$ requires the knowledge of $\mathcal{H}^{F(1)}$ and the LO calculation of $d\sigma^{F+jets}$, while on the other hand, the NNLO can be obtained by knowing the coefficient $\mathcal{H}^{F(2)}$ and also the NLO of $d\sigma^{F+jets}$.

4.2.2 Explicit formulae for NNLO QCD calculations

Now, for the sake of completeness and in order to provide the basis for the extension to the mixed order, we recall the expressions for the fixed order expansion of the resummed cross section up to NNLO in QCD as first addressed in Ref. [111].

If we take into account the resummed component of the transverse-momentum cross section (see Eq. (4.1.3) in section 4.1), we can expand the known structure (4.1.24) in powers of α_s and explicitly get the $\Sigma^{F(n;k)}$ coefficients schematized in Eq. (4.2.4), which read

$$\mathcal{W}^{F}_{ab}(b,M,\hat{s};\alpha_s,\mu_R^2,\mu_F^2,Q^2) = \sum_c \sigma^{(0)}_{c\bar{c},\,F}(\alpha_s,M)\Big\{\delta_{ca}\,\delta_{\bar{c}b}\,\delta(1-z) + \sum_{n=1}^{\infty}\left(\frac{\alpha_s}{\pi}\right)^n\left[\widetilde{\Sigma}^{F\,(n)}_{c\bar{c}\leftarrow ab}\left(z,\widetilde{L};\frac{M^2}{\mu_R^2},\frac{M^2}{\mu_F^2},\frac{M^2}{Q^2}\right) + \mathcal{H}^{F\,(n)}_{c\bar{c}\leftarrow ab}\left(z;\frac{M^2}{\mu_R^2},\frac{M^2}{\mu_F^2},\frac{M^2}{Q^2}\right)\right]\Big\}\,. \tag{4.2.7}$$

Here, $\widetilde{L} = ln\left(\frac{Q^2b^2}{b_0^2}+1\right)$ is the logarithmically divergent quantity in the $q_T \to 0$ limit with the constraint of perturbative unitarity in the large-q_T region[3], $z = M^2/\hat{s}$, $\alpha_s = \alpha_s(\mu_R^2)$, $\sigma^{(0)}_{c\bar{c},\,F}(\alpha_s,M) = \alpha_s^{p_{cF}}\,\sigma^{(\mathrm{LO})}_{c\bar{c},\,F}(M)$ and, in general, the power p_{cF} depends on the lowest-order partonic subprocess $c+\bar{c}\to F$. In Eq. (4.2.7), $\mathcal{W}^F_{ab}$ is the resummed cross section on the right-hand side of Eq. (4.1.3).

The form of the coefficient $\widetilde{\Sigma}^{F\,(n)}$ is a polynomial of degree $2n$ in $\widetilde{L}$. It vanishes by definition when $\widetilde{L}=0$ (i.e. in the large-q_T region corresponding to $b=0$) and the b-independent part is represented by the coefficient $\mathcal{H}^{F\,(n)}$.

As stated in Ref. [111], the perturbative coefficients in the expansion of Eq. (4.2.7) up to NNLO in α_s are

$$\widetilde{\Sigma}^{F\,(1)}_{c\bar{c}\leftarrow ab}(z,\widetilde{L}) = \Sigma^{F\,(1;2)}_{c\bar{c}\leftarrow ab}(z)\,\widetilde{L}^2 + \Sigma^{F\,(1;1)}_{c\bar{c}\leftarrow ab}(z)\,\widetilde{L}\,, \tag{4.2.8}$$

$$\widetilde{\Sigma}^{F\,(2)}_{c\bar{c}\leftarrow ab}(z,\widetilde{L}) = \Sigma^{F\,(2;4)}_{c\bar{c}\leftarrow ab}(z)\,\widetilde{L}^4 + \Sigma^{F\,(2;3)}_{c\bar{c}\leftarrow ab}(z)\,\widetilde{L}^3 + \Sigma^{F\,(2;2)}_{c\bar{c}\leftarrow ab}(z)\,\widetilde{L}^2 + \Sigma^{F\,(2;1)}_{c\bar{c}\leftarrow ab}(z)\,\widetilde{L}\,, \tag{4.2.9}$$

where the dependence on the scale ratios M^2/μ_R^2, M^2/μ_F^2 and M^2/Q^2 is understood. The b-independent coefficients $\Sigma^{F\,(1;k)}(z)$, $\mathcal{H}^{F\,(1)}(z)$, $\Sigma^{F\,(2;k)}(z)$ and $\mathcal{H}^{F\,(2)}(z)$ are presented by considering their N-moments with respect to z as

$$\Sigma^{F\,(1;2)}_{c\bar{c}\leftarrow ab,\,N} = -\frac{1}{2}A_c^{(1)}\,\delta_{ca}\delta_{\bar{c}b}\,, \tag{4.2.10}$$

$$\Sigma^{F\,(1;1)}_{c\bar{c}\leftarrow ab,\,N}(M^2/Q^2) = -\left[\delta_{ca}\delta_{\bar{c}b}\,\left(B_c^{(1)} + A_c^{(1)}\,\ell_Q\right) + \delta_{ca}\gamma^{(1)}_{\bar{c}b,\,N} + \delta_{\bar{c}b}\gamma^{(1)}_{ca,\,N}\right]\,, \tag{4.2.11}$$

$$\mathcal{H}^{F\,(1)}_{c\bar{c}\leftarrow ab,\,N}\left(\frac{M^2}{\mu_R^2},\frac{M^2}{\mu_F^2},\frac{M^2}{Q^2}\right) = \delta_{ca}\delta_{\bar{c}b}\left[H_c^{F\,(1)} - \left(B_c^{(1)} + \frac{1}{2}A_c^{(1)}\ell_Q\right)\ell_Q - p_{cF}\beta_0\ell_R\right] + \delta_{ca}C^{(1)}_{\bar{c}b,\,N} + \delta_{\bar{c}b}C^{(1)}_{ca,\,N} + \left(\delta_{ca}\gamma^{(1)}_{\bar{c}b,\,N} + \delta_{\bar{c}b}\gamma^{(1)}_{ca,\,N}\right)(\ell_F - \ell_Q)\,, \tag{4.2.12}$$

[3]The impact parameter b here is the variable conjugate to q_T, such that the limit $q_T \ll M$ corresponds to $Mb \gg 1$ (see Chapter 4.1 for more details on this parameter and on the $\widetilde{L}$ quantity).

$$\Sigma^{F\,(2;4)}_{c\bar{c}\leftarrow ab,\,N} = \frac{1}{8}\left(A^{(1)}_c\right)^2\,\delta_{ca}\delta_{\bar{c}b}\;, \tag{4.2.13}$$

$$\Sigma^{F\,(2;3)}_{c\bar{c}\leftarrow ab,\,N}(M^2/Q^2) = -\,A^{(1)}_c\left[\frac{1}{3}\,\beta_0\,\delta_{ca}\delta_{\bar{c}b} + \frac{1}{2}\,\Sigma^{F\,(1;1)}_{c\bar{c}\leftarrow ab,\,N}(M^2/Q^2)\right]\;, \tag{4.2.14}$$

$$\begin{aligned}\Sigma^{F\,(2;2)}_{c\bar{c}\leftarrow ab,\,N}\left(\frac{M^2}{\mu_R^2},\frac{M^2}{\mu_F^2},\frac{M^2}{Q^2}\right) &= -\,\frac{1}{2}\,A^{(1)}_c\left[\mathcal{H}^{F\,(1)}_{c\bar{c}\leftarrow ab,\,N}\left(\frac{M^2}{\mu_R^2},\frac{M^2}{\mu_F^2},\frac{M^2}{Q^2}\right) - \beta_0\,\delta_{ca}\delta_{\bar{c}b}\,(\ell_R-\ell_Q)\right]\\ &-\,\frac{1}{2}\sum_{a_1,b_1}\Sigma^{F\,(1;1)}_{c\bar{c}\leftarrow a_1b_1,\,N}(M^2/Q^2)\left[\delta_{a_1a}\gamma^{(1)}_{b_1b,\,N} + \delta_{b_1b}\gamma^{(1)}_{a_1a,\,N}\right]\\ &-\,\frac{1}{2}\left[A^{(2)}_c\,\delta_{ca}\delta_{\bar{c}b} + \left(B^{(1)}_c + A^{(1)}_c\,\ell_Q - \beta_0\right)\,\Sigma^{F\,(1;1)}_{c\bar{c}\leftarrow ab,\,N}(M^2/Q^2)\right]\;,\end{aligned} \tag{4.2.15}$$

$$\begin{aligned}\Sigma^{F\,(2;1)}_{c\bar{c}\leftarrow ab,\,N}\left(\frac{M^2}{\mu_R^2},\frac{M^2}{\mu_F^2},\frac{M^2}{Q^2}\right) &= \Sigma^{F\,(1;1)}_{c\bar{c}\leftarrow ab,\,N}(M^2/Q^2)\,\beta_0\,(\ell_Q-\ell_R)\\ &-\sum_{a_1,b_1}\mathcal{H}^{F\,(1)}_{c\bar{c}\leftarrow a_1b_1,\,N}\left(\frac{M^2}{\mu_R^2},\frac{M^2}{\mu_F^2},\frac{M^2}{Q^2}\right)\left[\delta_{a_1a}\delta_{b_1b}\left(B^{(1)}_c + A^{(1)}_c\,\ell_Q\right) + \delta_{a_1a}\gamma^{(1)}_{b_1b,\,N} + \delta_{b_1b}\gamma^{(1)}_{a_1a,\,N}\right]\\ &-\left[\delta_{ca}\delta_{\bar{c}b}\,\left(B^{(2)}_c + A^{(2)}_c\,\ell_Q\right) - \beta_0\left(\delta_{ca}C^{(1)}_{\bar{c}b,\,N} + \delta_{\bar{c}b}C^{(1)}_{ca,\,N}\right) + \delta_{ca}\gamma^{(2)}_{\bar{c}b,\,N} + \delta_{\bar{c}b}\gamma^{(2)}_{ca,\,N}\right]\;,\end{aligned} \tag{4.2.16}$$

$$\begin{aligned}&\mathcal{H}^{F\,(2)}_{c\bar{c}\leftarrow ab,\,N}\left(\frac{M^2}{\mu_R^2},\frac{M^2}{\mu_F^2},\frac{M^2}{Q^2}\right) = \delta_{ca}\delta_{\bar{c}b}\,H^{F\,(2)}_c + \delta_{ca}\,C^{(2)}_{\bar{c}b,\,N} + \delta_{\bar{c}b}\,C^{(2)}_{ca,\,N} + C^{(1)}_{ca,\,N}\,C^{(1)}_{\bar{c}b,\,N}\\ &+H^{F\,(1)}_c\left(\delta_{ca}\,C^{(1)}_{\bar{c}b,\,N} + \delta_{\bar{c}b}\,C^{(1)}_{ca,\,N}\right) + \frac{1}{6}\,A^{(1)}_c\,\beta_0\,\ell_Q^3\,\delta_{ca}\delta_{\bar{c}b} + \frac{1}{2}\left[A^{(2)}_c\,\delta_{ca}\delta_{\bar{c}b} + \beta_0\,\Sigma^{F\,(1;1)}_{c\bar{c}\leftarrow ab,\,N}(M^2/Q^2)\right]\ell_Q^2\\ &-\left[\delta_{ca}\delta_{\bar{c}b}\,\left(B^{(2)}_c + A^{(2)}_c\,\ell_Q\right) - \beta_0\left(\delta_{ca}C^{(1)}_{\bar{c}b,\,N} + \delta_{\bar{c}b}C^{(1)}_{ca,\,N}\right) + \delta_{ca}\gamma^{(2)}_{\bar{c}b,\,N} + \delta_{\bar{c}b}\gamma^{(2)}_{ca,\,N}\right]\ell_Q\\ &+\frac{1}{2}\,\beta_0\,\left(\delta_{ca}\gamma^{(1)}_{\bar{c}b,\,N} + \delta_{\bar{c}b}\gamma^{(1)}_{ca,\,N}\right)\ell_F^2 + \left(\delta_{ca}\gamma^{(2)}_{\bar{c}b,\,N} + \delta_{\bar{c}b}\gamma^{(2)}_{ca,\,N}\right)\ell_F - \mathcal{H}^{F\,(1)}_{c\bar{c}\leftarrow ab,\,N}\left(\frac{M^2}{\mu_R^2},\frac{M^2}{\mu_F^2},\frac{M^2}{Q^2}\right)\beta_0\ell_R\\ &+\frac{1}{2}\sum_{a_1,b_1}\left[\mathcal{H}^{F\,(1)}_{c\bar{c}\leftarrow a_1b_1,\,N}\left(\frac{M^2}{\mu_R^2},\frac{M^2}{\mu_F^2},\frac{M^2}{Q^2}\right) + \delta_{ca_1}\delta_{\bar{c}b_1}\,H^{F\,(1)}_c + \delta_{ca_1}\,C^{(1)}_{\bar{c}b_1,\,N} + \delta_{\bar{c}b_1}\,C^{(1)}_{ca_1,\,N}\right]\\ &\times\left[\left(\delta_{a_1a}\gamma^{(1)}_{b_1b,\,N} + \delta_{b_1b}\gamma^{(1)}_{a_1a,\,N}\right)(\ell_F-\ell_Q) - \delta_{a_1a}\delta_{b_1b}\left(\left(B^{(1)}_c + \frac{1}{2}\,A^{(1)}_c\,\ell_Q\right)\ell_Q + p_{cF}\,\beta_0\,\ell_R\right)\right]\\ &-\delta_{ca}\delta_{\bar{c}b}\,p_{cF}\left(\frac{1}{2}\,\beta_0^2\,\ell_R^2 + \beta_1\,\ell_R\right)\;.\end{aligned} \tag{4.2.17}$$

The right-hand side of Eqs. (4.2.10)–(4.2.17) is expressed in terms of the resummation-scheme independent coefficients given in section 4.1 and of the logarithms

$$\ell_R = \ln\frac{M^2}{\mu_R^2}\;,\quad \ell_F = \ln\frac{M^2}{\mu_F^2}\;,\quad \ell_Q = \ln\frac{M^2}{Q^2}\;. \tag{4.2.18}$$

As for the hard-virtual coefficients $H_c^{F(n)}$ in these expressions, they can be found up to $\mathcal{O}(\alpha_s^2)$ for the case of Drell Yan in the Appendix B.

With these coefficients we can obtain the fixed-order contributions of $d\hat{\sigma}^{(\text{res.})}_{F\,ab}$ and then construct the counterterm in Eq. (4.2.5), up to NNLO in α_s:

$$\left[\frac{d\hat{\sigma}^{(\text{res.})}_{F\,ab}}{dq_T^2}(q_T, M, \hat{s}=\frac{M^2}{z}; \alpha_s(\mu_R^2), \mu_R^2, \mu_F^2, Q^2)\right]_{\text{LO}} = \frac{\alpha_s(\mu_R^2)}{\pi}\,\frac{z}{Q^2}\sum_c \sigma^{(0)}_{c\bar{c},\,F}(\alpha_s(\mu_R^2), M) \times\left[\Sigma^{F\,(1;2)}_{c\bar{c}\leftarrow ab}(z)\;\widetilde{I}_2(q_T/Q) + \Sigma^{F\,(1;1)}_{c\bar{c}\leftarrow ab}\left(z;\frac{M^2}{Q^2}\right)\;\widetilde{I}_1(q_T/Q)\right]. \tag{4.2.19}$$

$$\left[\frac{d\hat{\sigma}^{(\text{res.})}_{F\,ab}}{dq_T^2}(q_T, M, \hat{s}=\frac{M^2}{z}; \alpha_s(\mu_R^2), \mu_R^2, \mu_F^2, Q^2)\right]_{\text{NLO}} = \left[\frac{d\hat{\sigma}^{(\text{res.})}_{F\,ab}}{dq_T^2}(q_T, M, \hat{s}; \alpha_s(\mu_R^2), \mu_R^2, \mu_F^2, Q^2)\right]_{\text{LO}} + \left(\frac{\alpha_s(\mu_R^2)}{\pi}\right)^2\,\frac{z}{Q^2}\sum_c \sigma^{(0)}_{c\bar{c},\,F}(\alpha_s(\mu_R^2), M)\sum_{k=1}^{4}\Sigma^{F\,(2;k)}_{c\bar{c}\leftarrow ab}\left(z;\frac{M^2}{\mu_R^2},\frac{M^2}{\mu_F^2},\frac{M^2}{Q^2}\right)\;\widetilde{I}_k(q_T/Q)\,, \tag{4.2.20}$$

On the right-hand side of Eqs. (4.2.19) and (4.2.20), the dependence on q_T is fully embodied in the functions $\widetilde{I}_n(q_T/Q)$, which are obtained by the following Bessel transformation:

$$\widetilde{I}_n(q_T/Q) = Q^2\int_0^\infty db\,\frac{b}{2}\,J_0(bq_T)\;\ln^n\left(\frac{Q^2b^2}{b_0^2}+1\right). \tag{4.2.21}$$

The term $\ln^n(1+Q^2b^2/b_0^2) = \widetilde{L}^n$ in the integrand comes from the replacement $L\to\widetilde{L}$ (see Eq. (4.1.8)).

4.3 Mixed QCD⊗QED contributions

In order to extend the formalism of the q_T-subtraction and apply it to the mixed corrections, we start by considering the QCD⊗QED perturbative expansion of the (differential) cross section for the production of the final state F in the sense of Eq. (2.2.1), by expanding in powers of the strong (α_s) and electromagnetic (α) couplings,

$$d\sigma^F = \sum_{i,j}\left(\frac{\alpha_s}{\pi}\right)^i\left(\frac{\alpha}{\pi}\right)^j d\sigma_F^{(i,j)}, \tag{4.3.1}$$

where $d\sigma_F^{(i,0)}$ stands for the pure QCD corrections, and $d\sigma_F^{(0,j)}$ for the pure QED ones. The *mixed* corrections are represented by $d\sigma_F^{(i,j)}$ with both $i,j\neq 0$, being the first mixed contribution

$d\sigma_F^{(1,1)}$.

Following a similar structure to the one valid in the pure QCD case (see section 4.2), the basic formula for the q_T-subtraction method in the case of mixed QCD⊗QED corrections can be expressed in the following way,

$$d\sigma_F^{(1,1)} = \mathcal{H}_F^{(1,1)} \otimes d\sigma_F^{(0,0)} + \left[d\sigma_{F+\text{jet}}^{(1,1)} - d\sigma_{F\,CT}^{(1,1)} \right] , \tag{4.3.2}$$

where $d\sigma_{F+\text{jet}}^{(1,1)}$ corresponds to the $F + \text{jet}$ production cross section at $\mathcal{O}(\alpha_s\alpha)$. It is important to note that in this context 'jet' stands for either quarks, antiquarks, gluons or photons in the final state and all of them need to be considered in the initial state as well. The term inside the square bracket in Eq. (4.3.2) is finite in the limit of vanishing transverse momentum of the F state, but the individual terms $d\sigma_{F+\text{jet}}^{(1,1)}$ and $d\sigma_{F\,CT}^{(1,1)}$ are separately divergent. In order to evaluate $d\sigma_{F+\text{jet}}^{(1,1)}$, we can make use of any NLO subtraction method (adapted, though, to the case of mixed QCD⊗QED corrections).

The subtraction counter-term $d\sigma_{F\,CT}^{(1,1)}$ encodes the singular behavior of the real scattering amplitudes in the small-q_T region. The coefficient function $\mathcal{H}_F^{(1,1)}$ restores the correct normalization to the total cross section and it has Born kinematics (*i.e.* it is proportional to $\delta(q_T)$). Both coefficient functions can be calculated, through the abelianisation procedures [39, 40], from Eqs. (4.2.10-4.2.17) in section 4.2.2. We have also made sure (as a self-consistency check) that the same coefficient functions can be obtained from first principles, *i.e* redefining Eq. (6) in Ref. [110] to take into account QED emissions and expanding it to a given fixed order.

Next we present the explicit expression of all the required terms needed for the subtraction at $\mathcal{O}(\alpha_s\alpha)$. These are constructed by convoluting the parton distributions with the corresponding partonic terms, which up to $\mathcal{O}(\alpha_s\alpha)$ are given by

$$\begin{aligned} d\sigma_{ab\,CT}^{F} &= \left(\frac{\alpha_s}{\pi}\right) d\sigma_{ab\,CT}^{F\,(1,0)} + \left(\frac{\alpha}{\pi}\right) d\sigma_{ab\,CT}^{F\,(0,1)} + \left(\frac{\alpha_s}{\pi}\right)\left(\frac{\alpha}{\pi}\right) d\sigma_{ab\,CT}^{F\,(1,1)} \\ &= \sum_c d\sigma_{c\bar{c},F}^{(0,0)} \Bigg\{ \left(\frac{\alpha_s}{\pi}\right) \widetilde{\Sigma}_{c\bar{c}\leftarrow ab}^{F(1,0)}(z, q_T/Q) + \left(\frac{\alpha}{\pi}\right) \widetilde{\Sigma}_{c\bar{c}\leftarrow ab}^{F(0,1)}(z, q_T/Q) \\ &+ \left(\frac{\alpha_s}{\pi}\right)\left(\frac{\alpha}{\pi}\right) \widetilde{\Sigma}_{c\bar{c}\leftarrow ab}^{F(1,1)}(z, q_T/Q) \Bigg\} \end{aligned} \tag{4.3.3}$$

and

$$\begin{aligned}\mathcal{H}_{ab}^{F}\otimes d\sigma_{LO}^{F} &= \left[1+\left(\frac{\alpha_s}{\pi}\right)\mathcal{H}_{ab}^{F(1,0)}+\left(\frac{\alpha}{\pi}\right)\mathcal{H}_{ab}^{F(0,1)}+\left(\frac{\alpha_s}{\pi}\right)\left(\frac{\alpha}{\pi}\right)\mathcal{H}_{ab}^{F(1,1)}\right]\otimes d\sigma_{LO}^{F}\\ &= \sum_{c} d\sigma_{c\bar{c},F}^{(0,0)}\Bigg\{\delta_{ca}\delta_{\bar{c}b}\delta(1-z)+\left(\frac{\alpha_s}{\pi}\right)\mathcal{H}_{c\bar{c}\leftarrow ab}^{F(1,0)}(z)\\ &+\left(\frac{\alpha}{\pi}\right)\mathcal{H}_{c\bar{c}\leftarrow ab}^{F(0,1)}(z)+\left(\frac{\alpha_s}{\pi}\right)\left(\frac{\alpha}{\pi}\right)\mathcal{H}_{c\bar{c}\leftarrow ab}^{F(1,1)}(z)\Bigg\}.\end{aligned} \tag{4.3.4}$$

In order to simplify the notation, we indicate by z the dependence on both partonic momentum fractions z_1 and z_2. The explicit dependence on either z_1 and z_2 can be easily understood in terms on the dependence on the partonic label a and b, respectively. Also, it is implicit the dependence on the renormalization (μ_R), factorization (μ_F) and resummation (Q) scales.

Note that, for the sake of generality, in the results contained in this section we keep the full dependence on the resummation scale [111]. This dependence is needed in the context of transverse-momentum resummation. The fixed-order cross-section is independent of this scale, and it is convenient to set $Q = M$ to simplify the corresponding expressions.

The contributions to the counter-term $\widetilde{\Sigma}_{c\bar{c}\leftarrow ab}^{F(i,j)}$ can be organized in the following way

$$\widetilde{\Sigma}_{c\bar{c}\leftarrow ab}^{F(1,0)}(z,q_T/Q) = \Sigma_{c\bar{c}\leftarrow ab}^{F(1,0)[1;2]}(z)\widetilde{I}_2\left(q_T/Q\right)+\Sigma_{c\bar{c}\leftarrow ab}^{F(1,0)[1;1]}(z)\widetilde{I}_1\left(q_T/Q\right), \tag{4.3.5}$$

$$\widetilde{\Sigma}_{c\bar{c}\leftarrow ab}^{F(0,1)}(z,q_T/Q) = \Sigma_{c\bar{c}\leftarrow ab}^{F(0,1)[1;2]}(z)\widetilde{I}_2\left(q_T/Q\right)+\Sigma_{c\bar{c}\leftarrow ab}^{F(0,1)[1;1]}(z)\widetilde{I}_1\left(q_T/Q\right), \tag{4.3.6}$$

$$\begin{aligned}\widetilde{\Sigma}_{c\bar{c}\leftarrow ab}^{F(1,1)}(z,q_T/Q) &= \Sigma_{c\bar{c}\leftarrow ab}^{F(1,1)[2;4]}(z)\widetilde{I}_4\left(q_T/Q\right)+\Sigma_{c\bar{c}\leftarrow ab}^{F(1,1)[2;3]}(z)\widetilde{I}_3\left(q_T/Q\right)\\ &+\Sigma_{c\bar{c}\leftarrow ab}^{F(1,1)[2;2]}(z)\widetilde{I}_2\left(q_T/Q\right)+\Sigma_{c\bar{c}\leftarrow ab}^{F(1,1)[2;1]}(z)\widetilde{I}_1\left(q_T/Q\right),\end{aligned} \tag{4.3.7}$$

according to their power of logarithmic enhancement. The dependence on the transverse momentum is given by the known integrals $\widetilde{I}_n\left(q_T/Q\right)$ presented in Eq. (4.2.21).

The corresponding coefficients for the expansion of $\widetilde{\Sigma}_{c\bar{c}\leftarrow ab}^{F(i,j)}$ and $\mathcal{H}_{c\bar{c}\leftarrow ab}^{F(i,j)}$ are more easily presented by considering their N-moments (Mellin) with respect to the variable z. At NLO in QCD and QED they are given by

$$\Sigma_{c\bar{c}\leftarrow ab,N}^{F(1,0)[1;2]} = -\frac{1}{2}A_c^{(1,0)}\delta_{ca}\delta_{\bar{c}b}\,, \tag{4.3.8}$$

$$\Sigma^{F(1,0)[1;1]}_{c\bar{c}\leftarrow ab,N} = -\left[\delta_{ca}\delta_{\bar{c}b}\left(B^{(1,0)}_c + A^{(1,0)}_c \ell_Q\right) + \delta_{ca}\gamma^{(1,0)}_{\bar{c}b,N} + \delta_{\bar{c}b}\gamma^{(1,0)}_{ca,N}\right] , \tag{4.3.9}$$

$$\Sigma^{F(0,1)[1;2]}_{c\bar{c}\leftarrow ab,N} = -\frac{1}{2}A^{(0,1)}_c \delta_{ca}\delta_{\bar{c}b} , \tag{4.3.10}$$

$$\Sigma^{F(0,1)[1;1]}_{c\bar{c}\leftarrow ab,N} = -\left[\delta_{ca}\delta_{\bar{c}b}\left(B^{(0,1)}_c + A^{(0,1)}_c \ell_Q\right) + \delta_{ca}\gamma^{(0,1)}_{\bar{c}b,N} + \delta_{\bar{c}b}\gamma^{(0,1)}_{ca,N}\right] , \tag{4.3.11}$$

$$\begin{aligned}\mathcal{H}^{F(1,0)}_{c\bar{c}\leftarrow ab,N} &= \delta_{ca}\delta_{\bar{c}b}\left[H^{F(1,0)}_c - \left(B^{(1,0)}_c + \frac{1}{2}A^{(1,0)}_c \ell_Q\right)\ell_Q\right] \\ &\quad + \delta_{ca}C^{(1,0)}_{\bar{c}b,N} + \delta_{\bar{c}b}C^{(1,0)}_{ca,N} + \left(\delta_{ca}\gamma^{(1,0)}_{\bar{c}b,N} + \delta_{\bar{c}b}\gamma^{(1,0)}_{ca,N}\right)(\ell_F - \ell_Q) ,\end{aligned} \tag{4.3.12}$$

$$\begin{aligned}\mathcal{H}^{F(0,1)}_{c\bar{c}\leftarrow ab,N} &= \delta_{ca}\delta_{\bar{c}b}\left[H^{F(0,1)}_c - \left(B^{(0,1)}_c + \frac{1}{2}A^{(0,1)}_c \ell_Q\right)\ell_Q\right] \\ &\quad + \delta_{ca}C^{(0,1)}_{\bar{c}b,N} + \delta_{\bar{c}b}C^{(0,1)}_{ca,N} + \left(\delta_{ca}\gamma^{(0,1)}_{\bar{c}b,N} + \delta_{\bar{c}b}\gamma^{(0,1)}_{ca,N}\right)(\ell_F - \ell_Q) ,\end{aligned} \tag{4.3.13}$$

while for the mixed QCD⊗QED corrections at $\mathcal{O}(\alpha_s\alpha)$ they are given by

$$\Sigma^{F(1,1)[2;4]}_{c\bar{c}\leftarrow ab,N} = \frac{1}{4}A^{(1,0)}_c A^{(0,1)}_c \delta_{ca}\delta_{\bar{c}b} , \tag{4.3.14}$$

$$\Sigma^{F(1,1)[2;3]}_{c\bar{c}\leftarrow ab,N} = -A^{(0,1)}_c \frac{1}{2}\Sigma^{F(1,0)[1;1]}_{c\bar{c}-ab,N} - A^{(1,0)}_c \frac{1}{2}\Sigma^{F(0,1)[1;1]}_{c\bar{c}-ab,N} , \tag{4.3.15}$$

$$\begin{aligned}\Sigma^{F(1,1)[2;2]}_{c\bar{c}\leftarrow ab,N} &= -\frac{1}{2}A^{(1,0)}_c \mathcal{H}^{F(0,1)}_{c\bar{c}\leftarrow ab,N} - \frac{1}{2}\sum_{a_1,b_1}\Sigma^{F(1,0)[1;1]}_{c\bar{c}\leftarrow a_1b_1,N}\left[\delta_{a_1a}\gamma^{(0,1)}_{b_1b,N} + \delta_{b_1b}\gamma^{(0,1)}_{a_1a,N}\right] \\ &\quad - \frac{1}{2}A^{(0,1)}_c \mathcal{H}^{F(1,0)}_{c\bar{c}\leftarrow ab,N} - \frac{1}{2}\sum_{a_1,b_1}\Sigma^{F(0,1)[1;1]}_{c\bar{c}\leftarrow a_1b_1,N}\left[\delta_{a_1a}\gamma^{(1,0)}_{b_1b,N} + \delta_{b_1b}\gamma^{(1,0)}_{a_1a,N}\right] \\ &\quad - \frac{1}{2}\left[A^{(1,1)}_c \delta_{ca}\delta_{\bar{c}b} + \left(B^{(1,0)}_c + A^{(1,0)}_c \ell_Q\right)\Sigma^{F(0,1)[1;1]}_{c\bar{c}\leftarrow ab,N} + \left(B^{(0,1)}_c + A^{(0,1)}_c \ell_Q\right)\Sigma^{F(1,0)[1;1]}_{c\bar{c}\leftarrow ab,N}\right] ,\end{aligned} \tag{4.3.16}$$

$$
\begin{aligned}
\Sigma^{F(1,1)[2;1]}_{c\bar{c}\leftarrow ab,N} = &- \sum_{a_1,b_1} \mathcal{H}^{F(1,0)}_{c\bar{c}\leftarrow a_1b_1,N} \left[\delta_{a_1a}\delta_{b_1b}\left(B_c^{(0,1)} + A_c^{(0,1)}\ell_Q\right) + \delta_{a_1a}\gamma^{(0,1)}_{b_1b,N} + \delta_{b_1b}\gamma^{(0,1)}_{a_1a,N}\right] \\
&- \sum_{a_1,b_1} \mathcal{H}^{F(0,1)}_{c\bar{c}\leftarrow a_1b_1,N} \left[\delta_{a_1a}\delta_{b_1b}\left(B_c^{(1,0)} + A_c^{(1,0)}\ell_Q\right) + \delta_{a_1a}\gamma^{(1,0)}_{b_1b,N} + \delta_{b_1b}\gamma^{(1,0)}_{a_1a,N}\right] \\
&- \left[\delta_{ca}\delta_{\bar{c}b}\left(B_c^{(1,1)} + A_c^{(1,1)}\ell_Q\right) + \delta_{ca}\gamma^{(1,1)}_{\bar{c}b,N} + \delta_{\bar{c}b}\gamma^{(1,1)}_{ca,N}\right] ,
\end{aligned}
\tag{4.3.17}
$$

$$
\begin{aligned}
\mathcal{H}^{F(1,1)}_{c\bar{c}\leftarrow ab,N} = &\ \delta_{ca}\delta_{\bar{c}b}H_c^{F(1,1)} + \delta_{ca}C^{(1,1)}_{\bar{c}b,N} + \delta_{\bar{c}b}C^{(1,1)}_{ca,N} + C^{(1,0)}_{ca,N}C^{(0,1)}_{\bar{c}b,N} + C^{(0,1)}_{ca,N}C^{(1,0)}_{\bar{c}b,N} \\
&+ H_c^{F(1,0)}\left(\delta_{ca}C^{(0,1)}_{\bar{c}b,N} + \delta_{\bar{c}b}C^{(0,1)}_{ca,N}\right) + H_c^{F(0,1)}\left(\delta_{ca}C^{(1,0)}_{\bar{c}b,N} + \delta_{\bar{c}b}C^{(1,0)}_{ca,N}\right) \\
&+ \frac{1}{2}A_c^{(1,1)}\delta_{ca}\delta_{\bar{c}b}\ell_Q^2 + \left(\delta_{ca}\gamma^{(1,1)}_{\bar{c}b,N} + \delta_{\bar{c}b}\gamma^{(1,1)}_{ca,N}\right)\ell_F \\
&- \left[\delta_{ca}\delta_{\bar{c}b}\left(B_c^{(1,1)} + A_c^{(1,1)}\ell_Q\right) + \delta_{ca}\gamma^{(1,1)}_{\bar{c}b,N} + \delta_{\bar{c}b}\gamma^{(1,1)}_{ca,N}\right]\ell_Q \\
&+ \frac{1}{2}\sum_{a_1,b_1}\left[\mathcal{H}^{F(1,0)}_{c\bar{c}\leftarrow a_1b_1,N} + \delta_{ca_1}\delta_{\bar{c}b_1}H_c^{F(1,0)} + \delta_{ca_1}C^{(1,0)}_{\bar{c}b_1,N} + \delta_{\bar{c}b_1}C^{(1,0)}_{ca_1,N}\right] \\
&\quad\times\left[\left(\delta_{a_1a}\gamma^{(0,1)}_{b_1b,N} + \delta_{b_1b}\gamma^{(0,1)}_{a_1a,N}\right)(\ell_F - \ell_Q) - \delta_{a_1a}\delta_{b_1b}\left(\left(B_c^{(0,1)} + \frac{1}{2}A_c^{(0,1)}\ell_Q\right)\ell_Q\right)\right] \\
&+ \frac{1}{2}\sum_{a_1,b_1}\left[\mathcal{H}^{F(0,1)}_{c\bar{c}\leftarrow a_1b_1,N} + \delta_{ca_1}\delta_{\bar{c}b_1}H_c^{F(0,1)} + \delta_{ca_1}C^{(0,1)}_{\bar{c}b_1,N} + \delta_{\bar{c}b_1}C^{(0,1)}_{ca_1,N}\right] \\
&\quad\times\left[\left(\delta_{a_1a}\gamma^{(1,0)}_{b_1b,N} + \delta_{b_1b}\gamma^{(1,0)}_{a_1a,N}\right)(\ell_F - \ell_Q) - \delta_{a_1a}\delta_{b_1b}\left(\left(B_c^{(1,0)} + \frac{1}{2}A_c^{(1,0)}\ell_Q\right)\ell_Q\right)\right] .
\end{aligned}
\tag{4.3.18}
$$

In the expressions above we have defined $\ell_Q = \ln M^2/Q^2$ and $\ell_F = \ln M^2/\mu_F^2$, while $\gamma^{(i,j)}_{ab,N}$ represent the corresponding (moments of the) splitting functions. The coefficients $A_c^{(i,j)}$ and $B_c^{(i,j)}$ arise from the mixed expansion of the Sudakov form factor,

$$
S_c(M,b) = \exp\left\{-\int_{b_0^2/b^2}^{M^2}\frac{dq^2}{q^2}\left[A_c\left(\alpha_s,\alpha\right)\ln\frac{M^2}{q^2} + B_c\left(\alpha_s,\alpha\right)\right]\right\} ,
\tag{4.3.19}
$$

with

$$
\begin{aligned}
A_c\left(\alpha_s,\alpha\right) &= \left(\frac{\alpha_s}{\pi}\right)A_c^{(1,0)} + \left(\frac{\alpha}{\pi}\right)A_c^{(0,1)} + \left(\frac{\alpha_s}{\pi}\right)\left(\frac{\alpha}{\pi}\right)A_c^{(1,1)} + \dots , \\
B_c\left(\alpha_s,\alpha\right) &= \left(\frac{\alpha_s}{\pi}\right)B_c^{(1,0)} + \left(\frac{\alpha}{\pi}\right)B_c^{(0,1)} + \left(\frac{\alpha_s}{\pi}\right)\left(\frac{\alpha}{\pi}\right)B_c^{(1,1)} + \dots ,
\end{aligned}
\tag{4.3.20}
$$

and their explicit expression for the quark-initiated case (which is the case in the Drell Yan mechanism) is given by

$$\begin{aligned} A_q^{(1,0)} &= C_F\,, \qquad A_q^{(0,1)} = e_q^2\,, \\ B_q^{(1,0)} &= -\frac{3}{2}C_F\,, \qquad B_q^{(0,1)} = -\frac{3}{2}e_q^2\,, \\ A_q^{(1,1)} &= 0\,, \qquad B_q^{(1,1)} = \frac{C_F e_q^2}{8}(-3+24\zeta_2-48\zeta_3)\,. \end{aligned} \tag{4.3.21}$$

Notice that the coefficients $A_q^{(1,1)}$ and $B_q^{(1,1)}$ can be calculated by abelianising the coefficients $A_q^{(2)}$ and $B_q^{(2)}$ in Eqs. (B.1) and (B.3) in the Appendix B, respectively.

Finally, we present the collinear functions, again for $c = q$, and the hard-virtual coefficients, the latter specifically for the DY case as they are a process-dependent quantity. The separation between C and H coefficients is scheme dependent. Those presented here are obtained in the so-called *hard* scheme [110]. Up to NLO in QCD and QED, the hard-virtual coefficients take the form

$$H_q^{DY(1,0)} = C_F\left(\frac{\pi^2}{2}-4\right) = \frac{C_F}{e_q^2}H_q^{DY(0,1)}\,, \tag{4.3.22}$$

and the collinear functions are given by

$$\begin{aligned} C_{qq}^{(1,0)}(z) &= \frac{C_F}{2}(1-z) = \frac{C_F}{e_q^2}C_{qq}^{(0,1)}(z)\,, \\ C_{qg}^{(1,0)}(z) &= \frac{1}{2}z(1-z) = C_{q\gamma}^{(0,1)}(z)\frac{T_R}{e_q^2 N_C}\,, \\ C_{gq}^{(1,0)}(z) &= \frac{C_F}{2}z = \frac{C_F}{e_q^2}C_{\gamma q}^{(0,1)}(z)\,. \end{aligned} \tag{4.3.23}$$

The hard-virtual coefficient needed for the first order in the mixed QCD⊗QED expansion takes the following form,

$$H_q^{DY(1,1)} = \frac{C_F e_q^2}{2}\left(-15\zeta_3+\frac{511}{16}-\frac{67\pi^2}{12}+\frac{17\pi^4}{45}\right)\,, \tag{4.3.24}$$

while the needed collinear functions are given by the following expressions:

$$
\begin{aligned}
C_{qq'}^{(1,1)}(z) = \delta_{qq'}\, e_q^2 C_F \Bigg\{ & \frac{1+z^2}{1-z}\left(\frac{\mathrm{Li}_3(1-z)}{2} + \frac{1}{2}\,\mathrm{Li}_2(z)\log(1-z) + \frac{3\,\mathrm{Li}_2(z)\log(z)}{2}\right. \\
& \left. - \frac{5\,\mathrm{Li}_3(z)}{2} + \frac{3}{4}\log(z)\log^2(1-z) + \frac{1}{4}\log^2(z)\log(1-z) - \frac{1}{12}\pi^2\log(1-z) + \frac{5\zeta_3}{2}\right) \\
& + (1-z)\left(-\mathrm{Li}_2(z) - \frac{3}{2}\log(1-z)\log(z) + \frac{2\pi^2}{3} - \frac{29}{4}\right) + \frac{1}{24}(1+z)\log^3(z) \\
& + \frac{1}{1-z}\left(\frac{1}{8}\left(-2z^2+2z+3\right)\log^2(z) + \frac{1}{4}\left(17z^2-13z+4\right)\log(z)\right) \\
& - \frac{z}{4}\log(1-z) - \frac{1}{4}\left[(2\pi^2-18)(1-z) - (1+z)\log z\right]\Bigg\},
\end{aligned}
\tag{4.3.25}
$$

$$
\begin{aligned}
C_{q\bar{q}'}^{(1,1)}(z) = \delta_{qq'}\, 2C_F e_q^2 \Bigg\{ & \frac{1+z^2}{1+z}\left(\frac{3\,\mathrm{Li}_3(-z)}{2} + \mathrm{Li}_3(z) + \mathrm{Li}_3\left(\frac{1}{1+z}\right) - \frac{\mathrm{Li}_2(-z)\log(z)}{2}\right. \\
& - \frac{\mathrm{Li}_2(z)\log(z)}{2} - \frac{1}{24}\log^3(z) - \frac{1}{6}\log^3(1+z) + \frac{1}{4}\log(1+z)\log^2(z) \\
& \left. + \frac{\pi^2}{12}\log(1+z) - \frac{3\zeta_3}{4}\right) + (1-z)\left(\frac{\mathrm{Li}_2(z)}{2} + \frac{1}{2}\log(1-z)\log(z) + \frac{15}{8}\right) \\
& - \frac{1}{2}(1+z)\left(\mathrm{Li}_2(-z) + \log(z)\log(1+z)\right) + \frac{\pi^2}{24}(z-3) + \frac{1}{8}(11z+3)\log(z)\Bigg\},
\end{aligned}
\tag{4.3.26}
$$

$$
\begin{aligned}
C_{qg}^{(1,1)}(z) = e_q^2 \Bigg\{ & \left(2z^2-2z+1\right)\left(\zeta_3 - \frac{\mathrm{Li}_3(1-z)}{8} - \frac{\mathrm{Li}_3(z)}{8} + \frac{1}{8}\,\mathrm{Li}_2(1-z)\log(1-z)\right. \\
& \left. + \frac{\mathrm{Li}_2(z)\log(z)}{8} - \frac{1}{48}\log^3(1-z) + \frac{1}{16}\log(z)\log^2(1-z) + \frac{1}{16}\log^2(z)\log(1-z)\right) \\
& - \frac{3z^2}{8} - \frac{1}{96}\left(4z^2-2z+1\right)\log^3(z) + \frac{1}{64}\left(-8z^2+12z+1\right)\log^2(z) \\
& + \frac{1}{32}\left(-8z^2+23z+8\right)\log(z) + \frac{5}{24}\pi^2(1-z)z + \frac{11z}{32} + \frac{1}{8}(1-z)z\log^2(1-z) \\
& - \frac{1}{4}(1-z)z\log(1-z)\log(z) - \frac{1}{16}(3-4z)z\log(1-z) - \frac{9}{32} \\
& - \frac{1}{4}\left[z\log z + \frac{1}{2}\left(1-z^2\right) + \left(\pi^2-8\right)z(1-z)\right]\Bigg\},
\end{aligned}
\tag{4.3.27}
$$

$$C_{q\gamma}^{(1,1)}(z) = 2C_F C_A C_{qg}^{(1,1)}(z)\,. \tag{4.3.28}$$

Note that the hard-virtual function $H^{DY(1,1)}$ in Eq. (4.3.24) and the collinear coefficients in Eqs. (4.3.25)-(4.3.28) could be calculated by means of the $C^{(2)}$ NNLO QCD coefficients in Eqs. (B.5)-(B.8) and the hard-virtual function $H^{DY(2)}$ in Eq. (B.9) in the Appendix B, by taking the corresponding abelian limit.

The results above provide all the ingredients needed for the application of the q_T-subtraction formalism to the calculation of mixed QCD⊗QED corrections. The same coefficients are required by the transverse-momentum resummation formalism, considering in this case the full dependence on the resummation scale Q.

4.4 Results and Phenomenology

In order to obtain quantitative results, our calculation is implemented in two independent parton-level Monte Carlo programs. One of them is based on MCFM [27] (including the NNLO QCD corrections), suitably modified to deal with mixed corrections and to apply the q_T-subtraction formalism. The other is a private implementation, which relies on the FKS subtraction method [67] to deal with the NLO-type divergences (adapted to the mixed QCD⊗QED case), and on analytic results for the relevant scattering amplitudes obtained from Ref. [128], plus an explicit calculation of the tree-level all-quarks channels using FeynCalc 9.2.0 [129].

For our phenomenological analysis we consider $n_F = 5$ massless quark flavours. We work in the G_μ scheme for the EW couplings, using the input values $G_\mu = 1.16639 \times 10^{-5}$ GeV^{-2}, $M_Z = 91.1876$ GeV and $M_W = 80.385$ GeV. The width of the Z boson is set to the value $\Gamma_Z = 2.4952$ GeV. For the parton luminosities and strong coupling, we use the NNPDF3.1luxQED set with five flavours [130] through the LHAPDF interface [108], always at NNLO accuracy, regardless the order of the calculation. Both renormalization and factorization scales are set to the default value $\mu_R = \mu_F = m_{\ell_1\ell_2}$. For the cutoff parameter of the subtraction method, $q_{T,\text{cut}}$, we choose the central value $q_{T,\text{cut}} = 0.2$ GeV. We checked that our results are compatible within uncertainties when varying this parameter around its central value by a factor of 2.

As a first check of our implementation, we computed the inclusive cross section for the production of an on-shell Z boson, and compared to the predictions obtained from the analytic results presented in Ref. [2] (see Chapter 3 of the present work). The corresponding

Channel	qq'	qg	$q\gamma$	$g\gamma$
q_T-subtraction [pb]	52.6(4)	-34.8(3)	-1.41(1)	0.569(2)
Analytic (Ref. [2]) [pb]	52.3	-35.0	-1.41	0.571

Table 4.1: The $\mathcal{O}(\alpha_s\alpha)$ contribution to the inclusive on-shell Z production cross section for the different partonic channels. The results obtained using q_T-subtraction are compared to the inclusive predictions obtained in Ref. [2]. Numerical uncertainties on the last digit are indicated in parenthesis for our predictions, while the uncertainties of the inclusive implementation are below the last digits shown. The category denoted by qq' includes all combinations of quarks and anti-quarks.

$\mathcal{O}(\alpha_s\alpha)$ contributions to the cross section, split into quark-quark, quark-gluon, quark-photon and gluon-photon initiated channels, are shown in table 4.1. As can be seen from the table, we can reach sub-percent precision for these inclusive predictions, and we find full agreement with the analytic results from Ref. [2]. As an additional validation, we have computed the NNLO QCD differential distributions using the public code MATRIX [131], finding full agreement with our results.

For all of the differential distributions presented here, we consider the following set of cuts,

$$p_{T,\ell_1} > 25\,\text{GeV}\,, \quad p_{T,\ell_2} > 20\,\text{GeV}\,, \quad |y|_{\ell_{1,2}} < 2.5\,, \quad m_{\ell_1\ell_2} > 50\,\text{GeV}, \tag{4.4.1}$$

where ℓ_1 and ℓ_2 represent the final-state leptons, ordered according to their transverse momentum. Since we consider only neutrinos in the final state, there is no need to recombine collinear leptons and photons.

We start by presenting the transverse momentum distribution of the leptons in figure 4.1. The kinematical dependence of the mixed corrections is highly non trivial. This feature is also shared by the pure QCD and QED corrections, and it is expected due to the particular features that these two distributions present at fixed order in perturbation theory. At LO both leptons are back-to-back, and therefore the distributions are identical. The radiative corrections produce the change of shape that render the p_{T,ℓ_1} spectrum harder than the p_{T,ℓ_2} one, producing therefore sizeable distortions in the distribution. Furthermore, some regions of the phase space are almost not populated at LO, and therefore radiative corrections become more relevant. This is the case for the region of p_{T,ℓ_2} below the lower cut on p_{T,ℓ_1}, which is directly not allowed for Born kinematics, or the region above $p_{T,\ell_{1,2}} \simeq M_Z/2$, which does not receive contributions from the Z peak at LO.

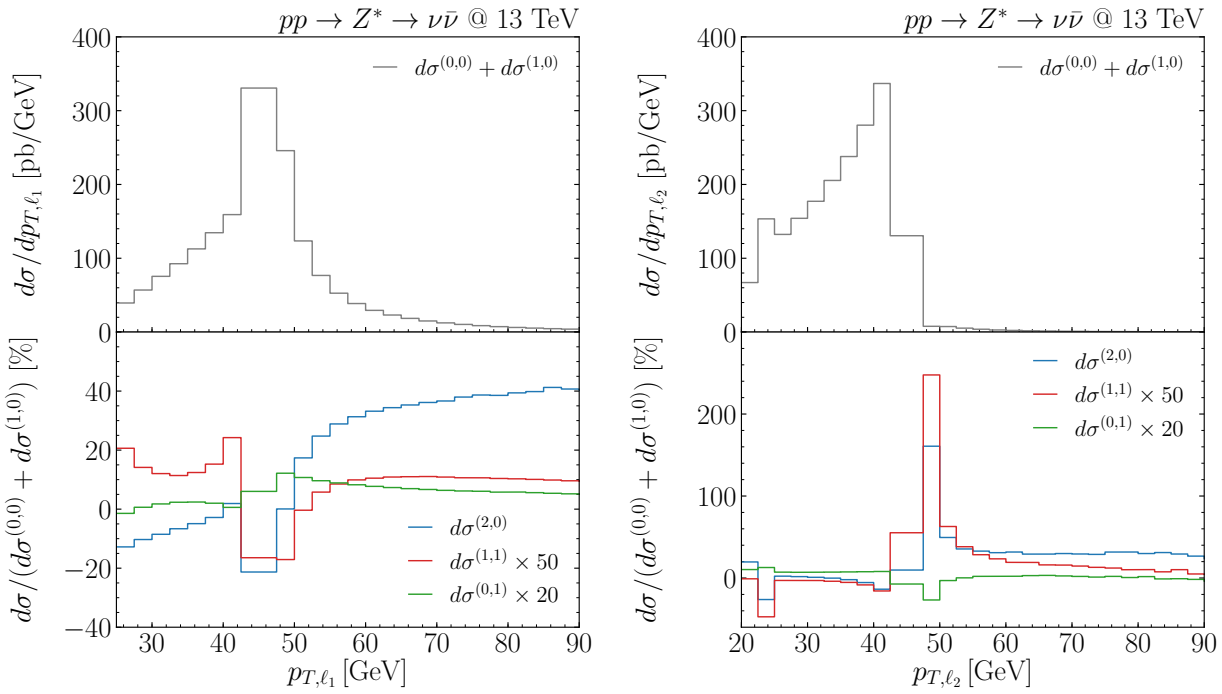

Figure 4.1: Transverse momentum distributions for the hardest (left) and softer (right) lepton. The upper panel shows the NLO QCD prediction, while the lower panel shows the NNLO QCD (blue), NLO QED (green) and mixed (red) corrections, normalized to the NLO result.

From figure 4.1 we can observe that for $p_{T,\ell_1} < M_Z/2$ the mixed corrections are positive, representing an increase of about 0.5% with respect to the NLO prediction. The corrections then change sign, being of the order of -0.5% in the first bins after $p_{T,\ell_1} = M_Z/2$, which corresponds to the expected Sudakov shoulder near the kinematic boundaries mentioned in the previous paragraph [132]. The mixed corrections then result smaller at the tail of the distribution. With respect to the softer lepton, we can observe that the corrections become very large around and slightly above $p_{T,\ell_2} = M_Z/2$, a pattern shared by the NNLO QCD corrections. In this region, the effect of the mixed QCD⊗QED contribution can reach the $\mathcal{O}(5\%)$ with respect to the NLO QCD result. In addition, we can also observe a small (negative) peak in the corrections around $p_{T,\ell_2} = 25$ GeV, which is related to the presence of a cut in p_{T,ℓ_1}, as mentioned before.

We continue by presenting the rapidity distributions of the leptons, again ordered according to their transverse momentum, in figure 4.2. In both cases, we can observe that the mixed corrections are extremely small, and show a very mild dependence on the corresponding kinematical variable. The reason for this particularly small value of the corrections is a very strong cancellation between the main partonic channels, that is the $q\bar{q}$ and qg initiated processes, over the whole rapidity range under consideration, a pattern that can also be observed

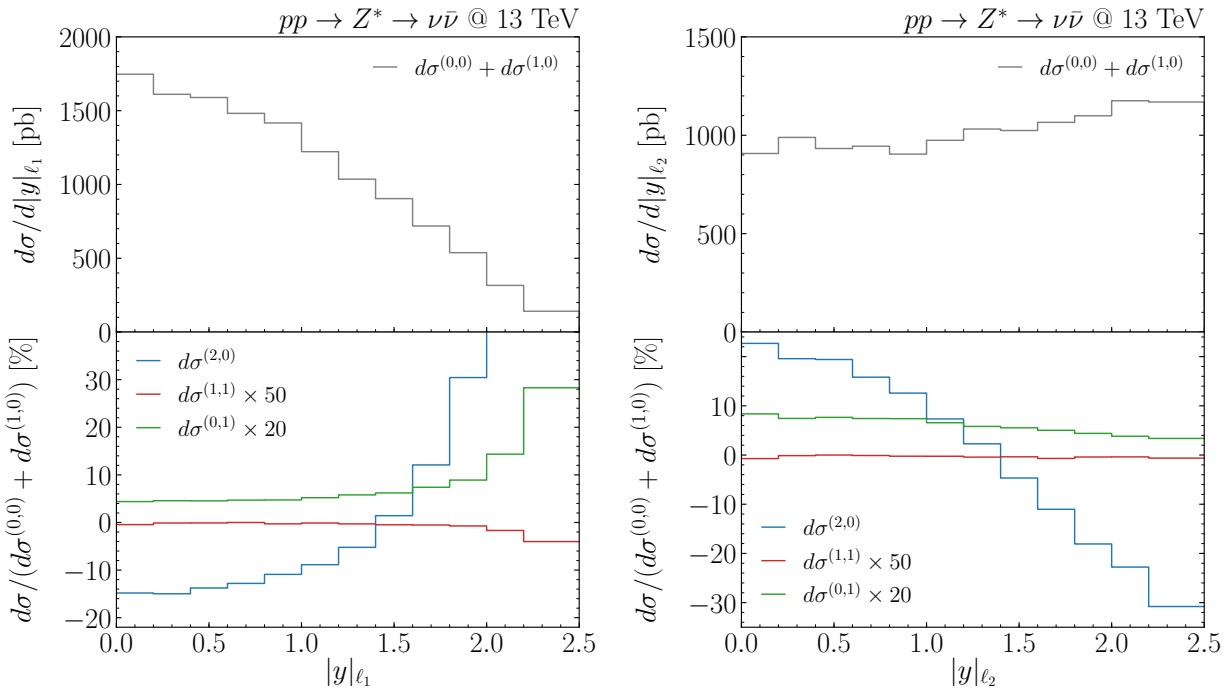

Figure 4.2: Rapidity distributions for the hardest (left) and softer (right) lepton. The upper panel shows the NLO QCD prediction, while the lower panel shows the NNLO QCD (blue), NLO QED (green) and mixed (red) corrections, normalized to the NLO result.

for instance at the level of the total cross section. We note that this effect is even stronger with the set of cuts in Eq. (4.4.1), compared to the fully inclusive case, with cancellations of about 90% between the different channels.

In figure 4.3 we present distributions for the lepton-pair system, specifically its transverse momentum and rapidity. The mixed corrections are negative below $p_{T,\ell_1\ell_2} \sim 15$ GeV, and diverge in the $p_{T,\ell_1\ell_2} \to 0$ limit. The sign of the mixed corrections in the low transverse momentum region is the same as the one of the NNLO QCD corrections, as one can infer from the sign of the logarithmic coefficient with highest power (see Eq. (4.3.14) for the mixed corrections and Eq. (66) of Ref. [111] for NNLO QCD). Above $p_{T,\ell_1\ell_2} \sim 15$ GeV the mixed corrections become positive, increasing the NLO QCD result by about 0.3%. In the same region the NLO QED corrections are of the order of 0.5%. As it is well known, at low-q_T, the large logarithmic corrections to the cross section have to be treated with transverse momentum resummation in order to recover the reliability of the prediction. This is true not only for the transverse momentum distribution but for any observable which presents a kinematical region directly related to $q_T = 0$.

The mixed corrections for the lepton-pair rapidity present a kinematic dependence that is similar to the one of the NNLO QCD contribution. They are negative for small $|y|_{\ell_1\ell_2}$, and

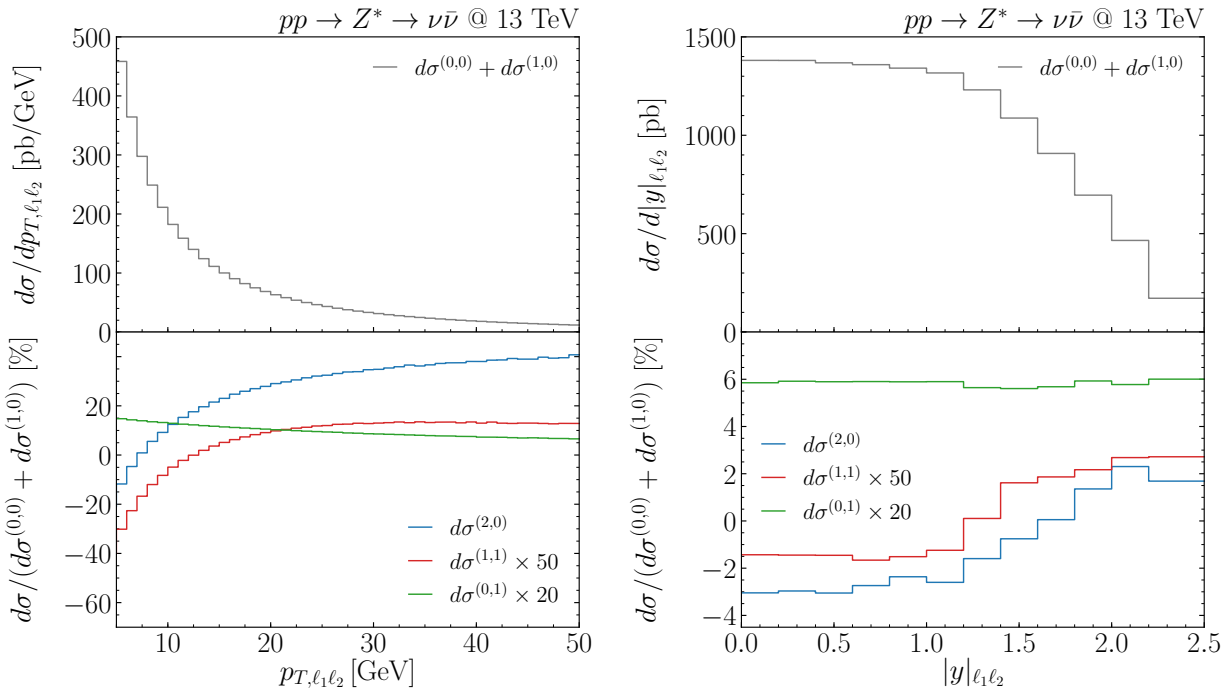

Figure 4.3: Lepton-pair transverse momentum (left) and rapidity (right) distributions. The upper panel shows the NLO QCD prediction, while the lower panel shows the NNLO QCD (blue), NLO QED (green) and mixed (red) corrections, normalized to the NLO result.

become positive for larger values of rapidity. The overall size of the mixed corrections is of course much smaller though, being of the order of 50 times smaller than the NNLO QCD corrections.

Finally, we present in figure 4.4 the ϕ^* and $\cos\theta^*$ distributions, defined as [133]

$$\begin{aligned} \phi^* &= \tan\left(\frac{\pi - \Delta\Phi}{2}\right) \sin\theta^* \\ \Delta\Phi &= \phi_{\ell_1} - \phi_{\ell_2} \\ \cos\theta^* &= \tanh\left(\frac{y_{\ell_1} - y_{\ell_2}}{2}\right) . \end{aligned} \tag{4.4.2}$$

Since at LO the two leptons are back-to-back, the ϕ^* distribution is trivial at that order, and contributions with $\phi^* \neq 0$ only start at NLO. As in the case of the transverse momentum, the small-ϕ^* region is not well behaved at fixed order and it is necessary the use of transverse resummation in order to recover the reliability of the prediction in those kinematical regions. The pattern of corrections, not only for the mixed but also for the NNLO QCD and NLO QED contributions, is very similar to the one observed in the $p_{T,\ell_1\ell_2}$ distribution, in particular with the mixed corrections being negative at small ϕ^* and becoming positive for larger values, and

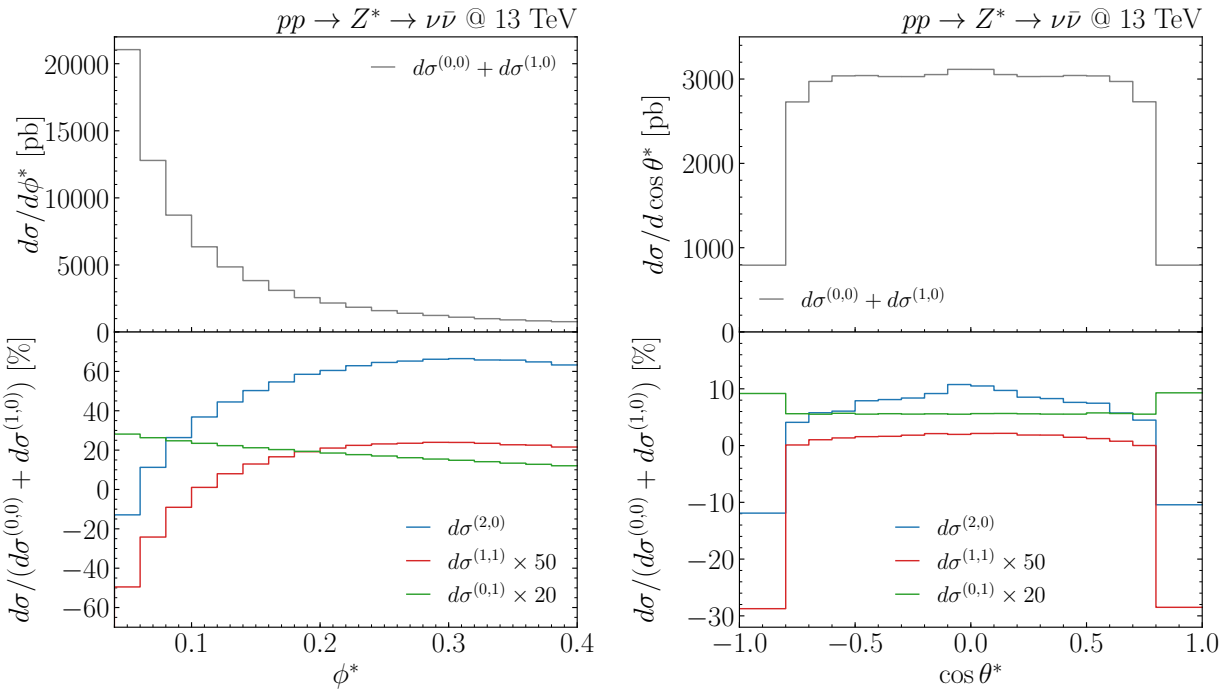

Figure 4.4: The ϕ^* distribution. The upper panel shows the NLO QCD prediction, while the lower panel shows the NNLO QCD (blue), NLO QED (green) and mixed (red) corrections, normalized to the NLO result.

about a factor of 2 smaller than the NLO QED corrections in the tail of the distribution.

In the case of $\cos\theta^*$, the distribution is rather flat in the central region, and presents a strong suppression for $\cos\theta^* = \pm 1$, which is only populated by events with very large and opposite rapidities of the corresponding leptons. This region is therefore particularly suppressed by the presence of the cuts on $y_{\ell_{1,2}}$, which directly forbid the region above $|\cos\theta^*| \sim 0.987$. From the lower panel of the figure we can observe that the perturbative corrections are rather flat in the region where the bulk of the cross section is located, and therefore they follow a pattern similar to the one observed for the total cross section. In particular, the mixed QCD⊗QED corrections are extremely small, and become more relevant only close to the boundaries, where they reach the 0.6% level (note that the last bin of the distribution is larger and extends from $|\cos\theta^*| = 0.8$ to 1).

Before going to the summary, it is interesting to compare the size of the mixed QCD⊗QED corrections computed here against the naive approximation in which QCD and QED corrections factorize. Specifically, defining for a given bin

$$d\Delta^{(i,j)} = d\sigma^{(i,j)}/d\sigma^{(0,0)}\,, \tag{4.4.3}$$

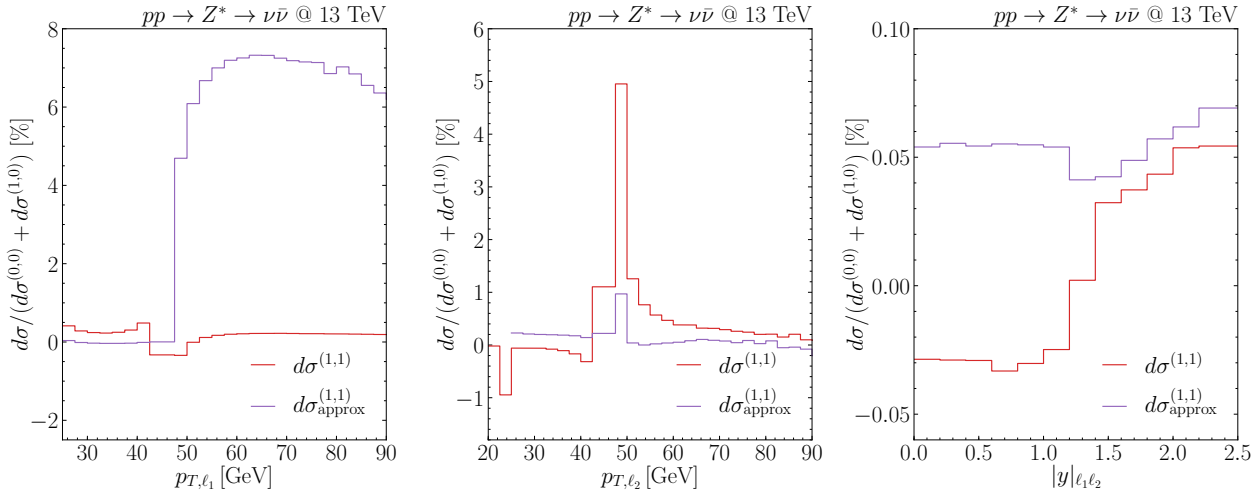

Figure 4.5: Comparison between the mixed QCD⊗QED corrections (red) and the naive factorization approximation (purple), for the transverse momentum of the hardest (left) and softer (center) lepton, and the rapidity of the pair (right).

the multiplicative approximation to the $\mathcal{O}(\alpha_s\alpha)$ based on NLO QCD and QED predictions is given by the product

$$d\sigma^{(1,1)}_{\text{approx}} = d\sigma^{(0,0)} d\Delta^{(1,0)} d\Delta^{(0,1)} \,. \tag{4.4.4}$$

In figure 4.5 we present the mixed QCD⊗QED corrections together with the approximation defined by Eq. (4.4.4), for the transverse momentum of the two leptons and the rapidity of the pair. The results are normalized to the NLO QCD prediction, as in the lower panels of the previous figures. We can observe that, in all cases, the multiplicative approach is a rather poor approximation to the full results. This is in line with the observations made for the total cross section in Ref. [2]. The discrepancies, however, can be strongly enhanced at the differential level. This can be seen for instance in the $p_{T,\ell_1} > M_Z/2$ region, where the exact $\mathcal{O}(\alpha_s\alpha)$ corrections are at the per-mille level, while the factorization approximation predicts $\sim 7\%$ corrections. The reason for this big discrepancy is the presence of large K-factors at NLO (both in QCD and QED), associated to the fact that at LO this region is only populated by events that are away from the Z peak. In the case of the p_{T,ℓ_2} distribution, we can observe that the multiplicative approach has the wrong sign for $p_{T,\ell_2} < M_Z/2$ (note that the approximation is not well defined for $p_{T,\ell_2} < 25$ GeV due to the cut in the hardest lepton), and fails to reproduce the correct size of the corrections around the peak located in $p_{T,\ell_2} \sim M_Z/2$. Finally, for the rapidity of the lepton pair we can see that the factorization approximation predicts a rather flat K-factor, failing to describe the kinematical dependence of the mixed corrections.

CHAPTER 5

Conclusions

It is undeniable that over the last decade, both the theoretical and experimental developments in particle physics have shown an impressive agreement. While no conclusive evidence for new physics has been found yet, BSM theories might not be available for direct detection in resonant searches, but only through small deviations between theory and the experiment.

These facts shape the need for precise theoretical computations to effectively test the predictions of the SM. Moreover, although the Large Hadron Collider was first meant to explore high energy sectors and discover new fundamental particles, such as the Higgs, the great accuracy of the measurements, which will be even enhanced in the High-Luminosity upgrade, makes it an useful and essential tool for precision testing.

Specifically, from all the experiments at the LHC, the Drell Yan mechanism gathers a big interest, since it is one of the most clean, sensitive and precise ways to access and test the EW and strong sectors of the SM. In this sense, all along this work we focused on reaching precise theoretical determinations for the Drell Yan cross section at the LHC, by including the electromagnetic effects within the perturbative expansion. These, although subdominant, become important in the current context of precision measurements.

As for any theoretical calculation, the path to reach precision is rather involved and non-lineal, especially concerning the higher orders. In the case of the mixed corrections to Drell Yan, both the photon PDF and the mixed order splitting functions were needed, and they were, in fact, recently computed [39–42]. With this in mind, in the first part of this work we presented the mixed QCD$\otimes$QED corrections to the total Z-production cross

section in hadronic collisions. These results were obtained for the first time and achieved via an *abelianisation* procedure that profits from the available pure QCD NNLO terms. Even more, we also computed the pure QED NNLO corrections, thus showing the versatility of the procedure and, most importantly, completing the set of NNLO contributions to the neutral current Drell Yan mechanism. These results were published in [2].

Furthermore, regarding the phenomenological impact, our analysis showed that the mixed corrections are of the order of per mille at the LHC, but only a factor of ~ 3.5 smaller than the pure QCD NNLO due to a sign change that occurs in the latter at $\sqrt{S} \sim 14$ TeV. On the other hand, pure QED NNLO terms were found to be negative small corrections of the order of 10^{-5}. Finally, the full QCD$\oplus$QED NNLO corrections are found to stabilize the scale dependence of the final result.

Additionally, the exact K-factor at order $\mathcal{O}(\alpha_s\alpha)$ was compared with the naive factorization approximation, which consists of the mixed order term of the product of QCD and QED NLO K-factors. It was shown that the latter fails to reproduce the exact result by a factor of two or more. Although in this specific situation the difference is not highly significant, due to the smallness of the overall contribution, this result hints that the factorization approximation may not work in a general case.

In a second part, we decided to go one step further and focus on the exclusive calculation of the mixed terms for the neutral-current Drell Yan process. To achieve this goal, we addressed the extension of the q_T-subtraction formalism in order to deal with the case of mixed QCD$\otimes$QED divergences in the $q_T = 0$ region. We extended the method to be applied to the fully exclusive calculation of the $\mathcal{O}(\alpha_s\alpha)$ corrections to the production of generic colorless and neutral final states (e.g. Z and Higgs bosons, photons, neutrinos). Specifically, we have provided all the relevant formulas for its implementation at $\mathcal{O}(\alpha_s\alpha)$ and used the formalism to address the production of an off-shell Z boson in hadronic collisions. Furthermore, our coefficient functions and the hard virtual coefficients are also of value for transverse momentum resummation and the expressions contain the full dependence on the resummation scale Q. Our results are published in [134].

As for the phenomenological impact, we studied the production of an off-shell Z boson, followed by a consequent decay into a pair of neutrinos. We presented differential distributions for the final-state leptons at the LHC, and found that the corrections can have a sizeable dependence on the kinematics, and not necessarily following the pattern of the NNLO QCD

corrections. The size of the corrections is typically very small and below 1%, though it can be enhanced in some particular phase space regions.

We have also compared the mixed QCD$\otimes$QED contribution with the factorization approximation based on the product of QCD and QED K-factors, this time at the differential level. We have found that this multiplicative approach is in general a bad approximation to the mixed corrections, and the disagreement can be quite extreme for some differential distributions.

APPENDIX

NNLO Correction Terms for Drell Yan

Here we present the expressions for the different correction terms needed for the full set of NNLO QCD⊕QED inclusive results. For the sake of completeness we include also the NLO Δ functions, which were first mentioned in section 3.1.

we recall the following distributions

$$\mathcal{D}_i(x) = \left[\frac{\log^i(1-x)}{1-x}\right]_+ \tag{A.1}$$

which appear in the soft terms regularizing the divergence of soft emission ($x \approx 1$) and defined as usual by

$$\int_0^1 \mathcal{D}_i(x) f(x) \mathrm{d}x = \int_0^1 \frac{\log^i(1-x)}{1-x} \left[f(x) - f(1)\right] \mathrm{d}x \,. \tag{A.2}$$

We also define an auxiliary variable to write the dependence on the factorization scale,

$$L_{\mu_F} = -\log\left(\frac{\mu_F^2}{Q^2}\right), \tag{A.3}$$

where μ_F is the factorization scale and Q the invariant mass of the produced Z.

The corrections needed for the NLO result are

$$\begin{aligned}\Delta_{q\bar{q}}^{(1)} =& 8\mathcal{D}_0(x)L_{\mu_F} + 16\mathcal{D}_1(x) + \delta(x-1)(6L_{\mu_F} + 8\zeta_2 - 16) \\ & - 4L_{\mu_F}(x+1) - \frac{4\left(x^2+1\right)\log(x)}{1-x} - 8(x+1)\log(1-x) \qquad \text{(A.4)} \\ \Delta_{qg}^{(1)} =& \frac{1}{2}\left(2\left(2x^2-2x+1\right)\left(L_{\mu_F} + 2\log(1-x) - \log(x)\right) - 7x^2 + 6x + 1\right). \qquad \text{(A.5)}\end{aligned}$$

For the second NNLO, several correction terms are introduced. We denote with a C_A superscript the corrections coming from the non-abelian part of the contributions (only relevant for the QCD NNLO contribution), with n_F the ones that involve a sum over fermion families (relevant for the QCD and QED NNLO result), and with C_F the rest of the abelian contributions.

The non-abelian contributions on the quark-antiquark channel are

$$\begin{aligned}\Delta_{q\bar{q}}^{(2)C_A} =& \Delta_{q\bar{q}}^{\text{NS},C_A} - \Delta_{q\bar{q}}^{C_F - C_A/2} \qquad \text{(A.6)} \\ \Delta_{q\bar{q}}^{(2)C_F} =& \Delta_{q\bar{q}}^{\text{NS},C_F} + 2\Delta_{q\bar{q}}^{C_F - C_A/2} \qquad \text{(A.7)} \\ \Delta_{q\bar{q}}^{(2)n_F} =& \frac{8}{27}\left(9\mathcal{D}_0(x)L_{\mu_F}^2 + L_{\mu_F}\left(36\mathcal{D}_1(x) - 30\mathcal{D}_0(x)\right) - 36\mathcal{D}_0(x)\zeta_2 + 28\mathcal{D}_0(x)\right. \\ & \left. -60\mathcal{D}_1(x) + 36\mathcal{D}_2(x)\right) + \frac{1}{18}\delta(x-1)\left(36L_{\mu_F}^2 - 204L_{\mu_F} - 224\zeta_2\right. \\ & \left. +144\zeta_3 + 381\right) + \frac{1}{27(x-1)}\left(2\left(2\left(18x^2\text{Li}_2(1-x) - (x-1)\right.\right.\right. \\ & \left.\left.\left.\times\left(9L_{\mu_F}^2(x+1) + L_{\mu_F}(6-66x) - 36x\zeta_2 + 103x - 36\zeta_2 - 47\right)\right)\right. \\ & \left. - 24\log(1-x)\left((x-1)(3L_{\mu_F}(x+1) - 11x + 1) - 6\left(x^2+1\right)\log(x)\right)\right. \\ & \left. + 18\left(4L_{\mu_F}\left(x^2+1\right) - 11x^2 + 10x - 9\right)\log(x) - 72\left(x^2-1\right)\log^2(1-x)\right. \\ & \left. -9\left(5x^2+7\right)\log^2(x)\right)\right)^{1}, \qquad \text{(A.8)}\end{aligned}$$

[1] Here we amend the result for $\Delta^{(2)}_{q\bar{q},A^2}$ given in Eq.(B.11) of ref [20] by adding the corresponding missing x factor to term $103x$ above.

where

$$
\begin{aligned}
\Delta_{q\bar{q}}^{\mathrm{NS},C_A} =& \frac{1}{180}\delta(x-1)\left(-1980L_{\mu_F}^2 - 4320L_{\mu_F}\,\zeta_3 + 11580L_{\mu_F}\right.\\
&\left.-432\zeta_2^2 + 11840\zeta_2 + 5040\zeta_3 - 23025\right) - \frac{4}{27}\left(99\mathcal{D}_0(x)L_{\mu_F}^2\right.\\
&+108\mathcal{D}_0(x)L_{\mu_F}\,\zeta_2 - 402\mathcal{D}_0(x)L_{\mu_F} - 396\mathcal{D}_0(x)\zeta_2 - 378\mathcal{D}_0(x)\zeta_3\\
&\left.+404\mathcal{D}_0(x) + 396\mathcal{D}_1(x)L_{\mu_F} + 216\mathcal{D}_1(x)\zeta_2 - 804\mathcal{D}_1(x) + 396\mathcal{D}_2(x)\right)\\
&+\frac{1}{27(x-1)}\left[2\left(36\mathrm{Li}_2(1-x)\left(3L_{\mu_F}\left(x^2+1\right) - 7x^2 + 3x + 3\right)\right.\right.\\
&+99L_{\mu_F}^2\left(x^2-1\right) + 6L_{\mu_F}(x-1)(2x(9\zeta_2 - 62) + 18\zeta_2 - 19)\\
&+270x^2\mathrm{S}_{1,2}(1-x) - 162\mathrm{S}_{1,2}(1-x) + 324\mathrm{Li}_3(1-x) - 450x^2\zeta_2 - 378x^2\zeta_3\\
&\left.+1139x^2 + 108x\zeta_2 - 1362x + 342\zeta_2 + 378\zeta_3 + 223\right) + 12\log(1-x)\\
&\times\left(36x^2\mathrm{Li}_2(1-x) + (x-1)(66L_{\mu_F}(x+1) + 36x\zeta_2 - 239x + 36\zeta_2\right.\\
&\left.-38) - 6\left(22x^2+13\right)\log(x)\right) - 18\log(x)\left(12\left(x^2+1\right)\mathrm{Li}_2(1-x)\right.\\
&+L_{\mu_F}\left(44x^2+26\right) + 12x^2\zeta_2 - 109x^2 + 83x + 12\zeta_2 - 78\right)\\
&\left.+792\left(x^2-1\right)\log^2(1-x) + 9\left(55x^2+32\right)\log^2(x)\right] \qquad \text{(A.9)}
\end{aligned}
$$

$$
\begin{aligned}
\Delta_{q\bar{q}}^{\mathrm{NS},C_F} =& L_{\mu_F}\left(-\mathcal{D}_0(x)(64\zeta_2+128)+96\mathcal{D}_1(x)+192\mathcal{D}_2(x)\right)+L_{\mu_F}^2\left(48\mathcal{D}_0(x)\right.\\
&\left.+64\mathcal{D}_1(x)\right)+256\mathcal{D}_0(x)\zeta_3-\mathcal{D}_1(x)(128\zeta_2+256)+128\mathcal{D}_3(x)+\delta(x-1)\\
&\times\left(L_{\mu_F}^2\left(18-32\zeta_2\right)+L_{\mu_F}\left(24\zeta_2+176\zeta_3-93\right)+\frac{8\zeta_2^2}{5}\right.\\
&\left.-70\zeta_2-60\zeta_3+\frac{511}{4}\right)+\frac{1}{3(x-1)}\left[2\left(12\left(\mathrm{Li}_2(1-x)\left(2L_{\mu_F}\left(x^2-3\right)\right.\right.\right.\right.\\
&\left.\left.\left.\left.-4x^2+x+3\right)+L_{\mu_F}^2\left(-\left(x^2+4x-5\right)\right)+L_{\mu_F}\left(x-1\right)(x(4\zeta_2+2)\right.\right.\right.\\
&\left.\left.\left.+4\zeta_2+15)+6x^2\mathrm{S}_{1,2}(1-x)+2\mathrm{S}_{1,2}(1-x)-4x^2\mathrm{Li}_3(1-x)+6\mathrm{Li}_3(1-x)-8x^2\zeta_2\right.\right.\right.\\
&\left.\left.\left.-16x^2\zeta_3+6x^2+16x\zeta_2-15x-8\zeta_2+16\zeta_3+9\right)+6\log(1-x)\right.\right.\\
&\left.\left.\times\left(6\left(x^2-3\right)\mathrm{Li}_2(1-x)-(x-1)\left(8L_{\mu_F}^2\left(x+1\right)-4L_{\mu_F}\left(x-7\right)\right.\right.\right.\right.\\
&\left.\left.\left.\left.-x(16\zeta_2+3)-16(\zeta_2+4))+4\left(L_{\mu_F}\left(9x^2+5\right)-7x^2+11x-4\right)\log(x)\right.\right.\right.\\
&\left.\left.\left.-12\left(2x^2+1\right)\log^2(x)\right)+12\log(x)\left(3\left(x^2+1\right)\mathrm{Li}_2(1-x)+L_{\mu_F}^2\left(3x^2+1\right)\right.\right.\right.\\
&\left.\left.\left.+L_{\mu_F}\left(-3x^2+10x-1\right)-12x^2\zeta_2+6x^2-19x-4\zeta_2-1\right)\right.\right.\\
&\left.\left.-6\log^2(1-x)\left(8(x-1)(3L_{\mu_F}\left(x+1\right)-2x+2)-\left(39x^2+23\right)\log(x)\right)\right.\right.\\
&\left.\left.-6\left(L_{\mu_F}\left(9x^2+3\right)-6x^2+8x-2\right)\log^2(x)-96\left(x^2-1\right)\log^3(1-x)\right.\right.\\
&\left.\left.+\left(25x^2+11\right)\log^3(x)\right)\right] \qquad \text{(A.10)}
\end{aligned}
$$

$$
\begin{aligned}
\Delta_{q\bar{q}}^{C_F-C_A/2} =& \frac{1}{3(x-1)}\Big(12\mathrm{Li}_2(1-x)\left(2L_{\mu_F}\,x^2+2L_{\mu_F}\,-9x^3+4x^2\right.\\
&\left.+4\left(x^2+1\right)\log(1-x)+2\left(2x^3+6x^2-4x-1\right)\log(x)+9x-1\right)\\
&+72(x-1)(x+1)^2\mathrm{Li}_2(-x)(\log(x)-2\log(x+1)+1)+84L_{\mu_F}\,x^2\\
&+12L_{\mu_F}\,x^2\log^2(x)-24L_{\mu_F}\,x^2\log(x)-180L_{\mu_F}\,x\\
&+12L_{\mu_F}\,\log^2(x)+60L_{\mu_F}\,\log(x)+96L_{\mu_F}\,+96x^3\mathrm{S}_{1,2}(1-x)\\
&-144x^3\mathrm{S}_{1,2}(-x)+300x^2\mathrm{S}_{1,2}(1-x)-144x^2\mathrm{S}_{1,2}(-x)-192x\mathrm{S}_{1,2}(1-x)\\
&+144x\mathrm{S}_{1,2}(-x)+12\mathrm{S}_{1,2}(1-x)+144\mathrm{S}_{1,2}(-x)-24x^3\mathrm{Li}_3(-x)-72x^2\mathrm{Li}_3(1-x)\\
&-24x^2\mathrm{Li}_3(-x)+24x\mathrm{Li}_3(-x)-24\mathrm{Li}_3(1-x)+24\mathrm{Li}_3(-x)+36x^3\zeta_2\\
&+24x^3\zeta_2\log(x)-72x^3\zeta_2\log(x+1)-78x^3+4x^3\log^3(x)-90x^3\log^2(x)\\
&-72x^3\log(x)\log^2(x+1)+60x^3\log^2(x)\log(x+1)+72x^3\log(x)\log(x+1)\\
&+36x^2\zeta_2+24x^2\zeta_2\log(x)-72x^2\zeta_2\log(x+1)-240x^2+6x^2\log^3(x)\\
&+24x^2\log(1-x)\log^2(x)+54x^2\log^2(x)-72x^2\log(x)\log^2(x+1)\\
&+60x^2\log^2(x)\log(x+1)+168x^2\log(1-x)-48x^2\log(1-x)\log(x)\\
&+42x^2\log(x)+72x^2\log(x)\log(x+1)-36x\zeta_2-24x\zeta_2\log(x)+72x\zeta_2\log(x+1)\\
&-24\zeta_2\log(x)+72\zeta_2\log(x+1)+762x-12x\log^3(x)-14\log^3(x)+84x\log^2(x)\\
&+72x\log(x)\log^2(x+1)-60x\log^2(x)\log(x+1)+24\log(1-x)\log^2(x)\\
&-93\log^2(x)+72\log(x)\log^2(x+1)-60\log^2(x)\log(x+1)-360x\log(1-x)\\
&+162x\log(x)-72x\log(x)\log(x+1)+192\log(1-x)+120\log(1-x)\log(x)\\
&-276\log(x)-72\log(x)\log(x+1)-36\zeta_2-444)
\end{aligned}
\tag{A.11}
$$

The singlet contributions for the (anti)quark-(anti)quark channel include terms arising from identical initial quarks, and non-identical ones. These are given by the following expressions.

$$
\begin{aligned}
\Delta_{qq}^{(2)\text{id}} =& 2\Bigg(L_{\mu_F}\ \Big(-\frac{1}{x+1}\left(4\left(x^2+1\right)\left(4\text{Li}_2(-x)-\log^2(x)+4\log(x+1)\log(x)+2\zeta_2\right)\right) \\
&+8(x+1)\log(x)-16(x-1)\Big)-\frac{1}{3(x+1)}\left(4\left(x^2+1\right)(-18\text{Li}_2(1-x)\log(x)\right. \\
&+12\text{Li}_2(-x)(2\log(1-x)-2\log(x)+\log(x+1))-24\text{Li}_3\left(\frac{1-x}{x+1}\right)+24\text{Li}_3\left(\frac{x-1}{x+1}\right) \\
&-24\text{S}_{1,2}(1-x)+12\text{S}_{1,2}(-x)+24\text{Li}_3(1-x)+6\text{Li}_3(-x)-9\zeta_2\log(x)+12\zeta_2\log(1-x) \\
&+6\zeta_2\log(x+1)+2\log^3(x)-6\log(1-x)\log^2(x)-21\log(x+1)\log^2(x) \\
&\left.+6\log^2(x+1)\log(x)+24\log(1-x)\log(x+1)\log(x)+3\zeta_3\right)\Bigg)+(1-x) \\
&\times\Bigg(-16\text{Li}_2(-x)\log(x+1)-16\text{S}_{1,2}(-x)+8\text{Li}_3(-x)+4\zeta_2\log(x)-8\zeta_2\log(x+1) \\
&-\frac{2}{3}\log^3(x)+4\log(x+1)\log^2(x)-8\log^2(x+1)\log(x)+32\log(1-x)+8\zeta_3-34\Bigg) \\
&+4(x+1)(2\text{Li}_2(-x)+4\log(1-x)\log(x)+2\log(x)\log(x+1)+\zeta_2) \\
&+8(x+3)\text{Li}_2(1-x)-4(3x+1)\log^2(x)+2(7x-9)\log(x)\Bigg)-\frac{4}{3}(x-1)^2 \\
&\times\left(6\text{Li}_2(1-x)(2\log(x)+3)+12\text{S}_{1,2}(1-x)-12\text{Li}_3(1-x)+2\log^3(x)+9\log^2(x)\right) \\
&+4(6x-7)\log(x)-26x^2+56x-30 \qquad \text{(A.12)} \\
\Delta_{qq}^{(2)\text{non-id}} =& \frac{1}{54x}\left(36\text{Li}_2(1-x)(x(12L_{\mu_F}\ (x+1)+x(8x+15)+39)+6x(x+1)\right. \\
&\times(4\log(1-x)+\log(x))+16)+6x\log(x)\left(18L_{\mu_F}^2\ (x+1)+36\log(1-x)\right. \\
&\times\left(2(L_{\mu_F}\ +3)x+2L_{\mu_F}\ +2(x+1)\log(1-x)+4x^2+3\right) \\
&\left.+18L_{\mu_F}\ \left(4x^2+6x+3\right)+20x^2-72(x+1)\zeta_2-48x+345\right) \\
&+(x-1)\left(-18L_{\mu_F}^2\ (x(4x+7)+4)+24\log(1-x)\right. \\
&\times(-3L_{\mu_F}\ (x(4x+7)+4)-3(x(4x+7)+4)\log(1-x)+(17-22x)x-22) \\
&\left.-12L_{\mu_F}\ (x(22x-17)+22)+703x^2+72(x(4x+7)+4)\zeta_2-1895x-116\right) \\
&-9x\log^2(x)(24L_{\mu_F}\ (x+1)+48(x+1)\log(1-x)+5(x(8x+15)+3)) \\
&\left.+432x(x+1)(3\text{S}_{1,2}(1-x)-2\text{Li}_3(1-x))+162x(x+1)\log^3(x)\right) \qquad \text{(A.13)}
\end{aligned}
$$

It is worth noticing the sign difference in the non-identical vectorial contribution for qq initial

state, with respect to $q\bar{q}$.

$$\begin{aligned}\Delta_{q\bar{q}}^{(2)\text{non-id, V}} =& -\Delta_{qq}^{\text{non-id, V}} = \frac{1}{3x}\Big(2\Big(12\text{Li}_2(-x)\Big(2\Big(2x^2+5\Big)\log(x)+5x(x+1)-6(x(x+2)+2)\\ &\times\log(x+1))-6x\text{Li}_2(1-x)(4x+(x-10)\log(x)-5)+6(3x((x-2)\text{Li}_3(1-x)\\ &-4(x+2)\text{S}_{1,2}(-x))+4(x(x+2)+2)\text{S}_{1,2}(1-x)+2(10-3x)x\text{Li}_3(-x))\\ &-144\text{S}_{1,2}(-x)+24\text{Li}_3(1-x)-120\text{Li}_3(-x)+30x(x(\zeta_2+4)+\zeta_2-4)\\ &+6\log(x+1)(5\log(x)(2x(x+1)+(x(x+2)+2)\log(x))-6(x(x+2)+2)\zeta_2)\\ &-x\log(x)(-6x\zeta_2+48x+x\log(x)(4\log(x)+39)-60\zeta_2+60)-18((x-6)x\\ &+4)\zeta_3-36(x(x+2)+2)\log(x)\log^2(x+1)\Big)\Big) \qquad \text{(A.14)}\\ \Delta_{q\bar{q}}^{(2)\text{non-id, A}} =& 4\text{Li}_2(1-x)((3x+2)\log(x)+1)+8\text{Li}_2(-x)(x+8\log(x)-6(x+2)\log(x+1)\\ &+1)+4(4(x+2)\text{S}_{1,2}(1-x)-x(12\text{S}_{1,2}(-x)+\text{Li}_3(1-x)-10\text{Li}_3(-x)))\\ &-96\text{S}_{1,2}(-x)+\frac{2}{3}(-72\text{Li}_3(-x)+6(x(\zeta_2+9\zeta_3+4)+\zeta_2-6\zeta_3-4)\\ &+6\log(x+1)\left(-6(x+2)\zeta_2+5(x+2)\log^2(x)+2(x+1)\log(x)\right)\\ &+\log(x)(6(5x\zeta_2+2\zeta_2-2)-x\log(x)(4\log(x)+3))\\ &-36(x+2)\log(x)\log^2(x+1)\Big)+8\text{Li}_3(1-x) \qquad \text{(A.15)}\end{aligned}$$

The correction terms that appear in the qg and $q\gamma$ channels are given by the following ex-

pressions:

$$
\begin{aligned}
\Delta_{qg}^{(2)C_A} =& \frac{1}{2}\Bigg(\frac{2}{9}L_{\mu_F}\Big(36\left(2x^2+6x+3\right)\mathrm{Li}_2(1-x)-36\left(2x^2+2x+1\right)\left(\mathrm{Li}_2(-x)\right.\\
&\left.+\log(x)\log(x+1)\right)-72\left(2x^2-x+1\right)\zeta_2+73x^2+54\left(2x^2-2x+1\right)\log^2(1-x)\\
&+6\left(-71x^2+54x+\frac{8}{x}+9\right)\log(1-x)+18\left(28x^2-2x+3\right)\log(x)\\
&+36\left(-2x^2+10x+1\right)\log(1-x)\log(x)-12x+\frac{44}{x}-36(3x+1)\log^2(x)-87\Big)\\
&-4\left(2x^2+2x+1\right)\Bigg(4\mathrm{Li}_2(-x)(\log(1-x)-\log(x))+2\mathrm{Li}_3(-x)-4\mathrm{Li}_3\left(\frac{1-x}{x+1}\right)\\
&+4\mathrm{Li}_3\left(\frac{x-1}{x+1}\right)-3\log(x+1)\log^2(x)+4\log(1-x)\log(x+1)\log(x)\Bigg)\\
&+\frac{4}{3}\left(44x^2+90x+\frac{16}{x}+33\right)\mathrm{Li}_2(1-x)+8\left(5x^2+10x+7\right)\mathrm{Li}_2(1-x)\log(1-x)\\
&+8\left(4x^2+5x+1\right)\left(\mathrm{Li}_2(-x)+\log(x)\log(x+1)\right)+8x\mathrm{Li}_2(1-x)\\
&+8x(7-2x)\mathrm{Li}_2(1-x)\log(x)+\frac{2}{3}L_{\mu_F}^2\Big(-31x^2+6\left(2x^2-2x+1\right)\log(1-x)\\
&+24x+\frac{4}{x}+6(4x+1)\log(x)+3\Big)+8\left(4x^2+16x+9\right)\mathrm{S}_{1,2}(1-x)-4\left(12x^2+34x\right.\\
&\left.+15\right)\mathrm{Li}_3(1-x)+\frac{4}{3}\left(107x^2-84x-\frac{8}{x}+15\right)\zeta_2-32\left(2x^2-x+1\right)\zeta_2\log(1-x)\\
&-4\left(2x^2+4x+1\right)\zeta_3+\frac{1837x^2}{27}+\frac{26}{3}\left(2x^2-2x+1\right)\log^3(1-x)\\
&+\frac{4}{3}\left(-77x^2+63x+\frac{8}{x}+6\right)\log^2(1-x)+4\left(-6x^2+22x+1\right)\log(x)\log^2(1-x)\\
&+4\left(2x^2-14x-3\right)\log^2(x)\log(1-x)-\left(\frac{346x^2}{3}+5\right)\log^2(x)+\frac{2}{9}\Big(74x^2+75x\\
&+\frac{88}{x}-210\Big)\log(1-x)+20\left(13x^2-2x+1\right)\log(x)\log(1-x)-\frac{2}{9}\left(457x^2+12x\right.\\
&\left.-354\right)\log(x)+16x(2x-5)\zeta_2\log(x)-\frac{1226x}{9}+\frac{116}{27x}+\frac{2}{3}(20x+9)\log^3(x)\\
&-4x\log^2(x)+8x\log(x)\log(1-x)-8x\log(x)+\frac{539}{9}\Bigg)
\end{aligned}
\tag{A.16}
$$

$$
\begin{aligned}
\Delta_{qg}^{(2)C_F} =& \frac{1}{2}\Bigg(L_{\mu_F} \left(-48x^2\mathrm{Li}_2(1-x) + \left(2x^2-2x+1\right)\left(36\log^2(1-x) - 8\zeta_2\right) + 22x^2\right. \\
&+ 8\left(4x^2-2x+1\right)\log^2(x) - 4\left(23x^2-34x+8\right)\log(1-x) + 2\left(46x^2-40x+5\right) \\
&\times \log(x) - 8\left(16x^2-10x+5\right)\log(1-x)\log(x) - 68x + 24\Big) + \left(2x^2-2x+1\right) \\
&\left(-16\mathrm{Li}_2(-x)\log(x) + 32\mathrm{Li}_3(-x) - 16\zeta_2\log(1-x) + \frac{70}{3}\log^3(1-x) + 100\zeta_3\right) \\
&+ 2\left(40x^2-28x+3\right)\mathrm{Li}_2(1-x) - 4\left(26x^2-6x+3\right)\mathrm{Li}_2(1-x)\log(1-x) \\
&- 16\left(3x^2+2x-1\right)\left(\mathrm{Li}_2(-x) + \log(x)\log(x+1)\right) + 8(x-3)\mathrm{Li}_2(1-x) + 4(1-2x) \\
&\times \mathrm{Li}_2(1-x)\log(x) + 3L_{\mu_F}^2 \left(\left(8x^2-8x+4\right)\log(1-x) + \left(-8x^2+4x-2\right)\right. \\
&\times \log(x) + 4x - 1) - 4\left(34x^2-22x+11\right)\mathrm{S}_{1,2}(1-x) + 4\left(18x^2+2x-1\right)\mathrm{Li}_3(1-x) \\
&+ 4\left(-12x^2+2x+5\right)\zeta_2 + 24\left(4x^2-2x+1\right)\zeta_2\log(x) - \frac{305x^2}{2} - \frac{1}{3}\left(52x^2-34x\right. \\
&\left.+17\right)\log^3(x) - \frac{1}{2}\left(4x^2-68x+35\right)\log^2(x) + 8\left(10x^2-6x+3\right)\log(1-x)\log^2(x) \\
&- 6\left(22x^2-14x+7\right)\log^2(1-x)\log(x) - 2\left(63x^2-80x+23\right)\log^2(1-x) - \left(174x^2\right. \\
&\left.-245x+59\right)\log(x) + 4\left(48x^2-50x+13\right)\log(1-x)\log(x) + 2\left(88x^2-147x+38\right) \\
&\times \log(1-x) - 12(x-1) + 233x - 4(x-3)\log^2(x) + (28-44x)\log(x) + 8(x-3) \\
&\left.\times \log(1-x)\log(x) + 24(x-1)\log(1-x) - \frac{181}{2}\right)
\end{aligned}
\tag{A.17}
$$

The last correction terms correspond to the ones contributing to the gg, $g\gamma$ and $\gamma\gamma$ channels.

$$\begin{aligned}\Delta_{gg}^{(2)C_A} =& \frac{C_A^2}{C_A^2-1}\frac{1}{3}\big(-8(x+1)^2\mathrm{Li}_2(-x)(9\log(x)-6\log(x+1)-2)-24(x-1)^2\mathrm{S}_{1,2}(1-x)\\ &+48(x+1)^2\mathrm{S}_{1,2}(-x)+72x(x+2)\mathrm{Li}_3(-x)+72\mathrm{Li}_3(-x)+x(x(8\zeta_2+48\zeta_3+191)\\ &+16(\zeta_2+6\zeta_3-9))+24\zeta_2\log(x+1)+4\log(x+1)\big(6x(x+2)\zeta_2+(x+1)^2(4\\ &-9\log(x))\log(x))+24(x+1)^2\log(x)\log^2(x+1)+2\log(x)(-x(75x+38)\\ &+(x(25x+2)-2)\log(x)-6)+8\zeta_2+48\zeta_3-47\big) \qquad \text{(A.18)}\\ \Delta_{qg}^{(2)C_F} =& L_{\mu_F}\ \big((2x+1)^2(2\log(x)(\log(x)-4\log(1-x))-8\mathrm{Li}_2(1-x))-67x^2+60\\ &x+16(x-1)(3x+1)\log(1-x)+2(1-4(x-2)x)\log(x)+7)-4(x+1)^2\\ &\times\big(\log(x+1)\left(4\mathrm{Li}_2(-x)-3\log^2(x)+2\log(x+1)\log(x)+2\zeta_2\right)+4\mathrm{S}_{1,2}(-x)\big)\\ &-4(2x+1)^2(\mathrm{Li}_2(1-x)(4\log(1-x)+\log(x))-4\mathrm{Li}_3(1-x)+\log(1-x)\\ &\times(2\log(1-x)-\log(x))\log(x))+4(2x(7x-2)-5)\mathrm{Li}_2(1-x)+8(x(x+4)+2)\\ &\times\mathrm{Li}_2(-x)\log(x)+8(x+1)(\mathrm{Li}_2(-x)+\log(x)\log(x+1))-2L_{\mu_F}^2\\ &\times\left(-6x^2+4x+(2x+1)^2\log(x)+2\right)-8(x(7x+10)+1)\mathrm{S}_{1,2}(1-x)+8((x-2)x\\ &-1)\mathrm{Li}_3(-x)+98x^2+4(3(3-4x)x+5)\zeta_2+4(10x(x+1)+3)\zeta_2\log(x)+4(2(x-1)x\\ &-1)\zeta_3-66x-\frac{2}{3}(8x(x+1)+3)\log^3(x)-2(x+1)(4x+3)\log^2(x)+16(x-1)\\ &\times(3x+1)\log^2(1-x)+(x(105x-64)-23)\log(x)+4(1-4(x-2)x)\log(1-x)\\ &\times\log(x)-2(x-1)(67x+7)\log(1-x)-32 \qquad \text{(A.19)}\end{aligned}$$

APPENDIX B

Resummation formalism up to $\mathcal{O}(\alpha_s^2)$

Here we complete the expressions (4.1.28)-(4.1.34) in section 4.1 by providing the second order perturbative coefficients needed to perform the transverse momentum resummation up to $\mathcal{O}(\alpha_S^2)$. We focus exclusively on the case of quark initiated processes, such as Drell Yan, and recall the functions $A_c^{(2)}$, $\widetilde{B}_{c,N}^{(2)}$ and $C_{ab}^{(2)}$ in the *hard scheme*, as presented in [110, 111, 124, 127] and [135], respectively. Furthermore, we also present the process dependent quantities H_c^F needed for the Drell Yan mechanism, as reported in the appendix A of [110].

On the one hand, the coefficient $A_c^{(2)}$ in the expansion (4.1.13) can be read from the Eq. (47) in [111]:

$$A_c^{(2)} = \frac{1}{2}\, C_c \left[\left(\frac{67}{18} - \frac{\pi^2}{6} \right) C_A - \frac{5}{9} N_f \right] \quad , \tag{B.1}$$

where $C_c = C_F$ if $c = q, \bar{q}$.

On the other hand, the function $\widetilde{B}_N^{(2)}$ in Eq. (4.1.25) can be expressed in terms of $B_c^{(2)}$, the first order collinear function $C_{cc,N}^{(1)}$ and the NLO anomalous dimensions $\gamma_{cc,N}^{(2)}$ as

$$\widetilde{B}_{c,N}^{(2)} = B_c^{(2)} - 2\beta_0\, C_{cc,N}^{(1)} + 2\gamma_{cc,N}^{(2)} \quad , \tag{B.2}$$

where the expression for the perturbative coefficient $B_c^{(2)}$ in the hard scheme reads (see Eq. (34) in [110]):

$$B_a^{(2)} = \frac{\gamma_{a(1)}}{16} + \pi\beta_0\, C_a\, \zeta_2 \ , \tag{B.3}$$

with $\gamma_{a(1)}$ ($a = q, g$) the coefficients of the $\delta(1-z)$ term in the NLO quark and gluon splitting functions [86,87]. In the case of quark initiated processes, the expression for $\gamma_{a(1)}$ is

$$\gamma_{q\,(1)} = \gamma_{\bar{q}\,(1)} = (-3 + 24\zeta_2 - 48\zeta_3)\, C_F^2 + \left(-\frac{17}{3} - \frac{88}{3}\zeta_2 + 24\zeta_3\right) C_F C_A + \left(\frac{2}{3} + \frac{16}{3}\zeta_2\right) C_F N_f \ , \tag{B.4}$$

and ζ_n is the Riemann zeta-function ($\zeta_2 = \pi^2/6, \zeta_3 = 1.202\ldots, \zeta_4 = \pi^4/90$).

As for the $C^{(2)}$ collinear coefficients from the expansion (4.1.15), they can be obtained from Eqs. (37-40) in [110]. Here we present the final forms of $C_{qq}^{(2)}(z)$, $C_{qg}^{(2)}(z)$, $C_{q\bar{q}}^{(2)}(z)$, $C_{qq'}^{(2)}(z)$ and $C_{q\bar{q}'}^{(2)}(z)$ in the hard scheme, relevant for the quark initiated processes, such as Drell Yan:

$$
\begin{aligned}
2C_{qq}^{(2)}(z) = C_A C_F \Bigg\{ & \left(\frac{7\zeta_3}{2} - \frac{101}{27}\right)\left(\frac{1}{1-z}\right)_+ \\
& + \frac{1+z^2}{1-z}\Bigg(- \frac{\mathrm{Li}_3(1-z)}{2} + \mathrm{Li}_3(z) - \frac{\mathrm{Li}_2(z)\log(z)}{2} - \frac{1}{2}\mathrm{Li}_2(z)\log(1-z) - \frac{1}{24}\log^3(z) \\
& - \frac{1}{2}\log^2(1-z)\log(z) + \frac{1}{12}\pi^2\log(1-z) - \frac{\pi^2}{8}\Bigg) + \frac{1}{1-z}\Bigg(- \frac{1}{4}\left(11 - 3z^2\right)\zeta_3 \\
& - \frac{1}{48}\left(-z^2 + 12z + 11\right)\log^2(z) - \frac{1}{36}\left(83z^2 - 36z + 29\right)\log(z) + \frac{\pi^2 z}{4}\Bigg) \\
& + (1-z)\Bigg(\frac{\mathrm{Li}_2(z)}{2} + \frac{1}{2}\log(1-z)\log(z)\Bigg) + \frac{z+100}{27} + \frac{1}{4}z\log(1-z)\Bigg\} \\
& + C_F n_F \Bigg\{ \frac{14}{27}\left(\frac{1}{1-z}\right)_+ \\
& + \frac{(1+z^2)}{72(1-z)}\log(z)(3\log(z)+10) + \frac{1}{108}(-19z-37)\Bigg\} \\
& + C_F^2 \Bigg\{ \frac{1+z^2}{1-z}\Bigg(\frac{\mathrm{Li}_3(1-z)}{2} - \frac{5\mathrm{Li}_3(z)}{2} + \frac{1}{2}\mathrm{Li}_2(z)\log(1-z) + \frac{3\mathrm{Li}_2(z)\log(z)}{2} \\
& + \frac{3}{4}\log(z)\log^2(1-z) + \frac{1}{4}\log^2(z)\log(1-z) - \frac{1}{12}\pi^2\log(1-z) + \frac{5\zeta_3}{2}\Bigg) \\
& + (1-z)\left(-\mathrm{Li}_2(z) - \frac{3}{2}\log(1-z)\log(z) + \frac{2\pi^2}{3} - \frac{29}{4}\right) + \frac{1}{24}(1+z)\log^3(z) \\
& + \frac{1}{1-z}\Bigg(\frac{1}{8}\left(-2z^2 + 2z + 3\right)\log^2(z) + \frac{1}{4}\left(17z^2 - 13z + 4\right)\log(z)\Bigg) - \frac{z}{4}\log(1-z) \\
& - \frac{1}{4}\left[\left(2\pi^2 - 18\right)(1-z) - (1+z)\ln z\right]\Bigg\} \\
& + C_F \Bigg\{ \frac{1}{z}(1-z)\left(2z^2 - z + 2\right)\left(\frac{\mathrm{Li}_2(z)}{6} + \frac{1}{6}\log(1-z)\log(z) - \frac{\pi^2}{36}\right) \\
& + \frac{1}{216z}(1-z)\left(136z^2 - 143z + 172\right) - \frac{1}{48}\left(8z^2 + 3z + 3\right)\log^2(z) \\
& + \frac{1}{36}\left(32z^2 - 30z + 21\right)\log(z) + \frac{1}{24}(1+z)\log^3(z)\Bigg\}\,, \qquad \text{(B.5)}
\end{aligned}
$$

$$
\begin{aligned}
C_{qg}^{(2)}(z) = C_A\Bigg\{ & -\frac{1}{12z}(1-z)\left(11z^2-z+2\right)\mathrm{Li}_2(1-z) \\
& + \left(2z^2-2z+1\right)\left(\frac{\mathrm{Li}_3(1-z)}{8} - \frac{1}{8}\mathrm{Li}_2(1-z)\log(1-z) + \frac{1}{48}\log^3(1-z)\right) \\
& + \left(2z^2+2z+1\right)\left(\frac{3\mathrm{Li}_3(-z)}{8} + \frac{\mathrm{Li}_3\left(\frac{1}{1+z}\right)}{4} - \frac{\mathrm{Li}_2(-z)\log(z)}{8} - \frac{1}{24}\log^3(1+z)\right. \\
& \left. + \frac{1}{16}\log^2(z)\log(1+z) + \frac{1}{48}\pi^2\log(1+z)\right) + \frac{1}{4}z(1+z)\mathrm{Li}_2(-z) + z\mathrm{Li}_3(z) \\
& - \frac{1}{2}z\mathrm{Li}_2(1-z)\log(z) - z\mathrm{Li}_2(z)\log(z) - \frac{3}{8}\left(2z^2+1\right)\zeta_3 - \frac{149z^2}{216} \\
& - \frac{1}{96}\left(44z^2-12z+3\right)\log^2(z) + \frac{1}{72}\left(68z^2+6\pi^2 z-30z+21\right)\log(z) + \frac{\pi^2 z}{24} + \frac{43z}{48} \\
& + \frac{43}{108z} + \frac{1}{48}(2z+1)\log^3(z) - \frac{1}{2}z\log(1-z)\log^2(z) - \frac{1}{8}(1-z)z\log^2(1-z) \\
& + \frac{1}{4}z(1+z)\log(1+z)\log(z) + \frac{1}{16}(3-4z)z\log(1-z) - \frac{35}{48}\Bigg\} \\
& + C_F\Bigg\{ \left(2z^2-2z+1\right)\left(\zeta_3 - \frac{\mathrm{Li}_3(1-z)}{8} - \frac{\mathrm{Li}_3(z)}{8} + \frac{1}{8}\mathrm{Li}_2(1-z)\log(1-z)\right. \\
& \left. + \frac{\mathrm{Li}_2(z)\log(z)}{8} - \frac{1}{48}\log^3(1-z) + \frac{1}{16}\log(z)\log^2(1-z) + \frac{1}{16}\log^2(z)\log(1-z)\right) \\
& - \frac{3z^2}{8} - \frac{1}{96}\left(4z^2-2z+1\right)\log^3(z) + \frac{1}{64}\left(-8z^2+12z+1\right)\log^2(z) \\
& + \frac{1}{32}\left(-8z^2+23z+8\right)\log(z) + \frac{5}{24}\pi^2(1-z)z + \frac{11z}{32} + \frac{1}{8}(1-z)z\log^2(1-z) \\
& - \frac{1}{4}(1-z)z\log(1-z)\log(z) - \frac{1}{16}(3-4z)z\log(1-z) - \frac{9}{32} \\
& - \frac{1}{4}\left[z\ln z + \frac{1}{2}(1-z^2) + (\pi^2-8)z(1-z)\right]\Bigg\}\,. \qquad \text{(B.6)}
\end{aligned}
$$

On the other hand, the flavour off-diagonal coefficients $C_{q\bar{q}}^{(2)}(z)$, $C_{qq'}^{(2)}(z)$ and $C_{q\bar{q}'}^{(2)}(z)$ are

$$
\begin{aligned}
C_{q\bar{q}}^{(2)}(z) = C_F\left(C_F-\frac{1}{2}C_A\right)\Bigg\{&\frac{1+z^2}{1+z}\left(\frac{3\mathrm{Li}_3(-z)}{2}+\mathrm{Li}_3(z)+\mathrm{Li}_3\left(\frac{1}{1+z}\right)-\frac{\mathrm{Li}_2(-z)\log(z)}{2}\right.\\
&-\frac{\mathrm{Li}_2(z)\log(z)}{2}-\frac{1}{24}\log^3(z)-\frac{1}{6}\log^3(1+z)+\frac{1}{4}\log(1+z)\log^2(z)\\
&\left.+\frac{\pi^2}{12}\log(1+z)-\frac{3\zeta_3}{4}\right)+(1-z)\left(\frac{\mathrm{Li}_2(z)}{2}+\frac{1}{2}\log(1-z)\log(z)+\frac{15}{8}\right)\\
&-\frac{1}{2}(1+z)\big(\mathrm{Li}_2(-z)+\log(z)\log(1+z)\big)+\frac{\pi^2}{24}(z-3)+\frac{1}{8}(11z+3)\log(z)\Bigg\}\\
&+C_F\Bigg\{\frac{1}{12z}(1-z)\left(2z^2-z+2\right)\left(\mathrm{Li}_2(z)+\log(1-z)\log(z)-\frac{\pi^2}{6}\right)\\
&+\frac{1}{432z}(1-z)\left(136z^2-143z+172\right)-\frac{1}{96}\left(8z^2+3z+3\right)\log^2(z)\\
&+\frac{1}{72}\left(32z^2-30z+21\right)\log(z)+\frac{1}{48}(1+z)\log^3(z)\Bigg\}\,,
\end{aligned}
\tag{B.7}
$$

$$
\begin{aligned}
C_{qq'}^{(2)}(z) = C_{q\bar{q}'}^{(2)}(z) = C_F\Bigg\{&\frac{1}{12z}(1-z)\left(2z^2-z+2\right)\left(\mathrm{Li}_2(z)+\log(1-z)\log(z)-\frac{\pi^2}{6}\right)\\
&+\frac{1}{432z}(1-z)\left(136z^2-143z+172\right)+\frac{1}{48}(1+z)\log^3(z)\\
&-\frac{1}{96}\left(8z^2+3z+3\right)\log^2(z)+\frac{1}{72}\left(32z^2-30z+21\right)\log(z)\Bigg\}\,,
\end{aligned}
\tag{B.8}
$$

As can be seen, from these expressions ((B.1), (B.3) and (B.5)-(B.8)) one can obtain, by taking the corresponding abelian limit according to the procedure detailed in Chapter 3, the mixed order coefficients $A_q^{(1,1)}$ and $B_q^{(1,1)}$ in Eq. (4.3.21) and the collinear functions $C_{qq'}^{(1,1)}(z)$, $C_{q\bar{q}'}^{(1,1)}(z)$, $C_{qg}^{(1,1)}(z)$ and $C_{q\gamma}^{(1,1)}(z)$ in Eqs. (4.3.25)-(4.3.28). Those are exactly the universal perturbative coefficients needed to perform the qt-subtraction up to mixed order $\mathcal{O}(\alpha_s\alpha)$.

Finally, we move to the process-dependent H_c^F coefficients and recall the NNLO hard-virtual function $H_q^{DY(2)}$ for the Drell Yan mechanism, in the *hard scheme*, as presented in [110,127]:

$$
\begin{aligned}
H_q^{DY(2)} = &\,C_FC_A\left(\frac{59\zeta_3}{18}-\frac{1535}{192}+\frac{215\pi^2}{216}-\frac{\pi^4}{240}\right)+\frac{1}{4}C_F^2\left(-15\zeta_3+\frac{511}{16}-\frac{67\pi^2}{12}+\frac{17\pi^4}{45}\right)\\
&+\frac{1}{864}C_FN_f\left(192\zeta_3+1143-152\pi^2\right)\,,
\end{aligned}
\tag{B.9}
$$

Here, just as in the case of the perturbative coefficients in Eqs. (B.1), (B.3) and (B.5)-(B.8), the abelian limit of Eq. (B.9) results in the expression for the mixed order hard-virtual coefficient $H_q^{DY(1,1)}$ in Eq. (4.3.24).

Bibliography

[1] **Particle Data Group** Collaboration, R. L. Workman et al., *Review of Particle Physics*, *PTEP* **2022** (2022) 083C01.
DOI: [10.1016/0550-3213(79)90040-3]. **INSPIRE-hep**: [hep-ex/2106994].

[2] D. de Florian, M. Der, and I. Fabre, *QCD⊕QED NNLO corrections to Drell Yan production*, *Phys. Rev. D* **98** (2018), no. 9 094008, [arXiv:1805.12214].
DOI: [10.1103/PhysRevD.98.094008].

[3] **ATLAS** Collaboration, G. Aad et al., *Observation of a new particle in the search for the Standard Model Higgs boson with the ATLAS detector at the LHC*, *Phys. Lett. B* **716** (2012) 1–29, [arXiv:1207.7214]. **DOI**: [10.1016/j.physletb.2012.08.020].

[4] **CMS** Collaboration, S. Chatrchyan et al., *Observation of a New Boson at a Mass of 125 GeV with the CMS Experiment at the LHC*, *Phys. Lett. B* **716** (2012) 30–61, [arXiv:1207.7235]. **DOI**: [10.1016/j.physletb.2012.08.021].

[5] **ATLAS, CMS** Collaboration, G. Aad et al., *Measurements of the Higgs boson production and decay rates and constraints on its couplings from a combined ATLAS and CMS analysis of the LHC pp collision data at $\sqrt{s} = 7$ and 8 TeV*, *JHEP* **08** (2016) 045, [arXiv:1606.02266]. **DOI**: [10.1007/JHEP0828201629045].

[6] M. Cepeda et al., *Report from Working Group 2: Higgs Physics at the HL-LHC and HE-LHC*, *CERN Yellow Rep. Monogr.* **7** (2019) 221–584, [arXiv:1902.00134].

[7] **ATLAS, CMS** Collaboration, A. Savin, *Electroweak measurements at High-Luminosity LHC*, *PoS* **LHCP2019** (2019) 242.
DOI: [10.22323/1.350.0242]. **INSPIRE-hep**: [hep-ex/1769965].

[8] **ALEPH, DELPHI, L3, OPAL, SLD, LEP Electroweak Working Group, SLD Electroweak Group, SLD Heavy Flavour Group** Collaboration, S. Schael et al.,

Precision electroweak measurements on the Z resonance, *Phys. Rept.* **427** (2006) 257–454, [hep-ex/0509008]. **DOI**: [10.1016/j.physrep.2005.12.006].

[9] **Gfitter Group** Collaboration, M. Baak, J. Cúth, J. Haller, A. Hoecker, R. Kogler, K. Mönig, M. Schott, and J. Stelzer, *The global electroweak fit at NNLO and prospects for the LHC and ILC*, *Eur. Phys. J. C* **74** (2014) 3046, [arXiv:1407.3792]. **DOI**: [10.1140/epjc/s10052-014-3046-5].

[10] S. Dittmaier, A. Huss, and C. Speckner, *Weak radiative corrections to dijet production at hadron colliders*, *JHEP* **11** (2012) 095, [arXiv:1210.0438]. **DOI**: [10.1007/JHEP1128201229095].

[11] S. Dittmaier, A. Huss, and C. Speckner, *Weak radiative corrections to dijet production at the LHC*, *PoS* **DIS2013** (2013) 283, [arXiv:1306.6298]. **DOI**: [10.22323/1.191.0283].

[12] S. D. Drell and T.-M. Yan, *Massive Lepton Pair Production in Hadron-Hadron Collisions at High-Energies*, *Phys. Rev. Lett.* **25** (1970) 316–320. [Erratum: Phys.Rev.Lett. 25, 902 (1970)]. **DOI**: [10.1103/PhysRevLett.25.316].

[13] **NNPDF** Collaboration, R. D. Ball et al., *Parton distributions for the LHC Run II*, *JHEP* **04** (2015) 040, [arXiv:1410.8849]. **DOI**: [10.1007/JHEP0428201529040].

[14] L. A. Harland-Lang, A. D. Martin, P. Motylinski, and R. S. Thorne, *Parton distributions in the LHC era: MMHT 2014 PDFs*, *Eur. Phys. J. C* **75** (2015), no. 5 204, [arXiv:1412.3989]. **DOI**: [10.1140/epjc/s10052-015-3397-6].

[15] S. Dulat, T.-J. Hou, J. Gao, M. Guzzi, J. Huston, P. Nadolsky, J. Pumplin, C. Schmidt, D. Stump, and C. P. Yuan, *New parton distribution functions from a global analysis of quantum chromodynamics*, *Phys. Rev. D* **93** (2016), no. 3 033006, [arXiv:1506.07443]. **DOI**: [10.1103/PhysRevD.93.033006].

[16] R. Brock et al., *Report of the Working Group on Precision Measurements*, in *Physics at Run II: QCD and Weak Boson Physics Workshop: 1st Meeting*, pp. 78–114, 3, 1999. hep-ex/0011009.

[17] M. L. Mangano, *Production of electroweak bosons at hadron colliders: theoretical aspects*, *Adv. Ser. Direct. High Energy Phys.* **26** (2016) 231–253, [arXiv:1512.00220]. **DOI**: [10.1142/97898147335190013].

[18] G. Altarelli, R. K. Ellis, and G. Martinelli, *Large Perturbative Corrections to the Drell-Yan Process in QCD*, *Nucl. Phys. B* **157** (1979) 461–497. **DOI**: [10.1016/0550-3213(79)90116-0]. **INSPIRE-hep**: [hep-ph/140456].

[19] R. Hamberg, W. L. van Neerven, and T. Matsuura, *A complete calculation of the order α_s^2 correction to the Drell-Yan K factor*, *Nucl. Phys. B* **359** (1991) 343–405. [Erratum: Nucl.Phys.B 644, 403–404 (2002)]. **DOI**: [10.1016/0550-3213(91)90064-5].

[20] W. L. van Neerven and E. B. Zijlstra, *The $O(\alpha_s^2)$ corrected Drell-Yan K factor in the DIS and MS scheme*, *Nucl. Phys.* **B382** (1992) 11–62. [Erratum: Nucl. Phys.B680,513(2004)]. **DOI**: [10.1016/j.nuclphysb.2003.12.019].

[21] R. V. Harlander and W. B. Kilgore, *Next-to-next-to-leading order Higgs production at hadron colliders*, *Phys. Rev. Lett.* **88** (2002) 201801, [hep-ph/0201206]. **DOI**: [10.1103/PhysRevLett.88.201801].

[22] S. Catani, L. Cieri, G. Ferrera, D. de Florian, and M. Grazzini, *Vector boson production at hadron colliders: a fully exclusive QCD calculation at NNLO*, *Phys. Rev. Lett.* **103** (2009) 082001, [arXiv:0903.2120]. **DOI**: [10.1103/PhysRevLett.103.082001].

[23] K. Melnikov and F. Petriello, *The W boson production cross section at the LHC through $O(\alpha_s^2)$*, *Phys. Rev. Lett.* **96** (2006) 231803, [hep-ph/0603182]. **DOI**: [10.1103/PhysRevLett.96.231803].

[24] K. Melnikov and F. Petriello, *Electroweak gauge boson production at hadron colliders through $O(\alpha_s^2)$*, *Phys. Rev. D* **74** (2006) 114017, [hep-ph/0609070]. **DOI**: [10.1103/PhysRevD.74.114017].

[25] R. Gavin, Y. Li, F. Petriello, and S. Quackenbush, *FEWZ 2.0: A code for hadronic Z production at next-to-next-to-leading order*, *Comput. Phys. Commun.* **182** (2011) 2388–2403, [arXiv:1011.3540]. **DOI**: [10.1016/j.cpc.2011.06.008].

[26] R. Gavin, Y. Li, F. Petriello, and S. Quackenbush, *W Physics at the LHC with FEWZ 2.1*, *Comput. Phys. Commun.* **184** (2013) 208–214, [arXiv:1201.5896].

[27] R. Boughezal, J. M. Campbell, R. K. Ellis, C. Focke, W. Giele, X. Liu, F. Petriello, and C. Williams, *Color singlet production at NNLO in MCFM*, *Eur. Phys. J. C* **77** (2017), no. 1 7, [arXiv:1605.08011]. **DOI**: [10.1140/epjc/s10052-016-4558-y].

[28] F. Caola, K. Melnikov, and R. Röntsch, *Nested soft-collinear subtractions in NNLO QCD computations*, *Eur. Phys. J. C* **77** (2017), no. 4 248, [arXiv:1702.01352]. **DOI**: [10.1140/epjc/s10052-017-4774-0].

[29] T. Ahmed, M. Mahakhud, N. Rana, and V. Ravindran, *Drell-Yan Production at Threshold to Third Order in QCD*, *Phys. Rev. Lett.* **113** (2014), no. 11 112002, [arXiv:1404.0366]. **DOI**: [10.1103/PhysRevLett.113.112002].

[30] S. Catani, L. Cieri, D. de Florian, G. Ferrera, and M. Grazzini, *Threshold resummation at N^3LL accuracy and soft-virtual cross sections at N^3LO*, *Nucl. Phys. B* **888** (2014) 75–91, [arXiv:1405.4827]. **DOI**: [10.1016/j.nuclphysb.2014.09.012].

[31] S. Camarda, L. Cieri, and G. Ferrera, *Drell–Yan lepton-pair production: qT resummation at N3LL accuracy and fiducial cross sections at N3LO*, *Phys. Rev. D* **104** (2021), no. 11 L111503, [arXiv:2103.04974]. **DOI**: [10.1103/PhysRevD.104.L111503].

[32] C. Duhr, F. Dulat, and B. Mistlberger, *Drell-Yan Cross Section to Third Order in the Strong Coupling Constant*, *Phys. Rev. Lett.* **125** (2020), no. 17 172001, [arXiv:2001.07717]. **DOI**: [10.1103/PhysRevLett.125.172001].

[33] C. Duhr, F. Dulat, and B. Mistlberger, *Charged current Drell-Yan production at N^3LO*, *JHEP* **11** (2020) 143, [arXiv:2007.13313]. **DOI**: [10.1007/JHEP1128202029143].

[34] C. Duhr and B. Mistlberger, *Lepton-pair production at hadron colliders at N^3LO in QCD*, *JHEP* **03** (2022) 116, [arXiv:2111.10379]. **DOI**: [10.1007/JHEP0328202229116].

[35] J. Baglio, C. Duhr, B. Mistlberger, and R. Szafron, *Inclusive production cross sections at N^3LO*, *JHEP* **12** (2022) 066, [arXiv:2209.06138]. **DOI**: [10.1007/JHEP1228202229066].

[36] X. Chen, T. Gehrmann, N. Glover, A. Huss, T.-Z. Yang, and H. X. Zhu, *Dilepton Rapidity Distribution in Drell-Yan Production to Third Order in QCD*, *Phys. Rev. Lett.* **128** (2022), no. 5 052001, [arXiv:2107.09085]. **DOI**: [10.1103/PhysRevLett.128.052001].

[37] X. Chen, T. Gehrmann, N. Glover, A. Huss, T.-Z. Yang, and H. X. Zhu, *Transverse mass distribution and charge asymmetry in W boson production to third order in QCD*, *Phys. Lett. B* **840** (2023) 137876, [arXiv:2205.11426].
DOI: [10.1016/j.physletb.2023.137876].

[38] X. Chen, T. Gehrmann, E. W. N. Glover, A. Huss, P. F. Monni, E. Re, L. Rottoli, and P. Torrielli, *Third-Order Fiducial Predictions for Drell-Yan Production at the LHC*, *Phys. Rev. Lett.* **128** (2022), no. 25 252001, [arXiv:2203.01565].
DOI: [10.1103/PhysRevLett.128.252001].

[39] D. de Florian, G. F. R. Sborlini, and G. Rodrigo, *QED corrections to the Altarelli–Parisi splitting functions*, *Eur. Phys. J. C* **76** (2016), no. 5 282, [arXiv:1512.00612].
DOI: [10.1140/epjc/s10052-016-4131-8].

[40] D. de Florian, G. F. R. Sborlini, and G. Rodrigo, *Two-loop QED corrections to the Altarelli-Parisi splitting functions*, *JHEP* **10** (2016) 056, [arXiv:1606.02887].
DOI: [10.1007/JHEP1028201629056].

[41] A. Manohar, P. Nason, G. P. Salam, and G. Zanderighi, *How bright is the proton? A precise determination of the photon parton distribution function*, *Phys. Rev. Lett.* **117** (2016), no. 24 242002, [arXiv:1607.04266].
DOI: [10.1103/PhysRevLett.117.242002].

[42] A. V. Manohar, P. Nason, G. P. Salam, and G. Zanderighi, *The Photon Content of the Proton*, *JHEP* **12** (2017) 046, [arXiv:1708.01256].
DOI: [10.1007/JHEP1228201729046].

[43] S. Dittmaier and M. Krämer, *Electroweak radiative corrections to W boson production at hadron colliders*, *Phys. Rev. D* **65** (2002) 073007, [hep-ph/0109062].
DOI: [10.1103/PhysRevD.65.073007].

[44] U. Baur and D. Wackeroth, *Electroweak radiative corrections to $p\bar{p} \to W^{\pm} \to \ell^{\pm}\nu$ beyond the pole approximation*, *Phys. Rev. D* **70** (2004) 073015, [hep-ph/0405191].
DOI: [10.1103/PhysRevD.70.073015].

[45] C. M. Carloni Calame, G. Montagna, O. Nicrosini, and A. Vicini, *Precision electroweak calculation of the charged current Drell-Yan process*, *JHEP* **12** (2006) 016, [hep-ph/0609170]. **DOI**: [10.1088/1126-6708/2006/12/016].

[46] U. Baur, O. Brein, W. Hollik, C. Schappacher, and D. Wackeroth, *Electroweak radiative corrections to neutral current Drell-Yan processes at hadron colliders*, *Phys. Rev. D* **65** (2002) 033007, [hep-ph/0108274]. **DOI**: [10.1103/PhysRevD.65.033007].

[47] U. Baur, S. Keller, and W. K. Sakumoto, *Qed radiative corrections to z boson production and the forward-backward asymmetry at hadron colliders*, *Phys. Rev. D* **57** (Jan, 1998) 199–215. **DOI**: [10.1103/PhysRevD.57.199].

[48] S. Actis, A. Ferroglia, M. Passera, and G. Passarino, *Two-Loop Renormalization in the Standard Model. Part I: Prolegomena*, *Nucl. Phys. B* **777** (2007) 1–34, [hep-ph/0612122]. **DOI**: [10.1016/j.nuclphysb.2007.04.021].

[49] S. Actis and G. Passarino, *Two-Loop Renormalization in the Standard Model Part II: Renormalization Procedures and Computational Techniques*, *Nucl. Phys. B* **777** (2007) 35–99, [hep-ph/0612123]. **DOI**: [10.1016/j.nuclphysb.2007.03.043].

[50] S. Actis and G. Passarino, *Two-Loop Renormalization in the Standard Model Part III: Renormalization Equations and their Solutions*, *Nucl. Phys. B* **777** (2007) 100–156, [hep-ph/0612124]. **DOI**: [10.1016/j.nuclphysb.2007.04.027].

[51] G. Degrassi and A. Vicini, *Two loop renormalization of the electric charge in the standard model*, *Phys. Rev. D* **69** (2004) 073007, [hep-ph/0307122]. **DOI**: [10.1103/PhysRevD.69.073007].

[52] R. Bonciani, F. Buccioni, N. Rana, and A. Vicini, *Next-to-Next-to-Leading Order Mixed QCD-Electroweak Corrections to on-Shell Z Production*, *Phys. Rev. Lett.* **125** (2020), no. 23 232004, [arXiv:2007.06518]. **DOI**: [10.1103/PhysRevLett.125.232004].

[53] F. Buccioni, F. Caola, M. Delto, M. Jaquier, K. Melnikov, and R. Röntsch, *Mixed QCD-electroweak corrections to on-shell Z production at the LHC*, *Phys. Lett. B* **811** (2020) 135969, [arXiv:2005.10221]. **DOI**: [10.1016/j.physletb.2020.135969].

[54] L. Buonocore, M. Grazzini, S. Kallweit, C. Savoini, and F. Tramontano, *Mixed QCD-EW corrections to $pp \to \ell\nu_\ell + X$ at the LHC*, *Phys. Rev. D* **103** (2021) 114012, [arXiv:2102.12539]. **DOI**: [10.1103/PhysRevD.103.114012].

[55] R. Bonciani, L. Buonocore, M. Grazzini, S. Kallweit, N. Rana, F. Tramontano, and A. Vicini, *Mixed Strong-Electroweak Corrections to the Drell-Yan Process*, *Phys. Rev. Lett.* **128** (2022), no. 1 012002, [arXiv:2106.11953]. **DOI**: [10.1103/PhysRevLett.128.012002].

[56] R. Bonciani, F. Buccioni, N. Rana, and A. Vicini, *On-shell Z boson production at hadron colliders through $\mathcal{O}(\alpha\alpha_s)$*, *JHEP* **02** (2022) 095, [arXiv:2111.12694]. **DOI**: [10.1007/JHEP02(2022)095].

[57] T. Armadillo, R. Bonciani, S. Devoto, N. Rana, and A. Vicini, *Two-loop mixed QCD-EW corrections to neutral current Drell-Yan*, *JHEP* **05** (2022) 072, [arXiv:2201.01754]. **DOI**: [10.1007/JHEP05(2022)072].

[58] F. Buccioni, F. Caola, H. A. Chawdhry, F. Devoto, M. Heller, A. von Manteuffel, K. Melnikov, R. Röntsch, and C. Signorile-Signorile, *Mixed QCD-electroweak corrections to dilepton production at the LHC in the high invariant mass region*, *JHEP* **06** (2022) 022, [arXiv:2203.11237]. **DOI**: [10.1007/JHEP06(2022)022].

[59] Q.-H. Cao and C. P. Yuan, *Combined effect of QCD resummation and QED radiative correction to W boson observables at the Tevatron*, *Phys. Rev. Lett.* **93** (2004) 042001, [hep-ph/0401026]. **DOI**: [10.1103/PhysRevLett.93.042001].

[60] G. Balossini, G. Montagna, C. M. Carloni Calame, M. Moretti, O. Nicrosini, F. Piccinini, M. Treccani, and A. Vicini, *Combination of electroweak and QCD corrections to single W production at the Fermilab Tevatron and the CERN LHC*, *JHEP* **01** (2010) 013, [arXiv:0907.0276]. **DOI**: [10.1007/JHEP01(2010)013].

[61] N. E. Adam, V. Halyo, S. A. Yost, and W. Zhu, *Evaluation of the Theoretical Uncertainties in the $W \to \ell\nu$ Cross Sections at the LHC*, *JHEP* **09** (2008) 133, [arXiv:0808.0758]. **DOI**: [10.1088/1126-6708/2008/09/133].

[62] Y. Li and F. Petriello, *Combining QCD and electroweak corrections to dilepton production in FEWZ*, *Phys. Rev. D* **86** (2012) 094034, [arXiv:1208.5967]. **DOI**: [10.1103/PhysRevD.86.094034].

[63] L. Barze, G. Montagna, P. Nason, O. Nicrosini, F. Piccinini, and A. Vicini, *Neutral current Drell-Yan with combined QCD and electroweak corrections in the POWHEG BOX*, *Eur. Phys. J. C* **73** (2013), no. 6 2474, [arXiv:1302.4606]. **DOI**: [10.1140/epjc/s10052-013-2474-y].

[64] S. Dittmaier, A. Huss, and C. Schwinn, *$O(\alpha_s\alpha)$ corrections to Drell-Yan processes in the resonance region*, *PoS* **LL2014** (2014) 045, [arXiv:1405.6897]. **DOI**: [10.22323/1.211.0045].

[65] S. Dittmaier, A. Huss, and C. Schwinn, *Mixed QCD-electroweak $\mathcal{O}(\alpha_s\alpha)$ corrections to Drell-Yan processes in the resonance region: pole approximation and non-factorizable corrections*, *Nucl. Phys. B* **885** (2014) 318–372, [arXiv:1403.3216]. **DOI**: [10.1016/j.nuclphysb.2014.05.027].

[66] S. Dittmaier, A. Huss, and C. Schwinn, *Dominant mixed QCD-electroweak $O(\alpha_s\alpha)$ corrections to Drell–Yan processes in the resonance region*, *Nucl. Phys. B* **904** (2016) 216–252, [arXiv:1511.08016]. **DOI**: [10.1016/j.nuclphysb.2016.01.006].

[67] S. Frixione, Z. Kunszt, and A. Signer, *Three jet cross-sections to next-to-leading order*, *Nucl. Phys. B* **467** (1996) 399–442, [hep-ph/9512328]. **DOI**: [10.1016/0550-3213(96)00110-1].

[68] T. Kinoshita, *Quantum electrodynamics*. World Scientific Publ., 1990. **DOI**: [10.1142/0495].

[69] S. G. Karshenboim, *Precision physics of simple atoms: QED tests, nuclear structure and fundamental constants*, *Phys. Rept.* **422** (2005) 1–63, [hep-ph/0509010]. **DOI**: [10.1016/j.physrep.2005.08.008].

[70] P. Langacker, *Precision tests of the Standard Model*, in *International Symposium on Neutrino Astrophysics*, 3, 1993. hep-ph/9303304.

[71] P. Langacker, *The Standard Model and Beyond*, Springer Science and Business Media LLC, aug, 2017. **DOI**: [10.1201/b22175].

[72] J. Erler and S. Su, *The Weak Neutral Current*, *Prog. Part. Nucl. Phys.* **71** (2013) 119–149, [arXiv:1303.5522]. **DOI**: [10.1016/j.ppnp.2013.03.004].

[73] F. Bloch and A. Nordsieck, *Note on the radiation field of the electron*, *Phys. Rev.* **52** (Jul, 1937) 54–59. **DOI**: [10.1103/PhysRev.52.54].

[74] T. Kinoshita, *Mass singularities of Feynman amplitudes*, *J. Math. Phys.* **3** (1962) 650–677. **DOI**: [10.1063/1.1724268]. **INSPIRE-hep**: [hep-ex/2272].

[75] T. D. Lee and M. Nauenberg, *Degenerate Systems and Mass Singularities*, *Phys. Rev.* **133** (1964) B1549–B1562.
DOI: [10.1103/PhysRev.133.B1549]. **INSPIRE-hep**: [hep-ph/23504].

[76] Y. L. Dokshitzer, V. A. Khoze, A. H. Mueller, and S. I. Troian, *Basics of perturbative QCD*. 1991. **DOI**: [BpQCD/27038173].

[77] A. Bassetto, M. Ciafaloni, and G. Marchesini, *Jet Structure and Infrared Sensitive Quantities in Perturbative QCD*, *Phys. Rept.* **100** (1983) 201–272.
DOI: [10.1016/Phys.Rept.].

[78] S. Catani and M. Grazzini, *The soft gluon current at one loop order*, *Nucl. Phys. B* **591** (2000) 435–454, [hep-ph/0007142]. **DOI**: [10.1016/S0550-3213(00)00572-1].

[79] S. Catani and M. H. Seymour, *A General algorithm for calculating jet cross-sections in NLO QCD*, *Nucl. Phys. B* **485** (1997) 291–419, [hep-ph/9605323]. [Erratum: Nucl.Phys.B 510, 503–504 (1998)]. **DOI**: [10.1016/S0550-3213(96)00589-5].

[80] G. Altarelli and G. Parisi, *Asymptotic Freedom in Parton Language*, *Nucl. Phys. B* **126** (1977) 298–318. **DOI**: [0550-3213/Nucl.Phys.B].

[81] A. Vogt, S. Moch, and J. Vermaseren, *Photon-parton splitting functions at the next-to-next-to-leading order of QCD*, *Acta Phys. Polon. B* **37** (2006) 683–688, [hep-ph/0511112].

[82] A. Vogt, S. Moch, and J. A. M. Vermaseren, *The Three-loop splitting functions in QCD: The Singlet case*, *Nucl. Phys. B* **691** (2004) 129–181, [hep-ph/0404111].
DOI: [10.1016/j.nuclphysb.2004.04.024].

[83] S. Moch, J. A. M. Vermaseren, and A. Vogt, *The Three loop splitting functions in QCD: The Nonsinglet case*, *Nucl. Phys. B* **688** (2004) 101–134, [hep-ph/0403192]. **DOI**: [10.1016/j.nuclphysb.2004.03.030].

[84] S. Moch, J. A. M. Vermaseren, and A. Vogt, *Next-to-next-to leading order QCD corrections to the photon's parton structure*, *Nucl. Phys. B* **621** (2002) 413–458, [hep-ph/0110331]. **DOI**: [10.1016/S0550-3213(01)00572-7].

[85] R. K. Ellis and W. Vogelsang, *The Evolution of parton distributions beyond leading order: The Singlet case*, hep-ph/9602356.

[86] W. Furmanski and R. Petronzio, *Singlet Parton Densities Beyond Leading Order*, *Phys. Lett. B* **97** (1980) 437–442. **DOI**: [10.1016/0370-2693(80)90636-X]. **INSPIRE-hep**: [155291/Phys.Lett.B].

[87] G. Curci, W. Furmanski, and R. Petronzio, *Evolution of Parton Densities Beyond Leading Order: The Nonsinglet Case*, *Nucl. Phys. B* **175** (1980) 27–92. **DOI**: [10.1016/0550-3213(80)90003-6]. **INSPIRE-hep**: [152873/Nucl.Phys.B].

[88] M. Roth and S. Weinzierl, *QED corrections to the evolution of parton distributions*, *Phys. Lett. B* **590** (2004) 190–198, [hep-ph/0403200]. **DOI**: [10.1016/j.physletb.2004.04.009].

[89] G. 't Hooft, *Dimensional regularization and the renormalization group*, *Nucl. Phys. B* **61** (1973) 455–468. **DOI**: [0550321373903763/Nucl.Phys.B].

[90] S. Weinberg, *New approach to the renormalization group*, *Phys. Rev. D* **8** (Nov, 1973) 3497–3509. **DOI**: [10.1103/PhysRevD.8.3497].

[91] R. K. Ellis, W. J. Stirling, and B. R. Webber, *QCD and Collider Physics*. Cambridge Monographs on Particle Physics, Nuclear Physics and Cosmology. Cambridge University Press, 1996. **DOI**: [10.1017/CBO9780511628788].

[92] D. J. Gross and F. Wilczek, *Ultraviolet Behavior of Nonabelian Gauge Theories*, *Phys. Rev. Lett.* **30** (1973) 1343–1346. **DOI**: [10.1103/PhysRevLett.30.1343].

[93] H. D. Politzer, *Reliable Perturbative Results for Strong Interactions?*, *Phys. Rev. Lett.* **30** (1973) 1346–1349. **DOI**: [10.1103/PhysRevLett.30.1346].

[94] L. Cieri, G. Ferrera, and G. F. R. Sborlini, *Combining QED and QCD transverse-momentum resummation for Z boson production at hadron colliders*, *JHEP* **08** (2018) 165, [arXiv:1805.11948]. **DOI**: [10.1007/JHEP08(2018)165].

[95] S. Frixione, *A General approach to jet cross-sections in QCD*, *Nucl. Phys. B* **507** (1997) 295–314, [hep-ph/9706545]. **DOI**: [10.1016/S0550-3213(97)00574-9].

[96] Z. Kunszt and D. E. Soper, *Calculation of jet cross-sections in hadron collisions at order α_s^3*, *Phys. Rev. D* **46** (1992) 192–221.
DOI: [10.1103/PhysRevD.46.192]. **INSPIRE-hep**: [hep-ph/332376].

[97] Z. Kunszt, A. Signer, and Z. Trocsanyi, *Singular terms of helicity amplitudes at one loop in QCD and the soft limit of the cross-sections of multiparton processes*, *Nucl. Phys. B* **420** (1994) 550–564, [hep-ph/9401294]. **DOI**: [10.1016/0550-3213(94)90077-9].

[98] R. K. Ellis and J. C. Sexton, *QCD Radiative Corrections to Parton Parton Scattering*, *Nucl. Phys. B* **269** (1986) 445–484.
DOI: [10.1016/0550-3213(86)90232-4]. **INSPIRE-hep**: [hep-ph/218454].

[99] S. Catani and M. Grazzini, *An NNLO subtraction formalism in hadron collisions and its application to Higgs boson production at the LHC*, *Phys. Rev. Lett.* **98** (2007) 222002, [hep-ph/0703012]. **DOI**: [10.1103/PhysRevLett.98.222002].

[100] R. Bonciani, F. Buccioni, R. Mondini, and A. Vicini, *Double-real corrections at $\mathcal{O}(\alpha\alpha_s)$ to single gauge boson production*, *Eur. Phys. J. C* **77** (2017), no. 3 187, [arXiv:1611.00645]. **DOI**: [10.1140/epjc/s10052-017-4728-6].

[101] R. Bonciani, S. Di Vita, P. Mastrolia, and U. Schubert, *Two-Loop Master Integrals for the mixed EW-QCD virtual corrections to Drell-Yan scattering*, *JHEP* **09** (2016) 091, [arXiv:1604.08581]. **DOI**: [10.1007/JHEP09(2016)091].

[102] B. Humpert and W. L. Van Neerven, *AMBIGUITIES IN THE INFRARED REGULARIZATION OF QCD*, *Phys. Lett. B* **84** (1979) 327. [Erratum: Phys.Lett.B 85, 471 (1979)]. **DOI**: [10.1016/0370-2693(79)91299-1].

[103] B. Humpert and W. L. van Neerven, *How to Regularize the Infrared and Mass Singularities in QCD*, *Phys. Lett. B* **89** (1979) 69–75.
DOI: [10.1016/0370-2693(79)90078-9]. **INSPIRE-hep**: [hep-ph/142710].

[104] A. P. Contogouris and J. Kripfganz, *Some quantum-chromodynamic corrections to the drell-yan formula*, *Phys. Rev. D* **20** (Nov, 1979) 2295–2303. **DOI**: [10.1103/PhysRevD.20.2295].

[105] T. Matsuura, S. C. van der Marck, and W. L. van Neerven, *The Calculation of the Second Order Soft and Virtual Contributions to the Drell-Yan Cross-Section*, *Nucl. Phys. B* **319** (1989) 570–622. **DOI**: [hep-ph/0550321389906202].

[106] T. Matsuura, S. C. van der Marck, and W. L. van Neerven, *The Order α_s^2 Drell-Yan K factor*, *Nucl. Phys. B Proc. Suppl.* **7** (1989) 80–89. **DOI**: [hep-ph/0920563289905884].

[107] T. Matsuura, R. Hamberg, and W. L. van Neerven, *The Contribution of the Gluon-gluon Subprocess to the Drell-Yan K Factor*, *Nucl. Phys. B* **345** (1990) 331–368. **DOI**: [hep-ph/055032139090391P].

[108] A. Buckley, J. Ferrando, S. Lloyd, K. Nordström, B. Page, M. Rüfenacht, M. Schönherr, and G. Watt, *LHAPDF6: parton density access in the LHC precision era*, *Eur. Phys. J. C* **75** (2015) 132, [arXiv:1412.7420]. **DOI**: [10.1140/epjc/s10052-015-3318-8].

[109] J. Butterworth et al., *PDF4LHC recommendations for LHC Run II*, *J. Phys. G* **43** (2016) 023001, [arXiv:1510.03865]. **DOI**: [10.1088/0954-3899/43/2/023001].

[110] S. Catani, L. Cieri, D. de Florian, G. Ferrera, and M. Grazzini, *Universality of transverse-momentum resummation and hard factors at the NNLO*, *Nucl. Phys. B* **881** (2014) 414–443, [arXiv:1311.1654]. **DOI**: [10.1016/j.nuclphysb.2014.02.011].

[111] G. Bozzi, S. Catani, D. de Florian, and M. Grazzini, *Transverse-momentum resummation and the spectrum of the Higgs boson at the LHC*, *Nucl. Phys.* **B737** (2006) 73–120, [hep-ph/0508068]. **DOI**: [10.1016/j.nuclphysb.2005.12.022].

[112] S. Catani, D. de Florian, and M. Grazzini, *Universality of nonleading logarithmic contributions in transverse momentum distributions*, *Nucl. Phys. B* **596** (2001) 299–312, [hep-ph/0008184]. **DOI**: [10.1016/S0550-3213(00)00617-9].

[113] J. C. Collins, D. E. Soper, and G. F. Sterman, *Transverse Momentum Distribution in Drell-Yan Pair and W and Z Boson Production*, *Nucl. Phys. B* **250** (1985) 199–224. **DOI**: [10.1016/0550-3213(85)90479-1]. **INSPIRE-hep**: [hep-ph/203059].

[114] J. Kodaira and L. Trentadue, *Summing Soft Emission in QCD*, *Phys. Lett. B* **112** (1982) 66. **DOI**: [hep-ph/0370269382909078].

[115] G. Parisi and R. Petronzio, *Small Transverse Momentum Distributions in Hard Processes*, *Nucl. Phys. B* **154** (1979) 427–440. **DOI**: [10.1016/0550-3213(79)90040-3]. **INSPIRE-hep**: [hep-ph/140188].

[116] G. Curci, M. Greco, and Y. Srivastava, *Qcd jets from coherent states*, *Nucl. Phys. B* **159** (1979), no. 3 451–468. **DOI**: [0550321379903456/Nucl.Phys.B].

[117] J. C. Collins and D. E. Soper, *Back-To-Back Jets in QCD*, *Nucl. Phys. B* **193** (1981) 381. [Erratum: Nucl.Phys.B 213, 545 (1983)].**DOI**: [10.1016/0550-3213(81)90339-4].

[118] J. C. Collins and D. E. Soper, *Back-to-back jets: Fourier transform from b to kt*, *Nucl. Phys. B* **197** (1982), no. 3 446–476. **DOI**: [0550321382904539/Nucl.Phys.B].

[119] J. Kodaira and L. Trentadue, *Single Logarithm Effects in electron-Positron Annihilation*, *Phys. Lett. B* **123** (1983) 335–338. **DOI**: [10.1016/0370-2693(83)91213-3]. **INSPIRE-hep**: [hep-ph/179471].

[120] G. Altarelli, R. K. Ellis, M. Greco, and G. Martinelli, *Vector Boson Production at Colliders: A Theoretical Reappraisal*, *Nucl. Phys. B* **246** (1984) 12–44. **DOI**: [hep-ph/0550321384901123].

[121] M. Dasgupta and G. P. Salam, *Resummation of the jet broadening in DIS*, *Eur. Phys. J. C* **24** (2002) 213–236, [hep-ph/0110213]. **DOI**: [10.1007/s100520200915].

[122] S. Catani, L. Trentadue, G. Turnock, and B. R. Webber, *Resummation of large logarithms in e+ e- event shape distributions*, *Nucl. Phys. B* **407** (1993) 3–42. **DOI**: [10.1016/0550-3213(93)90271-P]. **INSPIRE-hep**: [hep-ph/344540].

[123] S. Catani, D. de Florian, M. Grazzini, and P. Nason, *Soft gluon resummation for Higgs boson production at hadron colliders*, *JHEP* **07** (2003) 028, [hep-ph/0306211]. **DOI**: [10.1088/1126-6708/2003/07/028].

[124] S. Catani and L. Trentadue, *Resummation of the QCD Perturbative Series for Hard Processes*, *Nucl. Phys. B* **327** (1989) 323–352. **DOI**: [10.1016/0550-3213(89)90273-3]. **INSPIRE-hep**: [hep-ph/25461].

[125] C. T. H. Davies and W. J. Stirling, *Nonleading Corrections to the Drell-Yan Cross-Section at Small Transverse Momentum*, *Nucl. Phys. B* **244** (1984) 337–348. **DOI**: [10.1016/0550-3213(84)90316-X]. **INSPIRE-hep**: [hep-ph/200822].

[126] R. P. Kauffman, *Higher order corrections to Higgs boson p_T*, *Phys. Rev. D* **45** (11, 1991). **DOI**: [10.1103/PhysRevD.45.1512].

[127] S. Catani, L. Cieri, D. de Florian, G. Ferrera, and M. Grazzini, *Vector boson production at hadron colliders: hard-collinear coefficients at the NNLO*, *Eur. Phys. J.* **C72** (2012) 2195, [arXiv:1209.0158]. **DOI**: [10.1140/epjc/s10052-012-2195-7].

[128] L. J. Dixon, Z. Kunszt, and A. Signer, *Helicity amplitudes for $\mathcal{O}(\alpha_s)$ production of W^+W^-, $W^\pm Z$, ZZ, $W^\pm\gamma$, or $Z\gamma$ pairs at hadron colliders*, *Nucl. Phys.* **B531** (1998) 3–23, [hep-ph/9803250]. **DOI**: [10.1016/S0550-3213(98)00421-0].

[129] V. Shtabovenko, R. Mertig, and F. Orellana, *New Developments in FeynCalc 9.0*, *Comput. Phys. Commun.* **207** (2016) 432–444, [arXiv:1601.01167]. **DOI**: [10.1016/j.cpc.2016.06.008].

[130] **NNPDF** Collaboration, V. Bertone, S. Carrazza, N. P. Hartland, and J. Rojo, *Illuminating the photon content of the proton within a global PDF analysis*, *SciPost Phys.* **5** (2018), no. 1 008, [arXiv:1712.07053]. **DOI**: [10.21468/SciPostPhys.5.1.008].

[131] M. Grazzini, S. Kallweit, and M. Wiesemann, *Fully differential NNLO computations with MATRIX*, *Eur. Phys. J. C* **78** (2018), no. 7 537, [arXiv:1711.06631]. **DOI**: [10.1140/epjc/s10052-018-5771-7].

[132] S. Catani and B. R. Webber, *Infrared safe but infinite: Soft gluon divergences inside the physical region*, *JHEP* **10** (1997) 005, [hep-ph/9710333]. **DOI**: [10.1088/1126-6708/1997/10/005].

[133] S. Alioli et al., *Precision studies of observables in $pp \to W \to l\nu_l$ and $pp \to \gamma, Z \to l^+l^-$ processes at the LHC*, *Eur. Phys. J.* **C77** (2017), no. 5 280, [arXiv:1606.02330]. **DOI**: [10.1140/epjc/s10052-017-4832-7].

[134] L. Cieri, D. de Florian, M. Der, and J. Mazzitelli, *Mixed QCD⊗QED corrections to exclusive Drell Yan production using the q_T -subtraction method*, *JHEP* **09** (2020) 155, [arXiv:2005.01315]. **DOI**: [10.1007/JHEP09(2020)155].

[135] D. de Florian and M. Grazzini, *Next-to-next-to-leading logarithmic corrections at small transverse momentum in hadronic collisions*, *Phys. Rev. Lett.* **85** (2000) 4678–4681, [hep-ph/0008152]. **DOI**: [10.1103/PhysRevLett.85.4678].